

**Geological description of rock
domains and deformation
zones in the Simpevarp and
Laxemar subareas**

**Preliminary site description
Laxemar subarea – version 1.2**

Carl-Henric Wahlgren, Geological Survey of Sweden

Jan Hermanson, Ola Forsberg
Golder Associates AB

Philip Curtis, FB Engineering AB

Carl-Axel Triumf, Geovista AB

Henrik Drake, Earth Sciences Centre, Göteborg University

Eva-Lena Tullborg, Terralogica AB

December 2006

Svensk Kärnbränslehantering AB

Swedish Nuclear Fuel
and Waste Management Co
Box 5864
SE-102 40 Stockholm Sweden
Tel 08-459 84 00
+46 8 459 84 00
Fax 08-661 57 19
+46 8 661 57 19



Geological description of rock domains and deformation zones in the Simpevarp and Laxemar subareas

Preliminary site description Laxemar subarea – version 1.2

Carl-Henric Wahlgren, Geological Survey of Sweden

Jan Hermanson, Ola Forssberg
Golder Associates AB

Philip Curtis, FB Engineering AB

Carl-Axel Triumph, Geovista AB

Henrik Drake, Earth Sciences Centre, Göteborg University

Eva-Lena Tullborg, Terralogica AB

December 2006

This report concerns a study which was conducted for SKB. The conclusions and viewpoints presented in the report are those of the authors and do not necessarily coincide with those of the client.

A pdf version of this document can be downloaded from www.skb.se

Abstract

This report is focussed on the geological description and modelling of rock domains and deterministic deformation zones in the Laxemar part of the local model area, i.e. the Laxemar subarea and its immediate surroundings. However, updating has been carried out in the Simpevarp subarea as well.

In comparison to the rock domain model presented in Simpevarp SDM version 1.2, additional data, particularly a new bedrock map in the Laxemar subarea, have implied that major modifications have been made in the rock domain model in the Laxemar part of the local scale model domain. The dominant rock domain in central and northern parts of Laxemar is principally made up of Ävrö granite (RSMA01). The southern and southwestern part of the Laxemar subarea is dominated by quartz monzodiorite in the rock domain RSMD01. In between the RSMA01 and RSMD01 domains, an arc-shaped rock domain (RSMM01) occurs which is characterized by a high frequency of diorite to gabbro, especially in the Ävrö granite. The RSMM01 domain and the northern contact of RSMD01 domain dips to the north. Smaller domains made up of a mixture of Ävrö granite and fine-grained dioritoid (RSMBA) are embedded in the RSMM01 domain. The Laxemar and Simpevarp subareas are separated by two elongated domains (RSMP) which are characterized by a high frequency of low-grade ductile shear zones. Lithological heterogeneity comprises occurrence of subordinate rock types, e.g. fine-grained granite, pegmatite and fine-grained diorite to gabbro, and also compositional variations in the dominating rock types.

Two deterministic deformation zone models are presented; 1) a base case model, which consists of deformation zones of high, medium and low confidence of existence in the regional model area, and 2) an alternative model which consists of zones of only high and medium confidence of existence in the local model area. In comparison to the deformation zone model presented in Simpevarp SDM version 1.2, the base case model only comprises minor modifications in the geometry of the deformation zones. However, the geometries and the character of a number of regional and local major deformation zones in the Laxemar and Simpevarp subareas have been updated. The latter includes both upgrading of low confidence zones to medium or high confidence of existence and also rejection of a limited number of zones. In total, 35 deterministic deformation zones with high confidence of existence have been modelled in the local scale model area, five of which have been added since the SDM Simpevarp 1.2. Three main orientations are found among the high confidence zones. An east-west striking, south-dipping regional zone delimits the Laxemar subarea in the north. Furthermore, an east-west striking local major zone with variable northerly dip divides the Laxemar subarea. North-south striking deformation zones delimits the Laxemar subarea in the west, and northeast oriented low-grade ductile deformation zones separate the Laxemar from the Simpevarp subarea. The latter coincides with the RSMP domains.

One subhorizontal deformation zone has been incorporated in the deformation zone model in the central part of the Laxemar subarea. Its existence is based on the identification of a seismic reflector that occurs well below repository depth (> 770 m).

Both the rock domain and deterministic deformation zone models are judged to be stabilising, although modifications are anticipated in the Laxemar part of the local scale model volume in future model versions when new data are available, particularly from new cored boreholes.

Sammanfattning

Denna rapport omfattar i första hand en geologisk beskrivning och modellering av bergdomäner och deterministiska deformationszoner i Laxemardelen av det lokala modellområdet, dvs delområde Laxemar och dess närmaste omgivningar. Uppdateringar har dock även gjorts i modelleringen av delområde Simpevarp.

I jämförelse med bergdomänmodellen som presenterades i den platsbeskrivande modellen Simpevarp version 1.2, har nytillkomna data, inte minst en ny berggrundskarta över delområde Laxemar, inneburit att relativt stora förändringar har gjorts i bergdomänmodellen inom Laxemardelen av det lokala modellområdet. Den dominerande bergdomänen i centrala och norra Laxemar utgörs i huvudsak av Ävrögranit (RSMA01). Den södra och sydvästra delen av delområde Laxemar domineras av kvartsmonzodiorit i bergdomän RSMD01. Området mellan RSMA01 och RSMD01 utgörs av en bågformad bergdomän (RSMM01) vilken karakteriseras av en hög frekvens av diorit till gabbro, framförallt i Ävrögraniten. RSMM01 och den norra kontakten av RSMD01 stupar mot norr. Mindre domäner som utgörs av en blandning av Ävrögranit och finkornig dioritoid (RSMBA) förekommer inom RSMM01-domänen. Delområdena Laxemar och Simpevarp åtskiljs av bergdomäner som karakteriseras av en hög frekvens av lågradiga, plastiska skjuvzoner (RSMP). Litologiska heterogeniteter utgörs i första hand av underordnade bergarter, t ex finkornig granit, pegmatit, finkornig diorit till gabbro, men också sammansättningsvariationer i de dominerande bergarterna.

Två deterministiska deformationszonsmodeller har tagits fram; 1) en basmodell som utgörs av deformationszoner med hög, medelhög och låg konfidens kopplad till deras existens, och 2) en alternativ modell i vilken endast zoner med hög och medelhög konfidens inom det lokala modellområdet ingår. I jämförelse med den deformationszonsmodell som presenterades i modellversion Simpevarp 1.2, har endast mindre förändringar gjorts i deformationszonernas geometri i basmodellen. Geometrin och karaktären på ett antal regionala och lokala större zoner har emellertid uppdaterats i delområdena Laxemar och Simpevarp. Detta innefattar såväl uppgradering av lågkonfidenszoner till medelhög eller hög konfidens kopplad till deras existens, som slopandet av ett begränsat antal zoner. Totalt har 35 deterministiska zoner med hög konfidensnivå modellerats inom det lokala modellområdet, av vilka fem har tillkommit i jämförelse med modellversion Simpevarp 1.2. Zoner med hög konfidensnivå uppvisar tre huvudsakliga orienteringar. En öst-västlig regional zon med sydlig stupning avgränsar delområde Laxemar i norr. Vidare delar en öst-västlig zon med varierande nordlig stupning upp Laxemar. Nord-sydligt orienterade deformationszoner avgränsar delområdet i väster, och nordostligt orienterade lågradiga deformationszoner åtskiljer delområdena Laxemar och Simpevarp. De senare zonerna sammanfaller med RSMP-domänerna.

En subhorisontell deformationszon i centrala Laxemar ingår i deformationszonsmodellen, dock en bra bit under förvarsdjup (> 770 m). Dess förekomst baseras på identifieringen av en seismisk reflektor.

Både bergdomänmodellen och den deterministiska deformationszonsmodellen bedöms som relativt stabila. Modifieringar förväntas dock i Laxemardelen av den lokala modellvolymen i kommande modellversioner när nya data blir tillgängliga, framförallt från nya kärnbrunnar.

Contents

1	Introduction	7
1.1	State of knowledge at previous model version	8
2	Evaluation of primary data	11
2.1	Summary of data sources	11
2.2	Surface geology	13
2.2.1	Outcrop mapping and complementary analytical studies	14
2.2.2	Outcrop mapping	14
2.2.3	Complementary analytical studies	15
2.2.4	General classification of rock types in the Laxemar and Simpevarp subareas	18
2.2.5	Rock type distribution on the surface – bedrock map	19
2.2.6	Age relations	39
2.2.7	Petrophysical properties of rock types	40
2.2.8	Bedrock heterogeneity	45
2.2.9	Lineament identification	45
2.2.10	Observation of ductile and brittle structures from the surface	52
2.3	Surface geophysics	60
2.3.1	Older data	60
2.3.2	Data generated during the ongoing site investigation	62
2.4	Borehole data	62
2.4.1	Rock types in cored boreholes	63
2.4.2	Brittle structures in cored boreholes	68
2.4.3	Ductile structures in cored boreholes	68
2.4.4	Borehole radar and geophysical logs	68
2.4.5	Fracture mineralogy	71
2.4.6	Single hole geological interpretation	85
3	Rock domain model	89
3.1	Basis for modelling	89
3.2	Division into rock domains	90
3.2.1	Division of rock domains at the surface	90
3.2.2	Definition of rock domains in cored boreholes	93
3.3	Construction of the 3D rock domain model	94
3.3.1	Arc geometry	94
3.3.2	Lens geometry	94
3.4	The 3D rock domain model	95
3.5	Property of rock domains	97
3.5.1	Assignment of properties	97
3.6	Evaluation of ore potential	106
3.7	Evaluation of uncertainties	108
4	Deterministic deformation zone modelling	113
4.1	Modelling assumptions and input from other disciplines	113
4.2	Conceptual model of the kinematic evolution of deformation zones	115
4.3	Conceptual deformation zone model with potential alternatives	116
4.3.1	Conceptual base case deformation zone model	116
4.3.2	Alternative deformation zone model	122
4.4	Laxemar and Simpevarp subareas – divided by regional shear zones	123
4.5	Property assignment to the base case model with specification of high confidence zones within the local model volume	125

4.6	High confidence deformation zones – detailed descriptions	125
4.6.1	ZSMEW007A and ZSMEW900	125
4.6.2	ZSMNE005A (Äspö Shear zone)	134
4.6.3	ZSMEW002A (Mederhult shear zone)	138
4.6.4	ZSMNW042A	142
4.6.5	ZSMNS001A–D	146
4.6.6	ZSMEW009A (EW3 at Äspö)	148
4.6.7	ZSMEW013A (EW1a on Äspö)	151
4.6.8	ZSMEW023A	154
4.6.9	ZSMEW038A	158
4.6.10	ZSMNE004A	163
4.6.11	ZSMNE006A (NE1 on Äspö)	168
4.6.12	ZSMNE010A and ZSMNE011A	170
4.6.13	ZSMNE012A	172
4.6.14	ZSMNW928A	176
4.6.15	ZSMNE040A and ZSMNW929A	177
4.7	Evaluation of uncertainties	181
5	References	183
Appendix 1	Nomenclature of rock types (in English and Swedish), including rock codes applied in the site investigation at Oskarshamn	189
Appendix 2	Bedrock map	191
Appendix 3	Property tables for rock domains	193
Appendix 4	Dominant and subordinate rock type statistics	233
Appendix 5	Property tables for deformation zones	239

1 Introduction

This report covers the bedrock geology in the Laxemar part of the local model area, i.e. the Laxemar subarea and its immediate surroundings, and only minor updating in the Simpevarp subarea. What concerns the description and evaluation of the bedrock geology in the Simpevarp subarea, the reader is referred to the Simpevarp Site Descriptive Model (SDM) 1.1 and 1.2 reports /SKB 2004, 2005a/.

The bedrock geological model consists of three components; the rock domain model, the deterministic deformation zone model, and the statistical model of fractures and deformation zones, the so-called discrete fracture network (DFN) model. The work has been carried out according to the strategy described in /Munier et al. 2003/ and /Munier 2004/. This report does not comprise the DFN model which is reported in /Hermanson et al. 2005/. As in the case of model version Simpevarp 1.2, the rock domain and deterministic deformation zone models are presented for the whole regional model volume which encapsulates the local model volume. The DFN model has utilised fracture data essentially from within the rock mass of the local model volume situated outside deformation zones. An alternative model is presented for the deformation zone model.

A geological model of the bedrock and deformation zones rely on two types of data; indirect and direct data. Indirect data, acquired through airborne and ground geophysical measurements together with elevation surveys and photography, provide essential information of the extent and location of deformation zones. Direct data, acquired through excavated trenches, field mapping or core observations, can determine their existence and geological character.

One rock domain model is presented. Only very minor changes have been made in the regional model domain compared to version Simpevarp 1.2. Since the investigations in connection with the complete site investigation are entirely focused on the local scale model domain, no major modifications are to be expected in future model versions. Accordingly, the rock domain model in the regional model domain is, and will in future model versions, only be based on bedrock information of reconnaissance character that existed prior to the site investigation and which formed the base for the compilation of the Simpevarp SDM version 0. Consequently, the uncertainties what relate to the occurrence and geometry, and also the characterisation of the rock domains in the regional model area will persist throughout the site investigation. However, a significant increase in the amount of data, especially from the Laxemar subarea, implies that major modifications and changes have been made in the Laxemar part of the local scale model domain. By consideration of the changes compared to model version Simpevarp 1.2, it is considered that the rock domain model is stabilising, although modifications of the rock domain boundaries in the local scale model domain are anticipated when new data become available, in particular from future cored boreholes.

Two alternative deformation zone models are presented; 1) the base case model, which consists of deformation zones of high, medium and low confidence of existence in the regional model area, and 2) an alternative model which consists of only the high and medium confidence deformation zones in the local model area. Relatively minor changes in the geometries of the modelled zones of the base case model have occurred since the previous model version, even since most of the underlying primary data and lineaments have been reanalysed. Direct and indirect subsurface data together with better coverage of interpreted lineaments along the coast line has increased the knowledge of the geometries and the character of a number of regional and local major zones in the Laxemar subarea and on the Simpevarp peninsula. Several low confidence zones have been upgraded to high or medium confidence zones through confirmation by detailed indirect or by direct observations within the local model area. A few interpreted deformation zones in the Simpevarp 1.2 model have been rejected essentially through analyses of new subsurface data. One subhorizontal deformation zone

has been suggested, and is identified by a strong seismic reflector in the central part of the Laxemar subarea. The interpretation is that this zone is situated well below repository depth in the central part of the local model volume.

The base case deformation zone model is stabilising with regards to the locations and geometries of regional, and, to a large extent, local major zones in the local model volume, although small adjustments are expected in future model versions with the access to more detailed surface and subsurface data.

One or more components of the bedrock geological model provide a foundation for the modelling work in rock mechanics, thermal properties, bedrock hydrogeology and, to lesser extent, bedrock hydrogeochemistry and bedrock transport properties. All components of the geological model have also a direct influence on the location and detailed design of the repository. The model also constitutes a significant input to the safety analysis work.

1.1 State of knowledge at previous model version

The Simpevarp Site Descriptive Model version 1.2 related to the regional model area but the focus was on the eastern part of the local scale model area, i.e. principally the Simpevarp subarea /SKB 2005a/.

In model version Simpevarp 1.2, the surface geological information, i.e. the character and surface extension of dominant rock types, outside the Simpevarp subarea, were based on the SDM version 0. This variation in quality of the surface geological data and the limited subsurface information are the two most important factors that govern the uncertainties associated with the modelling of the rock domains in the Simpevarp SDM version 1.2. Consequently, the confidence of occurrence and geometry of the rock domains at the surface was judged to be medium to high in the part of the local model area making up the Simpevarp subarea, whereas it was judged to be low to medium outside the Simpevarp subarea. Due to the restricted subsurface information, the confidence of occurrence at depth was set to medium to low for most rock domains, except for the dominating rock domain RSMA01 (dominated by Ävrö granite) which forms the principal matrix in the local scale model volume. However, the geometrical relationships between rock domain RSMA01 and the other rock domains, in particular the major rock domains, were considered as highly uncertain.

The main uncertainties associated with the Simpevarp 1.2 rock domain model were:

- Nature of the bedrock below sea and on land outside the Simpevarp peninsula, Äspö and Ävrö in the regional model area (lower quality data in these areas).
- Spatial distribution of rock domains outside the Simpevarp subarea.
- Three-dimensional geometry of most rock domains.
- Proportion of rock types in domains (veins, patches, dykes, minor bodies; not evenly distributed at the 50–100 m scale and below). There could also be non-uniformity in their occurrence.
- Spatial distribution of compositional varieties of the Ävrö granite, i.e. granitic to granodioritic (“rich in quartz”) contra quartz monzodioritic (“poor in quartz”) varieties.
- Three-dimensional extent of “secondary red staining” (hydrothermal alteration).

A three-dimensional deformation zone model, which consists of 22 high confidence and 166 low confidence deformation zones in the whole regional model domain, was presented in the Simpevarp 1.2 site description. Deformation zones with a length of 1 km or more in the local model domain and zones with a length of 1.6 km or more in the regional model domain were addressed. The data coverage in the regional scale model domain did not allow the same high resolution as in the local scale model domain. Existing old structural models, a variety of

new surface and sub-surface data, and new linked lineament data from a larger area were used in the modelling. The linked lineaments were further post-processed to better reflect geology and in order to minimise effects of differences in data coverage over land and sea.

The interpretation of high confidence zones were supported by a variety of geological and geophysical information in addition to the interpreted lineaments. Two important types of deformation zones were present within this group:

- Regional deformation zones with northeasterly strike, confirmed already in model version 0 or in other previous models established in the Simpevarp area such as the Äspö shear zone (ZSMNE005).
- Local major fracture zones, which have been confirmed either by new borehole information or in previous models in the Simpevarp area such as ZSMEW007A.
- Smaller zones and fractures, with a surface extent of less than 1 km were not included deterministically in the model, but handled in a stochastic way through the geological DFN model.

2 Evaluation of primary data

2.1 Summary of data sources

This section summarises the data that were available at the time of the data freeze for Laxemar 1.2 and distinguishes data used and data not used in the geological site descriptive modelling. In the table below (Table 2-1), the first two columns set out the data available, columns 3 and 4 identify the data that were used. It is noted that the use of data from individual boreholes varied depending on the state of down-hole discipline-wise characterisation in the individual boreholes.

Table 2-1. Available bedrock geological and geophysical data and their handling in Laxemar 1.2.

Available primary data Data specification	Ref.	Usage in Simpevarp 1.2 Analysis/modelling
Bedrock mapping – outcrop data (rock type, ductile and some brittle structures at 353 observation points in the Simpevarp subarea and 1,169 observation points in the Laxemar subarea.	P-04-102, P-04-221, P-05-180	Rock type, ductile deformation in the bedrock, fracture statistics and identification of possible fracture zones at the surface
Bedrock map of the Äspö island	PR-25-88-12	Rock domain modelling
Marine geological survey	P-05-35	Identification of lineaments/deformation zones
Scan-line mapping of fractures at 16 outcrops in the Simpevarp subarea and 24 outcrops in the Laxemar subarea	P-04-102, P-04-244	Frequency and orientation of fractures
Detailed fracture mapping at four sites in the Simpevarp subarea and 2 sites in the Laxemar subarea	P-04-35, P-04-274	Fracture orientation, tracelength and other geological parameters (mineral infilling, alteration etc).
Modal analyses and geochemical analyses	P-04-102, P-05-180	Mineralogical and geochemical properties of the bedrock. Assessment of thermal properties.
Petrophysical rock parameters and in situ gamma-ray spectrometric data	P-03-97, P-04-294	Physical properties of the bedrock
Airborne geophysical data (magnetic, EM, VLF and gamma-ray spectrometric data)	P-03-25, P-03-63, P-03-100	Identification of lineaments/deformation zones and lithological boundaries
Detailed topographic data from airborne photography	P-02-02, P-03-99	Identification of lineaments/deformation zones
High resolution reflection seismics	P-03-71, P-03-72, P-04-52, P-04-204, P-04-215, TR-97-06, TR-02-04, TR-02-19, R-01-06 R-01-07, Geophysics 64, 662–667, Tectonophysics 355, 201–213	Identification of inhomogeneities in the bedrock that may correspond to boundaries between different types of bedrock or to deformation zones. Supportive information used from previous models (Laxemar, Ävrö and Äspö 96). Rock domain modelling
Surface geophysical data (magnetic, EM, refraction seismic and in situ gamma ray spectrometric data)	P-02-05, P-03-66, P-04-128, P-04-134, P-04-201, P-04-211 PR 25-89-13, PR 25-89-23	Identification of lineaments/deformation zones Rock domain modelling

Available primary data Data specification	Ref.	Usage in Simpevarp 1.2 Analysis/modelling
Regional gravity data and gravity data from profile measurements in the Laxemar subarea	P-04-128	Rock domain modelling
Interpretation of airborne geophysical and topographical data (linked lineament map)	P-03-100, P-03-99, P-04-49	Deterministic structural model
Simevarp site descriptive model v.0	R-02-35	Rock domain model and deterministic structural model
Simevarp site descriptive model v.1.2	R-05-08	Bedrock map, Rock domain model and deterministic structural
Laxemar area – testing the methodology for site descriptive modelling	TR-02-19	Deterministic structural model
RVS modelling, Ävrö	R-01-06	Deterministic structural model
ÄHRL, geological model	IPR-03-34	Deterministic structural model
Geophysical, radar and BIPS logging, interpretation of geophysical data, Boremap data, single-hole interpretation in KSH01A/B	P-03-15, P-03-16 P-03-73, P-04-01, P-04-28 P-04-32, P-04-218, P-04-250	Fracture statistics (including mineralogical analyses),, rock type proportion down to borehole depth 1,000 m in DFN (Discrete Fracture Network), rock domain and deformation zone models.
Geophysical, radar and BIPS logging, interpretation of geophysical data, Boremap data, single-hole interpretation in KSH02	P-03-16, P-03-73, P-03-109, P-03-111, P-04-28, P-04-77 P-04-131, P-04-133, P-04-218	Fracture statistics (including mineralogical analyses), rock type proportion down to borehole depth 1,000 m in DFN (Discrete Fracture Network), rock domain and deformation zone models
Geophysical, radar and BIPS logging, interpretation of geophysical data, Boremap data, single-hole interpretation in KSH03A/B	P-04-132, P-04-214, P-04-231	Fracture statistics (including mineralogical analyses), single hole interpretation, rock type proportion down to borehole depth 1,000 m in DFN (Discrete Fracture Network), rock domain and deformation zone models
Geophysical, radar and BIPS logging, interpretation of geophysical data, Boremap data, single-hole interpretation in KAV01	P-03-120, P-04-77, P-04-130, P-04-133, P-04-218	Fracture statistics (including mineralogical analyses, rock type proportion down to borehole depth 1,000 m in DFN (Discrete Fracture Network), rock domain and deformation zone models
Geophysical, radar and BIPS logging, interpretation of geophysical data, Boremap data, single-hole interpretation in KAV04A/B	P-04-217, P-04-308, P-05-22	Fracture statistics (including mineralogical analyses), single hole interpretation, rock type proportion down to borehole depth 1,000 m in DFN (Discrete Fracture Network), rock domain and deformation zone models
Petrocore data, geophysical loggings and interpretation of geophysical data for KLX01	P-05-34	Single hole interpretation, rock type proportion down to borehole depth 1,000 m, rock domain and deformation zone models
Geophysical, radar and BIPS logging, interpretation of geophysical data, Boremap data, single-hole interpretation in KLX02	P-03-111, P-03-120, P-04-214, P-04-129, P-04-231	Fracture statistics (including mineralogical analyses), single hole interpretation, rock type proportion down to borehole depth 1,000 m in DFN (Discrete Fracture Network), rock domain and deformation zone models
Geophysical, radar and BIPS logging, Boremap data, single-hole interpretation in KLX03	P-05-24, P-05-34	Fracture statistics (including mineralogical analyses), single hole interpretation, rock type proportion down to borehole depth 1,000 m in DFN (Discrete Fracture Network), rock domain and deformation zone models
Geophysical, radar and BIPS logging, Boremap data, single-hole interpretation in KLX04	P-05-23, P-05-34	Fracture statistics (including mineralogical analyses), single hole interpretation, rock type proportion down to borehole depth 1,000 m in DFN (Discrete Fracture Network), rock domain and deformation zone models

Available primary data Data specification	Ref.	Usage in Simpevarp 1.2 Analysis/modelling
Simplified mapping, radar and geophysical logging and interpretation of geophysical data of the cored borehole KLX05	P-05-189	Rock domain and deformation zone models
Simplified mapping, radar, geophysical logging and interpretation of geophysical data of the cored borehole KLX06	P-05-44	Rock domain and deformation zone models
Geophysical, radar and BIPS logging, interpretation of geophysical data, Boremap and single-hole interpretation in HSH01, HSH02 and HSH03	P-03-15, P-04-02, P-04-28 P-04-32, P-04-218	Rock domain and deformation zone models
Geophysical, radar and BIPS logging, interpretation of geophysical data, Boremap and single-hole interpretation in HAV09 and HAV10	P-04-214, P-04-231	Rock domain and deformation zone models
Geophysical logging, interpretation of geophysical data in HLX13	P-04-217	Rock domain and deformation zone models
Geophysical, radar and BIPS logging, Boremap and single-hole interpretation in HLX15	P-04-217, P-04-308	Rock domain and deformation zone models
BIPS, radar, geophysical logging and single-hole interpretation HLX21–28	P-05-34	Rock domain and deformation zone models

2.2 Surface geology

During the period between the data freezes for the model versions Simpevarp 1.2 and Laxemar 1.2, a considerable amount of new surface data have been generated from the Laxemar subarea. In contrast to the situation at the time of the Simpevarp 1.2 modelling, the Laxemar subarea is now covered by a detailed bedrock map compiled at the scale 1:10 000. As a complement to the outcrop database, generated during the bedrock mapping campaign, analytical work comprising modal, geochemical and petrophysical analyses has been carried out in order to characterise the various rock types. The results of this analytical work have subsequently been utilised in the characterisation of the identified rock domains in the geological modelling. The data from the surface is also complemented by new analytical data from cored boreholes.

The majority of the new primary data relate to the characterisation of the bedrock, mainly the various rock types, and not so much to the characterisation of the deformation zones. This is the explanation for the bias in the description below between the rock type related evaluation and description, and the evaluation of primary data related to the deformation zones.

In the Laxemar subarea and its immediate surroundings, the distribution, description and age of the various rock types have been documented with the help of the following information that to a major extent has been generated during recently performed site investigation activities:

- An outcrop database with numerical and descriptive data from 1,169 observation points /Persson Nilsson et al. 2004/, including repetitive measurements (commonly eight) of the magnetic susceptibility of the different rock types at every observation point.
- 51 modal analyses (mineral composition) of surface samples and 5 modal analyses from KLX03, recalculated and plotted in a QAPF diagram in order to classify the various rock types /Wahlgren et al. 2005/.
- Chemical analyses of 30 surface samples and 5 samples from KLX03, which have been used to characterise the various rock types /Wahlgren et al. 2005/.

- Petrophysical data, including density, magnetic and electric properties and porosity from laboratory measurements of 72 samples of different rock types, including scattered samples from the Simpevarp subarea and the remaining part of the regional model area /Mattsson et al. 2004a/.
- In situ gamma-ray spectrometry data from 171 locations, including locations in the Simpevarp subarea and the remaining part of the regional model area /Mattsson et al. 2004a/.
- Bedrock geological map compiled with the help of the outcrop database and magnetic data from airborne geophysical measurements /Wahlgren et al. 2005/, (see Section 2.2.5).
- Bedrock geological map at the scale 1:50 of two sites where detailed fracture mapping has been carried out on cleaned outcrops, one of which is the drill site for KLX05 /Cronquist et al. 2004/ (see Section 2.2.10.4).

Attention is given to the mineralogical and chemical composition, grain size, texture, structure and petrophysical properties, including those derived from in situ gamma ray spectrometry, of the rock types in the Laxemar part of the local scale model area. For reference, a comparison is made to corresponding results from the Simpevarp subarea.

2.2.1 Outcrop mapping and complementary analytical studies

The character of the different rock types in the Laxemar and Simpevarp subareas is defined primarily on the basis of two data sets:

- Outcrop database from bedrock mapping.
- Complementary analytical results of representative samples from the surface.

These data form the basis for the compilation of the bedrock map (see Section 2.2.5). Furthermore, in combination with corresponding information from the cored boreholes (see Section 2.4), they yield the properties of the rock types that define the different rock domains in the rock domain model.

2.2.2 Outcrop mapping

The bedrock in the Laxemar subarea is well exposed except for a minor area in the southern part (Figure 2-1).

Detailed bedrock mapping of the Laxemar subarea and its immediate surroundings was carried out during the summer 2004 /Persson Nilsson et al. 2004/ in conjunction with the ongoing site investigation programme (Figure 2-2). In the remaining part of the regional model area, the bedrock mapping campaign during 2004 only comprised selected target areas with the purpose of explaining geophysical anomalies, and, thus, the new bedrock information that has been gained from the surface is only of point character (Figure 2-2). In contrast to the local model area, which, except for the islands north of Ävrö (including the Äspö island), is covered by new detailed surface bedrock information, the surface bedrock geological information in the regional model area is only based on the SDM version 0 bedrock map. Hence, it is difficult to judge the quality of the bedrock information in the regional model area, since it is partly based on bedrock maps at the scale 1:250 000 /Bergman et al. 1998, 1999, SKB 2002/. Accordingly, the available bedrock data relating to the distribution and description of rock types within the regional model area are of variable quality, whereas the ages of the rock types are judged to be fairly well-constrained.

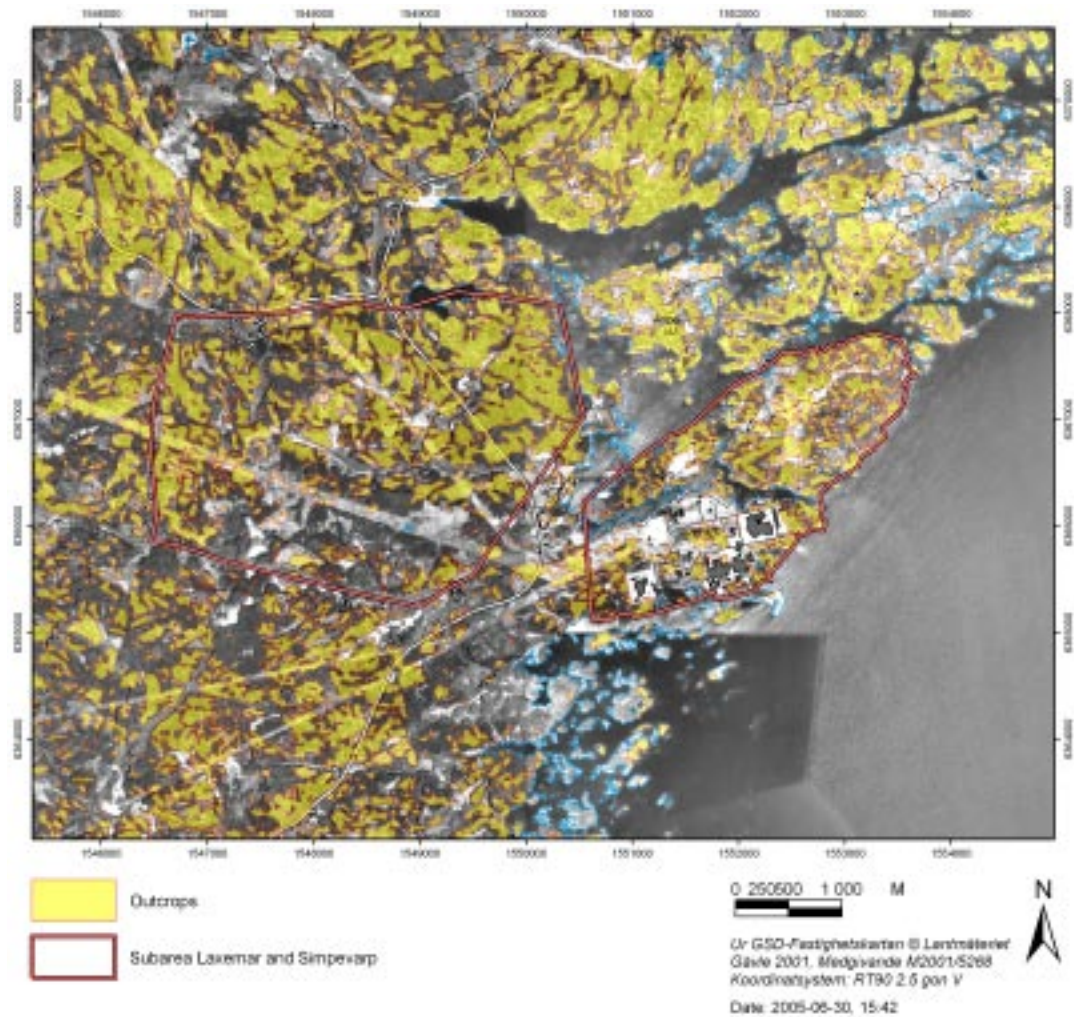


Figure 2-1. Outcrop map of the Laxemar and Simpevarp subareas and surroundings.

2.2.3 Complementary analytical studies

In order to characterise the different rock types, modal and geochemical analysis as well as determination of petrophysical properties, including density, magnetic and electric properties and porosity, have been performed of representative samples from the surface. Furthermore, in situ gamma-ray spectrometry measurements have been performed on selected outcrops. In Figure 2-3, the sample sites for the different analytical studies and the locations for the in situ gamma-ray measurements are displayed.

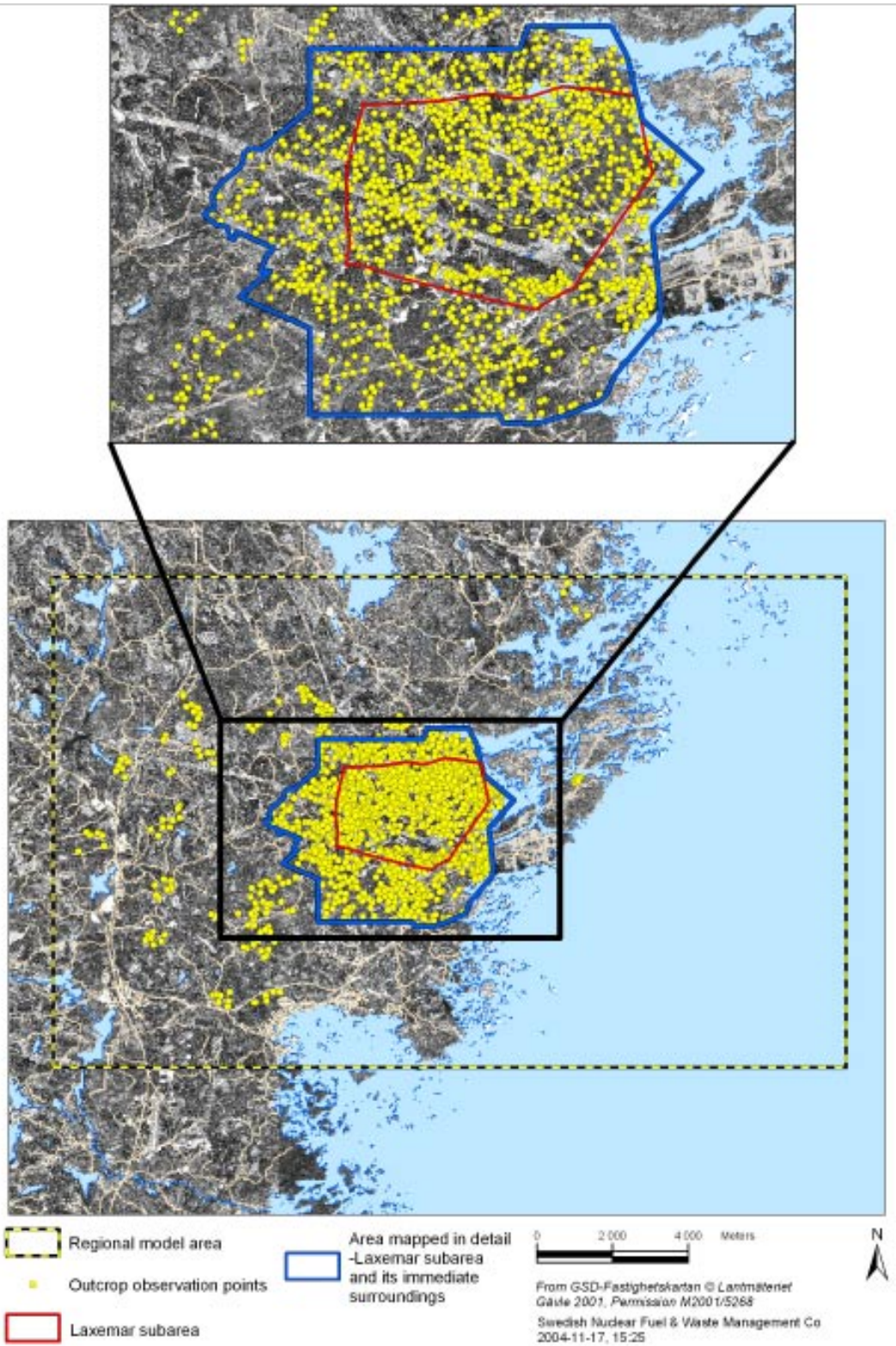


Figure 2-2. Observation points where outcrop data were collected during bedrock mapping in the summer 2004 are marked in yellow. The Laxemar subarea and immediate surroundings as well as the entire regional model area are displayed.

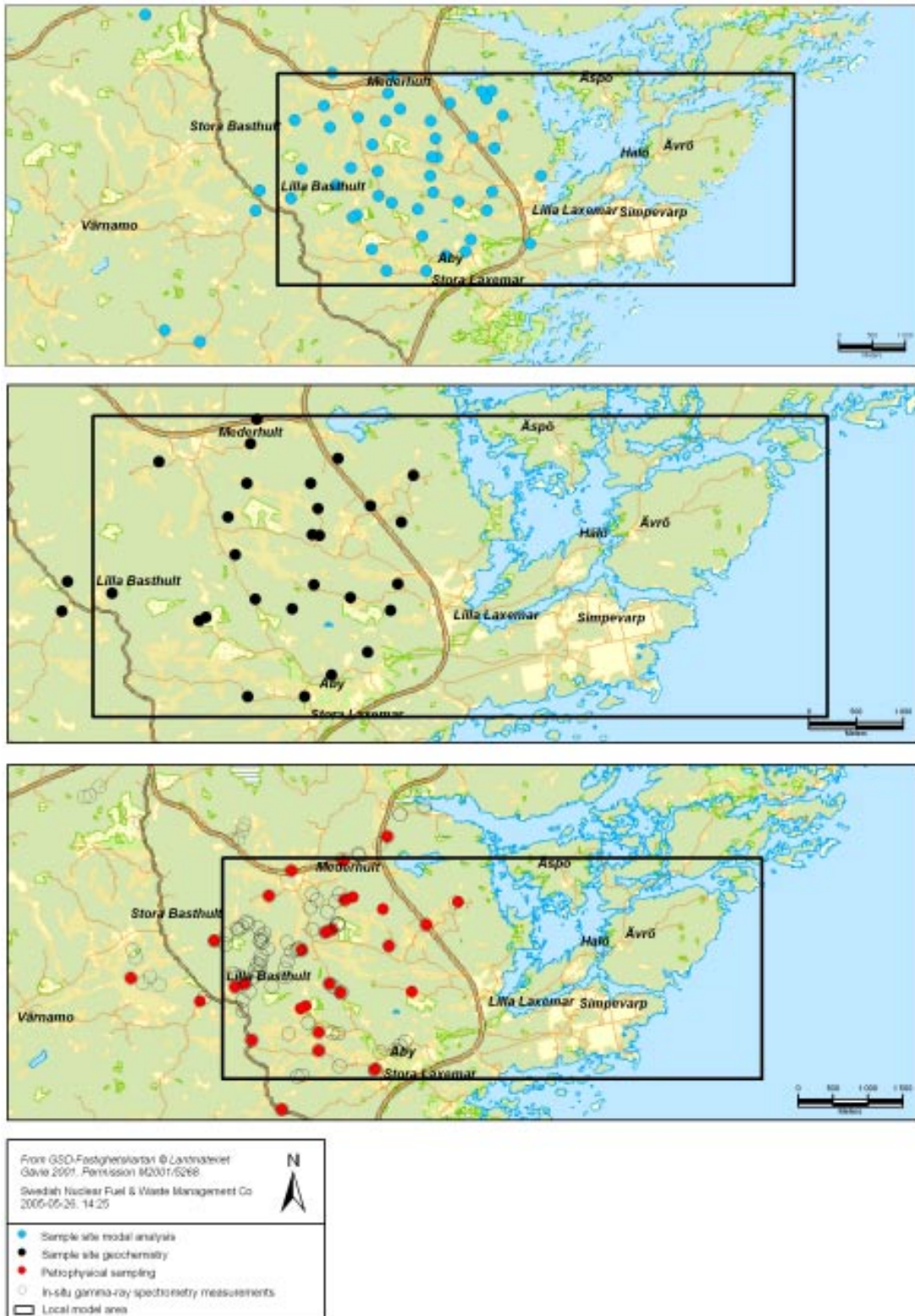


Figure 2-3. Sample sites for modal and geochemical analytical studies and petrophysical measurements, including locations for in situ gamma-ray spectrometric measurements in the Laxemar subarea and surroundings.

2.2.4 General classification of rock types in the Laxemar and Simpevarp subareas

As can be seen in the QAPF and geochemical classification diagrams (Figure 2-4, Figure 2-5 and Figure 2-6), the various rock types in the Simpevarp and Laxemar subareas display similar and overlapping compositional variations. Apart from the composition, the most important criteria employed in distinguishing between different rock types are texture and grain size.

The compositional alkali-calcic trend displayed in the QAPF and geochemical classification diagrams for the studied rock types is characteristic for granite-syenitoid-dioritoid-gabbroid rocks in the Transscandinavian Igneous Belt /e.g. Högdahl et al. 2004/. A comparison with corresponding rock types from the Bergslagen area and surroundings in south-central Sweden can be seen in Figure 2-5 and Figure 2-6. The descriptions and characterisations of the individual rock types are presented below in conjunction with the description of the bedrock map.

According to the International Union of Geological Sciences /LeMaitre 2002/, the classification of rocks should be based on the modal composition. Thus, the geochemical classification diagrams, cf. Figure 2-5 and Figure 2-6, should not be used strictly for classification purposes, but merely as an indication of the compositional trends of the different rock types.

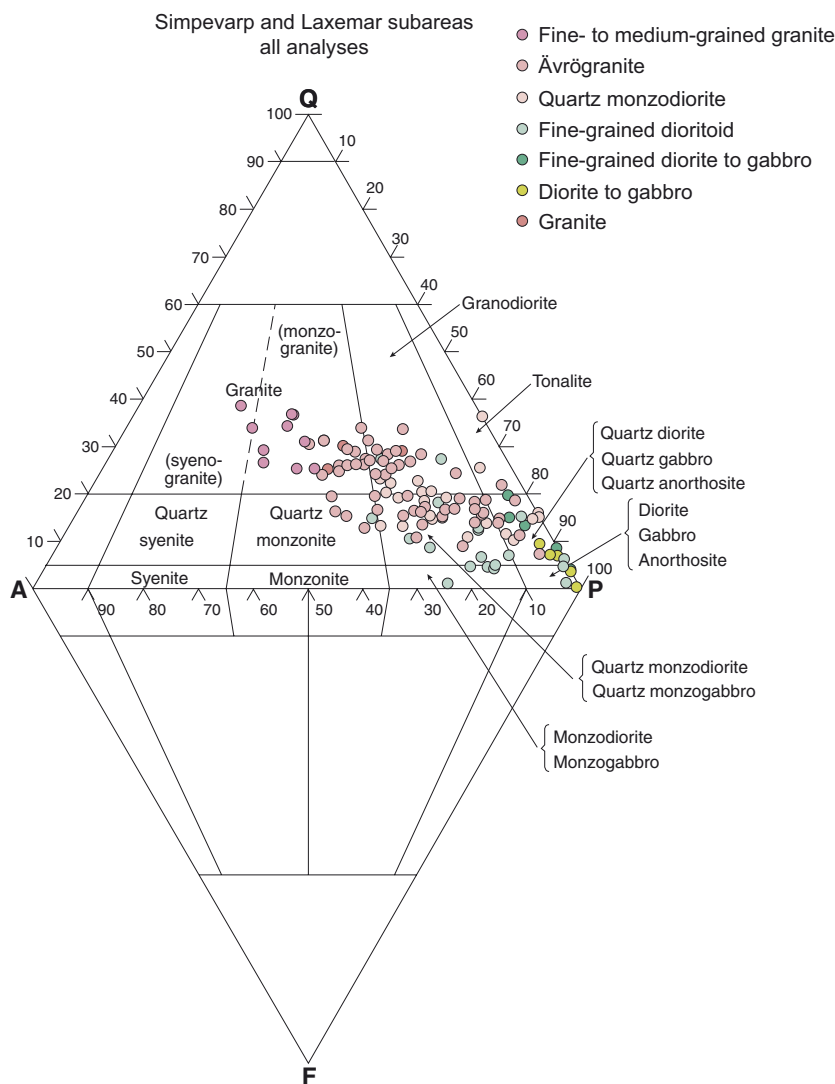


Figure 2-4. QAPF modal classification of rock types in the Simpevarp and Laxemar subareas according to /Streckeisen 1976/. All analysed samples are included.

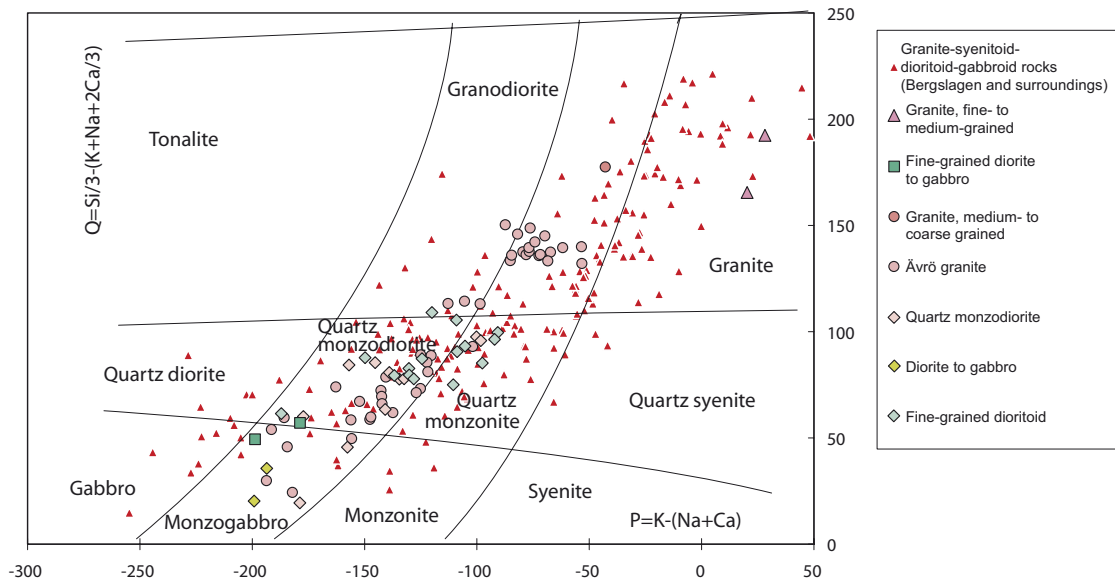


Figure 2-5. Geochemical classification of rocks from the Simpevarp and Laxemar subareas according to /Debon and LeFort 1983/. All analysed samples are included.

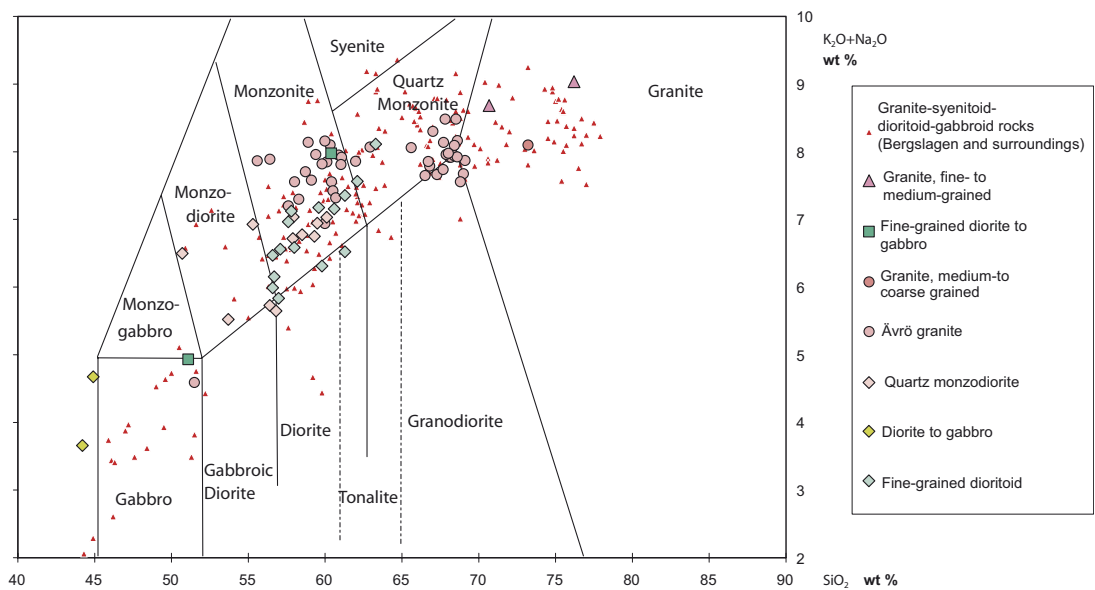


Figure 2-6. Geochemical classification of rocks from the Simpevarp and Laxemar subareas according to /Middlemost 1994/. All analysed samples are included.

2.2.5 Rock type distribution on the surface – bedrock map

The bedrock in the Simpevarp regional model area, as well as the major part of southeastern Sweden, is totally dominated by intrusive igneous rocks that belong to the approximately 1,810–1,760 Ma old generation of granite-syenitoid-dioritoid-gabbroid rocks in the 1,860–1,650 Ma old so-called Transscandinavian Igneous Belt (TIB). A characteristic feature is magma mingling and mixing relationships between the different rock types. The rocks are mostly well preserved and more or less isotropic, but a weak foliation is locally developed. However, low-grade ductile shear zones of mesoscopic to regional character do occur. A conspicuous rock type in the regional model area is a c. 1,450 Ma old granite.

The nomenclature of the rock types and associated rock codes applied in the Oskarshamn site investigation is presented in Appendix 1 in the Simpevarp 1.2 report /SKB 2005a/.

The bedrock in the Laxemar subarea and its immediate surroundings, which cover the western part of the local model area, is predominated by two rock types, namely:

- Ävrö granite (granite to quartz monzodiorite), medium-grained, generally porphyritic.
- Quartz monzodiorite, medium-grained, equigranular to weakly porphyritic.

The following rock types are subordinate in character, though they make up characteristic constituents in the bedrock and may be more or less frequently occurring:

- Granite, fine- to medium-grained.
- Pegmatite.
- Diorite to gabbro, fine-grained (mafic rock, fine-grained) .
- Granite, medium- to coarse-grained.
- Diorite to gabbro, medium-grained.
- Dioritoid, fine-grained, unequigranular.

The regional model area is composed of six dominant rock types, cf. Figure 2-7, namely:

- Ävrö granite (granite to quartz monzodiorite), medium-grained, generally porphyritic.
- Quartz monzodiorite, medium-grained, equigranular to weakly porphyritic.
- Granite, medium- to coarse-grained.
- Diorite to gabbro.
- Dioritoid, fine-grained, unequigranular.
- Götemar type granite, coarse-grained and fine- to medium-grained.

Subordinate rock types in the regional model area comprise:

- Granite, fine- to medium-grained.
- Pegmatite.
- Diorite to gabbro, fine-grained (mafic rock, fine-grained).

A new bedrock map at the scale 1:10 000 has been produced for the Laxemar subarea and its immediate surroundings /Wahlgren et al. 2005/. This bedrock map has been combined with the previously compiled bedrock map of the Simpevarp subarea /Wahlgren et al. 2004, SKB 2004/. Furthermore, a digitised version of the bedrock map of Äspö /Kornfält and Wikman 1988/ is included. Thus, the major part of the local model areas is now covered with a detailed bedrock map in the scale 1:10 000 (Appendix 2). It should be noted that the Äspö island has not been re-mapped in conjunction with the ongoing site investigation. Due to this, the Äspö diorite and the greenstone at Äspö have been given separate rock codes and thereby separate colours on the bedrock map, partly because they cannot be directly transformed to the decided rock codes for the site investigation, and partly to keep traceability to the underground mapping in the Äspö HRL.

In order to visualise the differences between the bedrock map of the Laxemar and Simpevarp subareas and the bedrock map from model version 0 in a simplified manner, these maps are merged in Figure 2-7. The obvious difference in resolution and amount of details between the two maps is obvious (Figure 2-7).

2.2.5.1 Ävrö granite

Ävrö granite is the dominating rock type in the central and northern part of the Laxemar subarea, as well as in the regional model area (Appendix 2 and Figure 2-7). The Ävrö granite concept comprises a suite of commonly porphyritic rocks that vary in composition from quartz monzodiorite to granite, including granodioritic, tonalitic, quartz dioritic and quartz monzonitic varieties (Figure 2-8). The geochemical classification of the Ävrö granite is displayed in Figure 2-9 and Figure 2-11. Corresponding classification for the Ävrö granite in the Simpevarp subarea is displayed in Figure 2-10 and Figure 2-12. As can be seen, the compositional variation is very similar to that in the Simpevarp subarea. The mineralogical composition of the Ävrö granite is displayed in Figure 2-18.

The Ävrö granite is reddish grey to greyish red, medium-grained and the phenocrysts are usually 1–2 cm in size but scattered larger phenocrysts exist. A characteristic feature in the Ävrö granite is the occurrence of enclaves of intermediate to mafic composition. Furthermore, the Ävrö granite commonly mixes and mingles with the surrounding rock types, especially with the equigranular quartz monzodiorite (see below). This is displayed by gradual and diffuse contact relationships, which indicate that the parent magmas were emplaced more or less synchronously /cf. SKB 2005a/. The latter is confirmed by obtained U-Pb zircon ages of 1,800±4 Ma and 1,802±4 Ma for the Ävrö granite and quartz monzodiorite, respectively (Table 2-2).

The Ävrö granite has not been subdivided in its different compositional varieties in the bedrock map, mainly due to difficulties to distinguish between the different varieties in hand specimen during the bedrock mapping. However, as can be seen in the QAPF classification diagram (Figure 2-8) and the geochemical classification diagrams (Figure 2-9 and Figure 2-11), it is indicated that the Ävrö granite in the Laxemar subarea constitute two populations, one richer in quartz (granodioritic to granitic) and one with a lower quartz content (quartz monzodioritic). This division in two populations is also indicated by in situ gamma-ray spectrometry and density results /Mattsson et al. 2004a/.

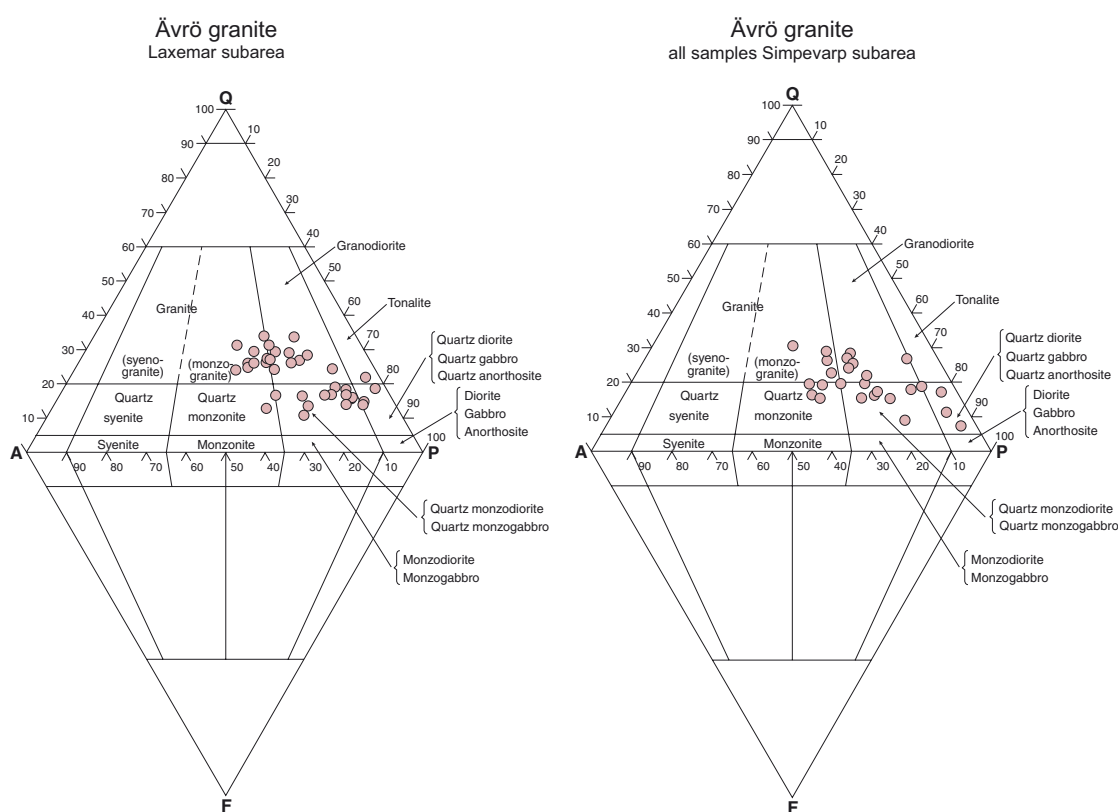


Figure 2-8. QAPF modal classification of Ävrö granite from the Laxemar subarea (left) and Simpevarp subarea (right) according to /Streckeisen 1976/.

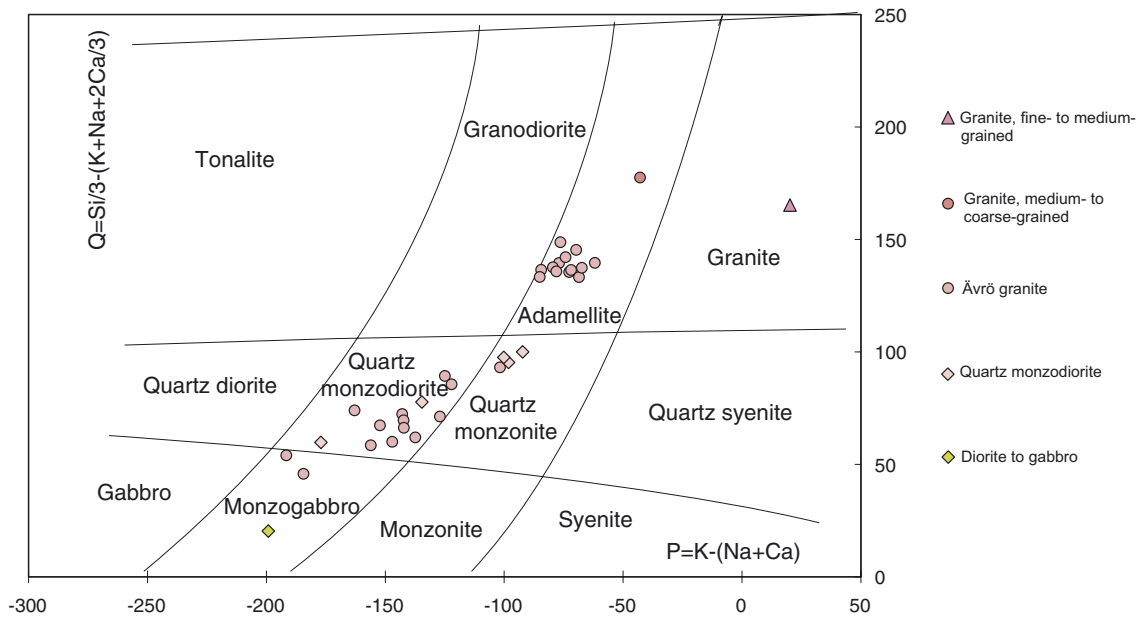


Figure 2-9. Geochemical classification of rocks from the Laxemar subarea according to /Debon and LeFort 1983/. Samples from KLX03 are also included.

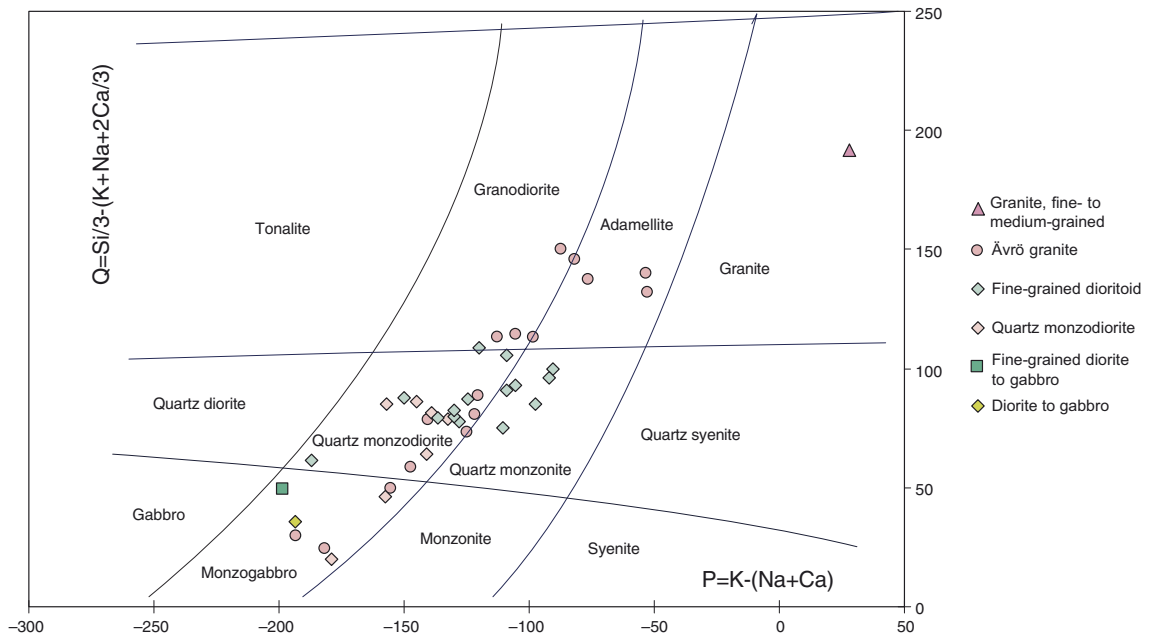


Figure 2-10. Geochemical classification of rocks in the Simpevarp subarea according to /Debon and Le Fort 1983/. Analyses data from boreholes KSH01A, KSH01B and KSH02 are also included.

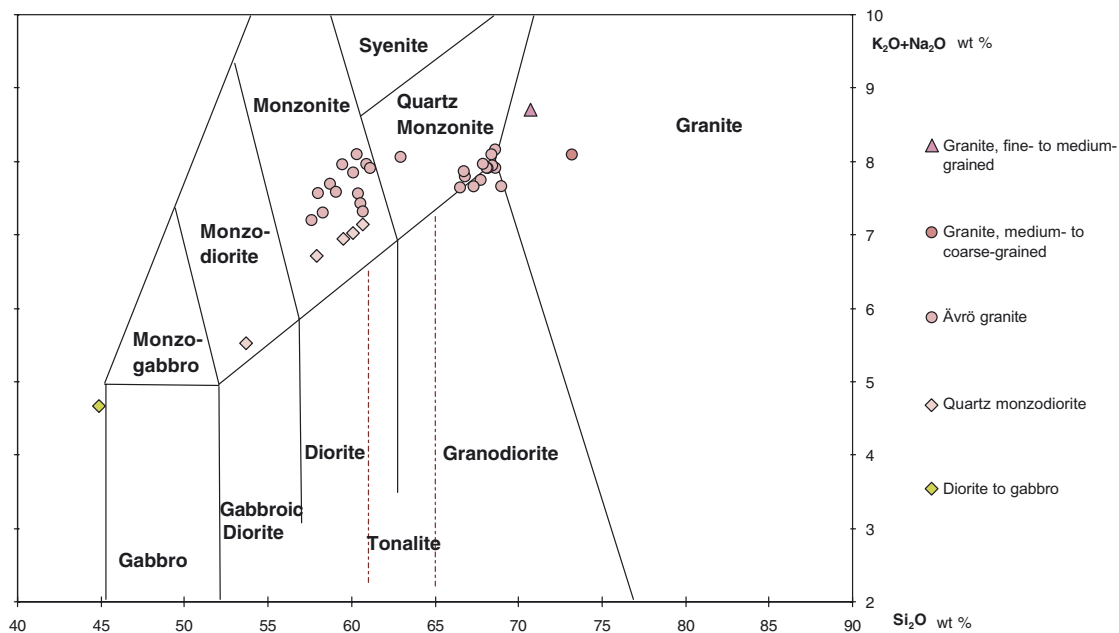


Figure 2-11. Geochemical classification of rocks from the Laxemar subarea according to /Middlemost 1994/. Samples from KLX03 are also included.

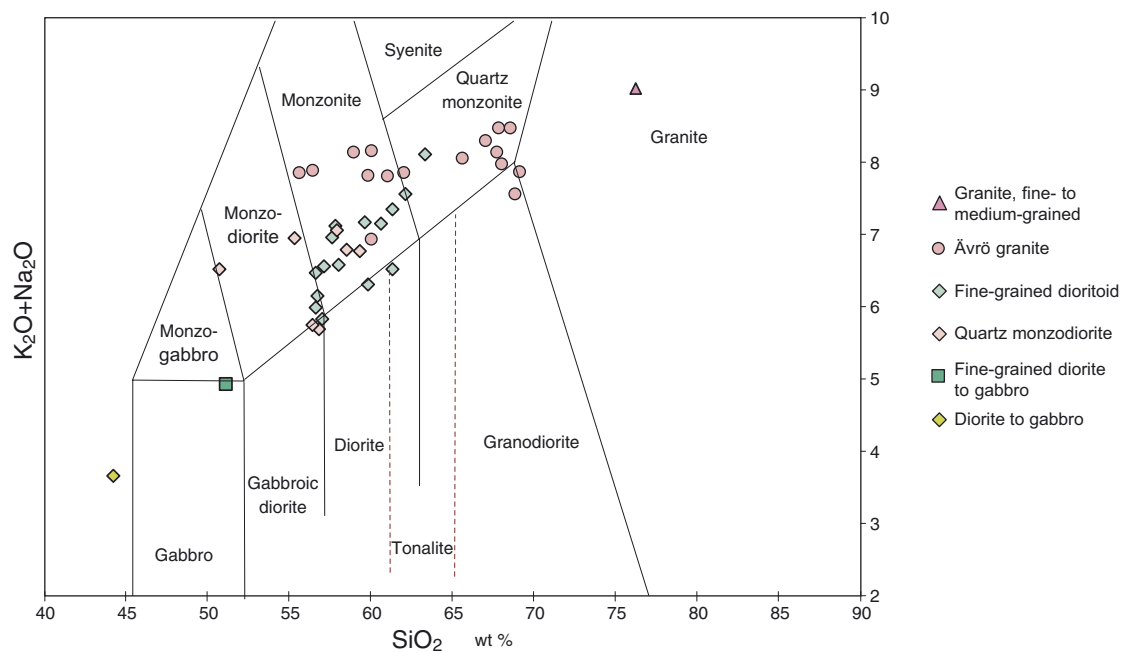


Figure 2-12. Geochemical classification of rocks from the Simpevarp subarea according to /Middlemost 1994/. Analyses data from boreholes KSH01A, KSH01B and KSH02 are also included.

In Figure 2-13 and Figure 2-14, quartz monzodioritic and granodioritic varieties of the Ävrö granite are displayed, respectively. Note the darker colour of the quartz monzodioritic variety (Figure 2-13) in comparison to the granodioritic variety (Figure 2-14) that has higher quartz content and lower content of dark minerals, i.e. biotite and hornblende. The differences in mineralogical composition between the two varieties are shown in Figure 2-15, in which the Ävrö granite in the southern part of the Laxemar subarea represents the quartz monzodioritic variety.



Figure 2-13. Ävrö granite with quartz monzodioritic composition.



Figure 2-14. Ävrö granite with granodioritic composition. Note the intermediate to mafic enclave (dark in colour) in the right part of the picture.

A useful indicator to demonstrate the compositional variation in the Ävrö granite is the quartz content. As can be seen in Figure 2-15 and Figure 2-16, the variation in quartz content is considerable and reflects the compositional variation seen in the QAPF diagram in Figure 2-8.

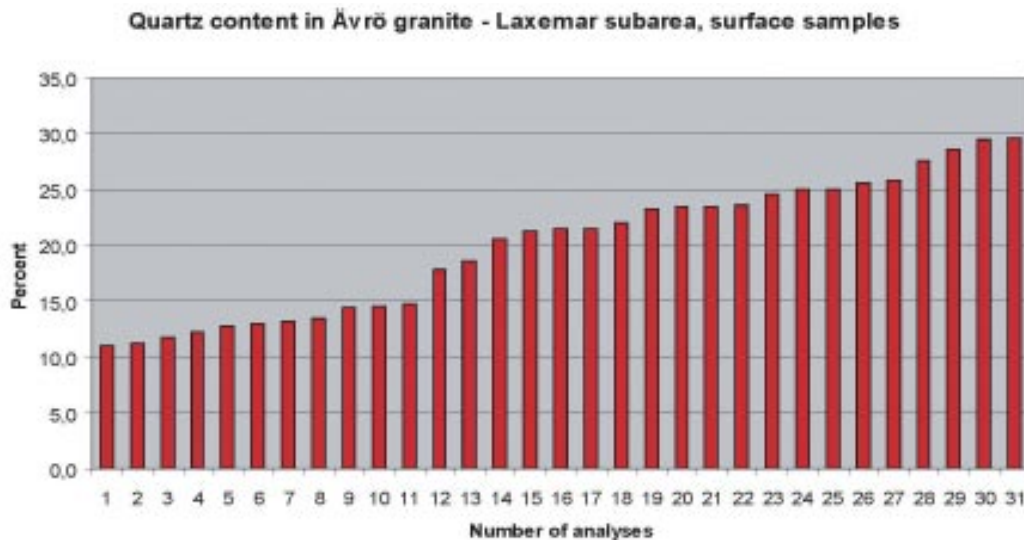


Figure 2-15. Histogram displaying the variation in quartz content (surface samples) in Ävrö granite within the Laxemar subarea.

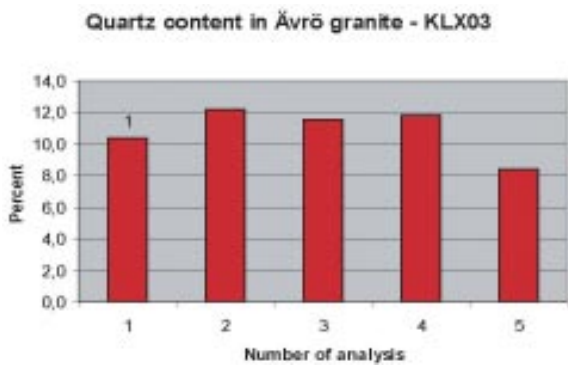


Figure 2-16. Histogram displaying the variation in quartz content in Ävrö granite in the cored borehole KLX03.

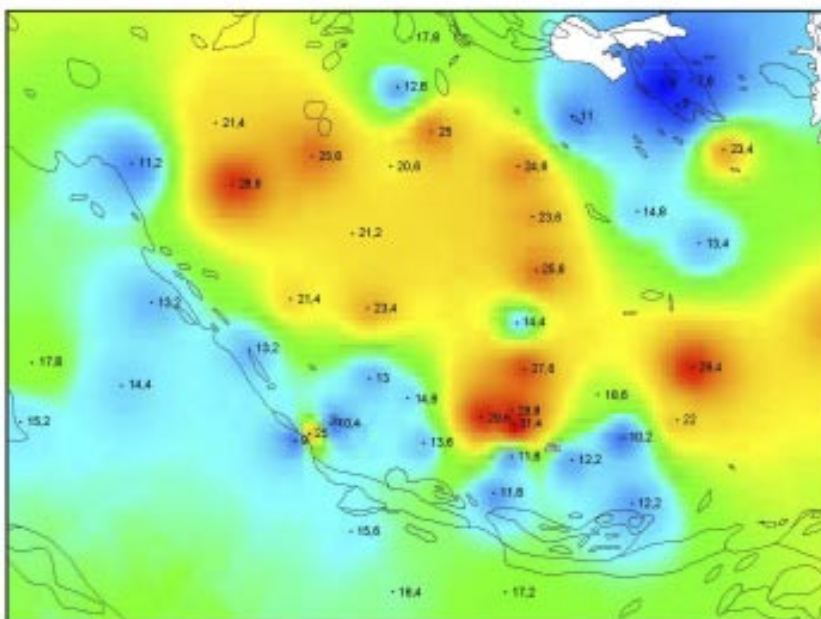


Figure 2-17. Map displaying the quartz content in the Ävrö granite and the quartz monzodiorite and an interpolation between the sample locations. The boundaries between the different rock types are shown as reference (cf. the bedrock map in Appendix 2).

In Figure 2-17, the quartz content from the modal analyses has been marked for the Ävrö granite and the quartz monzodiorite at different sample locations. Although a relatively restricted amount of data, the interpolation between the sample locations indicates a spatial distribution of the different compositional varieties of the Ävrö granite. The modal analyses indicate that the Ävrö granite in the central parts of the Laxemar subarea has a higher quartz content (granitic to granodioritic composition) compared with the peripheral parts which have a lower quartz content (quartz monzodioritic composition) that is similar to the quartz monzodiorite. This mineralogical variation has important implications for the thermal properties in the bedrock.

2.2.5.2 Quartz monzodiorite

The quartz monzodiorite dominates in the southern and southwestern part of the Laxemar subarea and neighbouring surroundings (Appendix 2). It also dominates in two minor areas southeast and west to westnorthwest of Lake Frisksjön in the northeastern part of the Laxemar subarea. It is grey to reddish grey, medium-grained, commonly equigranular (Figure 2-19).

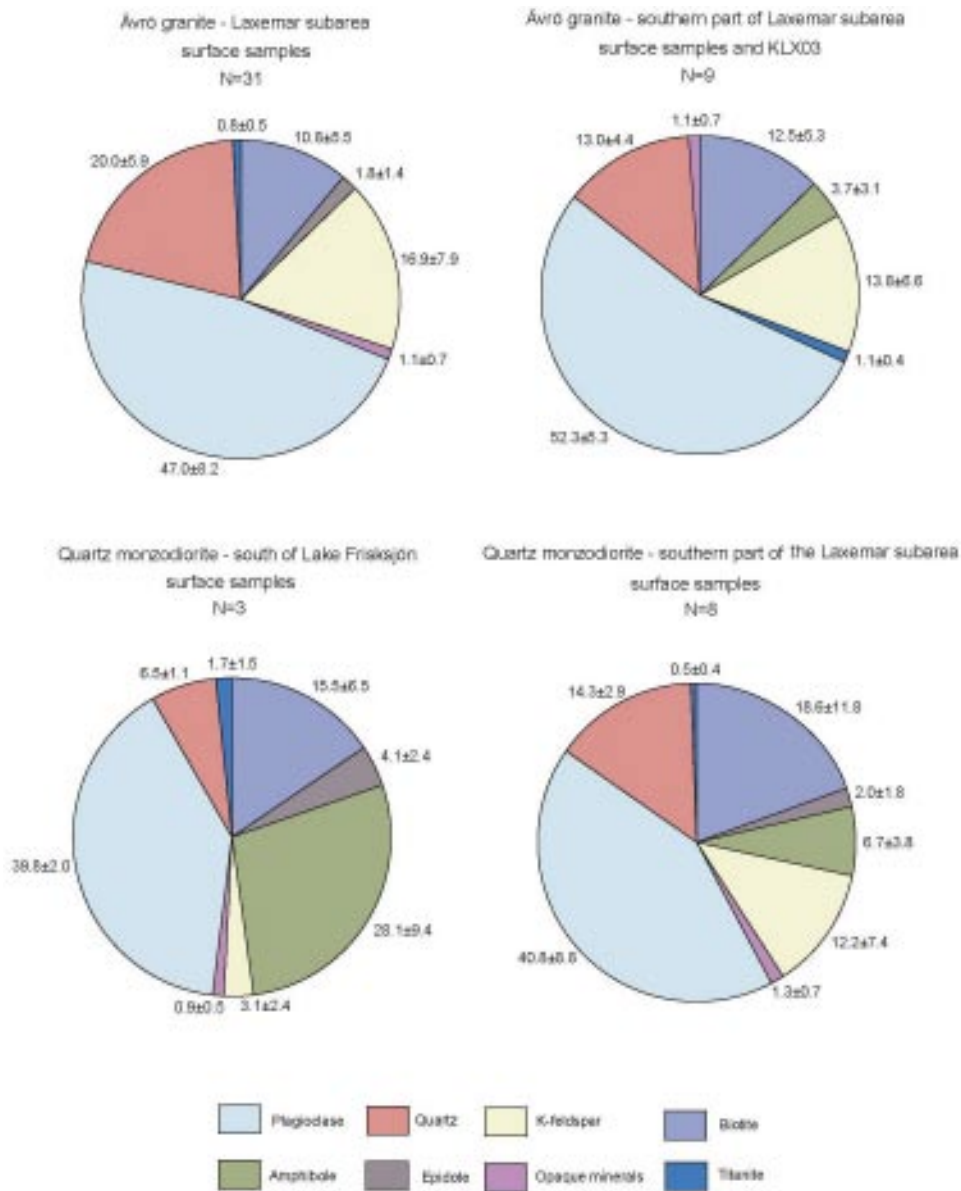


Figure 2-18. Diagrams showing the mineralogical composition (mean value and standard deviation) of the Ävrö granite and quartz monzodiorite in different parts of the Laxemar subarea.

The quartz monzodiorite has a relatively restricted compositional range (Figure 2-9, Figure 2-11, Figure 2-20), which is similar to that of the quartz monzodiorite in the Simpevarp subarea (Figure 2-20). The mineralogical composition of the quartz monzodiorite is displayed in Figure 2-18. It should be pointed out that the 3 points that plot in the lower right-hand part in



Figure 2-19. Characteristic appearance of equigranular quartz monzodiorite.

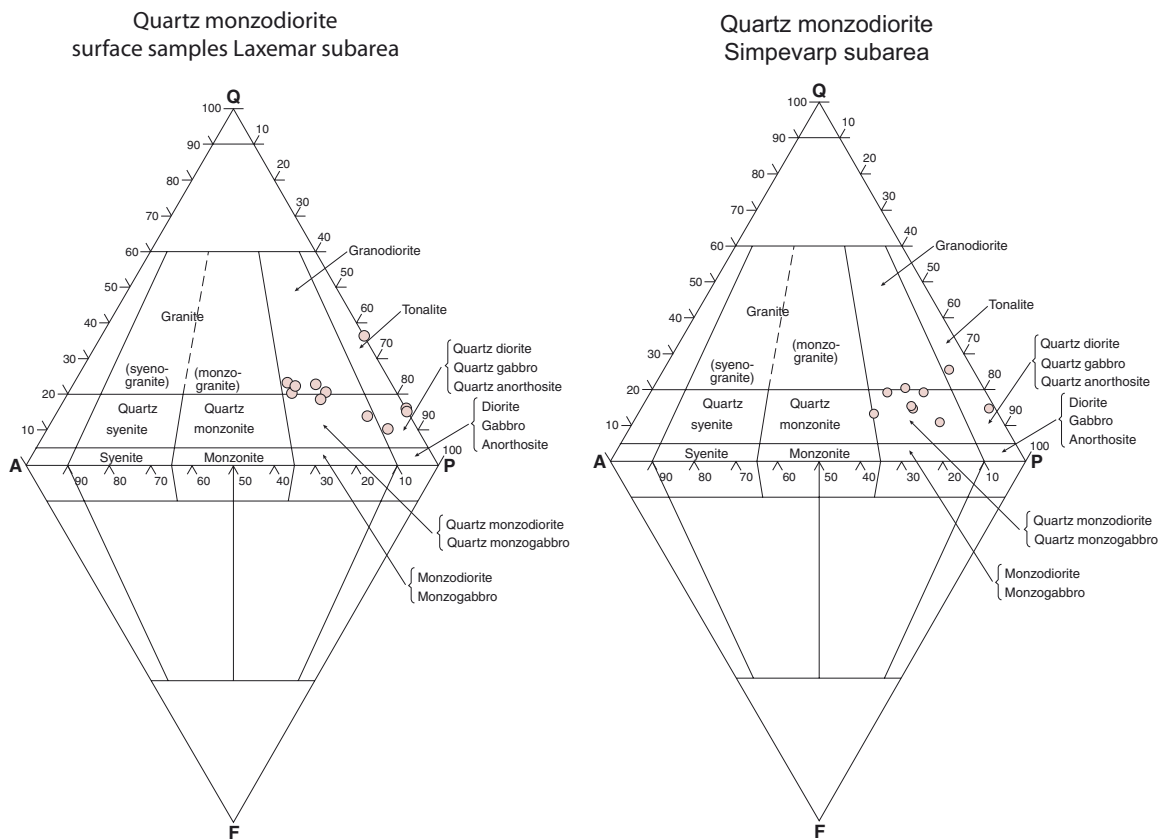


Figure 2-20. QAPF modal classification of quartz monzodiorite from surface samples in the Laxemar subarea (left) and Simpevarp subarea (right) according to /Streckeisen 1976/.

Figure 2-20 (Laxemar subarea) represents analyses from the quartz monzodiorite southeast of Lake Frisksjön. Consequently, this strongly indicates that this body differs in composition from the large body in southern and southwestern Laxemar (Appendix 2), since it has a quartz dioritic composition, i.e. lower content of potassium feldspar. Furthermore, it is indicated that the quartz monzodiorite in southern and southwestern Laxemar has a more homogeneous composition and slightly higher quartz content compared to the quartz monzodiorite in the Simpevarp subarea (Figure 2-20).

Based on the Simpevarp SDM version 0 /SKB 2002/, the quartz monzodiorite is also inferred to constitute isolated bodies elsewhere in the regional model area (Figure 2-7).

As mentioned above, the quartz monzodiorite displays diffuse and gradational contact relationships to the Ävrö granite, which strongly indicate that the two rock types have been emplaced more or less synchronously /cf. Wahlgren et al. 2004/.

2.2.5.3 Fine-grained dioritoid

Fine-grained dioritoid occurs in minor bodies in the southern part of the Laxemar subarea, particularly along the contact zone between the Ävrö granite and the quartz monzodiorite (Appendix 2, Figure 2-7). As can be seen in the bedrock map, the bodies along the contact zone diminish in size westwards. It is inferred that they originally formed parts of a coherent westward continuation of the large body of fine-grained dioritoid that covers the southern part of the Simpevarp peninsula (Appendix 2). Furthermore, the fine-grained dioritoid occurs as minor bodies or inclusions in especially the Ävrö granite and the quartz monzodiorite.

The fine-grained dioritoid is grey and commonly unequigranular with 3 to 5 mm large megacrysts of hornblende and plagioclase. Patches with inhomogeneous coarsening in cm to dm scale is a characteristic feature (Figure 2-21). The coarsening makes the fine-grained dioritoid resemble the quartz monzodiorite, and consequently, these two rock types are occasionally difficult to distinguish from one another. The contacts between the dioritoid and the country rocks are usually gradual, but locally the contact is sharp.

No modal or geochemical analyses exist from the fine-grained dioritoid in the Laxemar subarea. The variation in mineralogical and geochemical composition is judged to be similar to the fine-grained dioritoid in the Simpevarp subarea (cf. Figure 2-5, Figure 2-6 and Figure 2-22).



Figure 2-21. Fine-grained, unequigranular dioritoid displaying incipient inhomogeneous coarsening.

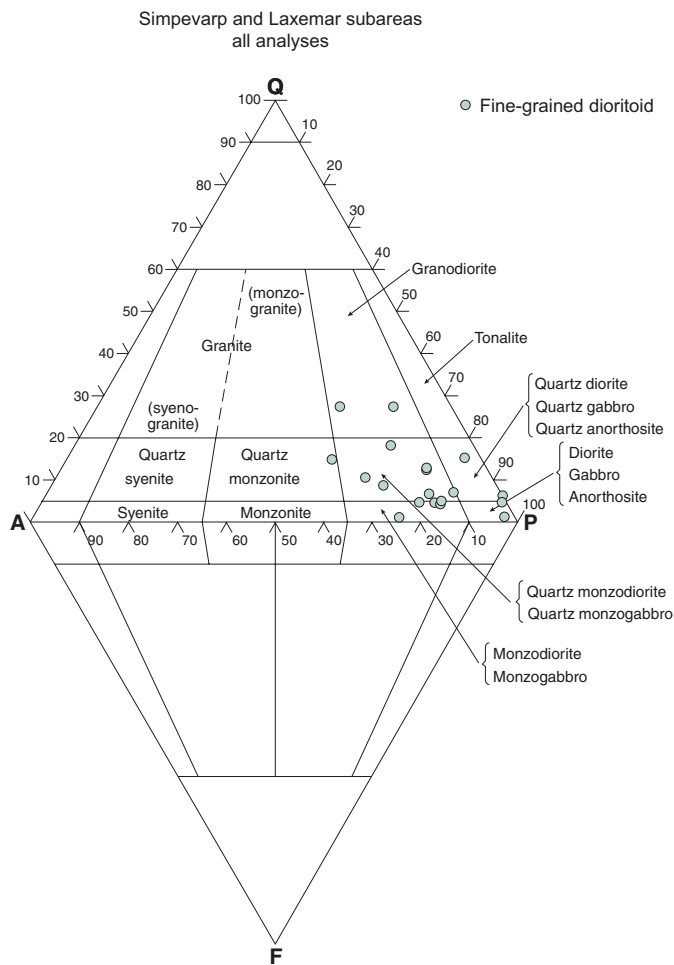


Figure 2-22. *QAPF modal classification of the fine-grained dioritoid from the Simpevarp subarea according to /Streckeisen 1976/.*

The fine-grained dioritoid has traditionally been classified as a volcanic rock of dacitic to andesitic composition /SKB 2002 and references therein/. However, except for being fine-grained, no characteristic criteria indicating that the rock is of volcanic origin were found during the bedrock mapping of the Simpevarp and Laxemar subareas. An alternative interpretation is that the rock constitutes a high-level intrusion that subsequently was intruded by its parent magma, which is presumed to be represented by the quartz monzodiorite in the country rock. The characteristic, inhomogeneous coarsening in the fine-grained dioritoid is inferred to be a late-magmatic phenomenon, presumably due to a thermal input during the emplacement of the quartz monzodiorite and possibly also the Ävrö granite.

2.2.5.4 Medium- to coarse-grained granite

Scattered minor bodies of red to greyish red, medium- to coarse-grained granite occur in the Laxemar subarea and its surroundings (Appendix 2, Figure 2-7 and Figure 2-24). In particular immediately north of the subarea, north of the deformation zone ZSMEW002A (see Section 4.3), small bodies are frequently occurring. Along the boundary zone between the Ävrö granite and the quartz monzodiorite in the southern part of the subarea, granite which is intimately mixed with diorite to gabbro occurs.

Medium- to coarse-grained granite also occurs as more or less large bodies in the northern and northwestern part of the regional model area /Figure 2-7, SKB 2002/. Furthermore, it occurs as both minor bodies and as mixed and mingled, diffusely delimited small occurrences in the Ävrö granite.

The variation in mineralogical and geochemical composition is exemplified in Figure 2-5, Figure 2-6 and Figure 2-23. The deviating sample with a granodioritic composition Figure 2-23) represents the granite which is mixed with diorite to gabbro in southern Laxemar (Appendix 2). Whether this sample is representative for the whole body is uncertain.

2.2.5.5 Diorite to gabbro

Diorit-gabbro occurs as scattered minor bodies in the Laxemar subarea and immediate surroundings (Appendix 2). Furthermore, diorite to gabbro occurs as separate larger bodies in the western part of the regional model area, and as scattered, minor bodies principally along the coast in the Simpevarp-Ävrö-Äspö and neighbouring area (Figure 2-7). As can be seen in the bedrock map in Appendix 2, the diorite to gabbro is not evenly distributed, and the central part of the Laxemar subarea is almost devoid of diorite to gabbro, except for minor inclusions and enclaves in the Ävrö granite (Figure 2-25, Figure 2-27 and Figure 2-28). The most conspicuous occurrence of diorite to gabbro is the concentration along the contact zone between the Ävrö granite and the quartz monzodiorite in the southern part of the Laxemar subarea (Appendix 2 and Figure 2-28). Furthermore, diorite to gabbro also frequently occurs as more or less minor bodies in the northern part and north of the Laxemar subarea.

The variation in mineralogical and geochemical composition can be seen in Figure 2-5, Figure 2-6 and Figure 2-26. It is evident from Figure 2-26, that quartz dioritic and/or quartz gabbroic varieties are included in the diorite to gabbro concept.

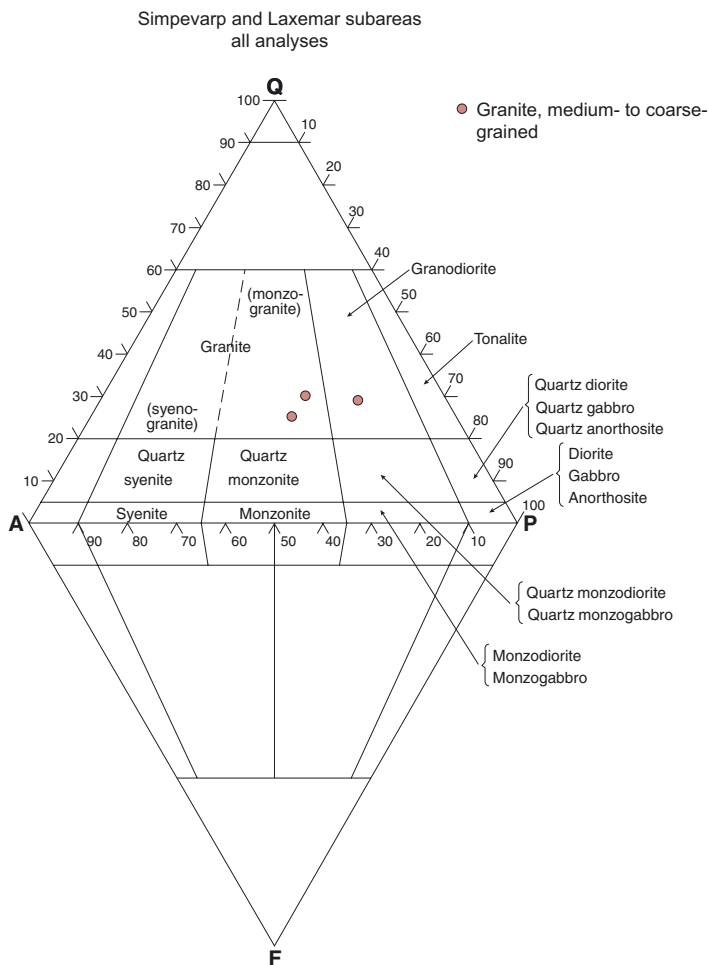


Figure 2-23. QAPF modal classification of medium- to coarse-grained granite from the Simpevarp and Laxemar subareas according to /Streckeisen 1976/.



Figure 2-24. Medium- to coarse-grained granite.



Figure 2-25. Inclusions of diorite to gabbro in Ävrö granite in the outcrop ASM000208 where detailed fracture mapping has been carried out (cf. Section 2.2.10.4). Northeastern part of the Laxemar subarea.

Modal analysis has been carried out of one sample of diorite to gabbro from the contact zone between the Ävrö granite and quartz monzodiorite in southern part of Laxemar. It has the following composition: 48.4% plagioclase, 20.6% biotite, 8.2% hornblende (secondary after pyroxene), 11.2% clinopyroxene (slightly altered to hornblende), 9.2% opaque minerals (hematite and magnetite), 1.8% quartz and 0.6% apatite.

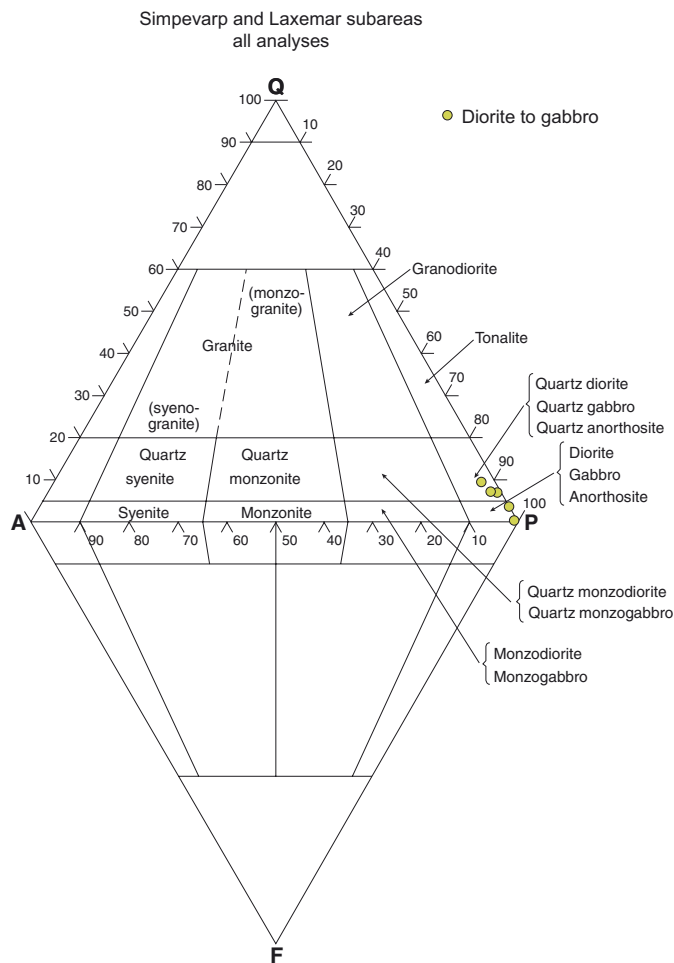


Figure 2-26. QAPF modal classification of diorite to gabbro from the Simpevarp and Laxemar subareas according to Streckeisen /1976/.

The majority of the diorite to gabbro bodies is spatially related to the Ävrö granite (Appendix 2). Furthermore, the distribution of the diorite to gabbro indicates a spatial and presumably also genetic relationship principally to the quartz monzodioritic varieties of the Ävrö granite.

The diorite to gabbro often displays mixing and mingling relationships with the country rock. Larger bodies are often medium-grained in its central part whereas they tend to be finer-grained towards their edges. However, a complex mixing of fine- and medium-grained varieties also occur.

2.2.5.6 Fine- to medium-grained granite

Fine- to medium-grained granite is the most common and characteristic subordinate rock type in the Laxemar subarea (Appendix 2, Figure 2-27, Figure 2-28 and Figure 2-30). It occurs as dykes of various thickness (generally 0.1–1 m), but also as veins and minor, irregular bodies in the other rock types. Furthermore, fine- to medium-grained granite constitutes some larger bodies outside the Laxemar subarea in the eastern part of the regional model area (Figure 2-7). U-Pb zircon dating indicates that the fine- to medium-grained granite is coeval with the country rocks and belongs to the same magmatic generation (Table 2-2).

The variation in mineralogical and geochemical composition can be seen in Figure 2-5, Figure 2-6 and Figure 2-29.

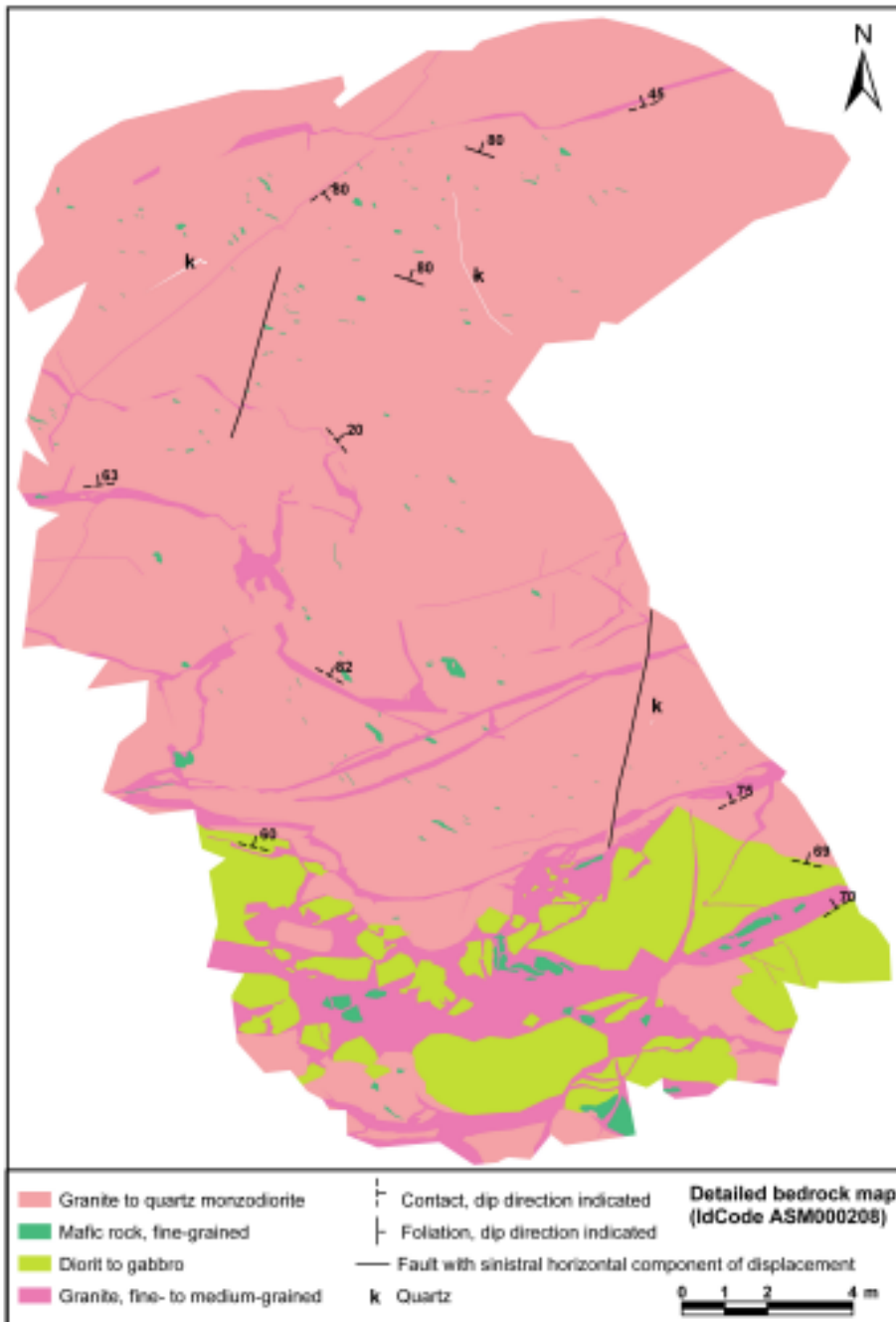


Figure 2-27. Detailed bedrock map of the outcrop ASM000208 where detailed fracture mapping has been carried out (cf. Section 2.2.10.4). Note the spatial relation between the diorite to gabbro and fine- to medium-grained granite.

In situ gamma-ray spectrometric measurements have shown that the fine- to medium-grained granite has a higher content of thorium than the other rock types in the area /Mattsson et al. 2004a/, and this confirms the findings from the Simpevarp subarea /SKB 2005a, Mattsson et al. 2003/. Fine- to medium-grained granite has also been documented to be a characteristic subordinate rock type in the regional model area /Wahlgren et al. 2003/.

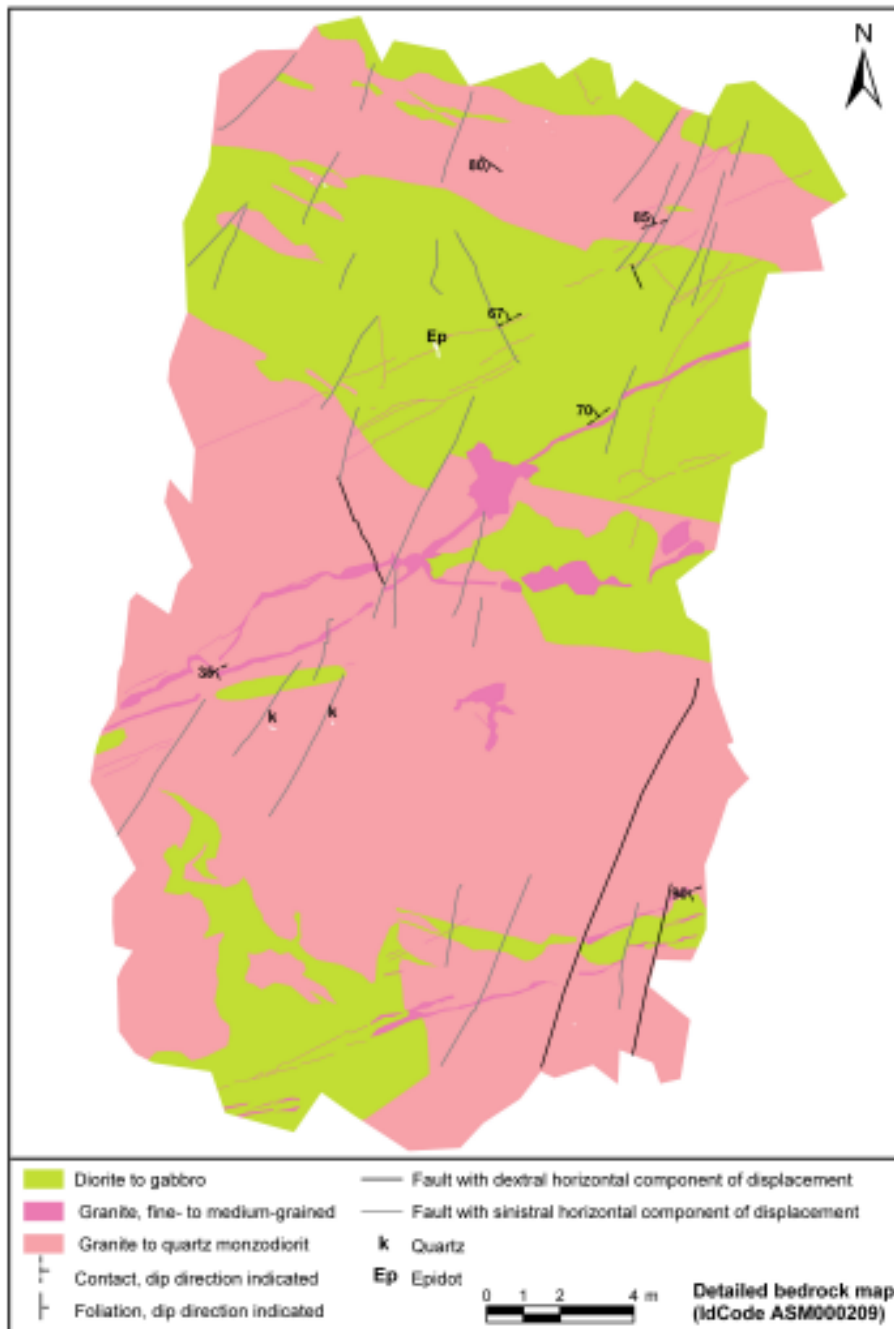


Figure 2-28. Detailed bedrock map of the outcrop ASM000209 where detailed fracture mapping has been carried out in the southern part of the Laxemar subarea (cf. Section 2.2.10.4). The map exemplifies the high amount of diorite to gabbro along the contact between the Ävrö granite and the quartz monzodiorite. Drill site for the cored borehole KLX05.

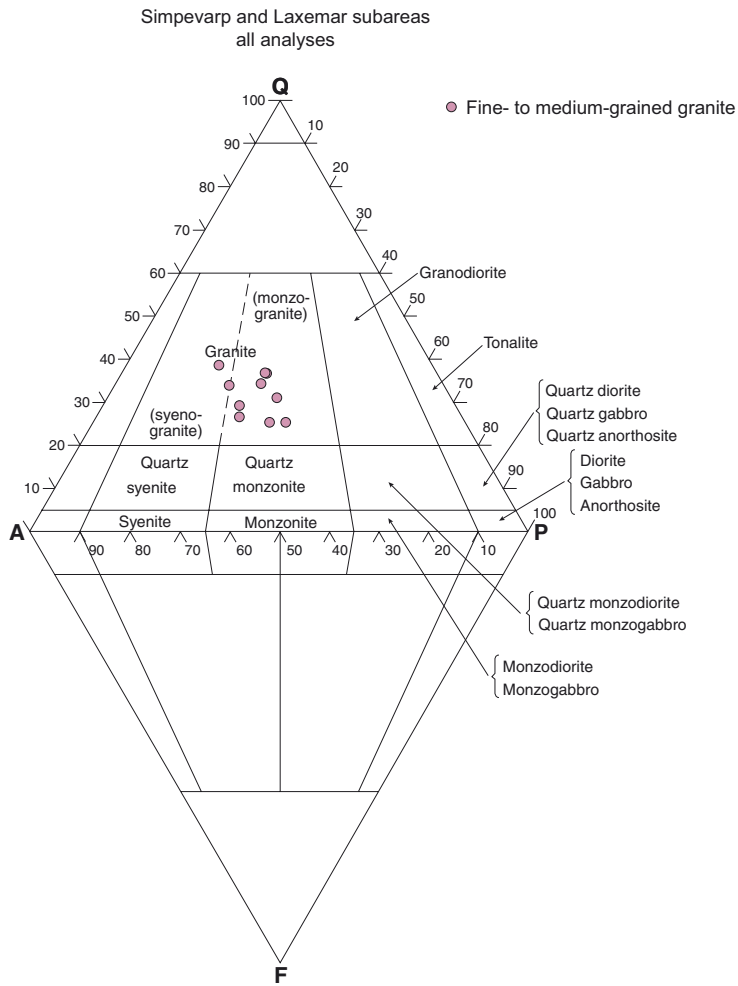


Figure 2-29. *QAPF modal classification of fine- to medium-grained granite from the Simpevarp and Laxemar subareas according to /Streckeisen 1976/.*



Figure 2-30. *Dyke of fine- to medium-grained granite (light red) in quartz monzodiorite.*

2.2.5.7 Pegmatite

Pegmatite is also a frequently occurring subordinate rock type (Figure 2-31), though in much less amount than the fine- to medium-grained granite. The pegmatite dykes are generally less than 0.3 m thick.

2.2.5.8 Orientation of fine-to medium-grained granite and pegmatite dykes

During the bedrock mapping of the Laxemar subarea and its immediate surroundings, the orientation of a number of dykes of fine- to medium-grained granite and pegmatite was documented /Persson Nilsson et al. 2004/. The orientation is displayed in Figure 2-32. Both sets of dykes display a dominant ENE-WSW to NE-SW strike, but the dip varies from vertical to horizontal, though there is a slight dominance for a southeasterly dip.



Figure 2-31. Pegmatite cross-cutting quartz monzodiorite.

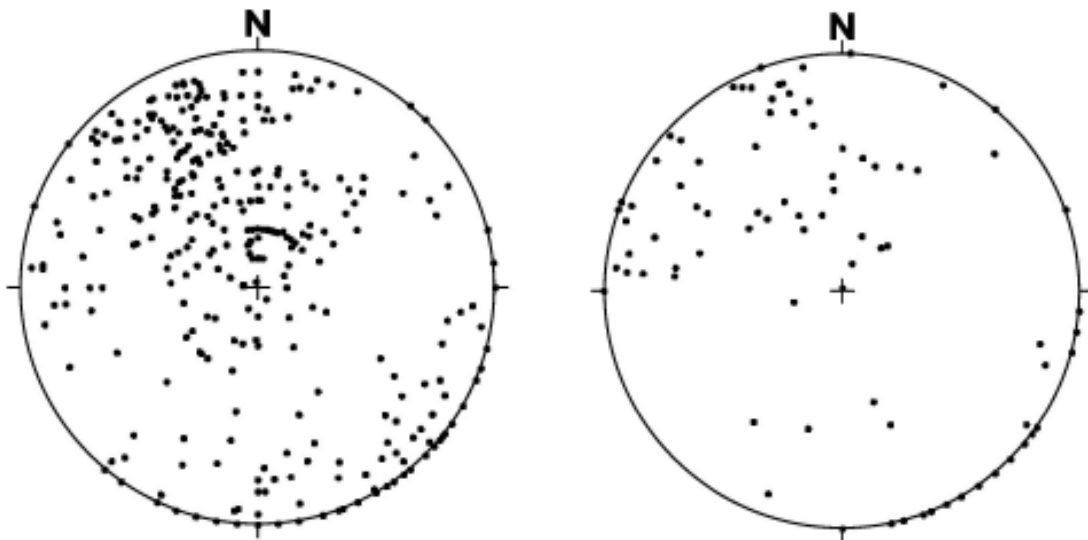


Figure 2-32. Orientation of dykes of fine- to medium-grained granite (left) and pegmatite (right) in the Laxemar subarea. Lower hemisphere of Schmidt equal area, stereographic plots.

A detailed study of fine- to medium-grained granitic dykes have been performed at the Äspö Hard Rock Laboratory /Jonsson 2004/. The measured dykes cluster in three different directions: ENE-WSW, NE-SW and WNW-ESE. The ENE-WSW oriented dykes are situated most distantly from the Äspö shear zone and coincide with the orientation of the main foliation, while the NE-SW oriented dykes mostly occur within the rock volume that is affected by the Äspö shear zone. Both these sets of dykes indicate that the structures in the bedrock control the dyke orientation.

The dyke orientations obtained from the bedrock mapping of the Laxemar subarea are consistent with results from the Äspö Hard Rock Laboratory. Hence, a dominating ENE-WSW to NE-SW trend for the granitic dykes is indicated in the local model area.

2.2.5.9 Fine-grained diorite to gabbro

Fine-grained diorite to gabbro commonly occurs as minor composite intrusions, dykes or bodies, in association with fine- to medium-grained granite (Figure 2-33). The fine-grained diorite to gabbro is generally porphyritic with 2–5 mm large megacrysts of hornblende and plagioclase. The variation in mineralogical and geochemical composition can be seen in Figure 2-5, Figure 2-6 and Figure 2-34. It is evident from Figure 2-34, that quartz dioritic to quartz gabbroic compositions dominate.

2.2.5.10 Göttemar type granite

This conspicuous rock type in the regional model area constitutes two large bodies of approximately 1,450 Ma old granite, the so-called Göttemar granite in the northern part and the so-called Uthammar granite in the southern part (Figure 2-7, Table 2-2). The granites are red to greyish red and commonly coarse-grained, but fine- to medium-grained varieties occur in the Göttemar granite (Figure 2-7).



Figure 2-33. Composite intrusion – fine-grained diorite to gabbro and fine- to medium-grained granite.

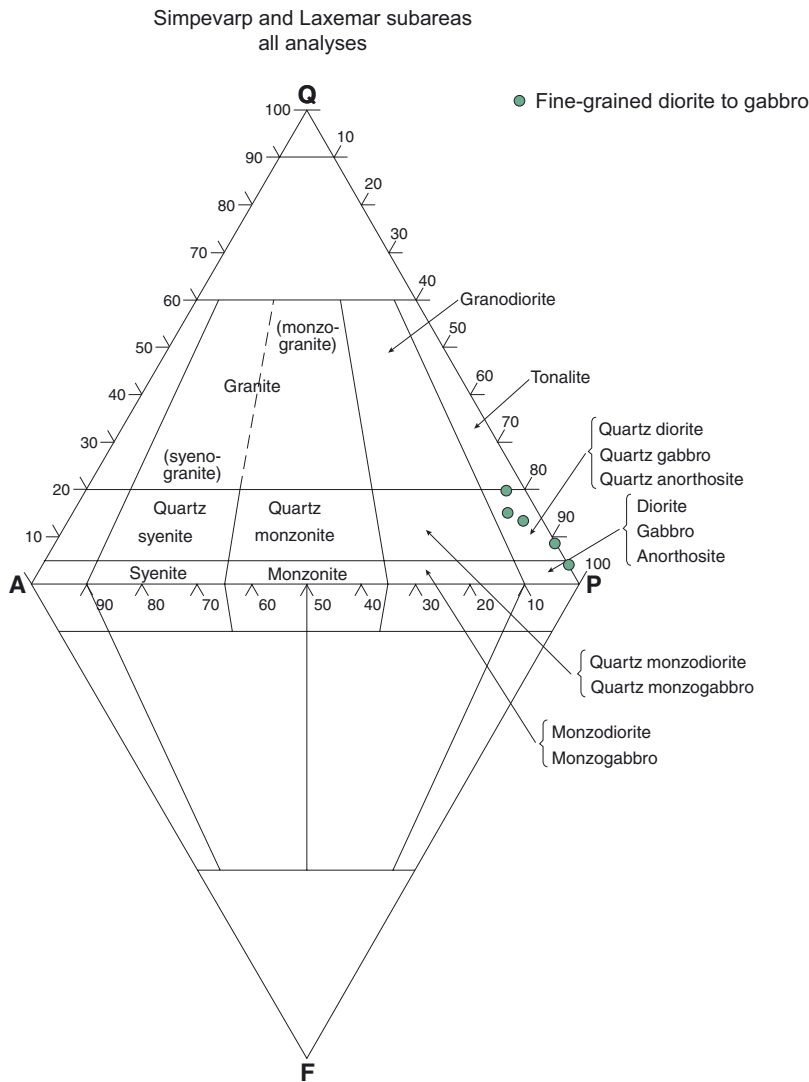


Figure 2-34. QAPF modal classification of fine-grained diorite to gabbro from the Simpevarp and Laxemar subareas according to /Streckeisen 1976/.

2.2.6 Age relations

The mixing and mingling relationships and diffuse contacts between the dominant rock types observed in the Laxemar and Simpevarp subareas strongly support the interpretation that they were formed more or less synchronously. However, based on field relationships, the following chronostratigraphy is indicated for the dominant and subordinate rock types:

Rock type	Relative age
Fine- to medium-grained granite and pegmatite	Youngest
Fine-grained diorite to gabbro	↑
Medium- to coarse-grained granite	
Ävrö granite	
Quartz monzodiorite	
Diorite to gabbro	
Fine-grained dioritoid	Oldest

In conjunction with the bedrock mapping of the Simpevarp subarea, the Ävrö granite and the quartz monzodiorite were sampled for U-Pb zircon and titanite dating. The Ävrö granite was sampled at the stripped outcrop at the site for the cored borehole KAV01. The quartz monzodiorite was sampled in a road cut north of the OIII nuclear reactor, in the eastern part of the Simpevarp peninsula.

Zircon and titanite was analyzed in both samples. The Ävrö granite yielded an upper intercept zircon and titanite age of $1,800 \pm 4$ Ma, and the quartz monzodiorite yielded an upper intercept zircon age of $1,802 \pm 4$ Ma and a slightly younger titanite upper intercept age of $1,793 \pm 4$ Ma. The obtained ages are in good agreement with earlier reported ages for intrusive rocks in the region (Table 2-2).

2.2.7 Petrophysical properties of rock types

A compilation of the petrophysical properties, including in situ gamma ray spectrometry, of the different rock types in the Laxemar subarea is presented in /Mattsson et al. 2004a/. The petrophysical properties are also included in the property table associated with each of the rock domains (see Section 3.5 and Appendix 3). A summary of the petrophysical properties follows below.

2.2.7.1 Magnetic susceptibility and density

Data obtained from surface samples of the rock types display overlapping magnetic susceptibilities, and partly overlapping density values, particularly for the medium- to coarse-grained granite and the granitic varieties of the Ävrö granite (Figure 2-35). Except for a slight overlap, it is obvious from Figure 2-35 that the quartz monzodiorite has a higher density than the Ävrö granite, although the Ävrö granite comprises quartz monzodioritic varieties. This is presumably caused by the higher content of biotite and hornblende in the quartz monzodiorite compared to the quartz monzodioritic varieties of the Ävrö granite (see Figure 2-18).

2.2.7.2 Porosity, electrical resistivity and induced polarization

Porosities of the investigated rocks in the Laxemar and Simpevarp subareas are low, in general below 1%, which is normal for unaltered crystalline Swedish bedrock. The distribution of measured porosities can be seen in the histograms in Figure 2-36. Although the porosity values overlap and the number of analyses is few, it is indicated that the fine-grained dioritoid and the diorite to gabbro have lower porosities than e.g. the Ävrö granite.

Table 2-2. Radiometric ages for intrusive rocks in the Simpevarp regional model area and surroundings.

Rock type	Northing (m)	Easting (m)	Depth (m.a.s.l.)	U-Pb zircon age	Reference
Fine-grained granite	6367111.8	1551572.7	-124.8	$1,794 + 16/-12$ Ma	/Kornfält et al. 1997, Wikman and Kornfält 1995/
Fine-grained granite	6367985.2	1551588.6	-395.7	$1,808 + 33/-30$ Ma	/Kornfält et al. 1997, Wikman and Kornfält 1995/
Äspö diorite	6367669.2	1551455.3	-318.4	$1,804 \pm 3$ Ma	/Kornfält et al. 1997, Wikman and Kornfält 1995/
Uthammar granite	636207	154827		$1,441 + 5/-3$ Ma	/Åhäll 2001/
Jungfru granite	63473	15590		$1,441 \pm 2$ Ma	/Åhäll 2001/
Götemar granite	637280	154980		$1,452 + 11/-9$ Ma	/Åhäll 2001/
Gersebo granite	637310	155148		$1,803 \pm 7$ Ma	/Åhäll 2001/
Virbo granite	6353848	1543959		c. 1,790 Ma	/Bergman et al. 2000/
Quartz monzodiorite	6366200	1552295		$1,802 \pm 4$ Ma	/Wahlgren et al. 2004/
Quartz monzodiorite	6366200	1552295		$1,793 \pm 4$ Ma (titanite)	/Wahlgren et al. 2004/
Ävrö granite	6367281	1553063		$1,800 \pm 4$ Ma (zircon+titanite)	/Wahlgren et al. 2004/

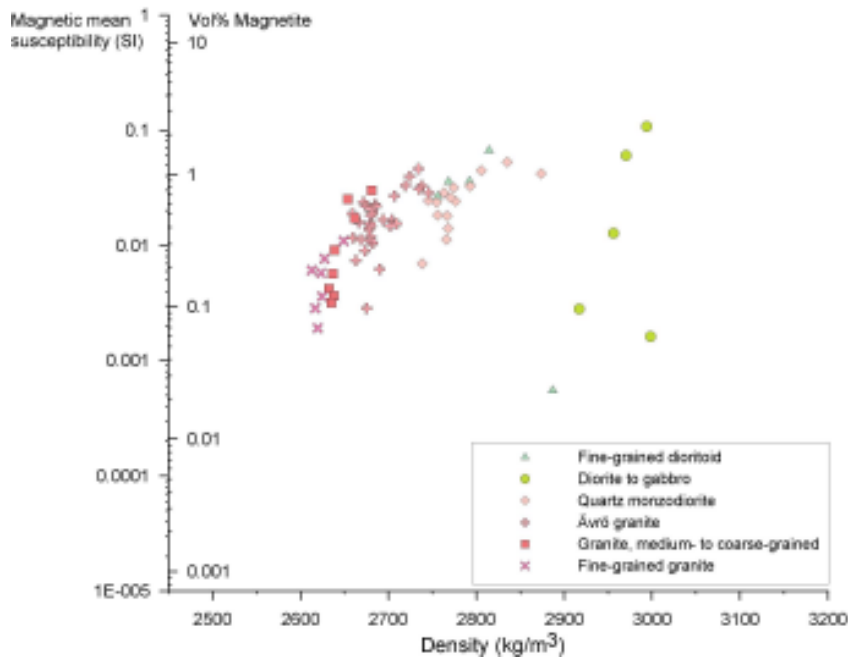


Figure 2-35. Diagram showing the density and magnetic susceptibility of rock types (surface samples) from the Simpevarp and Laxemar subareas. Figure from /Mattsson et al. 2004/.

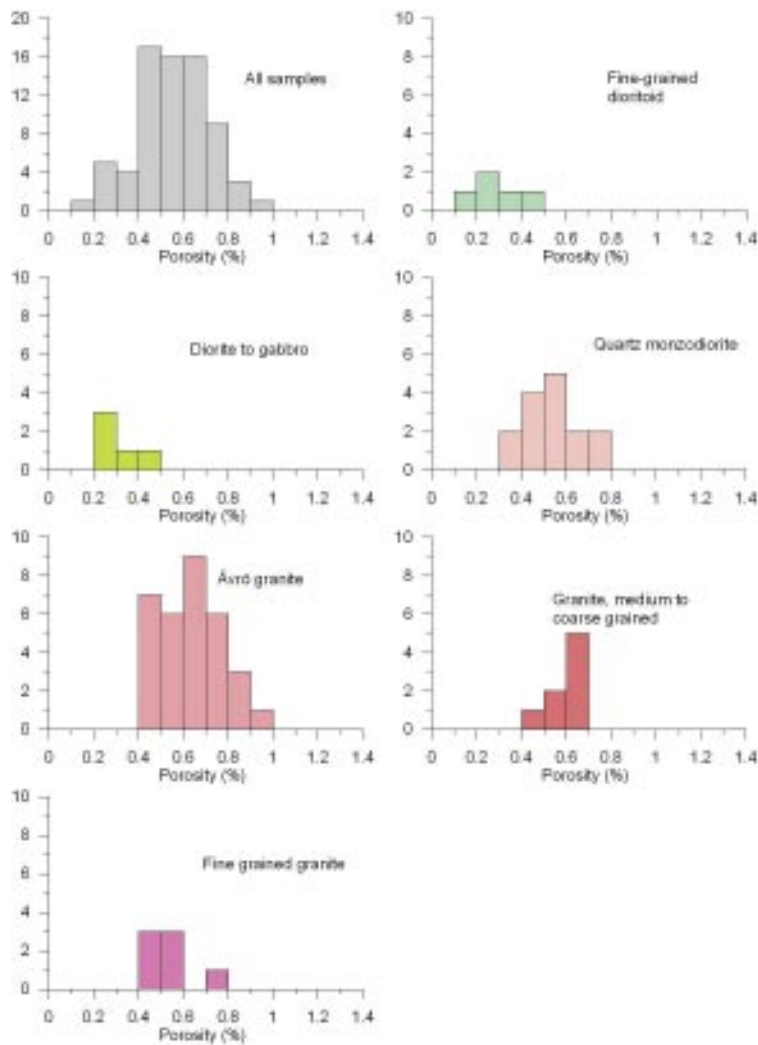


Figure 2-36. Histograms showing distribution of measured porosities for the rock types. Figure from /Mattsson et al. 2004/.

The resistivity values and IP-effect (phase angle) for the different rock types are displayed in Figure 2-37. The different rock types display overlapping values, but it is indicated that slightly higher resistivity is recorded for the fine-grained dioritoid and diorite to gabbro.

From Figure 2-38 and Figure 2-39, it is indicated that the Ävrö granite in central and northern Laxemar display higher porosity and lower resistivity values than the surrounding rock types /Mattsson et al. 2004a/.

2.2.7.3 In situ gamma-ray spectrometry

Apart from a special study of fine- to medium-grained granite at the Äspö and Ävrö islands and the Simpevarp peninsula /Mattsson et al. 2002/, 171 localities have been investigated with gamma-ray spectrometry in the Laxemar subarea and immediate surroundings (Figure 2-40), including some localities in the regional model area, during the ongoing site investigation /Mattsson et al. 2004a/.

The results from the in situ gamma-ray spectrometry measurements can be seen in Table 2-3.

The results of the in situ gamma ray spectrometry measurements show that the fine- to medium-grained granite has the highest content of potassium and thorium, which also has been observed in earlier studies /Mattsson et al. 2002/. Similar to the mineralogical and chemical variation in the Ävrö granite, the latter also display variations in the gamma ray spectrometric data. The thorium content is generally higher in the granitic varieties of the Ävrö granite compared to the quartz monzodioritic varieties.

All rock types in the Laxemar and Simpevarp subareas display low contents of uranium, except for pegmatite in which the uranium content locally exceeds 16 ppm (see Table 2-3). The latter is a critical value that corresponds to radium index=1, which must not be exceeded in rocks that will be used for the construction of buildings in which people are continuously present /BFS 1990/. Consequently, it is not a site discriminating factor.

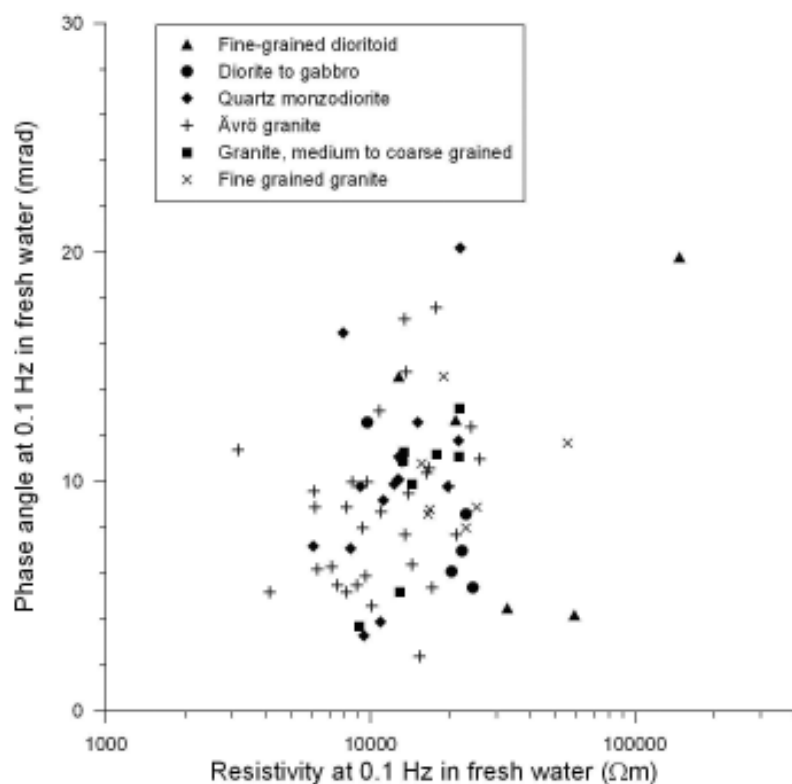


Figure 2-37. Resistivity and IP-effect (phase angle) for samples soaked in tap water. Figure from /Mattsson et al. 2004/.

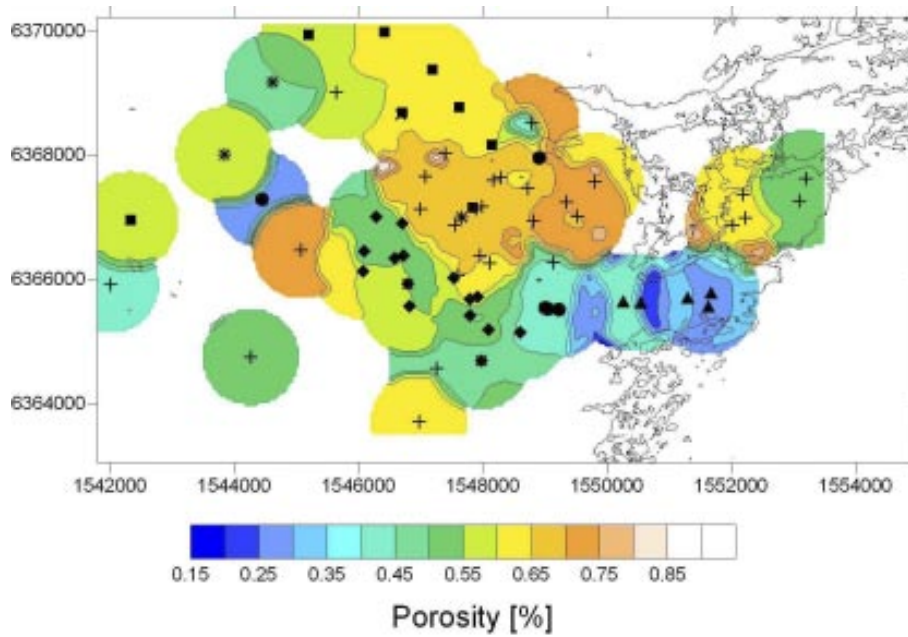


Figure 2-38. Map showing the measured porosity of rock samples. The symbols indicate the sampling locations and the symbol is in accordance with the legend in Figure 2-37. Note that more than one rock type has been sampled at some sites. The contour lines have been interpolated by taking the median value within a search radius of 800 metres. Figure from /Mattsson et al. 2004/.

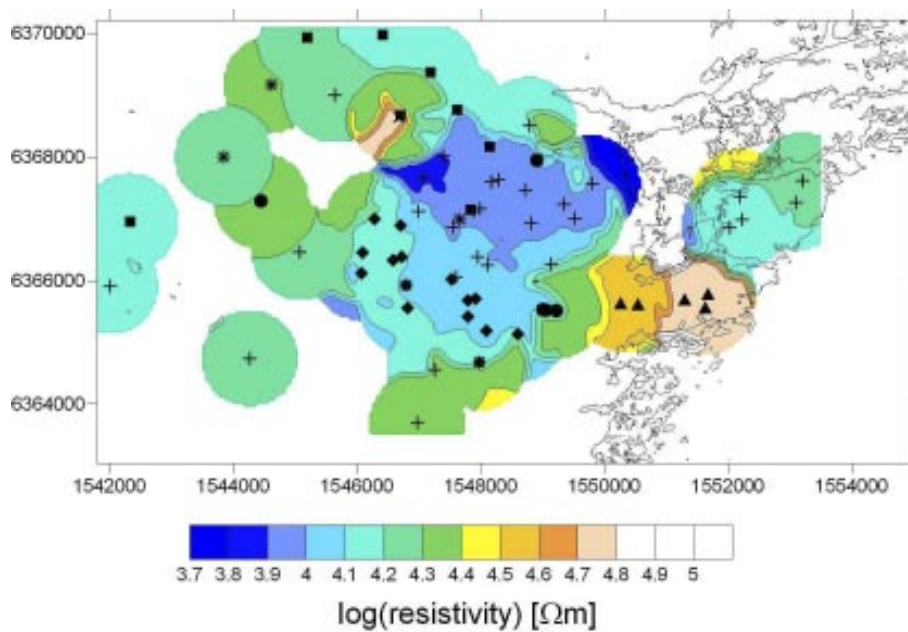


Figure 2-39. Map showing the resistivity of rock samples measured in fresh water. The symbols indicate the sampling locations and the symbol is in accordance with the legend in Figure 2-37. Note that more than one rock type has been sampled at some sites. The contour lines have been interpolated by taking the median value within a search radius of 800 metres. Figure from /Mattsson et al. 2004/.

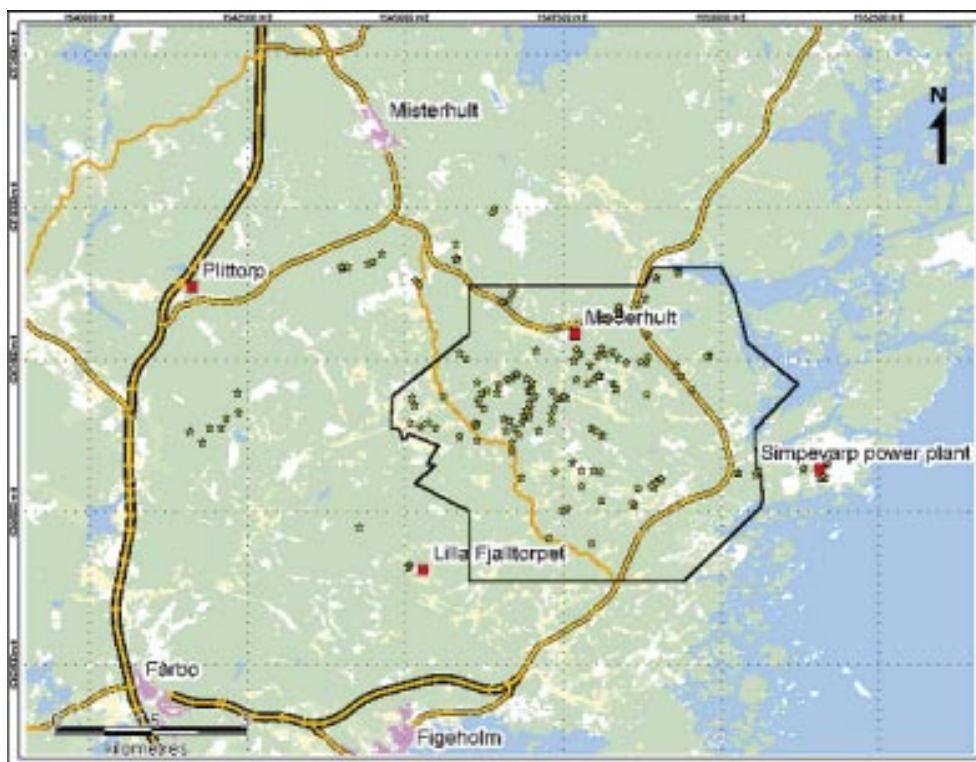


Figure 2-40. Distribution of the 171 localities studied with gamma-ray spectrometry during the ongoing site investigation. Localities from the special study of fine-to medium-grained granite at the Äspö and Ävrö islands and the Simpevarp peninsula /Mattsson et al. 2002/ are not included. The black frame marks the area covered by detailed bedrock mapping during 2004 /Persson Nilsson et al. 2004/.

Table 2-3. Gamma-ray spectrometry data (average and standard deviation) of rock types in the Laxemar subarea and surroundings. L=number of localities measured for each rock type. The shaded rows contain data from a previous investigation of fine-to medium-grained granite /Mattsson et al. 2002/. Slightly modified from /Mattsson et al. 2004a/.

Rock type and code	L	Potassium [%]	eUranium [ppm]	eThorium [ppm]
Fine-grained dioritoid (501030)	14	3.1±0.3	3.7±1.6	12.5±5.8
Diorite to gabbro (501033)	18	1.4±0.5	1.4±0.8	4.0±2.7
Quartz monzodiorite (501036)	38	3.0±0.3	3.2±0.8	9.9±1.8
Quartz monzodiorite to granodiorite (Äspö Island)	5	3.3±0.4	4.8±2.7	11.2±2.4
Ävrö granite (501044)	79	3.3±0.4	3.8±1.5	11.9±4.3
Ävrö granite (Ävrö Island)	7	3.6±0.2	4.9±0.8	16.6±6.6
Granite, medium- to coarse-grained (501058)	13	4.0±0.5	4.3±1.4	15.4±5.0
Pegmatite (501061)	1	2.7	6.8	11.4
Pegmatite	3	5.2±0.4	9.8±7.4	23.2±8.7
Fine-grained diorite to gabbro (505102)	1	1.5	0.7	3
Fine-to medium-grained granite (511058)	7	4.5±0.5	7.7±2.5	30.2±10.5
Granite, fine- to medium-grained (red dyke)	11	5.6±0.4	6.1±2.3	48.9±20.9

2.2.8 Bedrock heterogeneity

Bedrock heterogeneity can be assessed at different scales. The most common factors to consider are:

- Occurrences of subordinate rock types, e.g. dykes, veins, patches, enclaves, inclusions or minor bodies, in a dominating rock type.
- A general mixture of various rock types with different composition and character.
- More or less large compositional variations within a dominating rock type.
- A combination of the above mentioned factors.

The subordinate rock types in the Laxemar subarea, as well as in the Simpevarp subarea, have been registered in the outcrop database /Wahlgren et al. 2004, Persson Nilsson et al. 2004/ at every observation point during the bedrock mapping. The bedrock map in Appendix 2 and the detailed bedrock maps of the cleared outcrops in Figure 2-27 and Figure 2-28 reveal provisionally and approximately the contents of subordinate rock types. In particular, fine- to medium-grained granite, but also pegmatite and locally diorite to gabbro, are characteristic and constitute the most important factor contributing to heterogeneity.

As can be seen in the bedrock map in Appendix 2, the area along the contact between the Ävrö granite and the quartz monzodiorite in southern and southwestern Laxemar contains a large amount of diorite to gabbro. The latter occurs as minor enclaves up to more or less large bodies. In addition, fine- to medium-grained granite, pegmatite and fine-grained dioritoid occur. Consequently, this area is most heterogeneous when considering the implications of a mixture of different rock types.

Regarding compositional variations within a dominant rock type, this is represented by the data on the Ävrö granite (cf. Figure 2-8, Figure 2-9, Figure 2-11, Figure 2-15 and Figure 2-17).

The degree of bedrock inhomogeneity is also evident from the variation of rock types in the cored boreholes (see Section 2.4.1).

2.2.9 Lineament identification

2.2.9.1 Primary data and types of inferred lineaments

Lineaments in the regional model area have been identified on the basis of a joint integrated interpretation of different sets of lineaments, each of which has been identified separately from the following data sets /Rønning et al. 2003, Triumph et al. 2003, Wiklund 2002, Elhammer and Sandkvist 2005/:

- Helicopter-borne geophysical survey data, i.e. data on the total magnetic field, electromagnetic (EM) multifrequency data and very low frequency electromagnetic (VLF) data.
- Fixed-wing airborne, very low frequency electromagnetic (VLF) data.
- Detailed topographic data (terrain model).
- Terrain model of the sea bottom and bedrock surface in the sea area outside Simpevarp.

The helicopter-borne magnetic, EM multifrequency and VLF data were obtained during 2002 /Rønning et al. 2003/. Measurements were performed along north-south flight lines with a spacing of 50 m. The nominal instrument flight altitude during the measurements was 30–60 m. In a smaller area immediately east of the Simpevarp nuclear power plants, measurements were made along 36 lines perpendicular to the coast with a line spacing of 100 m. No measurements were carried out over the area occupied by the power plants (Figure 2-41), which implies that a large portion of the Simpevarp peninsula is devoid of airborne geophysical data. Furthermore, there are local disturbances in the measured data induced along existing power lines.

The data processing and methodology used in the interpretation of the helicopter- and fixed-wing borne geophysical survey data and the resulting different sets of identified lineaments are described in /Triumpf et al. 2003/. Maps of the total magnetic field, apparent resistivity calculated from fixed-wing VLF data and apparent resistivity calculated from EM multi-frequency data are shown in Figure 2-42, Figure 2-43 and Figure 2-44, respectively.

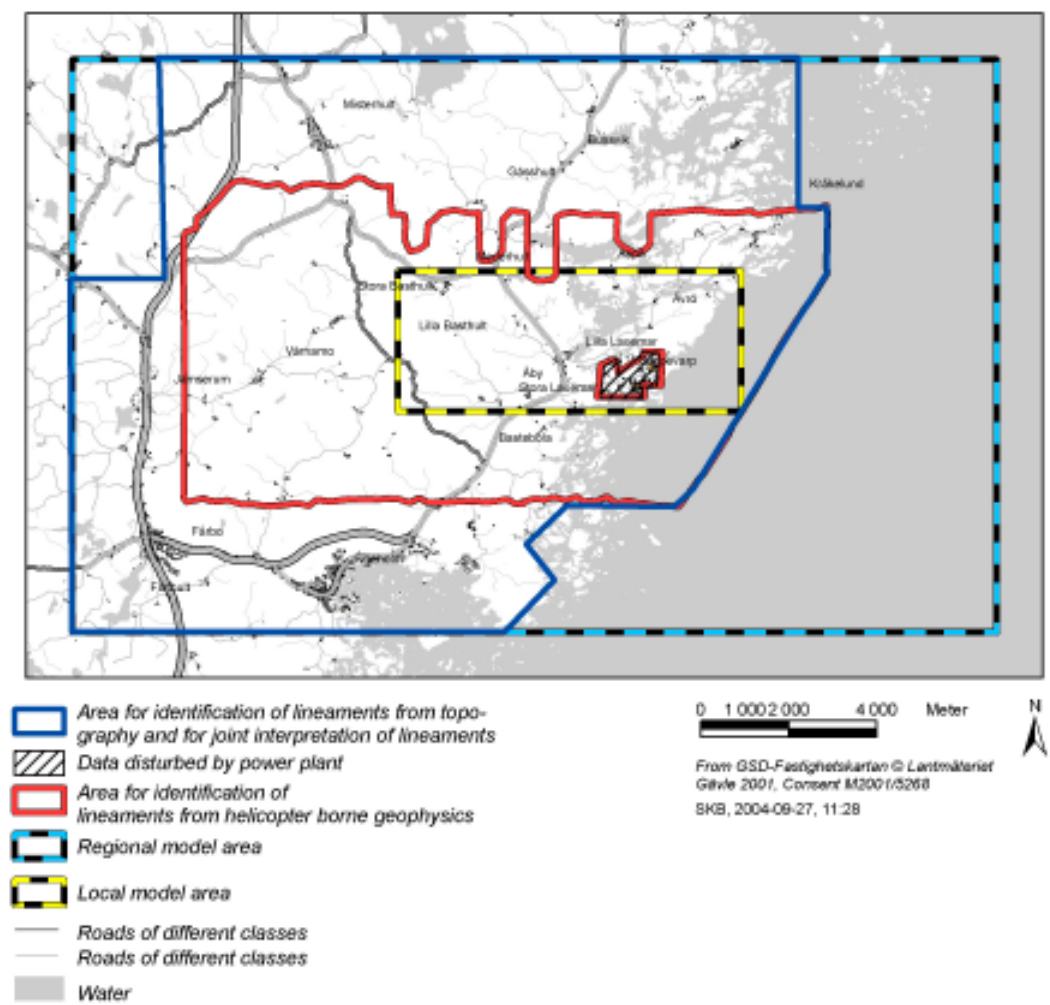


Figure 2-41. Map showing helicopter-borne geophysical and topographic data coverage. Note that no data were acquired in the area that is occupied by the nuclear power plants and their infrastructure.

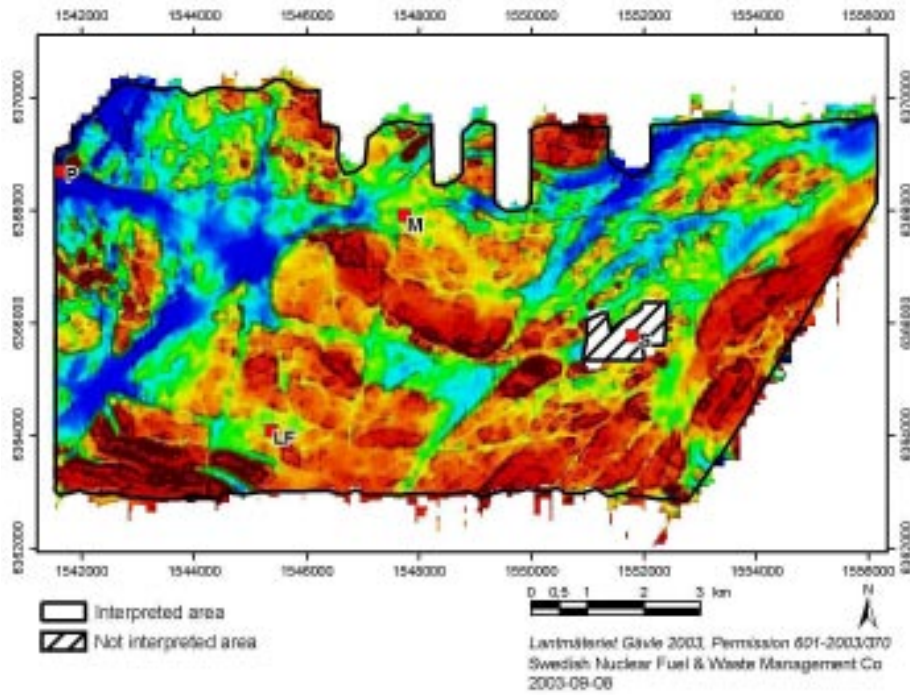


Figure 2-42. Map showing the total magnetic field from the helicopter survey. Reddish brown colour = strongly magnetic bedrock, blue colour = weakly magnetic bedrock.

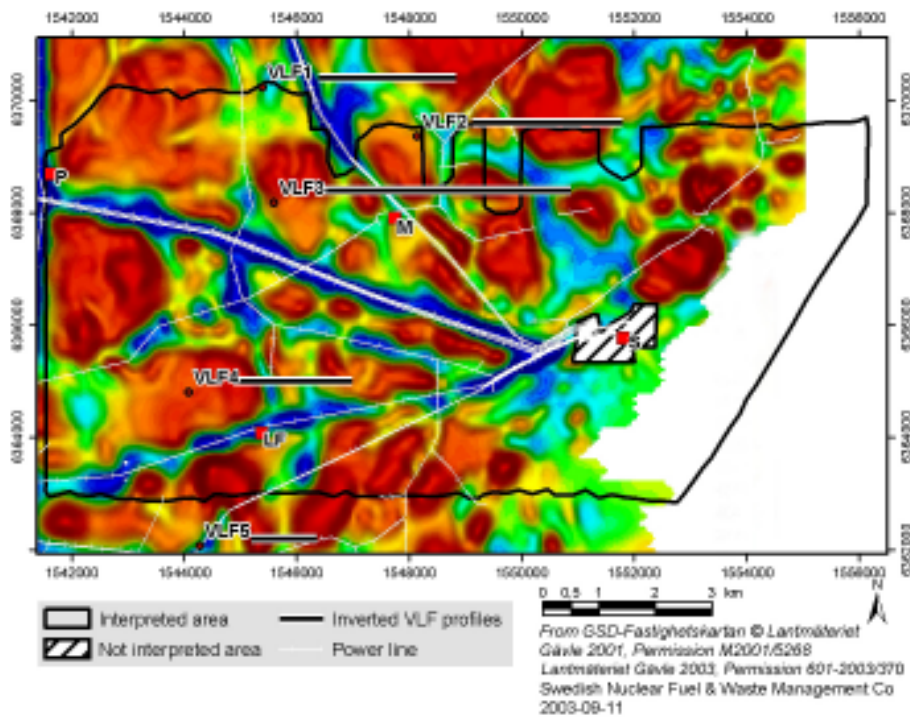


Figure 2-43. Map showing apparent resistivity calculated from fixed-wing VLF data. Reddish brown colour = high resistivity, blue colour = low resistivity.

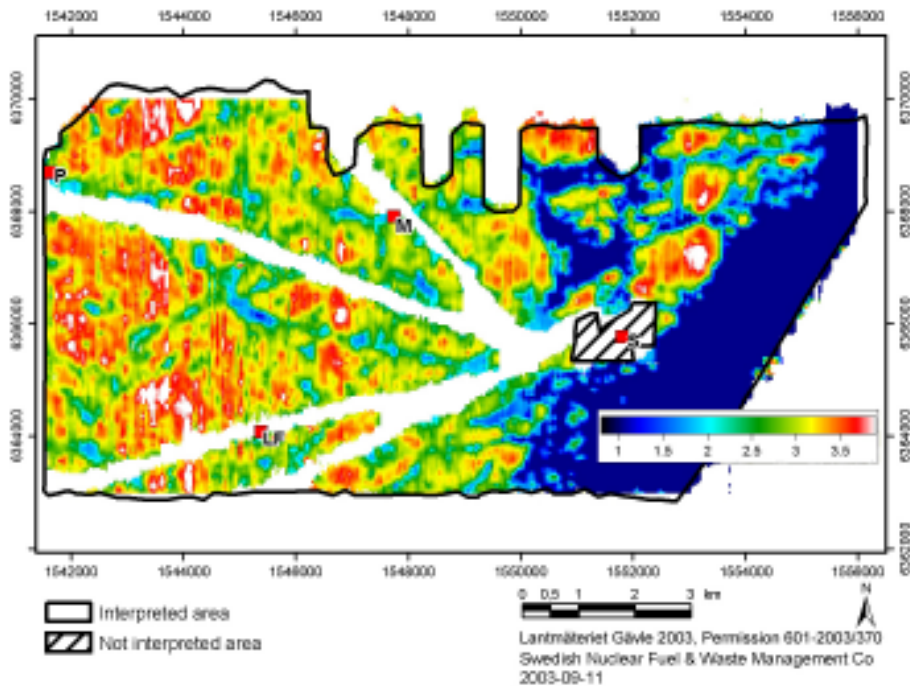


Figure 2-44. Map showing apparent resistivity calculated from helicopter-borne EM multi frequency data. Reddish colour = high resistivity, blue colour = low resistivity.

The topographic data are based on detailed airborne photography carried out 2001 with an instrument flight altitude of 2300 m and a spatial resolution of 0.2 m /Wiklund 2002/. The processing of the data resulted in a new detailed digital terrain model. The latter forms the basis for the identification of topographic lineaments. The processing of the topographic data, the methodology used in the interpretation work and the identified topographic lineaments are reported by /Triumpf 2003/.

The terrain model of the sea floor and bedrock surface offshore Simpevarp are based on a detailed marine geological survey carried out 2002 /Elhammer and Sandkvist 2005/. (Note: this report is not distributed yet because of security restrictions imposed by Swedish authorities). In the primary investigation area, i.e. close to the coast off the Simpevarp peninsula, the survey line spacing was 100 m, while the line spacing was 1,000 m in the remainder of the investigation area. The lineaments interpreted offshore are reported by /Triumpf 2004a/.

2.2.9.2 Evaluation

The process of joint interpretation of lineaments consists of the following major steps (cf. Figure 2-45 and definitions in the adjoining text):

- Construction of “co-ordinated lineaments” from “method-specific lineaments”,
- Parameterisation of the “coordinated lineaments”,
- Construction of “linked lineaments”,
- Parameterisation of “linked lineaments”.

A “method-specific lineament” is a lineament identified in a single specific type of data set, e.g. topography, helicopter-borne magnetic data, multifrequency electromagnetic (EM) data or data from the marine geological measurements (e.g. bathymetric data). A “coordinated lineament” is a single interpreted lineament that accounts for all “method-specific lineaments” along a segment of a given single lineament. A “linked lineament” here implies a lineament composed of one or several “coordinated” lineaments with a total extension in most cases longer than the underlying interpreted coordinated lineaments, cf. Figure 2-45.

The final result of the joint interpretation is the map of linked lineaments where the latter have been assigned attributes relating to their origin and character /Triumpf 2004a/. The linked lineaments identified in the Simepvarp regional model area are presented in Figure 2-46, where their assigned class (regional > 10 km or local major 1–10 km) are identified. The latter is an expert judgement that relates to the degree of clarity in surface expression of the lineaments where 1=low, 2=medium and 3=high uncertainty. A weighted average is calculated according to the length of each segment in the linked lineament. For a more detailed explanation, see /Triumpf 2004a/.

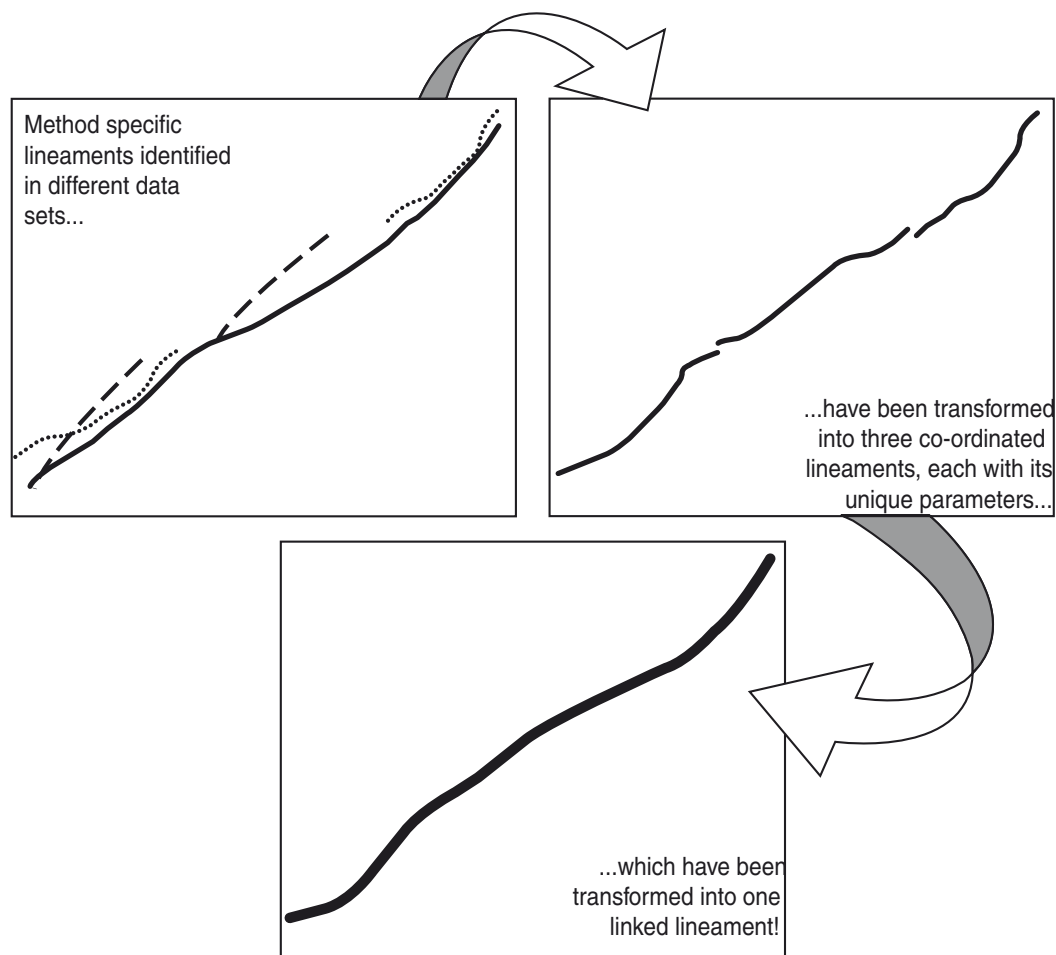


Figure 2-45. Schematic explanation of the joint lineament interpretation process.

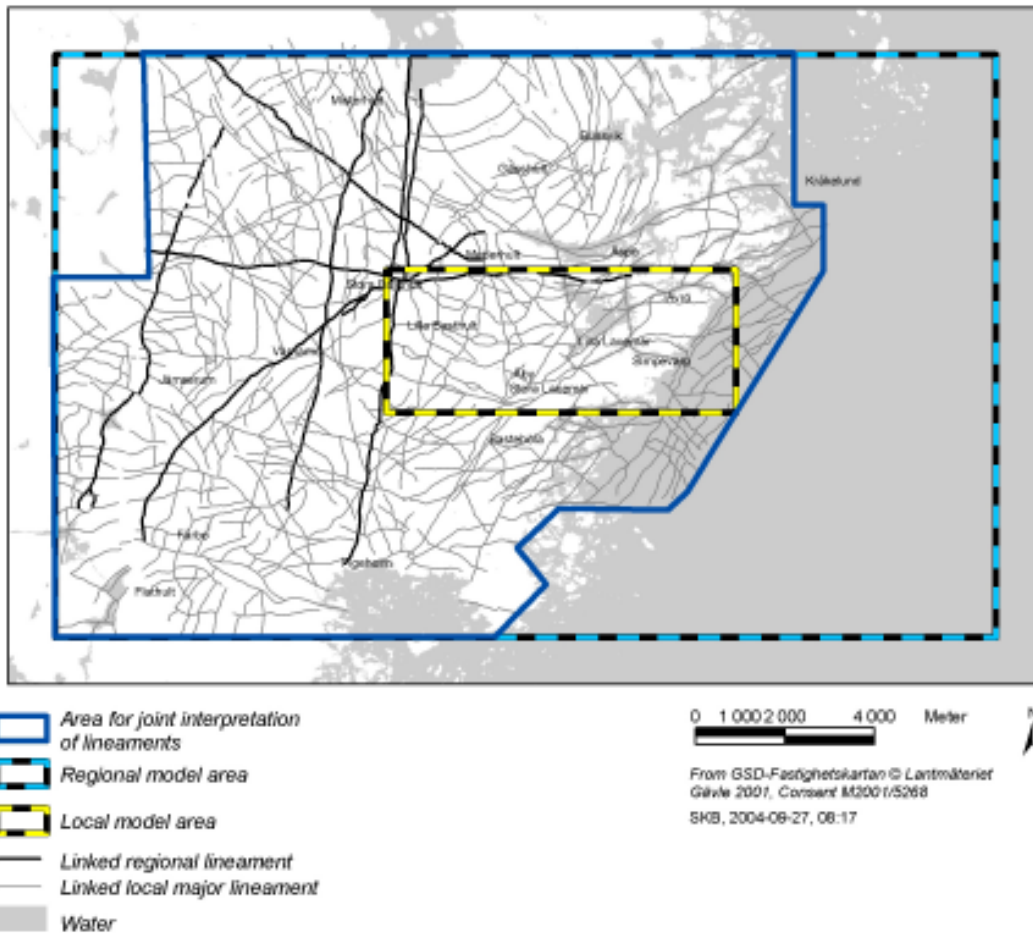


Figure 2-46. Interpreted linked lineaments in the Simpevarp regional model area.

The map of linked lineament covers a smaller area than the regional scale model area, cf. Figure 2-46. For modelling purposes, lineaments from earlier work (Simpevarp SDM version 0) have been evaluated and merged with the linked lineaments in areas with no detailed coverage.

The linked lineament interpretation was evaluated also on more structural geological grounds. Several connections were suggested to lineaments that were;

- segmented going from land to sea,
- segmented but still approximately linear and continuous.

Each suggested connection (see Figure 2-47) was reviewed by the geophysicist responsible for the original interpretation of the linked lineaments. The resulting merged linked lineament map covers the whole regional model domain and was aimed to be used as the common surface data deck for developing the 3D deformation zone model and the evaluation of DFN parameters.

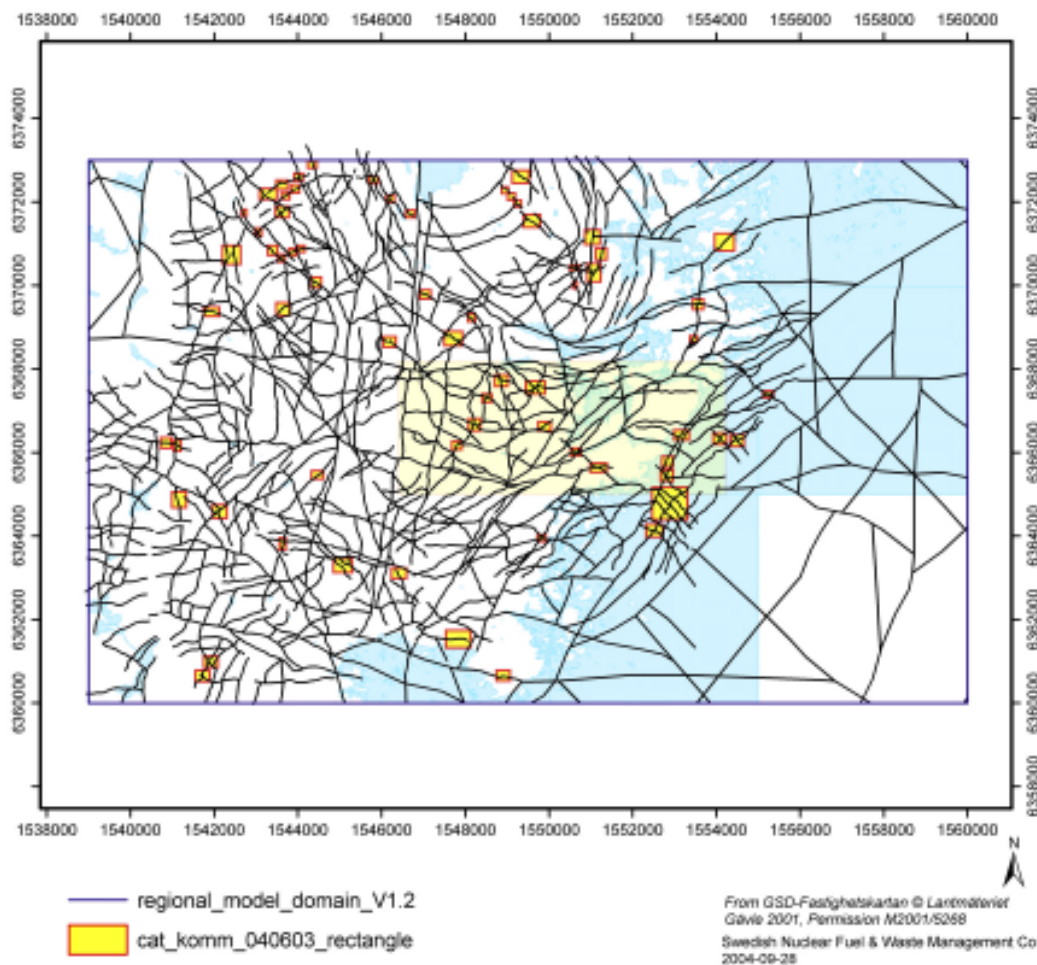


Figure 2-47. Geometrical improvements to the linked lineament map (small yellow rectangles) combined with the Version 0 lineament map in areas outside of the area of detailed linement coverage.

However, due to time constraints, the merged lineament evaluation was not completely finished when the deformation zone modelling and DFN analysis was initialised. The DFN analysis was consequently based only on available data at the time, i.e. merged and linked lineaments in the high resolution area (cf. Figure 2-46), whereas the deformation zone model utilised early versions of, and later also the final, merged linked lineament map inside the whole regional model domain shown in Figure 2-48.

It is important to note that the interpreted lineaments are not related with certainty to basement structures at this stage, except for a few where there is strong evidence from other independent sources of direct or indirect information as to their being basement structures, e.g. borehole data and/or seismic reflections or refractions. It is considered likely that many, but not all of the interpreted lineaments are associated with basement structures given that the overburden in Simpevarp is very thin or non-existing over large areas. However, at the moment it is not possible to discard lineaments as possible deformation zones if there are no data to support this. All merged and linked lineaments have therefore been considered in the modelling of deformation zones and evaluation of DFN parameters.

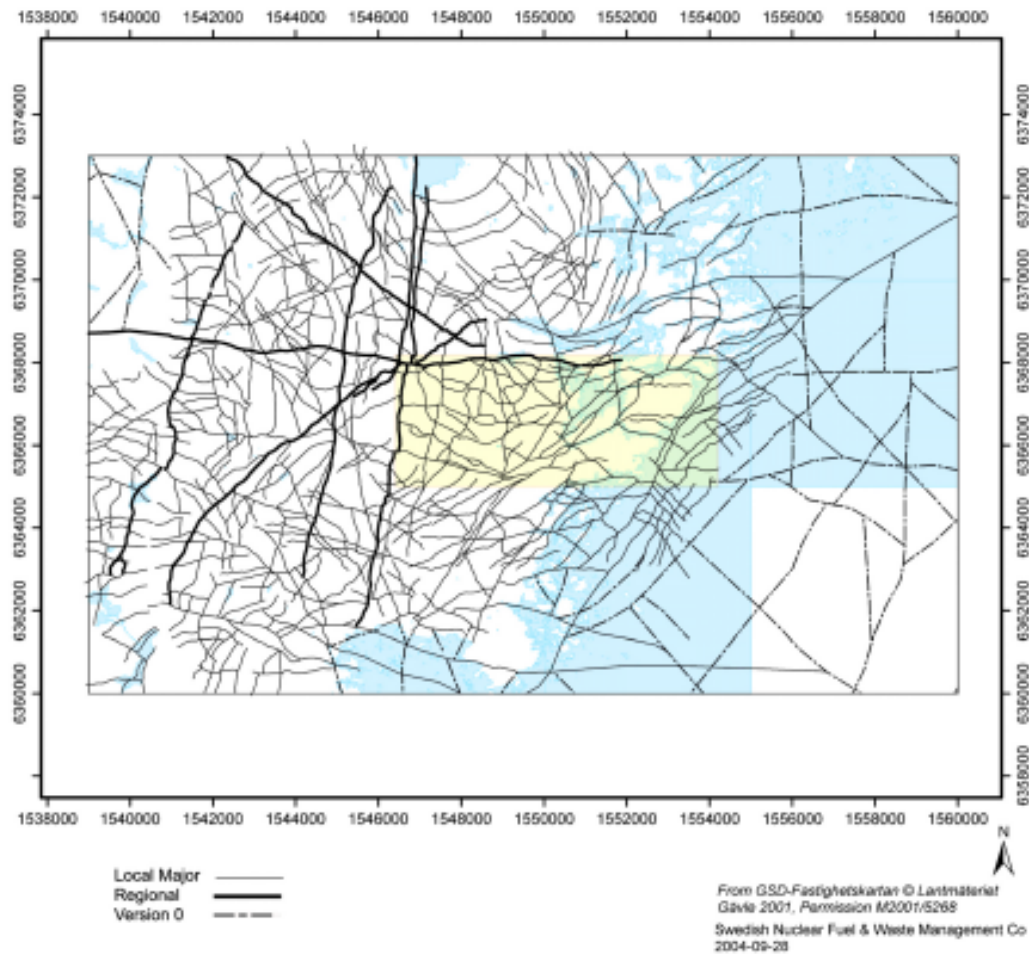


Figure 2-48. The lineament map (merged linked lineament map) used for the regional scale model area.

2.2.10 Observation of ductile and brittle structures from the surface

Data that document the character and orientation of ductile and brittle structures at the surface in the Laxemar subarea and surroundings originate from observations made in conjunction with the bedrock mapping of the Laxemar subarea and immediate surroundings during 2004. Available data comprise:

- 1,395 measurements of ductile and brittle structures and bedrock contacts at 1,350 observation points, including 181 observation points in the regional model area, that were documented during the bedrock mapping /Persson Nilsson et al. 2004/.
- Laboratory measurements of the anisotropy of the magnetic susceptibility (AMS) of samples from 66 outcrops /Mattsson et al. 2004a/, the majority of which is located in the Laxemar subarea and its immediate surroundings (see Figure 2-3).
- Documentation of fracture fillings by visual inspection at 333 of the 1,350 observation points referred to above /Persson Nilsson et al. 2004/.
- Detailed mapping of fractures (including fracture fillings) that are longer than 50 cm at two cleaned outcrops in the Laxemar subarea /Cronquist et al. 2004/ and four in the Simpevarp subarea /Hermanson et al. 2004/.
- Scan-line mapping of frequency and orientation of fractures that are longer than 100 cm at 24 observation points in the Laxemar subarea and immediate surroundings /Berglund 2004/ and 16 in the Simpevarp subarea /Wahlgren et al. 2004/ – fracture fillings were also noted when identified.

2.2.10.1 Ductile structures

The rocks in the Laxemar as well as in the Simpevarp subarea generally are well-preserved and more or less undeformed (this is presumably valid also for the rocks in the remainder of the regional model area). However, locally a weak foliation is developed that is defined by the preferred orientation of mainly biotite. Concerning the commonly porphyritic Ävrö granite, the foliation principally affects the matrix whereas the feldspar megacrysts show no or only weak preferred orientation.

The foliation in the Laxemar subarea and immediate surroundings has an east-west to north-westerly strike and a variable dip, whereas the foliation in the Simpevarp subarea displays an east-west to northeasterly strike and steep dip (Figure 2-49). Thus, a difference in the orientation of the foliation is obvious between the two subareas. Furthermore, the foliation is more or less concordant to the contacts between the dominant rock types which suggests a genetic relationship between the formation of the foliation and the formation of the rocks.

However, the most spectacular and characteristic ductile, structural features in the overall relatively well preserved rocks in both the Laxemar and Simpevarp subareas are the occurrence of protomylonitic to mylonitic, low-grade ductile to brittle-ductile shear zones (Figure 2-50 and Figure 2-51). Low-grade ductile to brittle-ductile shear zones, independent of thickness, are documented at 185 of a total of 1,350 observation points in the Laxemar subarea and surroundings, and at 47 of a total of 353 observation points in the Simpevarp subarea. The shear zones vary in thickness from decimetre up to tens of metres. At several places it appears that the ductile shear zones have undergone a later brittle reactivation. The alignment of some of the shear zones implies that they form part of one and the same zone of local major character. The dotted pattern in the bedrock map in Appendix 2 defines two areas or rather belts with a high concentration of low-grade ductile to brittle-ductile shear zones. The regional scale shear zones within this belt have a northeast-southwest strike and a vertical to subvertical dip (Figure 2-52), which, on a local scale, can be seen as two branches, denoted Äspö shear zone (ZSMNE005A) and zone ZSMNE004A, of a larger regional structure that divides Laxemar from Simpevarp, see Section 4.2.3

In several places, low-grade ductile shear zones have been observed in rock exposures close to identified lineaments during the bedrock mapping. This is an indication that the lineament represents a deformation zone.

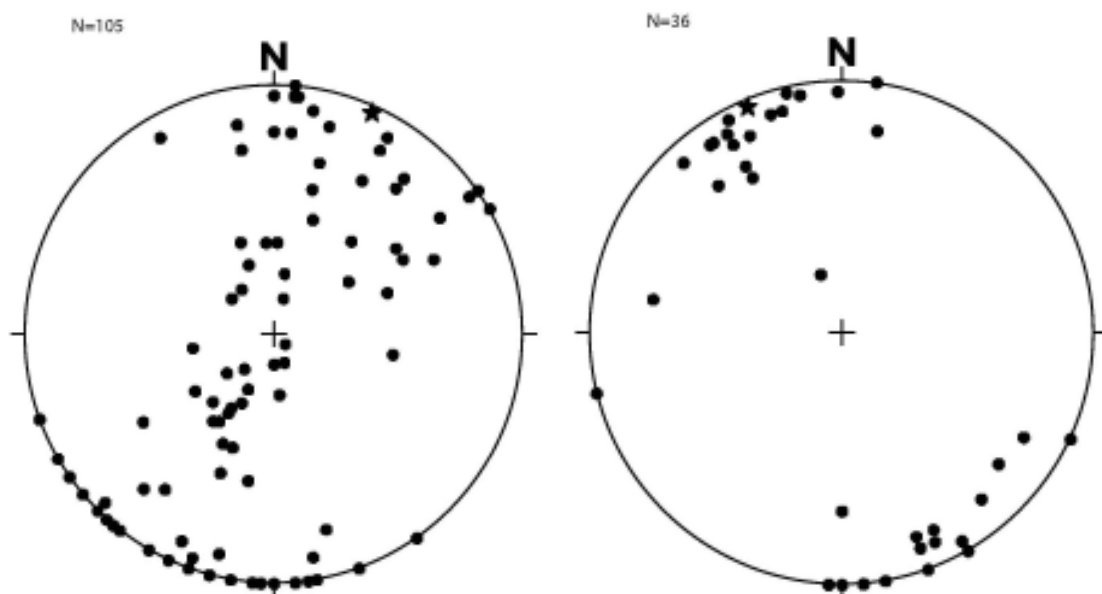


Figure 2-49. Poles to foliation in the Laxemar subarea and immediate surroundings (left) and Simpevarp subarea (right). Lower hemisphere of Schmidt equal area, stereographic plots.



Figure 2-50. Strongly deformed, protomylonitic Ävrö granite within ZSMNE004A, see Chapter 4.



Figure 2-51. Close-up of the protomylonitic Ävrö granite in Figure 2-50.

2.2.10.2 Overprinting by ductile shear zones – division in structural domains

The documentation of ductile shear zones during the bedrock mapping of the Laxemar and Simpevarp subareas /Persson Nilsson et al. 2004, Wahlgren et al. 2004/ indicates that the Simpevarp subarea is more strongly affected by low-grade ductile shear zones than the Laxemar subarea. This is also strongly indicated in the magnetic anomaly map where the Simpevarp subarea, i.e. east of the Äspö shear zone, is characterised by a much more banded, anomaly pattern than the Laxemar subarea west of the Äspö shear zone (Figure 2-42). This difference is interpreted to be a result of overprinting of the ductile shear zones. Thus, the Simpevarp and Laxemar subareas may be considered as two different structural domains, and indicates that the Simpevarp subarea is situated in a spaced ductile shear belt, while the Laxemar subarea more or less have escaped this ductile shearing and in respect to the latter constitute a “tectonic lens”.

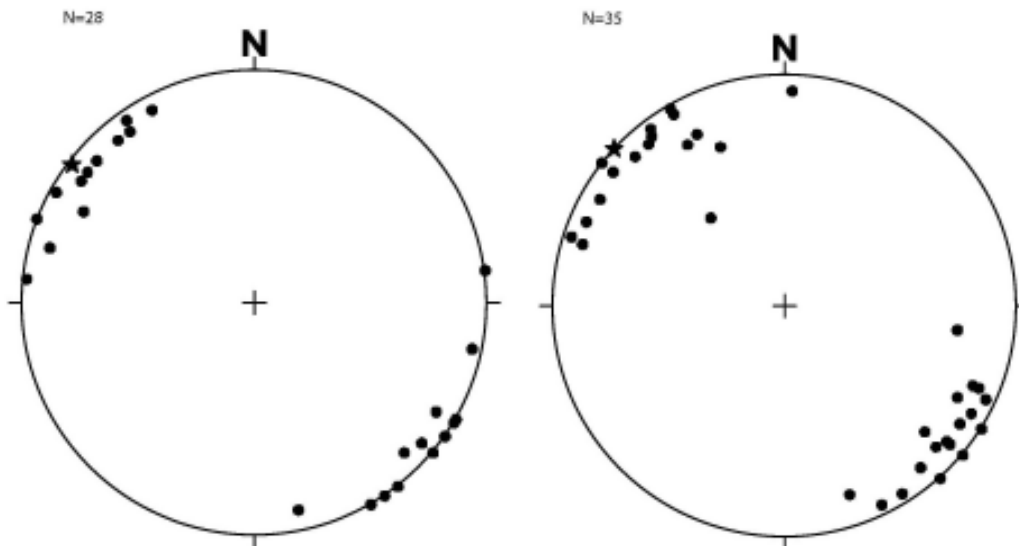


Figure 2-52. Poles to protomylonitic to mylonitic foliation in ductile shear zones in zone ZSMNE005 (Äspö shear zone) (left) and ZSMNE004A (right), see Section 4.2.3. Star marks the mean pole. Lower hemisphere of Schmidt equal area, stereographic plots.

A sinistral strike-slip component of movement has been suggested for the ductile deformation in the Äspö shear zone /Talbot and Munier 1989, Munier 1989/, and this is also indicated by the change in orientation of the magnetic anomaly pattern along both sides of the zone (Figure 2-53). Sinistral displacements along the NE-trending Äspö shear zone, may explain and is inferred to have caused the change in orientation of the lithological boundaries and the weakly developed foliation from northwesterly in the Laxemar subarea to northeasterly in the Simpevarp subarea.

A special study will be carried out in order to try to assess the sense of movement (kinematics) of the ductile shear zones. The results of this study will have important implications for the future modelling work and understanding of the structural and tectonic evolution in the area.

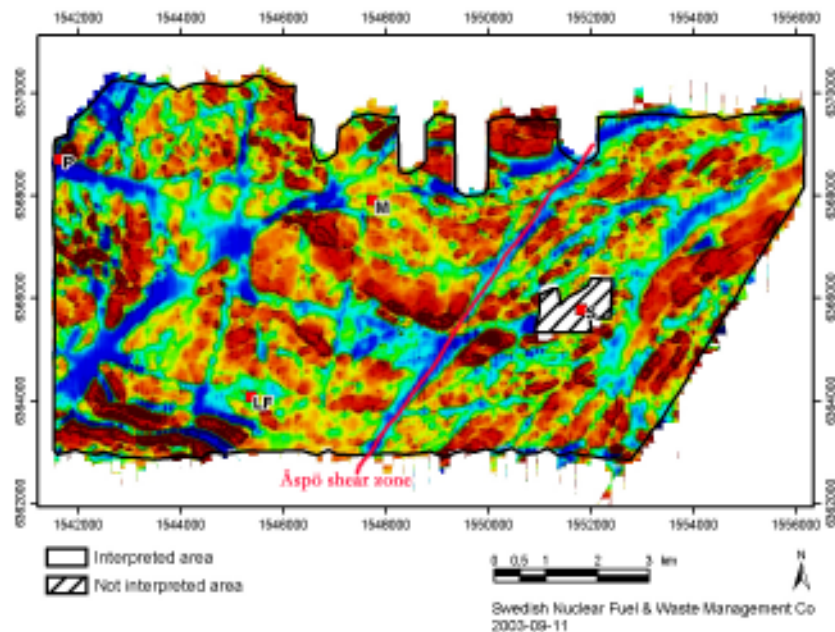


Figure 2-53. Map showing the total magnetic field from the helicopter survey. Reddish brown colour = strongly magnetic bedrock, blue colour = weakly magnetic bedrock.

2.2.10.3 Anisotropy of the magnetic susceptibility (AMS)

The anisotropy of the magnetic susceptibility (AMS) measurements constitute a means to calculate the principal directions and principal susceptibilities ($K_1 \geq K_2 \geq K_3$) of the magnetic susceptibility anisotropy ellipsoid for each sample /Mattsson et al. 2003/. By analysing the mean values of the principal magnetic susceptibilities for several samples, the degree of anisotropy and the shape of the anisotropy ellipsoid can be estimated for a rock object. The ellipsoid may be prolate (dominated by magnetic lineation), spherical or oblate (dominated by magnetic foliation). By analysing the principal directions it is possible to estimate the magnetic fabric orientation in 3D, which is related to structural parameters of the rocks such as lineation and foliation. Thus, the AMS data may be an important and useful tool in revealing an anisotropic fabric in rocks that appear well preserved and lack a clear visible tectonic fabric.

The anisotropy of magnetic susceptibility is primarily governed by the grain shape and orientation of the magnetite grains in the Simpevarp and Laxemar subareas. The AMS-ellipsoids show a continuous variation in shapes from strongly prolate (“cigar-shape”) to strongly oblate (“disc-shape”) and the degree of anisotropy is below 1.3 for most of the samples. This indicates that a majority of the rocks within the site investigation area are well preserved and unaffected by any major deformation. However, the AMS principal axis orientations clearly show a consistent pattern in spite of the fact that a vast majority of the sampled rocks appear to be of primary origin and lack visible tectonic fabrics.

The poles to the magnetic foliation (K_{min} , corresponding to the short axis of the strain ellipsoid) and the orientation of the magnetic lineations (K_{max} , corresponding to the long axis of the strain ellipsoid) are shown separately for the Laxemar and Simpevarp subareas (Figure 2-54, Figure 2-55, Figure 2-56 and Figure 2-57).

The poles to the foliation (K_{min}) form a girdle distribution, which indicates a folded geometry (Figure 2-54). However, the folded geometry is only apparent since the geographical distribution of the foliations is not consistent with a folding of the foliation /Mattsson et al. 2004a/. Two samples that are located close to the Äspö shear zone display orientations of magnetic foliations that are similar to the orientation of the shear zone. Hence, it is inferred that the girdle distribution of the magnetic foliations in Figure 2-54 is caused by a mixture of the regional foliations and foliations related to or disturbed by the low-grade ductile shear zones. In general, the strikes of the foliations follow the east-west to east-southeast – west-northwest orientation of the major lithological boundaries. Together with the generally low degrees of anisotropy, this probably indicates that most rocks carry a primary magnetic fabric related to the tectonic situation (stress field) that prevailed during the emplacement of the rocks.

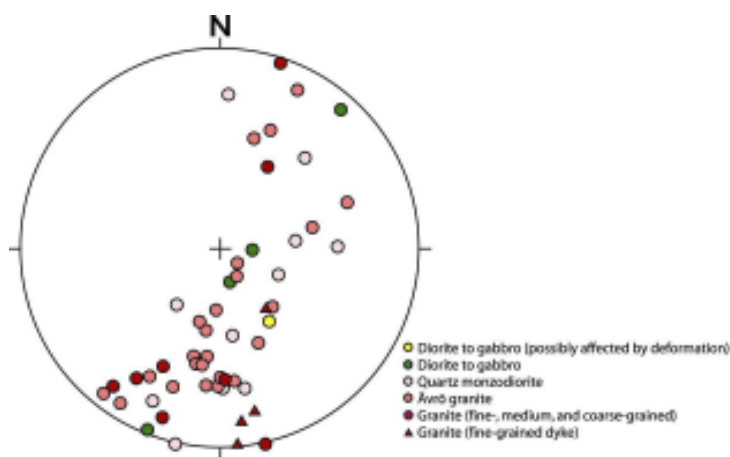


Figure 2-54. Equal area projection plots of minimum (poles to foliation) site mean anisotropy axes for rocks in the Laxemar subarea.

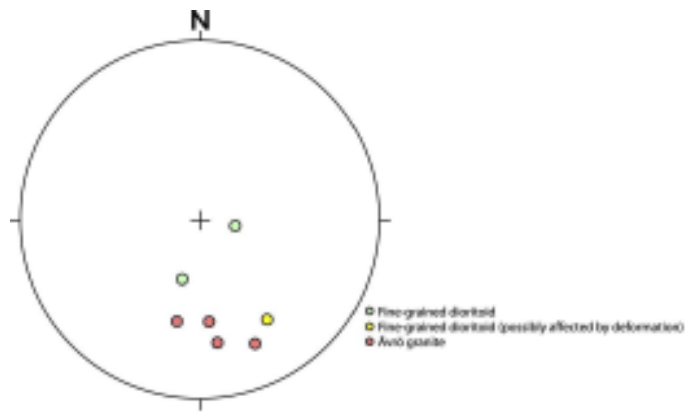


Figure 2-55. Equal area projection plots of minimum (poles to foliation) site mean anisotropy axes for rocks in the Simpevarp subarea.

The magnetic lineation (maximum strain) directions show consistent northwesterly to westnorthwesterly orientations at both the Laxemar and Simpevarp subareas (Figure 2-56 and Figure 2-57). Plunges are generally moderate to shallow. Note that for many site locations where the foliation planes vary in orientation, the orientation of the lineation is fairly constant.

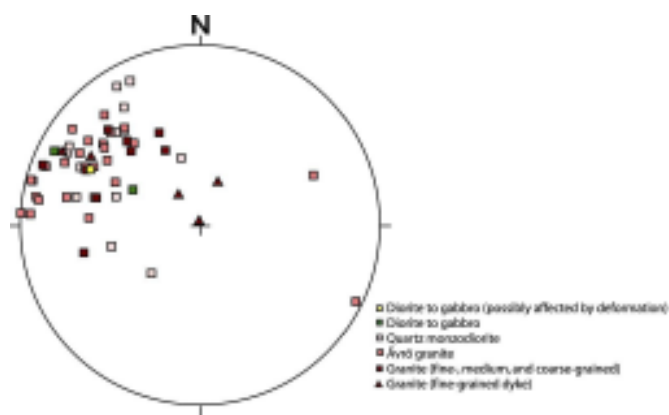


Figure 2-56. Equal area projection plots of maximum (lineation) site mean anisotropy axes for rocks in the Laxemar subarea.

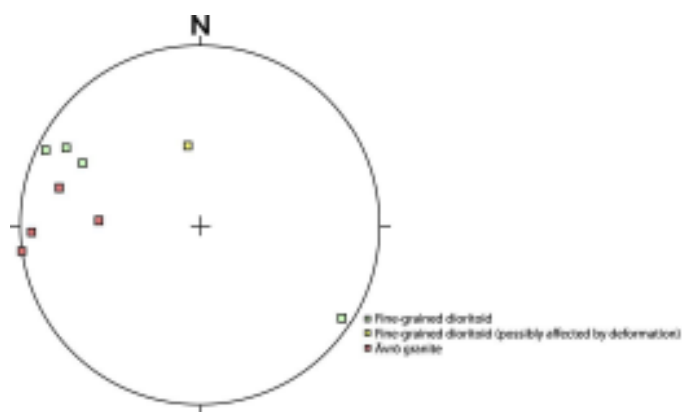


Figure 2-57. Equal area projection plots of maximum (lineation) site mean anisotropy axes for rocks in the Simpevarp subarea.

A contour plot of the dip of the foliation planes and plunge of the lineations are displayed in Figure 2-58. The contour lines have been interpolated by taking the mean value of values within a search radius of 600 meters. The contour plot of the magnetic foliations shows that the investigated area roughly can be divided into three structural regions; a southern dominated by moderate to steep dips, a central region dominated by shallow to moderate dips and a northern region dominated by steeply dipping foliation planes. The contour plot of the plunge of the lineations roughly supports a division of the investigated area into three structural regions.

The orientation of the foliations revealed by the AMS-measurements /Mattsson et al. 2004a/ support and are similar to the strike of the commonly weakly developed foliations documented during the bedrock mapping of the Laxemar and Simpevarp subareas /Persson Nilsson et al. 2004, Wahlgren et al. 2004/. However, no lineations have been observed during the bedrock mapping, so a comparison with the AMS results cannot be made.

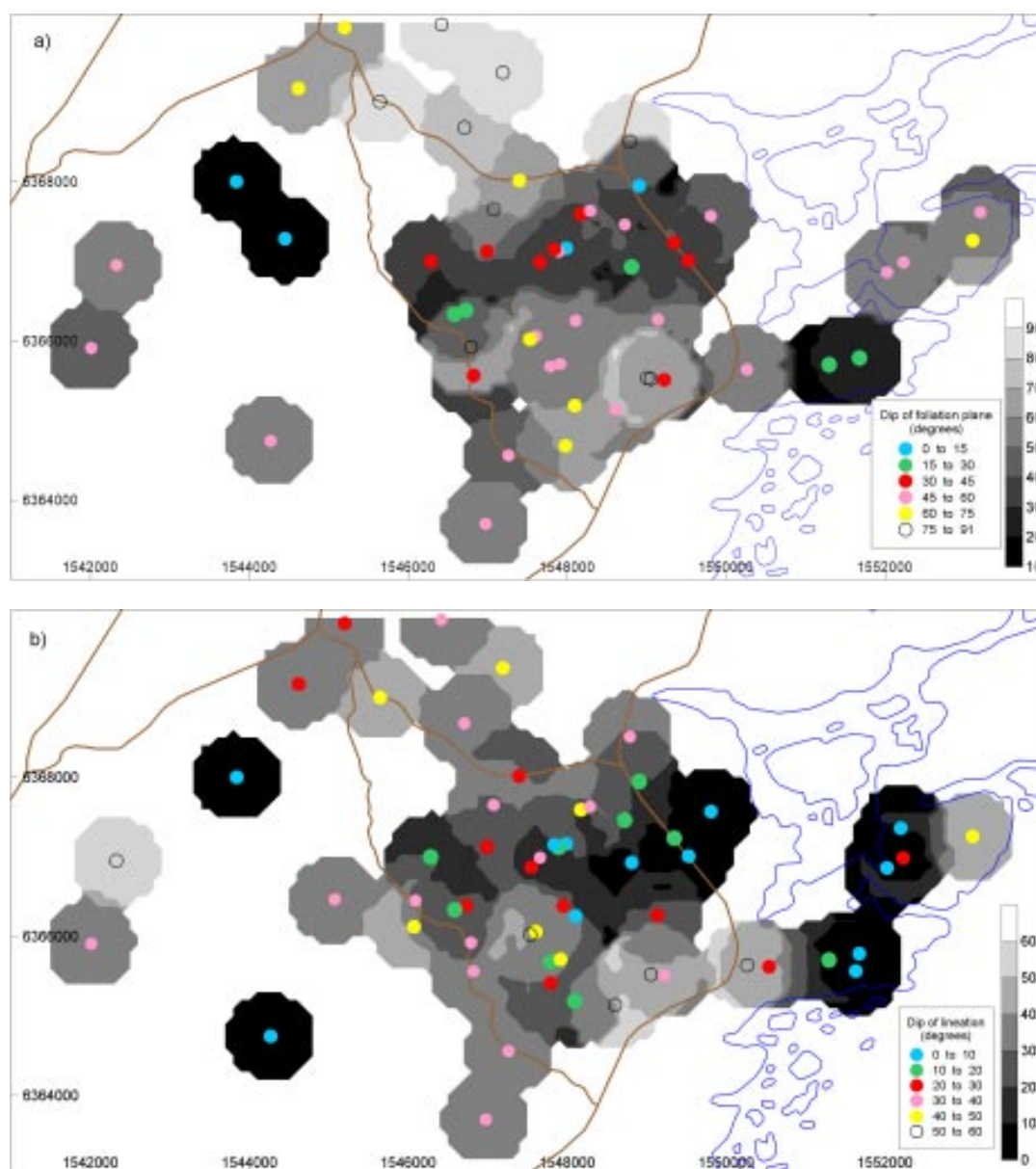


Figure 2-58. a) Contour plot of the dip of the magnetic foliation planes (symbols denote sampling position and dip of foliation in intervals of 15°). b) Contour plot of the plunge of the magnetic lineations (symbols denote sampling position and dip of foliation in intervals of 10°). Figure from /Mattsson et al. 2004a/.

2.2.10.4 Detailed fracture mapping

Description and evaluation of the detailed and scan-line fracture mapping in the Laxemar and Simpevarp subareas is reported in /Hermanson et al. 2005/.

2.2.10.5 Brittle deformation and alteration

Brittle deformation has been documented during the bedrock mapping of the Laxemar subarea and immediate surroundings. In several places, rock exposures close to identified lineaments show signs of brittle deformation such as high fracture frequency, cataclastic deformation, alteration etc. which is an indication that the lineament represents a deformation zone (Figure 2-59).

Epidote is the dominant fracture filling mineral observed during the bedrock mapping of the Laxemar subarea. Other common fracture filling minerals are quartz, prehnite and chlorite. Larger veins of hydrothermal quartz are also present.

So far, there are not sufficient data to evaluate the relationship between the fracture filling minerals and the orientation of the fractures. The fracture filling mineralogy is more extensively described in Section 2.4.5.

The extensive but inhomogeneous, red staining which is a characteristic phenomenon in the Simpevarp subarea was not observed to be of same extent in the Laxemar subarea and surroundings during the bedrock mapping. In the latter area, the red staining mainly occurs along and around fractures and interpreted deformation zones (Figure 2-59 and Figure 2-60) in contrast to the Simpevarp subarea where the red staining also affected the rock volumes in between the prominent, mesoscopic fractures. Numerous, small-scale, sealed fractures occur in these rock volumes, and presumably these fractures acted as conduits for the penetrating hydrothermal fluids.

The red staining alteration process is focussed on in the site investigation in an ongoing project /Drake and Tullborg 2004, Drake et al. 2004, SKB 2004, cf. Eliasson 1993/.



Figure 2-59. Brittle deformation and red staining in Ävrö granite close to the deformation zone ZSMNW929A (see Chapter 4) in the northern part of the Laxemar subarea. Note the red staining (oxidation).



Figure 2-60. Red staining along fractures in Ävrö granite and fine- to medium-grained granite.

As mentioned above, the Simpevarp and Laxemar subareas are inferred to have responded differently what relates to the overprinting of ductile shear zones, and the observed difference in the degree of red staining indicates that the Simpevarp subarea also responded differently than the Laxemar subarea during the brittle deformation/reactivation during the subsequent geological evolution. This may have great implications for the overall understanding of how the Simpevarp and Laxemar subareas are related, e.g. hydraulically and hydrogeochemically. This will be more closely considered and evaluated in the future modelling work.

Similarly to the ductile shear zones, a special study is carried out on the kinematics in the brittle deformation zones. The latter includes studies both at the surface and in identified deformation zones in drill cores, and will generate important complementary information for the understanding of the structural evolution.

2.3 Surface geophysics

Various types of surface geophysical measurements have been carried out during the ongoing site investigation. These provide indirect information to study the occurrence of possible deformation zones or to help constrain the depth existence of rock types, rock units and rock domains, dependent of the kind of method applied. Independent data, e.g. outcrop and borehole data are necessary to compare with the geophysical anomalies in order to confirm or refute the presence of e.g. a deformation zone.

2.3.1 Older data

Within the area of the Simpevarp peninsula many surface geophysical measurements were carried out during the investigation phases of OKG I-III and CLAB1-2. The resulting interpretations of major structures have been considered in the current project. However, due to the lack of the original raw data, no reassessment or reinterpretation of these data has been possible to carry out. In addition, since these surveys were followed up by drilling and actual excavation, a greater emphasis has been given to the results of tunnel and excavation mapping.

During 1989, magnetometry and VLF profile measurements were carried out across lineaments within the regional model area /Stenberg and Sehlstedt 1989/. Some of these profiles were also investigated by a refraction seismic survey /Rydström and Gereben 1989/.

Reflection seismic studies have been carried out prior to the site investigation in the Laxemar subarea /Bergman et al. 2001, 2002, Juhlin et al. 2002/ and on the island of Ävrö /Juhlin and Palm 1999/. These have been evaluated in connection with the SDM Simpevarp 1.2.

Important surface geophysical measurements for the site descriptive modelling work are displayed in Figure 2-61.

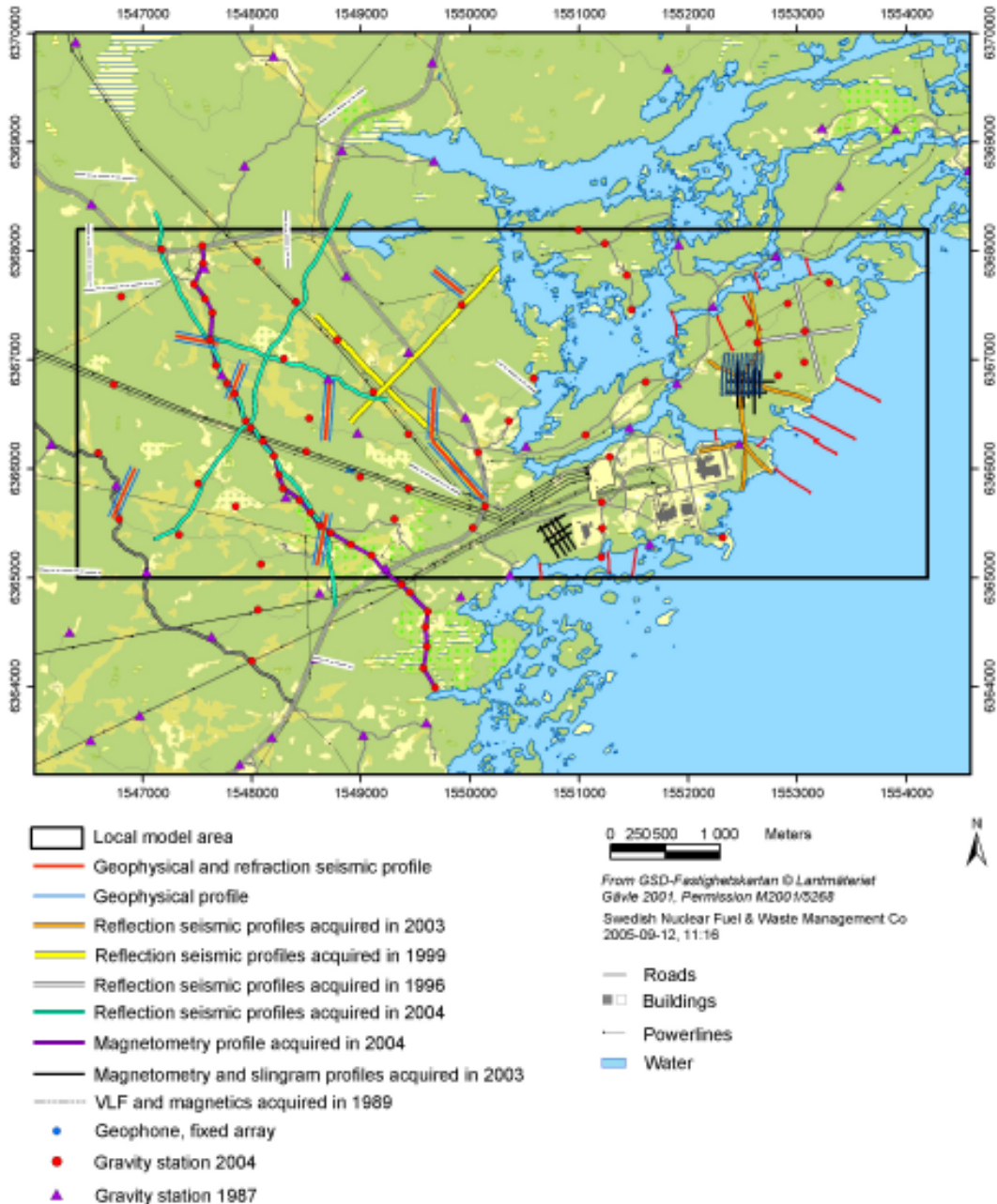


Figure 2-61. Location of surface geophysical measurements in the Laxemar and Simpevarp subareas utilised in the site descriptive modelling.

2.3.2 Data generated during the ongoing site investigation

In the Simpevarp subarea, the following surface geophysical measurements have been carried out:

- Magnetic and slingram measurements on the Simpevarp peninsula and at the island of Ävrö /Triumpf 2003/.
- Refraction seismic measurements in the sea area around the island of Ävrö and the Simpevarp peninsula /Lindqvist 2004a/.
- Reflection seismic measurements at the island of Ävrö and the Simpevarp peninsula /Schmelzbach and Juhlin 2004, Juhlin et al. 2004b/.

In the Laxemar subarea, the following surface geophysical measurements have been carried out:

- Gravity and accompanying total magnetic field measurements, including an approximately 5 km long profile, in the Laxemar subarea and surroundings /Triumpf 2004b/.
- Refraction seismic measurements across identified lineaments /Lindqvist 2004b/.
- Magnetic, electric resistivity and electromagnetic slingram measurements across lineaments /Thunehed et al. 2004/.
- Reflection seismic measurements /Juhlin et al. 2004a/.

All the surface geophysical investigations in the Laxemar subarea, except for the gravity and magnetic total field measurements, have been focussed on an improved understanding of whether lineaments constitute deformation zones and to better verify and characterize these deformation zones. The evaluation of the results is described in conjunction with the description of the deformation zones (Chapter 4).

The gravity and accompanying total magnetic field measurements in the Laxemar subarea focussed on a better understanding of the geometry and extension at depth of the rock types. Of special interest is the rock volume containing a high frequency of diorite to gabbro in the southern part of the Laxemar subarea and also the contact relationship between the Götemar granite and surrounding rocks north of the Laxemar subarea. The evaluation of the results of these measurements is described in conjunction with the description of the rock domain modelling.

2.4 Borehole data

The geological mapping and geophysical logging programmes for the boreholes have generated subsurface data that bear on the character of rock type (including alteration) and ductile and brittle deformation including fractures. These programmes are of vital importance for all three components in the geological modelling work, i.e. rock domain, deformation zone and DFN modelling. Due to the lack of a drill core, and thereby a somewhat more uncertain identification of rock types and deformation zones in the percussion boreholes, combined with the limited borehole length, the rock domain and deformation zone modelling work have focussed on data from the cored boreholes.

Data from KLX01, KLX02, KLX03, KLX04A/B, KLX05 and KLX06, i.e. approximately 6,800 metres of cored boreholes in the Laxemar subarea, and KSH01A/B, KSH02, KSH03A/B, KAV01 and KAV04A/B, i.e. c. 4,700 metres of cored boreholes in the Simpevarp subarea (Figure 2-62), have been used in the rock domain and deformation zone modelling work in the Laxemar SDM model version 1.2. Boremap data exist for KLX02 (200–1,006 m), KLX03, KLX04A/B, KSH01A/B, KSH02, KSH03A/B, KAV01 and KAV04A/B. It shall be noted that the preliminary and simplified mapping of KLX02 (1,006–1,700 m), KLX05 and KLX06 have

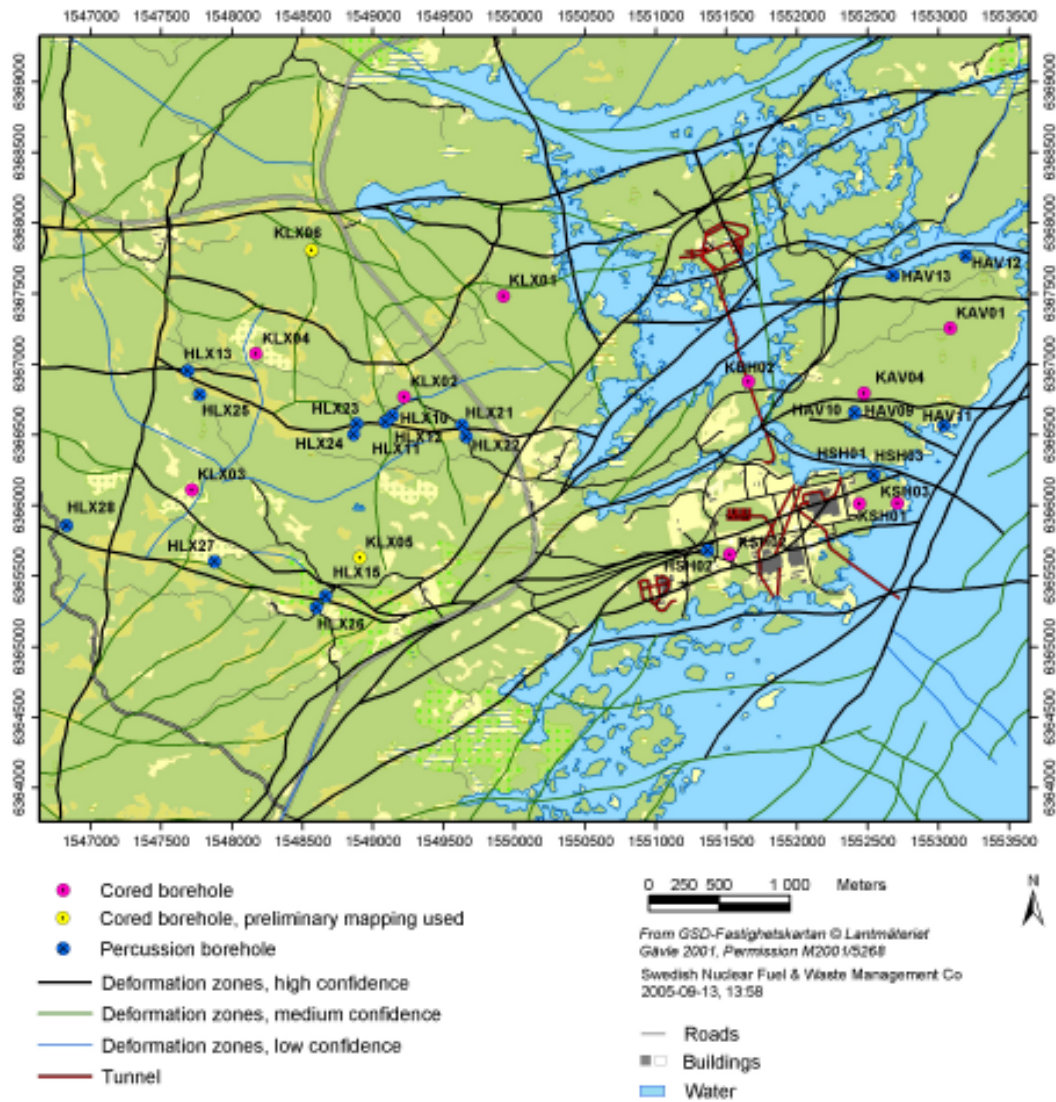


Figure 2-62. Location of cored and percussion boreholes in the Laxemar and Simpevarp subareas that have been utilised in the rock domain and deformation zone modelling.

been utilised only in the rock domain modelling. The bedrock information from KLX01 has not been updated by new Boremap mapping in conjunction with the ongoing site investigation due to the lack of BIPS images. However, the rock nomenclature from the old mapping has been evaluated and translated to the nomenclature used in the site investigation (see Appendix 1).

Fracture statistics from borehole data is described in /Hermanson et al. 2005/.

2.4.1 Rock types in cored boreholes

The proportion of rock types, based on the Boremap mapping /Ehrenborg and Stejskal 2004abcde, 2005, Ehrenborg and Dahlin 2005ab/ in the cored boreholes KLX01 (not mapped by the Boremap system), KLX02, KLX03 and KLX04A and simplified mapping of KLX06 in the Laxemar subarea, and KSH01A, KSH02, KSH03A, KAV01 and KAV04A in the Simpevarp subarea is displayed in Figure 2-63 and Figure 2-64, respectively. Note that the Boremap mapping of KLX02 only comprises the section 200–1,006 m although the borehole is c. 1,700 m deep.

Laxemar subarea Rock types in cored boreholes

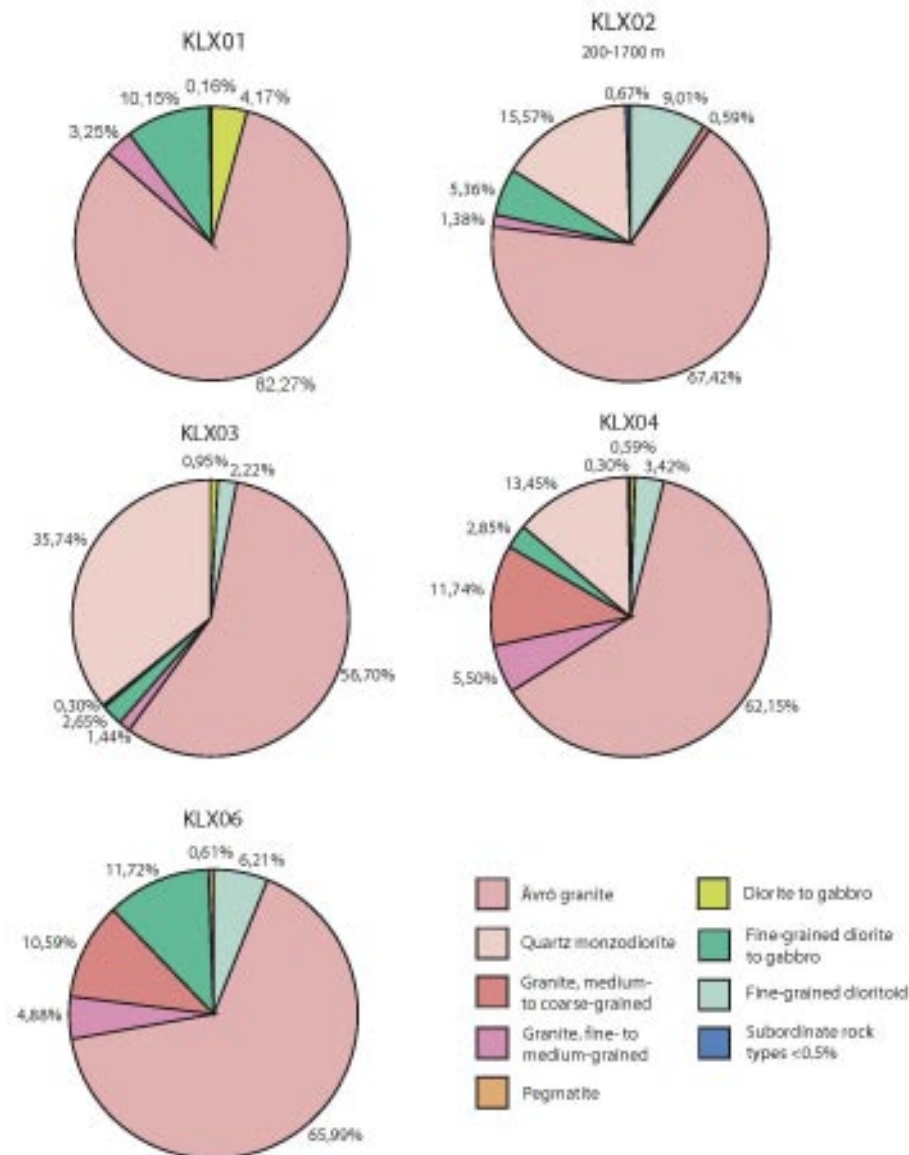


Figure 2-63. Proportion of rock types in cored boreholes in the Laxemar subarea. Note that the proportion of rock types in KLX02 between c. 1,006 and 1,700 m and in KLX06 is based only on simplified (preliminary) mapping. Furthermore, the drillcore from KLX01 has not been remapped, but the existing mapping has been translated to the rock nomenclature applied by SKB in the ongoing site investigation.

The percentage of every rock type represents the sum of the length of all sections of the rock type along each borehole. This implies that a particular rock type may be distributed in several more or less long sections in the boreholes mixed with other rock types as is exemplified by KLX02 in Figure 2-65.

In Figure 2-66, the distribution of rock types from the Boremap mapping between –400 and –600 m (envisaged repository depth) is displayed for the cored boreholes KLX01, KLX02, KLX03 and KLX04.

As can be seen in Figure 2-63 and Figure 2-66, Ävrö granite is the dominating rock type at depth in the Laxemar subarea. If the total borehole length is considered, Ävrö granite makes up between approximately 57 and 82% of the bedrock (Figure 2-63). However, if envisaged

Simpevarp subarea
Rock types in cored boreholes

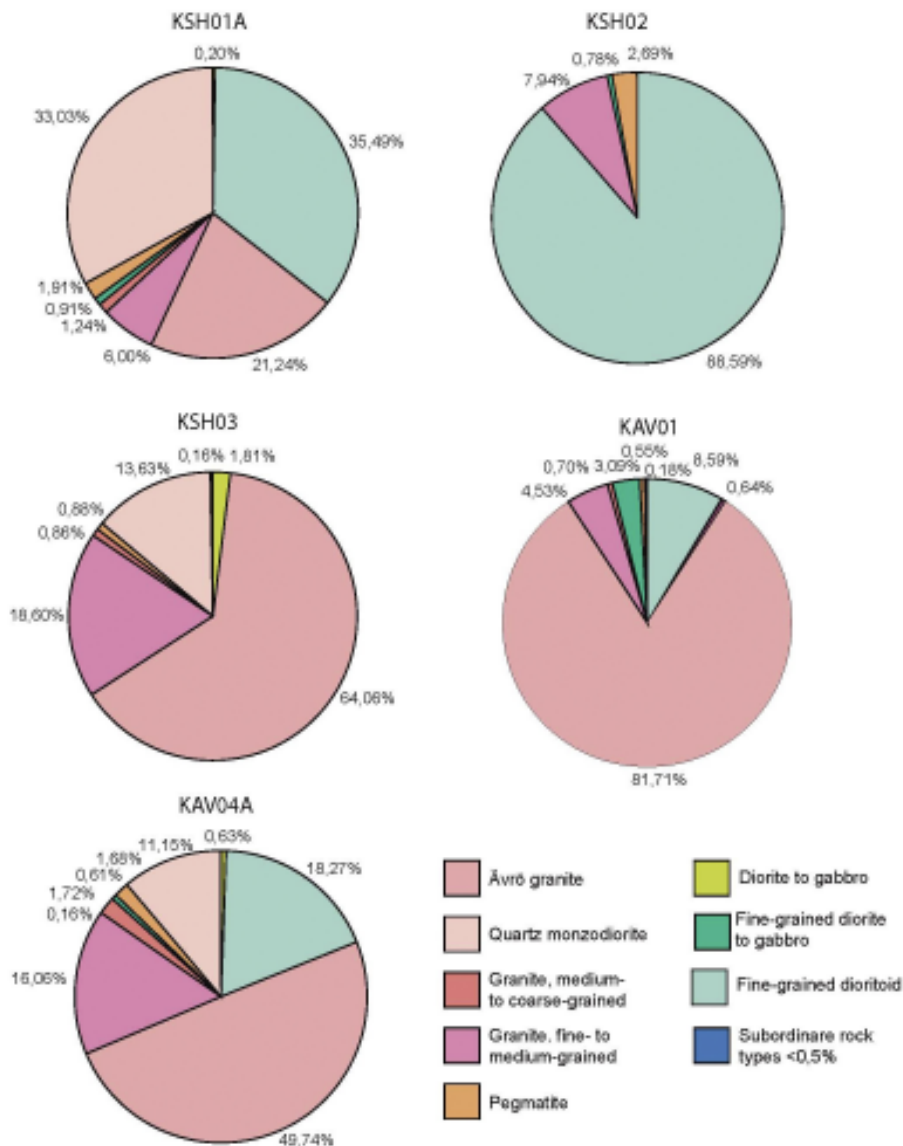


Figure 2-64. Proportion of rock types in cored boreholes in the Simpevarp subarea.

repository depth interval is considered, the proportion of Ävrö granite increases in KLX02 and KLX03, decreases in KLX04 and is the same in KLX01 in comparison to the proportion along the total borehole (cf. Figure 2-63, Figure 2-66). As can be seen in Figure 2-65, the variation (mixture) of rock types along a borehole may be unevenly distributed. In the forthcoming site descriptive modelling work, efforts will be made to try to analyse and present the variation in the distribution of subordinate rock types in the bedrock.

Table 2-4). The latter is evident from the actual distribution of these rock types along the boreholes. In KLX02 and KLX03, the quartz monzodiorite is concentrated in and dominates the sections c. 1,450–1,700 m and c. 620–1,000 m, respectively, whereas the quartz monzodiorite in KLX04 makes up several more or less long sections in the interval c. 385–745 m. Consequently, the mixture of different rock types at repository depth is different in KLX04 compared to KLX02 and KLX03. Note that the cored borehole KLX06 has been omitted what concerns the proportion of rock types at repository depth since the drill core penetrates the envisaged repository depth outside (north of) the Laxemar subarea.

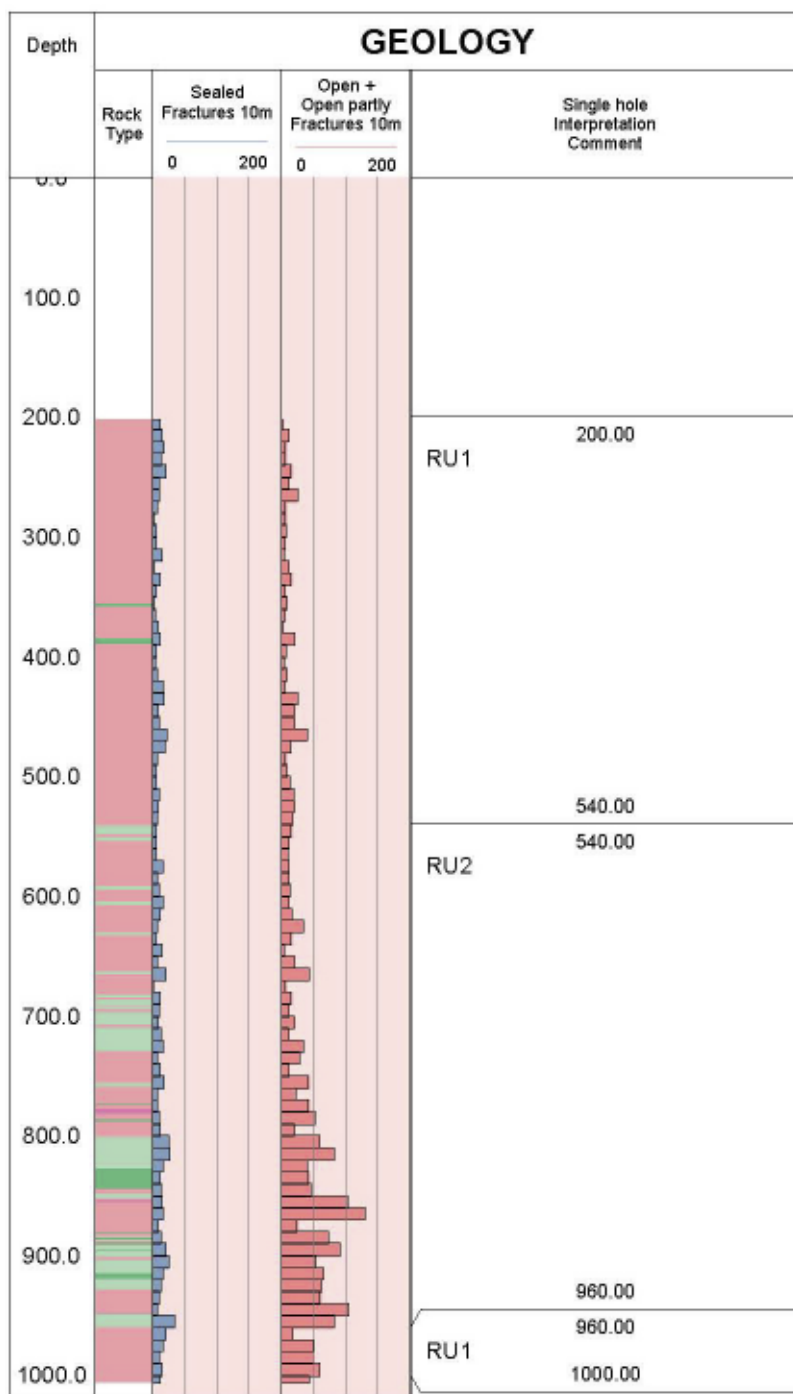


Figure 2-65. Overview of the distribution of rock types in the cored borehole KLX02. Legend of rock types according to Figure 2-63.

As can be seen in Figure 2-65, the variation (mixture) of rock types along a borehole may be unevenly distributed. In the forthcoming site descriptive modelling work, efforts will be made to try to analyse and present the variation in the distribution of subordinate rock types in the bedrock.

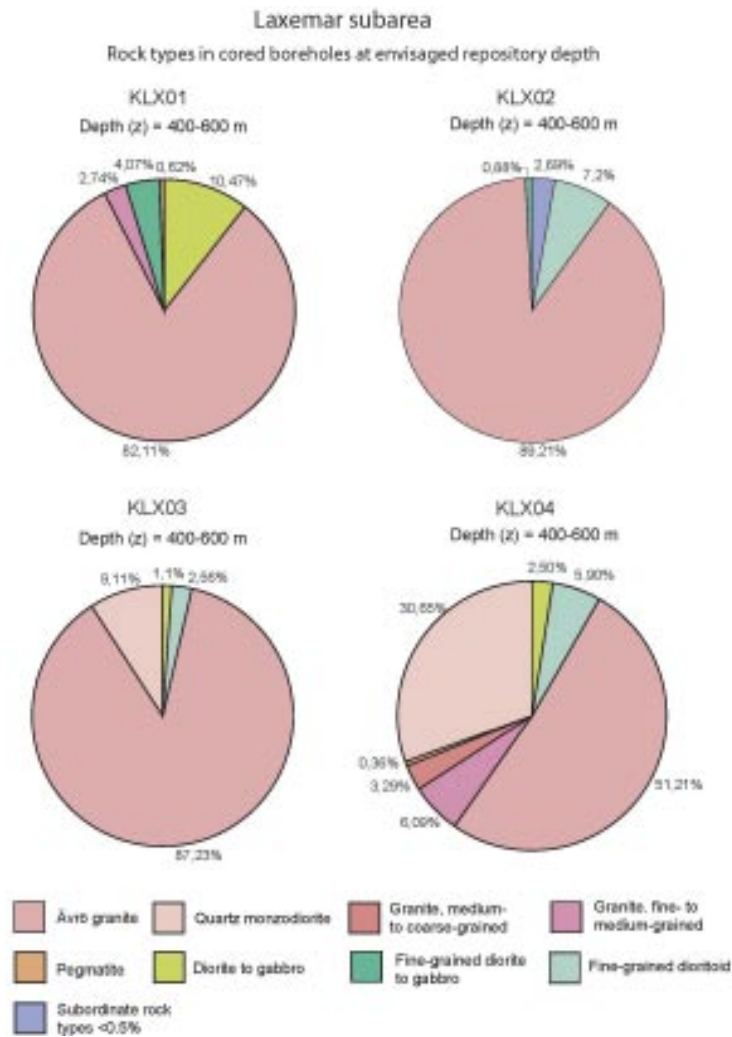


Figure 2-66. Proportion of rock types between –400 and –600 m (envisaged repository depth interval) in the Laxemar subarea, based on cored boreholes.

Table 2-4. Comparison of the proportion of rock types between total borehole length and envisaged repository depth interval (z=–400–600 m) in cored boreholes in the Laxemar subarea.

Rock type	KLX01		KLX02		KLX03		KLX04	
	Total borehole	Envisaged repository depth	Total borehole	Envisaged repository depth	Total borehole	Envisaged repository depth	Total borehole	Envisaged repository depth
Ävrö granite	82.27%	82.11%	67.24%	89.21%	56.70%	87.23%	62.15%	51.21%
Quartz monzodiorite	–	–	15.57%	–	35.74%	9.11%	13.45%	30.65%
Granite, medium- to coarse-grained	–	–	0.59%	–	–	–	11.74%	3.29%
Granite, fine- to medium-grained	3.25%	2.74%	1.38%	–	1.44%	–	5.50%	6.09%
Pegmatite	0.16%	0.62%	–	–	0.30%	–	–	–
Diorite to gabbro	4.17%	10.47%	–	–	0.95%	1.10%	0.59%	2.50%
Fine-grained diorite to gabbro	10.15%	4.07%	5.36%	0.88%	2.65%	–	2.85%	–
Fine-grained dioritoid	–	–	9.01%	7.20%	2.22%	2.56%	3.42%	5.90%
Various subordinate rock types	–	–	0.67%	2.69%	–	–	0.59%	–

The distribution of rock types in the cored boreholes clearly indicates the inhomogeneity in the bedrock from a pure lithological perspective. However, this must not necessarily be a discriminating factor without considering properties of the different rock types that may be critical for the construction of a deep repository.

Based on the Boremap mapping of the cored boreholes, the bedrock in the Laxemar and Simpevarp subareas display similar variation of rock types, apart from the cored borehole KSH02 that is drilled in the fine-grained dioritoid that dominates the southern part of the Simpevarp peninsula (Figure 2-63 and Figure 2-64).

2.4.2 Brittle structures in cored boreholes

For the evaluation of fractures in cored boreholes, see /Hermanson et al. 2005/.

2.4.3 Ductile structures in cored boreholes

As mentioned in Section 2.2.10, the rocks in the Laxemar subarea as well as in the Simpevarp subarea, generally are well-preserved and more or less isotropic, but locally a weak foliation is developed.

Foliated varieties of the rock types have also been documented in the Boremap mapping of the cored boreholes. In Figure 2-67 and Figure 2-68, orientation of all foliations documented in cored boreholes, excluding deformation zones, from the Laxemar and Simpevarp subareas is displayed, respectively. As can be seen in the figures, the majority of the foliations have been classified as weak to faint.

As can be seen in Figure 2-67, the recorded foliations from the cored boreholes in the Laxemar subarea exhibit a great deal of scatter and deviates from the NW-SE orientation documented at the surface during the bedrock mapping campaign (cf. Figure 2-49), and neither do they correlate with magnetic foliations from the AMS study (Figure 2-54). It should be noted that the majority of the recorded foliations are from KLX04 and do not represent any geographical spread.

In contrast, the orientation of the foliations recorded from the cored boreholes in the Simpevarp subarea coincides relatively well with those documented at the surface (Figure 2-49) and also with the few AMS measurements (Figure 2-55). However, the foliations documented at the surface are more steeply dipping.

The discrepancies between the orientations of the foliations documented at the surface, in the cored boreholes and the AMS study, especially for the Laxemar subarea is not understood and has to be evaluated in future work. A possible explanation for the deviating orientations between the surface and the borehole data might be that the foliations in the cored boreholes also include protomylonitic to mylonitic foliations related to shearing. The latter have been separated from the weakly developed foliations of more regional character during the bedrock mapping of the Laxemar and Simpevarp subareas /Wahlgren et al. 2004, Persson Nilsson et al. 2004/.

2.4.4 Borehole radar and geophysical logs

Besides production of an oriented image of the wall of each borehole with the help of the *Borehole Image Processing System* (BIPS) for use in the Boremap mapping of the boreholes, radar measurements and geophysical logs have been generated in all the boreholes. A combination of some of the geophysical data (e.g. density, natural gamma radiation) with the relevant petrophysical data provides a support to the mapping of the bedrock in the boreholes, especially in the percussion boreholes (see above). The borehole radar measurements and geophysical logs also provide an important input to the geological single hole interpretation (see Section 2.4.6).

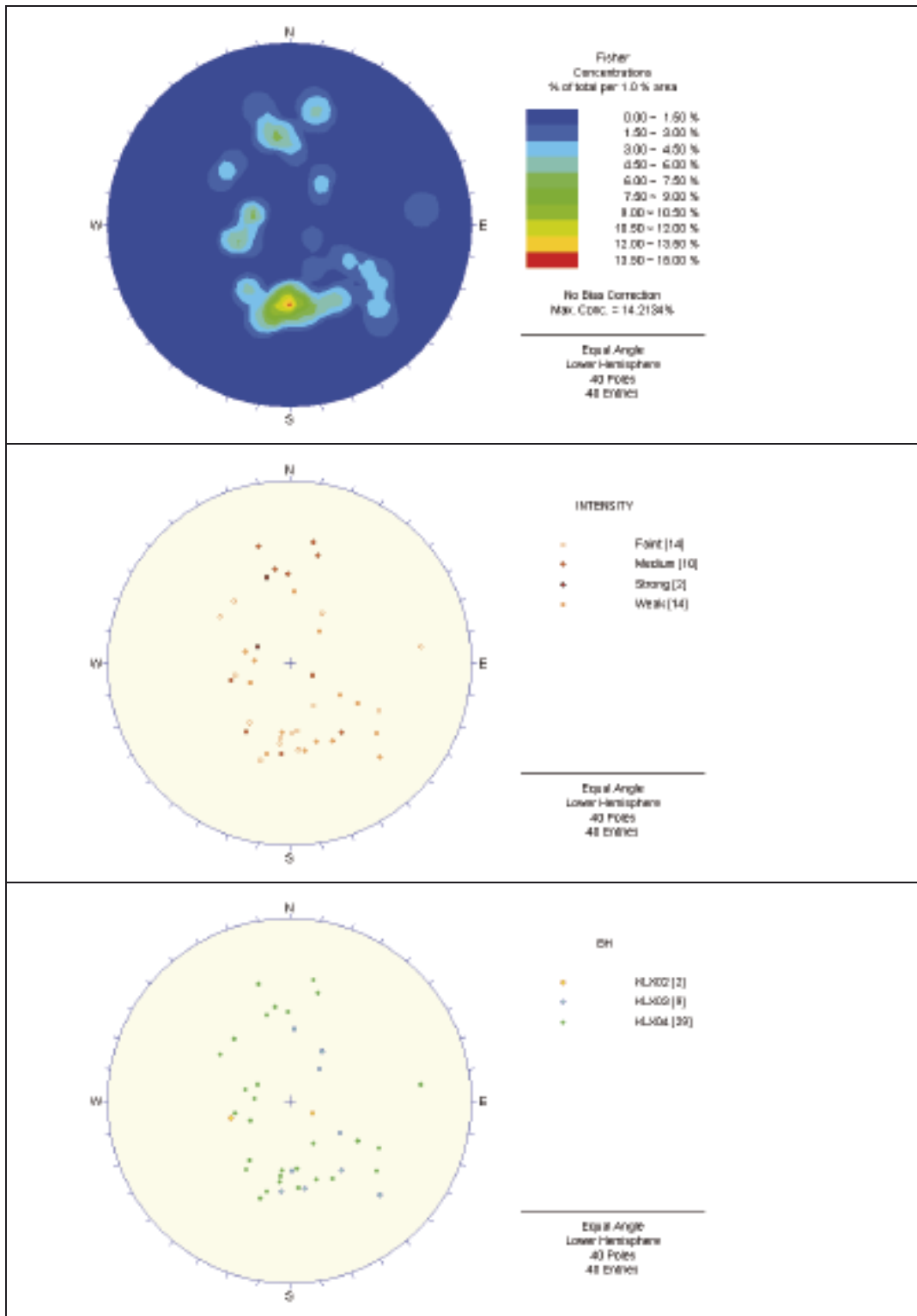


Figure 2-67. Orientation of foliations in the cored boreholes KLX02, KLX03 and KLX04 in the Laxemar subarea. Lower hemisphere of Schmidt equal area, stereographic plots.

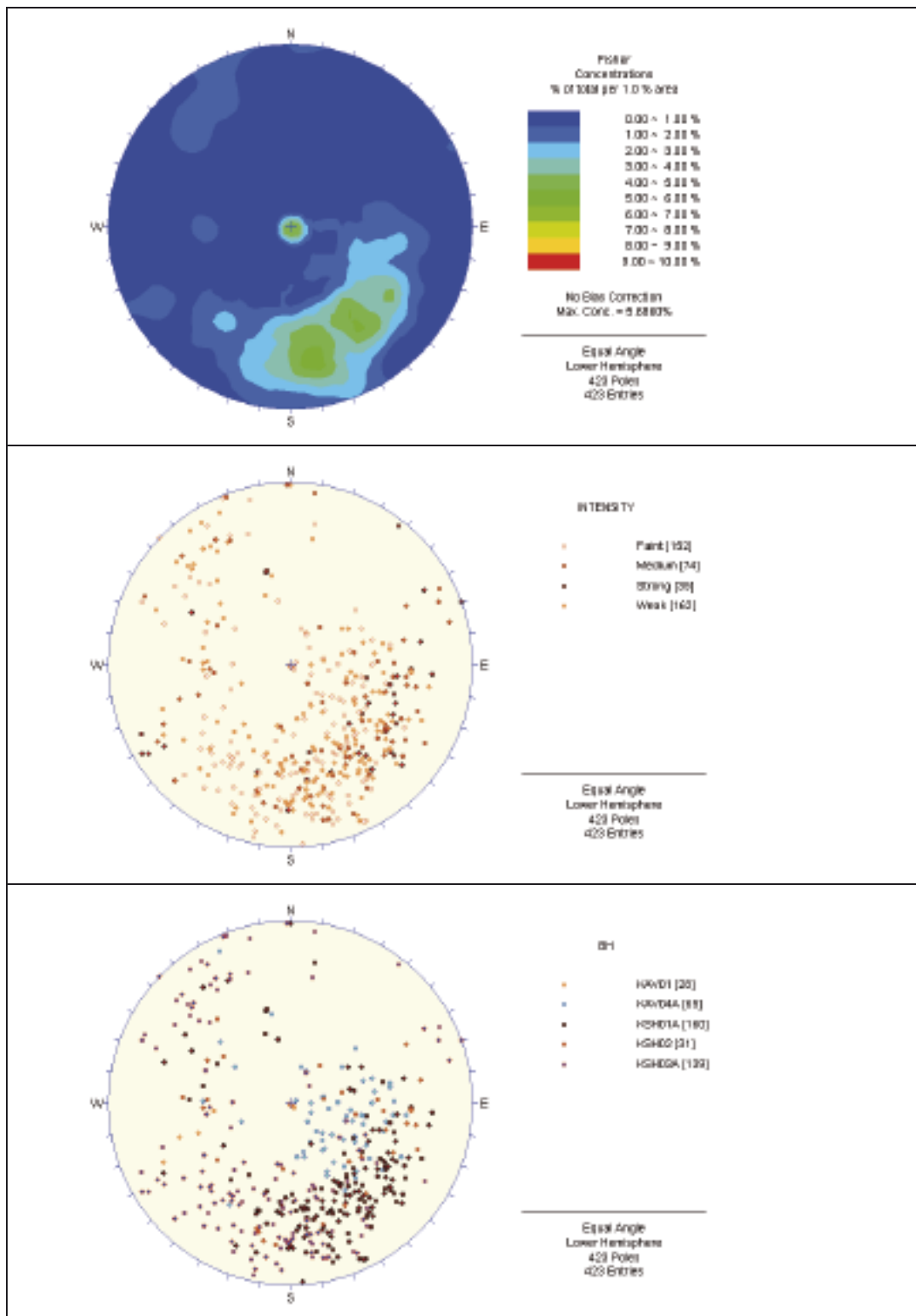


Figure 2-68. Orientation of foliations in the cored boreholes, KSH01A, KSH02, KSH03A, KAV01 and KAV04A in the Simpevarp subarea. Lower hemisphere of Schmidt equal area, stereographic plots.

The interpretation of borehole radar reflectors has been carried out for each borehole. An attempt has been made in several boreholes to document the orientation of these reflectors. However, this approach has been of varied success and the results must be treated with care.

The following geophysical data have been generated in the logging procedure for each borehole:

- Density (gamma-gamma).
- Magnetic susceptibility.
- Natural gamma radiation.
- A variety of electrical measurements (e.g. focused guard resistivity, normal resistivity, single point resistance (SPR) .
- P-wave velocity (sonic) measurements.
- Caliper measurements.

The interpretation of the geophysical logs has been carried out in a separate exercise. Density, magnetic susceptibility and natural gamma radiation measurements have been combined to provide an independent control on the composition of the rock types. The calculated silicate density, for example, can be linked to the composition of igneous rocks. However, the effects of alteration can disturb the simple correlation between density and composition. The natural gamma radiation correlates with the occurrence of fine- to medium-grained granite that commonly show significantly higher contents of thorium (see Section 2.2.7.3). Finally, the magnetic susceptibility measurements provide some constraints on the occurrence of bedrock alteration that is related to oxidation processes and the conversion of magnetite to hematite.

The occurrences of larger individual fractures have been inferred from a combined analysis of the resistivity, SPR, P-wave velocity and mean caliper measurements. The fracture frequency along sections that are 5 m in length has been calculated with the help of a calibration against the fracture frequency that was established during the mapping of several cored boreholes. However, the interpretation of fractures by this indirect method is of little use in the recognition of sealed fractures and sealed fracture networks.

2.4.5 Fracture mineralogy

Fracture minerals are mapped and determined macroscopically using the Boremap system. Many of the minerals are difficult to identify by eye and small crystals are easily overlooked. Therefore fracture mineral analyses have been carried out for identification, mainly comprising: 1) X-ray diffractometry; especially used for identification of clay minerals and gouge material composition and 2) Microscopy of fracture fillings; thin sections and fracture surfaces have been studied by SEM, /Drake and Tullborg 2004, 2006/.

The most common fracture minerals at the Simpevarp site are chlorite and calcite which occur in several different varieties and are present in most of the open fractures. Other common minerals are epidote, prehnite, laumontite, quartz, adularia (low-temperature K-feldspar), fluorite, hematite and pyrite. Fracture minerals that have been identified in small amounts include albite, harmotome (Ba-zeolite), barite, muscovite, titanite, chalcopyrite, apatite, galena, sphalerite, Ti-oxide (probably anatase), REE-carbonate, gypsum, U-silicate and apophyllite.

Clay minerals identified are in addition to chlorite; corrensitite (mixed layer chlorite/smectite or chlorite/vermiculite clay, the smectite or vermiculite layer are swelling), illite, mixed-layer illite/smectite (swelling) and a few occurrences of smectites.

Calcite has been analysed for its isotopic composition of $^{13}\text{C}/^{12}\text{C}$, $^{18}\text{O}/^{16}\text{O}$ and $^{87}\text{Sr}/^{86}\text{Sr}$ in order to sort out calcites of different generations, gain knowledge of formation conditions and support relative dating of different fracture filling generations.

2.4.5.1 Results from XRD analyses

Samples for XRD identification have mainly been taken from open and usually water conducting fractures with loose and clayish coatings, often of fault gouge type. The sampled fractures mostly occur in relation to identified (deterministic) fractures zones but also to minor fracture zones and occur at all depths throughout the drill cores. The fine fraction from each sample has been separated and oriented samples on glass were prepared for the clay mineral identification.

Most of the samples contain quartz, K-feldspar and albite in addition to calcite, chlorite and clay minerals. From previous identifications of open fractures at Äspö it is known that altered rock fragments dominate the gouge material /Andersson et al. 2002b/. It is therefore probable that most of the quartz and feldspars, together with the few observations of amphibole and biotite belong to these rock fragments or that the samples are contaminated with wall rock material. The total clay mineral contents in the open fractures is very difficult to determine in an appropriate way and the XRD analyses should not be regarded as necessarily representative for the entire filling but more of the specific sample. However, in fractures filled with fault gouge a reasonable estimate is that the amounts of clay mineral (chlorite not included) usually does not exceed 10–20 weight %. Thin coatings attached to the fracture wall can consist of 90–100% chlorite and clay minerals. The amounts are relatively small as these coatings are usually thin (< 100 m) but their surface can be very large (cf. SEM photos of clay mineral coatings in the section “Fracture mineral characteristics” below). Smectite which is significantly swelling clay mineral has been identified in a few samples. Other swelling clays like corrensite and mixed layer clay of illite/smectite are much more common.

Minerals constituting less than 5–10% may not be detected in the diffractograms and e.g. hematite and pyrite are thus left out in some analyses.

2.4.5.2 Results from microscopy and SEM studies

The fractures sampled for microscopy comprise open as well as sealed fractures from the entire boreholes. All sample descriptions and results from SEM/EDS analyses of different fracture minerals are accounted for in /Drake and Tullborg 2004, 2006/. The aim of the microscopy, in addition to identification of minerals, has been to find out different mineral parageneses and their sequences of formation and also to find out the different chemical varieties of minerals present (primarily chlorite and calcite).

The fracture mineralogy, as revealed in the drill cores shows several generations of mineralizations accounted for in Table 2-5 and Figure 2-69. Fractures are commonly re-activated, and especially in deformation zones even repeatedly re-activated. The formation temperatures of the different fracture filling generations range from moderate (greenschist facies) to low temperature conditions (zeolite facies) grading into present conditions. The outermost coatings along the hydraulically conductive fractures consist mainly of clay mineral illite and mixed layer clays (corrensite=chlorite/smectite and illite/smectite) together with calcite and minor grains of pyrite. It is assumed that especially the calcite and pyrite formation is ongoing processes although the amounts of possible recent precipitates are low.

The relative sequence of events (Table 2-5) starts with greenschist facies mylonites dominated by epidote and quartz and some chlorite (generation 1). Subsequent re-activation of the mylonites during semi-ductile conditions induced cataclasites dominated by epidote (early, generation 2a) and hematite (late, generation 2b), both in association with K-feldspar, quartz and chlorite. Coarse-grained fillings of quartz, calcite, chlorite, epidote, pyrite, fluorite and K-feldspar (generation 3) are presumed to be formed in relation to the intrusion of the adjacent c. 1.45 Ga Götemar granite /Åhäll 2001/. These fillings may be coeval with the cataclasites and the re-activation of the mylonites. The coarse-grained quartz-calcite fillings are cut by fractures filled with prehnite (generation 4) and later by calcite, laumontite, adularia, illite, Mg-chlorite and fine-grained adularia, Mg-chlorite and hematite-rich fillings (generation 5). Isotope studies



Figure 2-69. Drill-core sample from KSH03 showing fractures filled with calcite (white) cross-cutting a green filling dominated by illite.

of calcite indicate that all of these fillings are formed in rather close relation to the quartz-calcite fillings and thus not too distant in time from the intrusion of the Göttemar granite. Some of the calcite-laumontite fillings are however obviously formed later than the Göttemar intrusion but before fillings of generation 6. The minerals in generation 5c may thus be formed at several different events. Red-staining of the wall-rock due to hydrothermal alteration and oxidation is prominently related to prehnite filled fractures but also to mylonites, cataclasites and quartz-calcite filled fractures, i.e. generation 1–4, and possibly also generation 5.

Even later calcite fillings (generation 6) are assumed to be of Palaeozoic age since they cut through sandstone filled fractures of presumed Cambrian age. The calcite is sometimes found in paragenesis with some of the minerals adularia, Fe-chlorite, hematite, fluorite, pyrite, barite, harmotome, REE-carbonate, apophyllite, gypsum, illite (in ML-clay), corrensite, chalcopryrite, galena, sphalerite, Ti-oxide, U-silicate and laumontite. Fluorite from calcite-fluorite-galena filled fractures from the Göttemar granite has been dated to 405 ± 27 Ma /Sundblad et al. 2004/. The isotope composition of these Göttemar calcite-fillings as well as paragenetic minerals /Drake and Tullborg 2006/ suggest that some of the calcite in generation 6 in the Simpevarp might be of essentially the same age as the Göttemar-fillings dated by /Sundblad et al. 2004/. Even later fillings are composed of calcite and pyrite grown in open fractures at several different events until recent times.

Table 2-5. A schematic fracture filling-sequence from the oldest (1) to the youngest (7) for Simpevarp/Laxemar/Äspö is as follows:

-
1. Quartz- and epidote-rich mylonite, occasionally including muscovite, titanite, Fe/Mg-chlorite, albite, (apatite), (calcite), (K-feldspar).
 2. a. Epidote-rich cataclasite with quartz, titanite, Fe/Mg-chlorite, (K-feldspar), (albite).
 3. b. Hematite-rich cataclasite with epidote, K-feldspar, quartz, albite, chlorite.
 4. Euhedral quartz, epidote, Fe/Mg chlorite, calcite, pyrite, fluorite, muscovite, (K-feldspar).
 5. Prehnite, (fluorite).
 6. a. Calcite, (fluorite, hematite).
 7. b. Dark red/brown filling - Adularia, Mg-chlorite (also as mixed layer clay (ML-clay) with illite), hematite (quartz), (apatite); sometimes cataclastic.
 8. c. Calcite, adularia, laumontite, Mg-chlorite, quartz, illite (also as ML-clay with chlorite), hematite, (albite).
 9. Calcite, adularia, Fe-chlorite, hematite, fluorite, pyrite, barite, harmotome, REE-carbonate, apophyllite, gypsum, illite/chlorite (ML-clay), corrensite, chalcopryrite, galena, sphalerite, Ti-oxide, U-silicate, laumontite.
 10. Calcite, pyrite, FeOOH (near surface).
-

From the fracture mineral data available hitherto it can be concluded that:

The overall fracture mineralogy in Laxemar and Simpevarp subareas is very similar to earlier observations in the Äspö HRL. The frequency and intensity of different fracture mineralizations do however vary between the different subareas and Äspö.

The major differences between the fracture mineralogy in the Laxemar and Simpevarp subareas are essentially a matter of abundance and intensity of the different fracture minerals; The Simpevarp subarea shows more signs of brittle deformation with a higher degree of cataclasis-formation. These cataclasites often contain hematite and gouge. Also prehnite and associated red-stained wall rock is also more frequently found in the drill cores from the Simpevarp subarea while quartz-calcite-chlorite-pyrite-fluorite (generation 3) are more abundant in the Laxemar subarea, possibly because of the proximity to the Göttemar intrusion. Gypsum is identified in a number of fractures in KLX03 and KLX06 but has not been detected in Äspö and Ävrö islands or in the Simpevarp peninsula boreholes except for some findings in KSH03A east of fracture zone ZSMNE024A. One possible explanation is that gypsum that may have been present in the fractures is now dissolved except for in low permeable part of the rock. Apophyllite and barite are also found in a higher degree in the Laxemar subarea.

The studied drill cores are well preserved (flushing and grinding have been minimized), which has facilitated sampling of relatively undisturbed clay mineral samples. Furthermore calcite and pyrites grown on the fracture edge as well as soft or brittle zeolites minerals have been possible to study. This has e.g. resulted in the identification harmotome (Ba-zeolite), barite, apophyllite and other brittle minerals.

The red-staining of the wall rock around many fractures and fractures zones corresponds to hydrothermal alteration/oxidation, which has resulted in alteration of plagioclase to albite and K-feldspar, breakdown of biotite to chlorite and oxidation of Fe(II) to form hematite, mainly present as micrograins in secondary K-feldspar and albite in plagioclase pseudomorphs giving the red colour. However, there is not always a perfect correspondence between the extent of hydrothermal alteration and red staining. The red-staining is mainly found adjacent to early formed fractures filled with fillings of generation 1–4 (preferentially prehnite), and possibly generation 5.

Within the fractures several generations of hematite and pyrite are present. The findings of small pyrite grains in the outermost layers of the fracture coatings are in agreement with the present reducing groundwater chemistry /SKB 2006/. More detailed studies of the redox sensitive minerals and the timing of the hydrothermal oxidation is ongoing.

It has so far, not been possible to tie different fracture minerals to different fracture orientations. This has previously also been proven difficult within the large data set from Äspö /Munier 1993/.

The sequence of minerals, going from greenschist (epidote) facies in combination with ductile deformation, over to brittle deformation during prehnite facies and subsequent zeolite facies and further decreasing formation temperature series, indicate that the fractures were initiated relatively early in the geological history of the host rock and has been reactivated during several different periods of various physiochemical conditions.

The locations of the hydraulically conductive fractures are mostly associated with the presence of gouge filled faults produced by brittle reactivation of earlier ductile precursors or hydrothermally sealed fractures. The outermost coatings along the hydraulically conductive fractures consists mainly of clay minerals usually illite and mixed layer clays (corrensite = chlorite/smectite and illite/smectite) together with calcite and minor grains of pyrite.

2.4.5.3 Fracture mineral characteristics

A brief description of the most common fracture minerals in the Simpevarp area is found below along with pictures of the minerals from the area.

Epidote: $\text{Ca}_2\text{Al}_2(\text{Al},\text{Fe}^{3+})\text{OOH}[\text{Si}_2\text{O}_7][\text{SiO}_4]$

Epidote is characteristic in rocks of the greenschist and epidote-amphibolite facies, cf.

Figure 2-70. In greenschist-facies rocks, epidote is characteristically associated with chlorite, albite and quartz. Epidote also occurs as a product of the hydrothermal alteration (saussuritization) of plagioclase and along joints and fissures.

Chlorite: $(\text{Mg},\text{Fe}^{2+},\text{Fe}^{3+},\text{Al})_{12}[(\text{Si},\text{Al})_8\text{O}_{20}](\text{OH})_{16}$

Chlorite is a very common and often abundant mineral, that can be formed at temperatures up to about 400°C and pressures of a few kilo bars, cf. Figure 2-71. Partial and complete chloritization of biotite is common in the fracture wall rock. In the lower part of the zeolite facies chlorite is associated with e.g. laumontite, whereas in the upper part of the zeolite facies, chlorite occurs in assemblages with prehnite and pumpellyite. Continuous solid solution extends from Mg-rich chlorite (clinocllore) to Fe-rich chlorite (chamosite). Mg-, Mg/Fe- and Fe-rich chlorites have been identified in the Simpevarp area.



Figure 2-70. Fracture filled with epidote (green) and quartz (grey). Note the red colour of the wall rock due to hydrothermal alteration. Picture from KLX02.



Figure 2-71. Fracture filled with chlorite (arrow), calcite (white) and quartz (grey). KLX03.

Prehnite: $\text{Ca}_2(\text{Al,Fe}^{3+})[\text{AlSi}_3\text{O}_{10}](\text{OH})_2$

Prehnite is a hydrothermal mineral often associated with quartz, calcite and fluorite, cf. Figure 2-72. The upper limit of prehnite stability occurs at about 400°C at 2–4 kbar. The low-temperature alteration of prehnite may produce zeolites or chlorite/clay minerals.

Calcite: CaCO_3

Calcite is a common mineral of hydrothermal and secondary mineralization, cf. Figure 2-73. In the Simpevarp area calcite of several generations are found grading formation conditions from greenschist facies to possibly present groundwater conditions. One association commonly found is together with fluorite and barite ± sulphides. Isotope investigations on calcite (O, C, Sr) are used in order to distinguish different generations of calcite and the variation in physiochemical conditions with time.

Hematite: Fe_2O_3

Hematite is stable in the weathering environment and is commonly produced by weathering or hydrothermal alteration of iron-bearing minerals, cf. Figure 2-74. Hematite has partly replaced magnetite in the fracture wall rock and is also present mostly as minute grains covering other fracture minerals. Hematite at Simpevarp is a hydrothermal mineral.



Figure 2-72. Fracture filled with prehnite. Note the red colour of the wall rock due to hydrothermal alteration. From KSH01A.

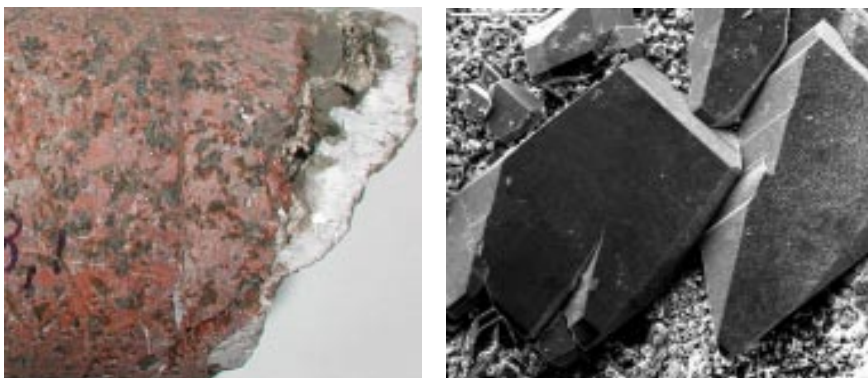


Figure 2-73. Fracture coating of calcite. KSH01. SEM-image of calcite crystals on fracture coating in open fracture. Scale bar is 200 μm . KSH01A.



Figure 2-74. Fracture surface covered with hematite. The white fracture filling is earlier formed calcite. KLX04.

Titanite: CaTiOSiO_4

Titanite may be produced by alteration of biotite or clinopyroxene in association to chloritization, cf. Figure 2-75.

Anatase (Ti-oxide): TiO_2

Anatase is a low-temperature polymorph of rutile (TiO_2) and is found as a minor constituent, cf. Figure 2-76. It also occurs as an alteration product of other Ti-bearing minerals such as titanite and ilmenite.



Figure 2-75. Fracture filled with quartz, epidote and titanite (arrows). KLX03.

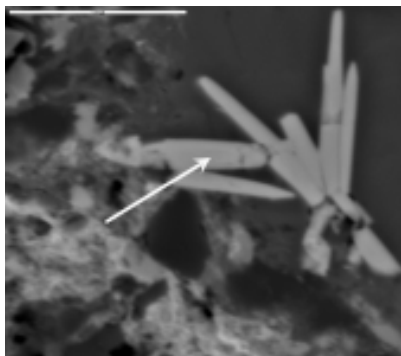


Figure 2-76. SEM-image of fine-grained anatase crystals in fracture filling from KSH01A. Scale bar is $20 \mu\text{m}$.

Albite: (Plagioclase) $\text{NaAlSi}_3\text{O}_8$

Plagioclase close to the fractures is partly or completely altered to albite, K-feldspar, sericite, saussurite, calcite, clay or zeolites, cf. Figure 2-77. Fracture fillings of albite are occasionally found in the Simpevarp area.

Pyrite: FeS_2

Pyrite is most abundant of the sulphide minerals and occurs in veins of hydrothermal origin but also in more low temperature fillings, cf. Figure 2-78. Sulphur isotope ratios are used to determine the origin of the sulphide-sulphur (hydrothermal or biogenic etc.).

Adularia: KAlSi_3O_8

Adularia is a low-temperature K-feldspar, defined based on its habitus and occurrence, cf. Figure 2-79. In most cases adularia is crystallized at low temperatures (< roughly 450°C) i.e. hydrothermal conditions. The alteration products are sericite and clay. Paragenesis may include chlorite, quartz, albite, apatite and corrensite. The colour of adularia varies but it is usually grey or greenish grey although red varieties are common in association to hematite.



Figure 2-77. Fracture filled with albite (arrow) and calcite (white) is cutting a fracture filled with prehnite. KSH01A.

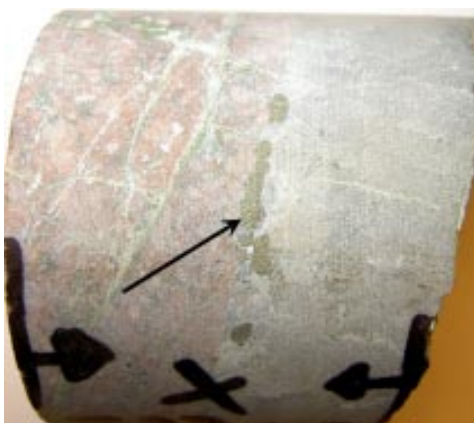


Figure 2-78. Fracture filled with quartz (grey) and pyrite (arrow). KLX03.

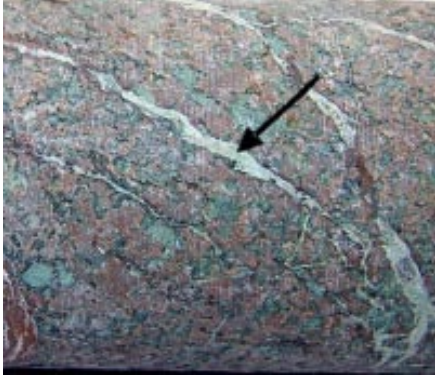


Figure 2-79. Fracture filled with adularia (arrow) and hematite (red). KSH03B.

Apophyllite: $(K,Na)Ca_4Si_8O_{20}F \cdot 8H_2O$

Apophyllite is a hydrothermal sheet silicate with white to silvery surface often associated with hydrothermal minerals like prehnite, cf. Figure 2-80.

Apatite: $Ca_5(PO_4)_3(OH,F,Cl)$

Apatite is a common accessory mineral in many types of rocks. Apatite also occurs in hydrothermal veins and cavities (Figure 2-81) and is found together with quartz, adularia, chlorite etc.



Figure 2-80. SEM-image of apophyllite fracture coating in an open fracture. KLX03. Scale bar is 200 μm .

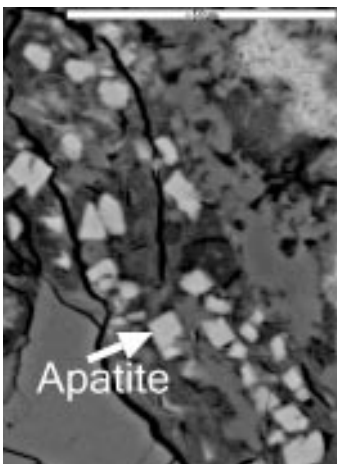


Figure 2-81. SEM-image of apatite in a sealed fracture. KSH01A. Scale bar is 50 μm .

Barite: BaSO₄

Barite is a sulphate mineral that is occasionally found in hydrothermal veins and cavity-fillings, cf. Figure 2-82. The sulphur isotope composition of barite can be used to determine the fluid composition and conditions (redox, open-closed system, bacterial influence) of formation.

Gypsum: CaSO₄ * 2H₂O

Gypsum is an easily dissolved sulphate mineral present in some fractures in the Simpevarp area (Figure 2-83). The sulphur isotope composition of gypsum can be used to determine the fluid composition and conditions (redox, open-closed system, bacterial influence) of formation.

Fluorite: CaF₂

Fluorite is a cubic mineral usually dark violet in colour and mainly hydrothermal in origin, cf. Figure 2-84. Fluorite is probably formed as a result of released F in association with breakdown of biotite along the fracture paths ways but F has also been introduced by the Göttemar granite.

Zeolites:

Zeolites are chemically related to feldspars but have much more open structures and contain water molecules. In low-grade metamorphic rocks they occur as a result of hydrothermal activity and by burial metamorphism. Zeolite minerals may alter to clay or to other zeolite minerals. Below are described the two zeolites identified at the Simpevarp site.

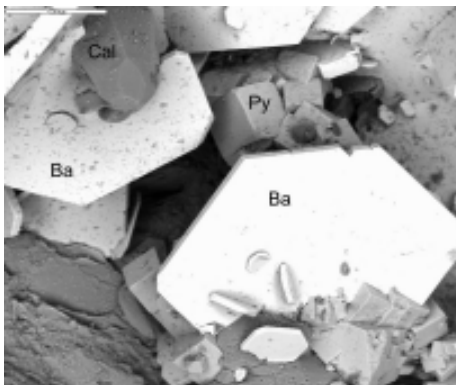


Figure 2-82. SEM-image of fracture coating in an open fracture. Fracture minerals are barite (Ba), calcite (Cal) and pyrite (Py). Scale bar is 200 µm. KLX03.



Figure 2-83. Photograph and SEM-image of gypsum and fluorite crystals on a fracture surface. Scale bar (right) is 200 µm. KLX06.



Figure 2-84. Fracture coating of purple fluorite and white calcite. KLX04.

Laumontite: $\text{Ca}_4[\text{Al}_8\text{Si}_{16}\text{O}_{48}] * 18\text{H}_2\text{O}$

Laumontite is the most widespread zeolite which occurs in large amounts in some of the deformation zones (e.g. ZSMEW002A; the Mederhult Zone), cf. Figure 2-85. It is white in colour, but may be red-stained by minute hematite crystals. The stability field of laumontite ranges from c. 150–250°C.

Harmotome: $\text{Ba}_2(\text{Na}, \text{Ca}_{0.5})[\text{Al}_5\text{Si}_{11}\text{O}_{32}] * 12\text{H}_2\text{O}$

Harmotome occurs as glassy small euhedral crystals on open fracture surfaces. It is a low temperature zeolite with a stability field that is somewhat lower than that of laumontite, although the stability field of harmotome has not been as extensively studied as that of laumontite, cf. Figure 2-86.



Figure 2-85. Fracture fillings of laumontite (arrow), calcite (white), adularia (red, coating laumontite filled fractures) and hematite-rich cataclasite (red, left). KSH03A.

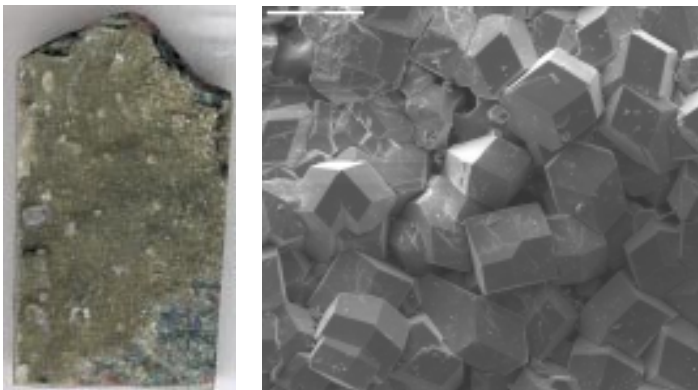


Figure 2-86. Fracture coating of harmotome. Width of photo (left): 15 mm. Scale bar on SEM-image (right) is 200 μm. KSH01A.

Clay minerals:

Illite: $(K, H_2O)Al_2[(Al,Si)Si_3O_{10}](OH)_2$

Illite occurs as micro – to cryptocrystalline, micaceous flakes. Illite is together with corrensite the most frequently found clay mineral in the Simpevarp area.

Smectite: e.g. $(Mg_3(Si_4O_{10})(OH)_2 \cdot nH_2O)$,

Smectite can vary in composition and occurs as dominantly as Mg- and Fe-rich varieties. Smectite is a swelling clay.

Mixed-Layer clays:

Mixed layer clay is usually applied on clays having alternating layers of e.g. illite and smectite, cf. Figure 2-87. The ratio between the illite and smectite layers varies due to degree of re-crystallisation; the larger the illite component the higher the formation temperature.

Mixed illite/smectite clay is swelling.

Corrensite: $((Mg,Fe)_9(Si,Al)_8O_{20}(OH)_{10} \cdot xH_2O)$

Corrensite is a chlorite-like mixed layer clay (swelling) with layers of chlorite and smectite/vermiculite, usually with ratio of 1:1, cf. Figure 2-88. Corrensite is very common in the water conducting fractures at the Simpevarp site.

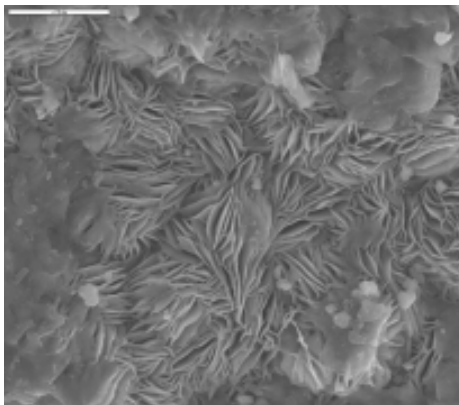


Figure 2-87. SEM photo showing mixed layer clay on a fracture surface from KSH01A (scale bar = 20 μm).

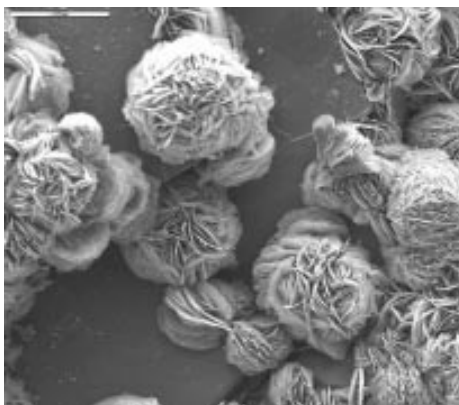


Figure 2-88. SEM photo showing corrensite aggregates on a fracture surface. (Scale bar = 200 μm). KLX06.

2.4.5.4 Fracture mineral frequencies

The above given fracture mineral description is based on detailed studies of thin sections. A statistic representation of the various fracture minerals needs however to be based on Boremap data from SICADA, although comments on suspected over/under representation of certain minerals are based on the detailed studies.

The total numbers of fractures in boreholes KLX02, KLX03, KLX04, KLX05 and KLX06 are in the order of 3,000 to 6,000 fractures/1,000 m borehole. Only 9 to 37% of these fractures are mapped as open. This figure is significantly larger for borehole KLX02 (68%) but this borehole is drilled with a less sophisticated technique (single instead of triple tube) and in addition, it has not been BIPs logged, instead, televiewer technique was applied. Together this means that the fracture mapping results from KLX02 may not be fully comparable with results from KLX03 and KLX04. Therefore KLX02 results has not been included in the plots and in order to compensate for this (get a better statistic representation) Boremap data from KLX05 and KLX06 have been included.

Based on the Boremap data the most common fracture minerals in the Laxemar subarea are chlorite and calcite (Figure 2-89 and Figure 2-90). Other common minerals are epidote, quartz, clay minerals, prehnite, laumontite, adularia (low-temperature K-feldspar), pyrite, hematite and fluorite. Quartz and epidote are more common in sealed fractures than in open fractures and clay minerals and pyrite are more common in open fractures than in sealed fractures. Prehnite is underrepresented in the Boremap data for KLX03–06 while epidote and quartz is overrepresented, since the present prehnite has been mapped as quartz or epidote.

The mineralogy in sealed and open fractures (including fractures in deformation zones, excluding crush zones) shows no significant variation with depth (Figure 2-91 and Figure 2-92). However, frequencies of calcite, pyrite and Fe-oxides in open fractures are expected to vary in the upper 100 meters due to interaction with recharge water but there are very few observations in this near surface interval so far; more near surface data will be available in forthcoming versions. Notably, pyrite is most common in the depth interval 300–600 m and gypsum is commonly found in the interval 500–600 m (vertical depth). The mineralogy in the water conducting

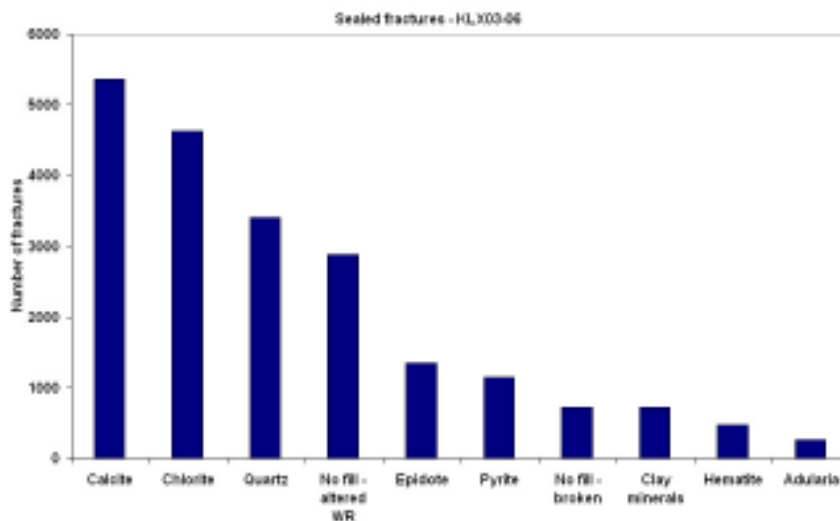


Figure 2-89. Number of observations of sealed fractures with a given mineral observed in boreholes KLX03 through KLX06 (Min1-Min4). “No fill – altered WR” = extremely narrow, sealed fractures with altered wall rock and no visible fracture filling, “No fill – broken” = most certainly broken during drilling. The total number of sealed fractures is 14,585.

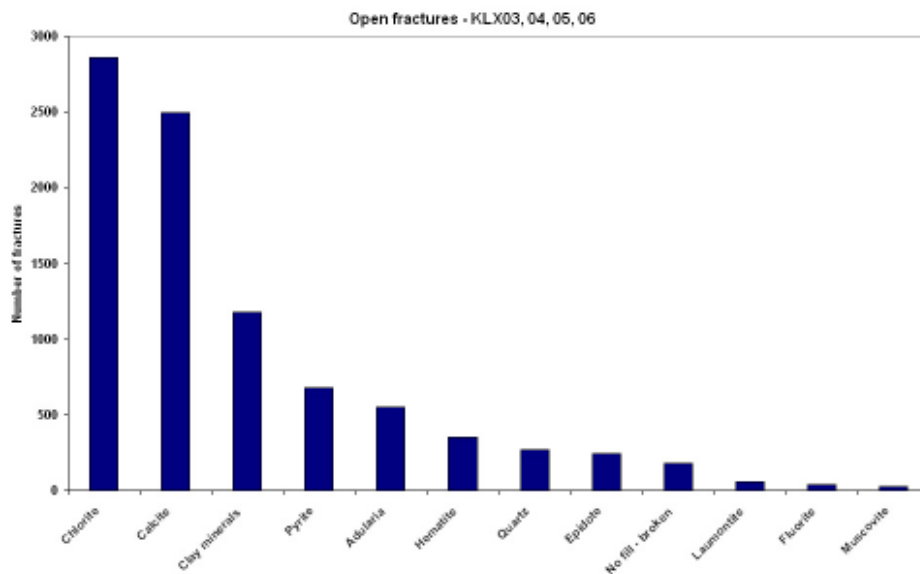


Figure 2-90. Number of observations of open fractures with a given mineral from observed in bore-holes KLX03 through KLX06 (Min1-Min4). “No fill – broken” = most certainly broken during drilling. The total number of open fractures is 4,049.

fractures is largely similar to that of the total group of fractures mapped as open (cf. Chapter 10 in L 1.2 SDM). It should be noted that the fracture mineral frequencies shown in Figure 2-89, Figure 2-90, Figure 2-91 and Figure 2-92 cannot be directly translated to amounts; e.g. pyrite is present in 5 to 30% of the fractures but the amount is still very small.

Clay minerals identified are in addition to chlorite; corrensite (mixed layer chlorite/smectite or chlorite/vermiculite clay, the smectite or vermiculite layers are swelling), illite, mixed-layer illite/smectite (swelling) and a few occurrences of smectites.

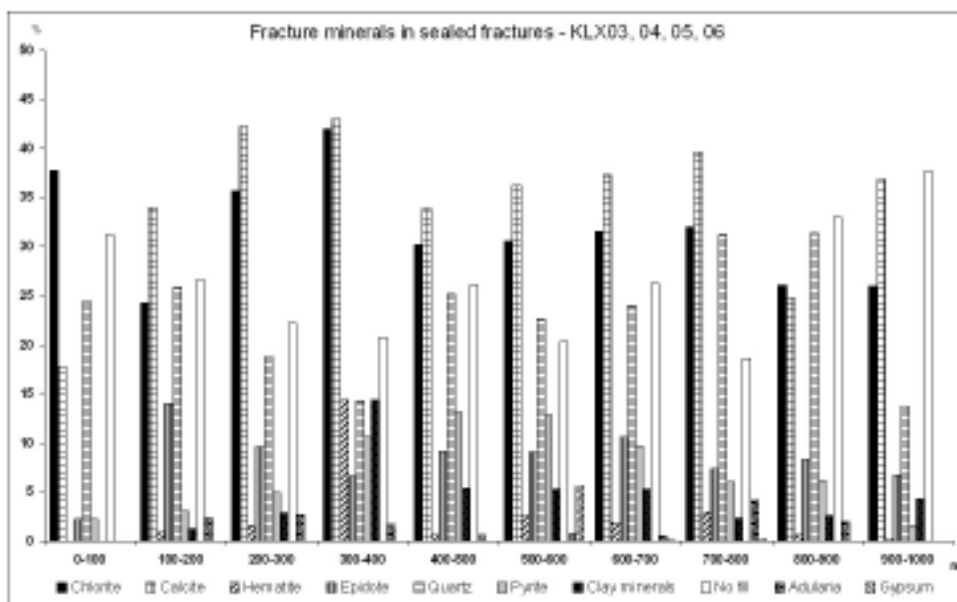


Figure 2-91. Variation in observations of fracture mineralogy (Min1-Min4) in sealed fractures as a function of depth. “No fill” = narrow, sealed fractures with altered wall rock and no visible fracture filling. Depth is given as vertical depth. Note that the observations from 0–100 m depth are very few.

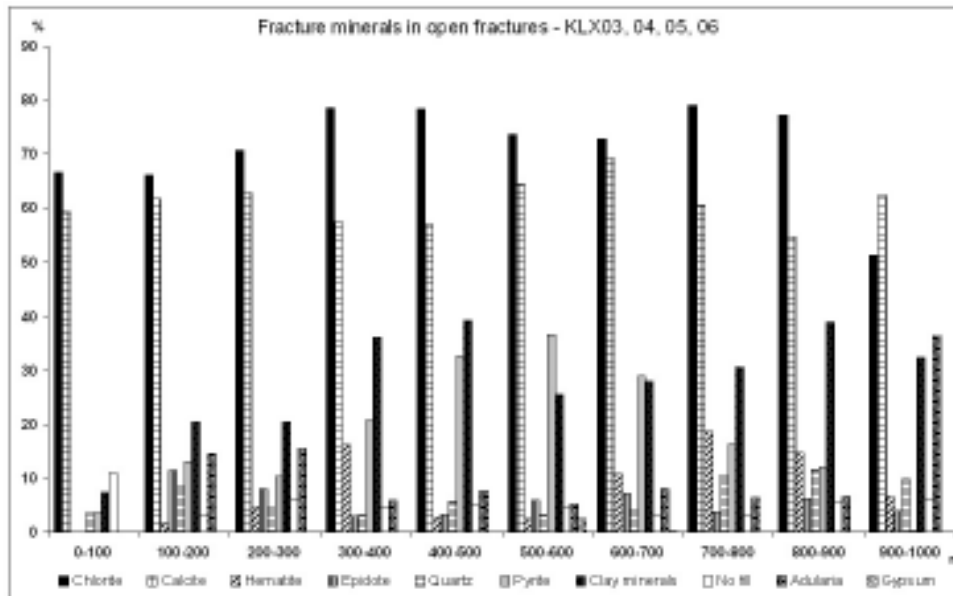


Figure 2-92. Variation in observations of fracture mineralogy (Min1-Min4) in open fractures as a function of depth. “No fill” = most certainly broken during drilling. Depth is given as vertical depth. Note that the observations from 0–100 m depth are very few.

2.4.6 Single hole geological interpretation

The single hole geological interpretation (SHI) provides a synthesis of all geological and geophysical data from a borehole. It forms an important link between all the detailed borehole data that are generated and the subsequent geological modelling work. It therefore has a similar role as the bedrock map that forms an important intermediate step between the detailed outcrop data generated during the bedrock mapping and the site descriptive modelling work. The SHI aims to document rock units with a minimum length of 5 m along the borehole as well as all deformation zones that intersect the borehole, i.e. define fixed data points at depth for the rock domain and deterministic deformation zone modelling. Note that these geological features are unique for each borehole, i.e. rock unit 1 (RU1) in one borehole may not correspond to RU1 in another borehole. Correlation of the geological data from the SHI and the surface forms an important step in the 3D modelling work.

The following data have been used in all SHI:

- Geological mapping data using BIPS and the Boremap system.
- Borehole radar data and their interpretation.
- Geophysical logs and their interpretation.

Short descriptions of the interpreted rock units and deformation zones for the cored boreholes KSH01A/B, KSH02, KSH03A/B and KLX02, and the percussion boreholes HSH01, HSH02, HSH03, HAV09 and HAV10 are provided in /Mattsson et al. 2004bc, Hultgren et al. 2004/.

The SHI of the cored boreholes KAV04A/B, KLX01 and KLX04, and the percussion boreholes HLX15, HLX21, HLX22, HLX23, HLX24 and HLX25 have also been utilised in the modelling although the P-reports were not available at the time of the analysis. Sealed fractures are distinguished from open and partly open in the fracture orientation plots.

The confidence in the interpretation of the rock units and deformation zones have been assessed using the following encoding: 3=certain, 2=probable, 1=possible.

2.4.6.1 Rock units

Ävrö granite is the dominant rock type in the majority of the defined rock units in the different boreholes. However, although the Ävrö granite may constitute the dominant rock type, different rock units can be defined based on the amount and type of subordinate rock type in the borehole section (Figure 2-93). With the exception of the Ävrö granite, quartz monzodiorite is the only rock type that dominates larger sections in the boreholes. Certain rock units do not have a rock types that are obviously dominant, but comprise a more or less complete mixture of two or more different rock types, for instance in the section 540–960 m in KLX02 (Figure 2-94).

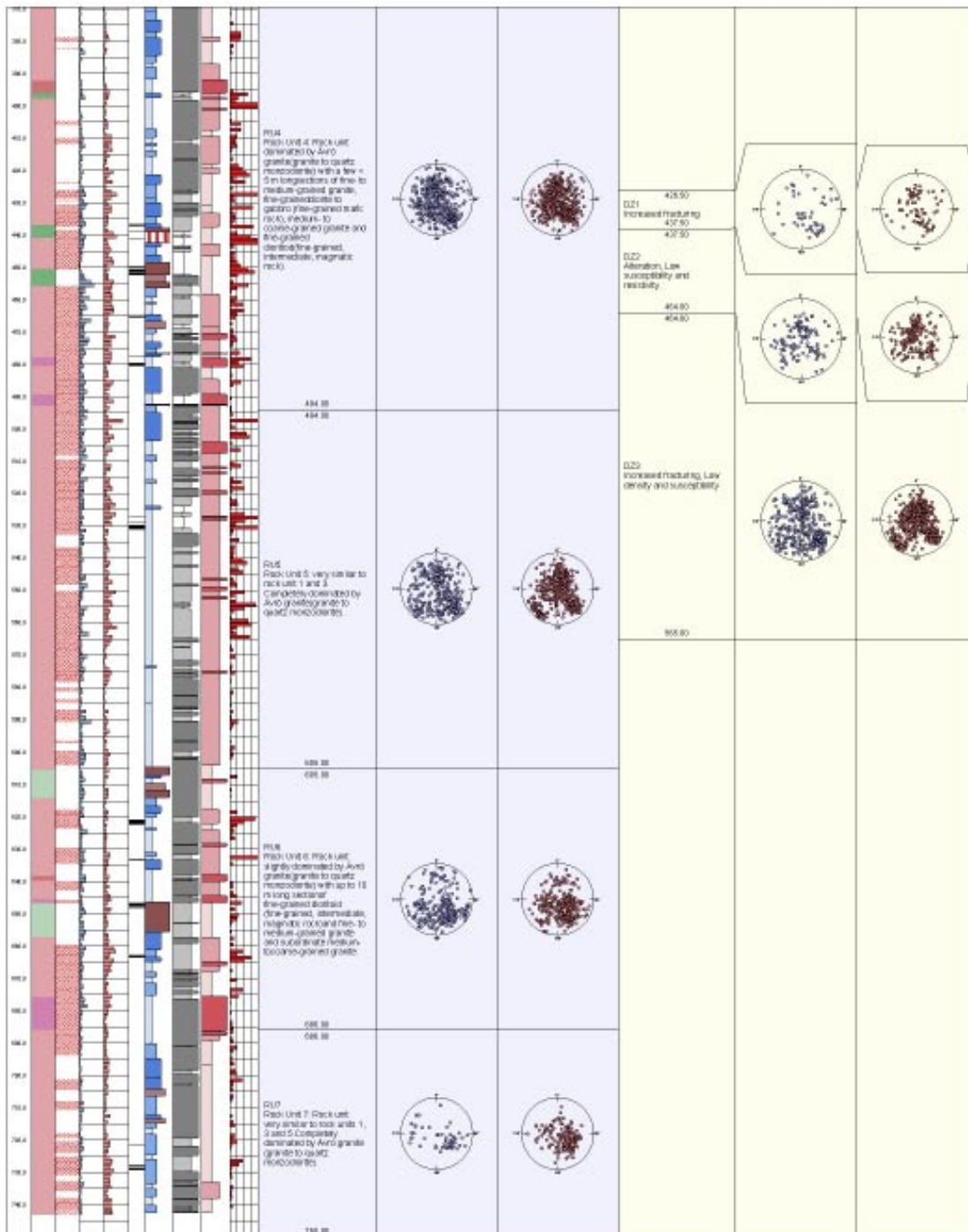


Figure 2-93. Example of different rock units in which the Ävrö granite dominates but the amount and type of subordinate rock types differ. Single hole interpretation of KAV01.

It should be noted that the Ävrö granite and the quartz monzodiorite, which constitute the two dominating rock types at the surface and in the boreholes in the Laxemar subarea, may also appear as subordinate rock types in rock units defined in the SHI. For example, the Ävrö granite may constitute a subordinate rock type in a rock unit dominated by quartz monzodiorite and vice versa. Otherwise, the subordinate rock types in the rock units are the same as at the surface. Accordingly, fine-to medium-grained granite is a characteristic subordinate rock type in most rock units.

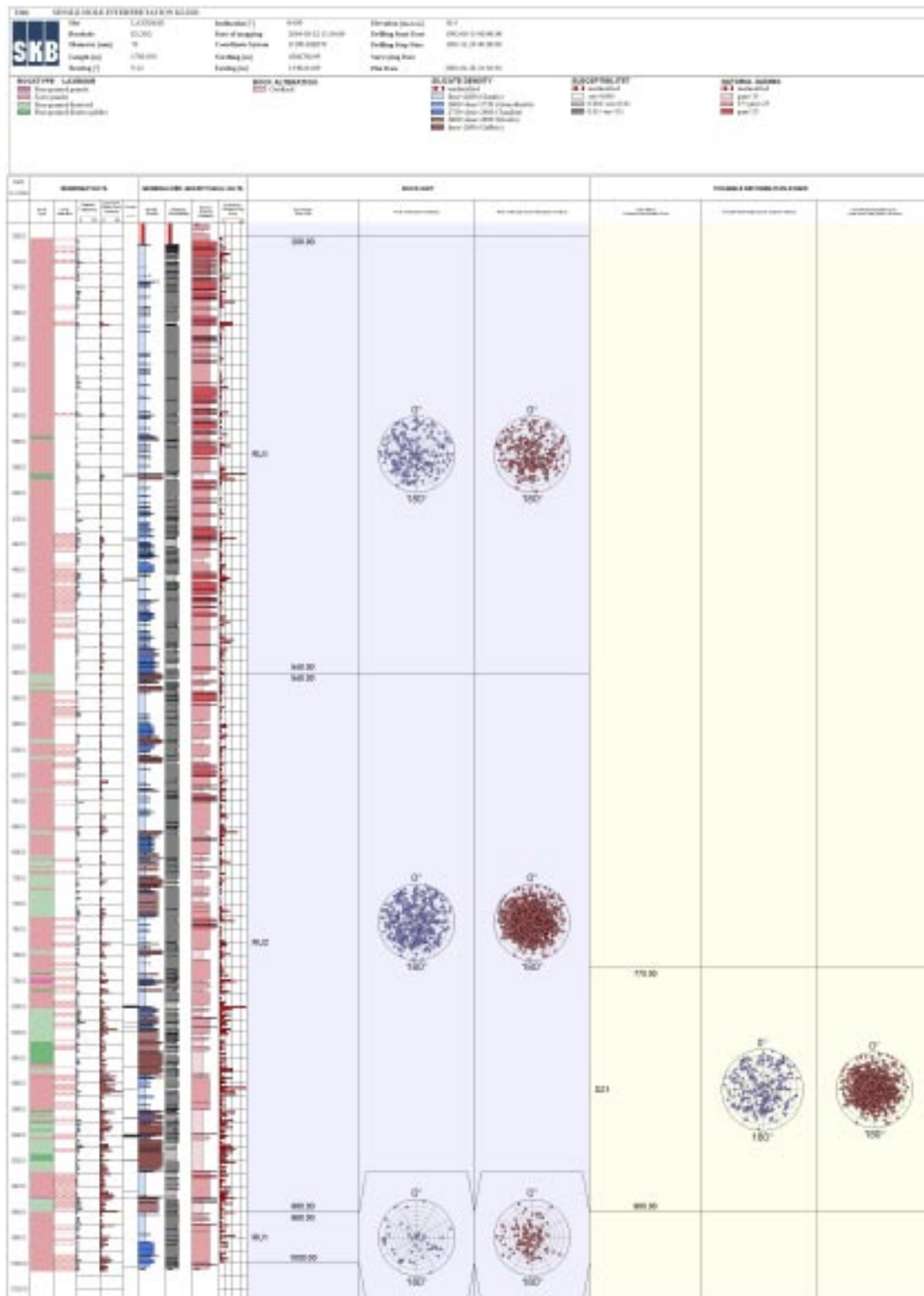


Figure 2-94. Single hole geological interpretation of KLX02 (200–1,000 m). Note the rock unit defined by the mixture of Ävrö granite and fine-grained dioritoid between 540 and 969 m.

2.4.6.2 Deformation zones

The majority of the possible deformation zones identified in the SHI are brittle in character. These zones have been recognised primarily on the basis of the frequency of fractures /Hermanson et al. 2005/, according to the recommendations in /Munier et al. 2003/. Both the transitional part and the cored part, if developed, have been included in each interpreted zone (Figure 2-95). The presence of bedrock alteration, the occurrence of an inferred orientation of radar reflectors, resistivity, SPR, P-wave velocity, caliper and magnetic susceptibility logs have also played a significant role in the interpretation of the zones.

Some deformation zones, or parts thereof, are characterised by ductile deformation under low-grade metamorphic conditions, as evidenced by protomylonitic to mylonitic or phyllonitic foliation. Purely ductile deformation zones are relatively thin, commonly a decimetre to a couple of metres in thickness, e.g. as seen in KSH01A. Most of the thicker deformation zones are characterised by brittle deformation. However, a mixture of ductile and overprinting and dominating brittle deformation is not uncommon, exemplified by the deformation zones between 162 and 275 metres in KSH03A and 722.5 and 814 in KLX03. This testifies for the importance of reactivation of the zones, by one or several phases of brittle deformation, which is characteristic for virtually all identified deformation zones.

In an ongoing study, a detailed geological characterisation, including kinematic studies, of the identified deformation zones in the SHI is carried out.

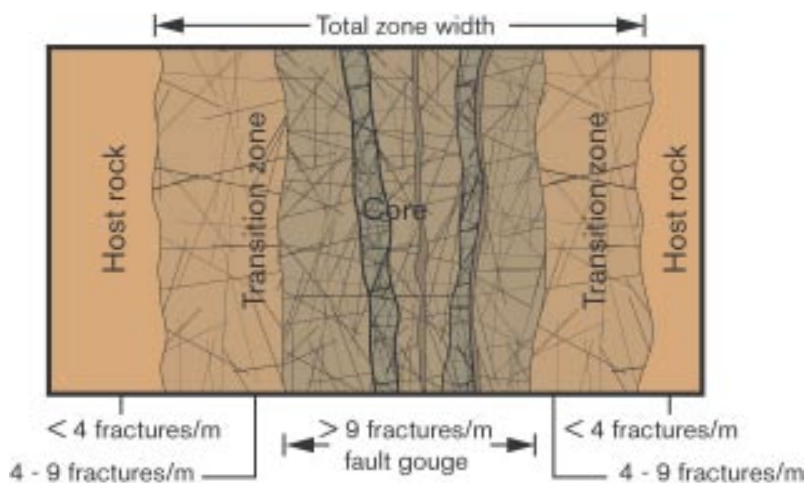


Figure 2-95. Terminology for characterisation of brittle deformation zones (after /Munier et al. 2003/).

3 Rock domain model

This section describes how the three-dimensional rock domain model of the local scale and regional model volumes has been constructed in the Laxemar SDM 1.2. The Simpevarp 1.2 site descriptive rock domain model forms the basis for present modelling which comprise the entire regional model area. In the SDM version 0 /SKB 2002/, no three-dimensional model was presented. A lithological model as a vertical section across Äspö is presented in /Rhén et al. 1997/. Also, a tentative three-dimensional rock domain model has been presented for Ävrö /Markström et al. 2001/. Furthermore, as a result of the testing of the methodology for the site descriptive modelling procedure, a three-dimensional rock domain model was presented for Laxemar /Andersson et al. 2002a/, i.e. the model area of which encompasses the easternmost part of the Laxemar subarea. However, this model has not been evaluated and incorporated in the present lithological model, mainly because the mentioned Laxemar project was designed only as a methodology test. Furthermore, there were significant limitations in the input data and the scope of analysis.

3.1 Basis for modelling

The terms rock units and rock domains are used here according to the terminological guidelines for geological site descriptive modelling given in /Munier et al. 2003/. Rock units are defined on the basis of the mineralogical composition, grain size, texture, structure and age of the dominant rock type. In particular, composition and grain size are judged to have relevance for the construction of a repository. Rock domains are defined on the basis of an integration of the rock units taking into account these geological criteria. In addition, a complex and intimate mixing of rock units has also been used as a criterion in the definition of a given rock domain.

The construction of the rock domain model in the local scale model area is principally based on existing bedrock data from the surface, i.e. the combined bedrock map of the Laxemar and Simpevarp subareas and the version 0 bedrock map in the remaining part of the model area. At depth the most important information comes from the cored boreholes KLX01, KLX02, KLX03, KLX04A/B and preliminary mapping of KLX05 and KLX06 in the Laxemar subarea, and KSH01A/B, KSH02, KSH03A/B, KAV01, KAV04A/B in the Simpevarp subarea. In addition, modelling of gravity and magnetic data /Triumpf 2004b/ is also important input information that has been used as support for the geometrical relationships between rock domains in the local scale model domain. Furthermore, modelling of gravity and magnetic data has been used to establish the geometry of the Göttemar and Uthammar granites in the regional model domain /Nisca 1987, Triumpf et al. 2003/.

The following list is a summary of important data that have been utilised in the Laxemar 1.2 rock domain modelling:

- SDM Simpevarp version 1.2.
- Combined bedrock map of the Simpevarp and Laxemar subareas (1:10 000), including outcrop databases.
- Bedrock map version 0 (1:100 000).
- Boremap data and SHI for the cored boreholes KSH01A/B, KSH02, KSH03A/B, KAV01, KAV04A/B, KLX01, KLX02, KLX03, KLX04A/B and preliminary/simplified mapping of KLX02 (1,006–1,700 m), KLX05 and KLX06.
- Modal and geochemical analyses.
- Petrophysical rock parameters.
- In situ gamma-ray spectrometric data.

- Reflection seismic data.
- Geophysical modelling based on gravimetric and magnetic data.

Apart from the cored boreholes, information from a number of percussion boreholes is available in the local scale model area (Figure 2-62). However, due to the somewhat more uncertain recognition of rock types (lack of drill core) and the limited depth to which these boreholes were drilled, they were considered to be of less importance for the rock domain modelling.

3.2 Division into rock domains

Based on the Simpevarp 1.2 modelling, the following working stages have been followed during the Laxemar 1.2 rock domain modelling:

- Integration of the new combined bedrock map of the Laxemar and Simpevarp subareas with the bedrock map that was used in the version 0 report /SKB 2002/, as well as the Simpevarp 1.2 rock domain model /SKB 2005a/.
- Definition of the areal extents of rock domains at the surface.
- Definition of rock domains in the cored boreholes.

3.2.1 Division of rock domains at the surface

The first stage in the modelling procedure includes identification of rock domains at the surface. Since the available information at depth is restricted, the identification of rock domains at the surface involves a simplification of the bedrock map, this in order to enable correlation of data at the surface with that at depth in the modelling volume.

The definition of rock domains at the surface involves seven principal rock units that originate from the bedrock map (cf. Appendix 2). These rock units and their characteristics are displayed in Table 3-1.

The simplification and integration procedures applied to the surface data have yielded a rock domain map that shows rock domains in the regional scale (Figure 3-1) and local scale (Figure 3-2 and Figure 3-3) model areas. On this basis, 33 rock domains have been identified at surface in the regional model area, 14 of which occur in the local scale model area.

Note the higher resolution in the local scale model area than in the remaining part of the model area. This is due to the much higher resolution in the bedrock map of the Laxemar and Simpevarp subareas than in the regional model area.

Table 3-1. Bedrock components used in the rock domain modelling procedure and their principal characteristics and encoding.

Rock units – composition, grain size and texture of dominant rock type			
Code (SKB)	Composition	Complementary characteristics	
501044	Granite to quartz monzodiorite	Medium-grained	Porphyritic
501036	Quartz monzodiorite	Medium-grained	Equigranular
501030	Dioritoid	Fine-grained	Unequigranular
501058	Granite	Medium- to coarse-grained	Equigranular to slightly porphyritic
511058	Granite	Fine- to medium-grained	Equigranular
501033	Diorite to gabbro	Medium-grained	Equigranular
521058	Granite (“Göttemar type”)	Coarse-grained and fine- to medium-grained	Equigranular to slightly porphyritic
Independent	Independent	Protomylonitic to mylonitic foliation	

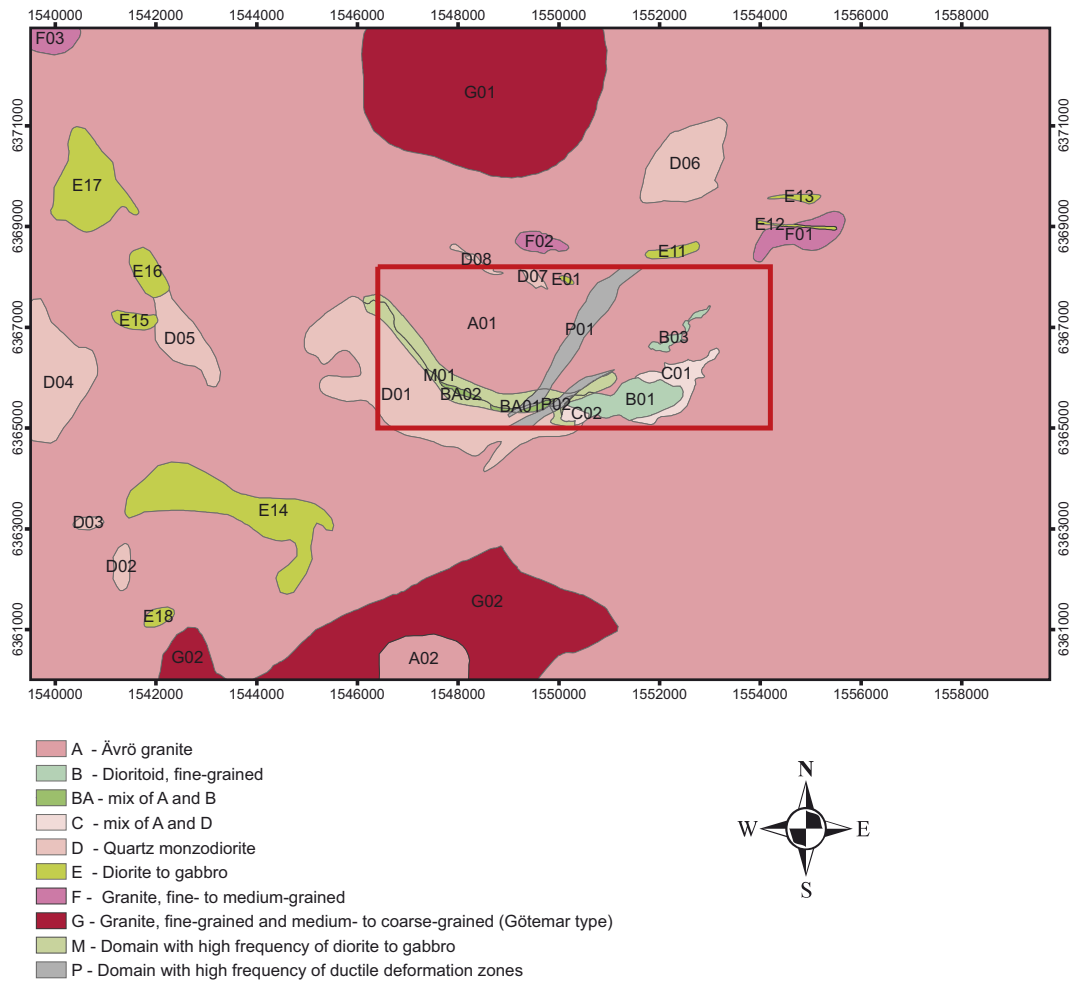


Figure 3-1. Surface view of the rock domains used in the regional model area ($N=33$), including the rock domains in the local scale model area (cf. Figure 3-2). For reasons of simplicity the prefix RSM has been excluded from the map. Note that the legend only indicates the main characteristic for the rock domain.

The rock domains have been given different codes where domains denominated with the same capital letter are dominated by the same characteristics as displayed below:

- RSMA-domains: dominated by Ävrö granite.
- RSMB-domains: dominated by fine-grained dioritoid.
- RSMBA-domains: characterized by a mixture of Ävrö granite and fine-grained dioritoid.
- RSMC-domains: characterized by a mixture of Ävrö granite and quartz monzodiorite.
- RSMD-domains: dominated by quartz monzodiorite.
- RSME-domains: dominated by diorite to gabbro.
- RSMF-domains: dominated by fine- to medium-grained granite.
- RSMG-domains: dominated by the Götemar type granite.
- RSM domains: characterized by a high frequency of minor bodies to small enclaves of diorite to gabbro in particularly Ävrö granite and quartz monzodiorite.
- RSM domains: characterized by a high frequency of low-grade ductile shear zones in the above mentioned rock types.

Rock domains of the same character that are physically separated are given different numbers, e.g. RSMC01 and RSMC02.

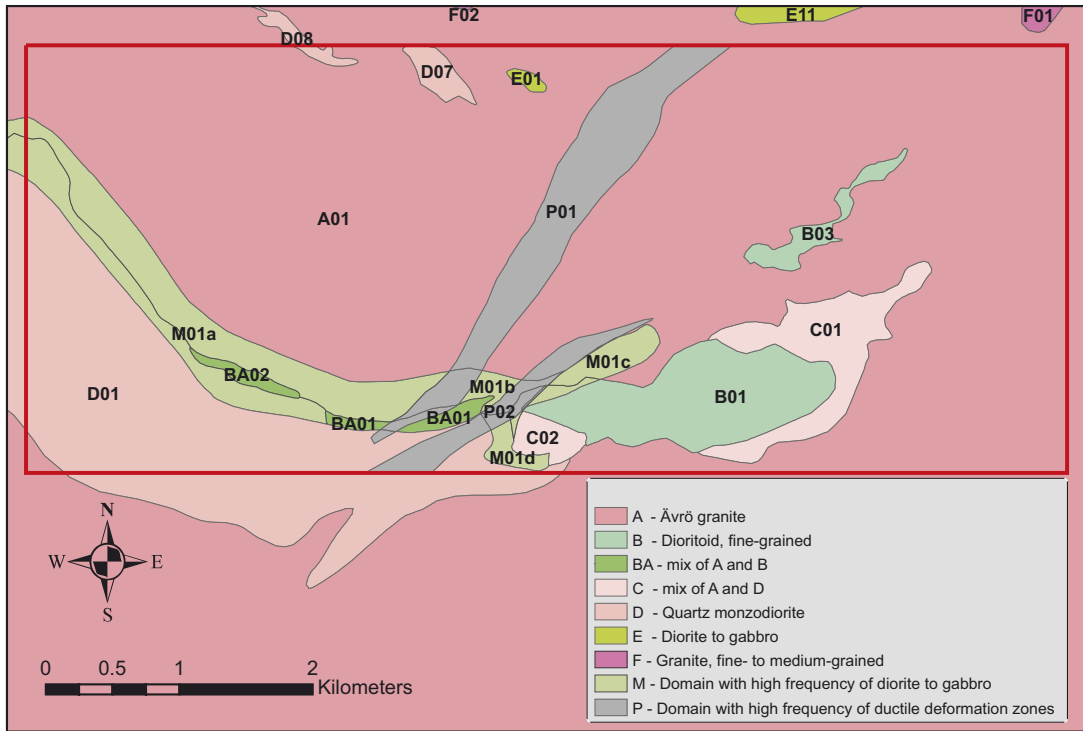


Figure 3-2. Surface view of the rock domains used in the local scale model area in the modelling procedure (N=14). For reasons of simplicity the prefix RSM has been excluded from the map. Note that the legend only indicates the main characteristic for the rock domain.

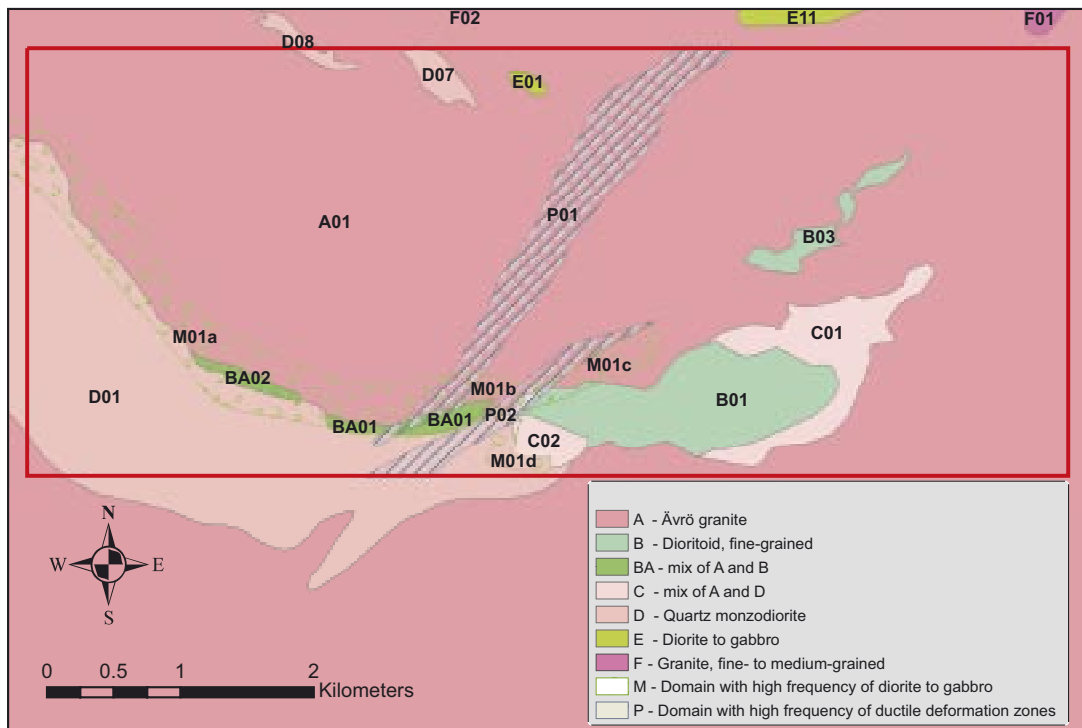


Figure 3-3. Surface view of the rock domains used in the local scale model area in the modelling procedure (N=14). The overlapping character of RSM domains are displayed by transparent raster. For reasons of simplicity the prefix RSM has been excluded from the map. Note that the legend only indicates the main characteristic for the rock domain.

As can be seen in Figure 3-2 and Figure 3-3, a number of domains overlap the boundaries of surrounding rock domains. This implies that the rock domains are in fact nested and partly inherit properties from the underlying domains (cf. Figure 3-3). This is easily visualised in 2D with a transparent raster for the RSMM01, RSMP01 and RSMP02 domains, but in 3D this kind of raster are not applicable for visualization. As can be seen in Figure 3-2 and Figure 3-3, the overlapping character of the RSMP01 and RSMP02 domains result in a subdivision of the RSMM01 domain into the subdomains RSMM01a–d.

The black line in the western part of the RSMM01 domain (RSMM01a; Figure 3-2) marks the boundary between the Ävrö granite in the northern to northeastern part and the quartz monzodiorite in the southern to southwestern part (cf. Figure 3-3), while the black line in the RSMM01c domain marks the boundary between the Ävrö granite in the north and the fine-grained dioritoid (cf. Figure 3-2 and Figure 3-3).

3.2.2 Definition of rock domains in cored boreholes

Rock domains have been defined in the cored boreholes, based on the Boremap mapping and single hole geological interpretation, as well as preliminary mapping of the drill cores from KLX05 and KLX06 (Table 3-2). The boundaries between the rock domains coincide with those reported in the SHI except for KLX05 and KLX06 since no SHI existed for these boreholes at the datafreeze.

Table 3-2. Definition of rock domains in cored boreholes. Entries in SICADA are rounded off to even metres.

Borehole	Sec up – Sec low (m)	Rock domain
KSH01A	100–322	RSMC01
KSH01A	322–631	RSMB01
KSH01A	631–1,001	RSMC01
KSH02	80–1,007	RSMB01
KSH03A	100–270	RSMC01
KSH03A	270–1,000	RSMA01
KAV01	20–750	RSMA01
KAV04A	101–289	RSMA01
KAV04A	289–690	RSMC01
KAV04A	690–1,003	RSMA01
KLX01	1–1,078	RSMA01
KLX02	200–540	RSMA01
KLX02	540–960	RSMB03
KLX02	960–1,450	RSMA01
KLX02	1,450–1,700	RSMD01
KLX03	101–798	RSMM01
KLX03	798–998	RSMD01
KLX04	101–991	RSMA01
KLX05 (Preliminary mapping)	100–400	RSMM01
KLX05 (Preliminary mapping)	400–465	RSMB01
KLX05 (Preliminary mapping)	465–649 (1,000)	RSMD01
KLX06 (Preliminary mapping)	100–995	RSMA01

3.3 Construction of the 3D rock domain model

The bedrock in both the local and regional model areas employed for the Laxemar 1.2 rock domain model is dominated by more or less pristine igneous rocks. Hence, there are, with some exceptions, no ductile structural frameworks that can be adopted as a guide for the three-dimensional geometric modelling of the domains (cf. the rock domain modelling in the Forsmark area /SKB 2005b/). The measured anisotropy of magnetic susceptibility indicates that the degree of anisotropy is only low to moderate (see Section 2.2.10.3). Thus, this anisotropy has not been considered an important guide in the construction of the geometry of the rock domains. However, the importance of the ductile structures for the geometric modelling will be more fully evaluated in future modelling work. Consequently, no real modelling concept has been applied in the downward projection of the rock domains defined at the surface. Accordingly, the shape of the rock domains is mainly determined by the defined rock domain boundaries at the surface and in the cored boreholes.

3.3.1 Arc geometry

The bedrock map of the Laxemar and Simpevarp subareas (Appendix 2) clearly demonstrate that the dominant rock types, except for the Ävrö granite that forms the matrix in the local scale model volume, are elongated and that the boundaries change orientation from northwest-southeast in the Laxemar subarea to northeast-southwest in the Simpevarp subarea. Accordingly, the rock domains follow the same trend having the concave side towards the north. This arc-shaped geometry is primarily displayed by the combined extension of the RSMD01, RSMM01, RSMB01, RSMC01 and the RSMB03 domains (Figure 3-1 and Figure 3-2).

Modelling of both gravity and magnetic data suggest that the whole arc-shaped complex is dipping to the north or northwest in the Laxemar subarea /Triumf 2004b/. This is confirmed by the definition of rock domains RSMA01 and RSMD01 in the cored boreholes KLX02, KLX03, and KLX05. The intervening rock domain RSMM01 is not that well-defined in the boreholes. However, from the bedrock map, the concentration of diorite to gabbro along the contact between the Ävrö granite in the rock domain RSMA01 and quartz monzodiorite in the rock domain RSMD01 is evident. In conclusion, there are strong indications that the general extension at depth of the boundaries between the major rock domains RSMA01, RSMD01 and RSMM01 is to the north. The geometry in the 3D modelling is primarily based on the domain intercepts in the cored boreholes, but the modelled geometry is also strongly supported by the geophysical modelling, although the latter indicates a more shallow extension at depth than that obtained from the defined domain boundaries in the cored boreholes.

There is no cored borehole in the southern part of the rock domain RSMD01. The geophysical modelling indicates that the quartz monzodiorite in rock domain RSMD01 extends much further to the south than what is indicated on the 2D rock domain map. In absence of reliable information, the southern boundary of the rock domain RSMD01 is modelled vertically towards the bottom of both the local and the regional model volume.

3.3.2 Lens geometry

The lens geometry concept implies that the dioritoid dominated domains (RSMB and RSMBA) that are aligned in the arc-shaped complex, have the shape of subvertical lenses oriented along the transitions between the above mentioned arc-shaped major rock domains. Apart from being visually appealing, this finding is supported by a number of borehole observations. The cored borehole KSH02 confirms a deep shape of RSMB01 of at least 1,000 metres. Moreover, the segment between 322 and 631 m that is defined as RSMB01 (see Table 3-2) in the cored borehole KSH01, indicates an extension of the domain at depth which could be explained by the domain being lens-shaped with its centre located below ground surface. Thus, based on subsurface information, the maximum lens radius is greater than what is visible at the surface.

Further the concept finds support in the cored borehole KLX05, which suggests a significant depth of the RSMBA01 domain as well.

Apart from being lens shaped, it is anticipated that these domains follow the same trend at depth as the surrounding major rock domains.

3.4 The 3D rock domain model

For the rock domain modelling in the Simpevarp SDM 1.2 the reader is referred to /SKB 2005a/.

No remodelling of the Simpevarp SDM 1.2 has been performed if no additional data has been available. Therefore, most of the rock domains in the regional model volume have not been modified. The exception is the geometries of the Götemar and Uthammar granites (RSMG01 and RSMG02) to the north and south of the local model area, respectively (see Figure 3-1), due to an updated geophysical modelling /Triumf 2004b/. Furthermore, some domains in the immediate surrounding of the local model area have been modified since new surface data has been available from the detailed bedrock map.

However, the new detailed bedrock map of the Laxemar subarea and surroundings, and additional information from new cored boreholes, have resulted in considerable modifications of the local scale rock domain model. Apart from defining new domains and modify the geometry of existing domains, some minor domains, particularly RSME-domains (dominated by diorite to gabbro) have been omitted from the model for simplicity reasons. These are now treated as subordinate rock types in the surrounding principal rock domain.

The local scale model volume contains a higher degree of details than the remaining part of the model. This is due to the much higher resolution in the bedrock map in the local model area, and the general lack of subsurface data in the regional model volume.

34 principal rock domains have been identified in the regional model volume, 15 of which make up the local scale model volume. Note that one of the rock domains (RSMBA03) cannot be seen in the 2D rock domain map (Figure 3-1, Figure 3-2 and Figure 3-3) since it only occurs at depth. However, in modelling terms there are far more “domains” due to the complications that arise with the nesting of domains, i.e. the overlapping character of the rock domains RSMM01, RSMP01 and RSMP02 (Section 3.2.1). Considering this, the regional model volume contains 57 and the local scale model volume 42 blocks and fragments. For example the RSMD01 domain in the regional model volume is divided into 8 blocks. One block is pure RSMD01 while three blocks lie within the RSMM01 domain and 4 blocks within the RSMP01 and RSMP02 domains.

The three-dimensional rock domain model of the regional model domain, with the local scale model domain inserted, is displayed in Figure 3-4. For the characterization of the rock domains, see Section 3.2.1.

As can be seen in Figure 3-5, the rock domains RSMA01 and RSMD01 dominate the local scale model volume. Focussing only at the Laxemar part of the local scale model volume, the RSMA01 and RSMD01 domains dominate the northern to northeastern and the southern to southwestern part, respectively. The northward extension at depth of the RSMD01 domain is confirmed by intercepts in the cored boreholes KLX02, KLX03 and KLX05.

As mentioned above (Section 3.3.1), the domains dominated by fine-grained dioritoid (RSMB and RSMBA domains), form elongated bodies along or close to the contact between the Ävrö granite in RSMA01 and the quartz monzodiorite in RSMD01 and between the RSMC01 and RSMC02 domains. Following the concept in Section 3.3.2 the domains have been modelled as lenses with a northerly extension at depth similar to RSMM01 (see Figure 3-6).

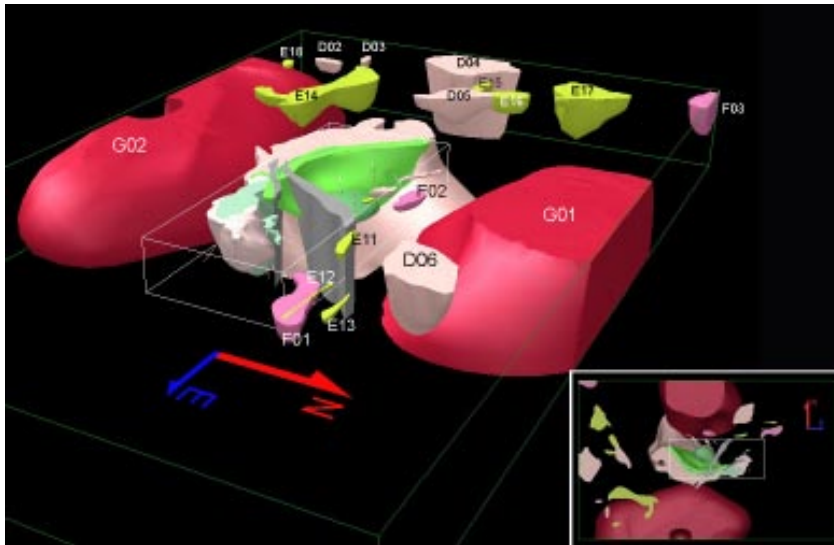


Figure 3-4. Regional rock domain model with the local scale model domain inserted. In the regional model volume, modifications are mainly restricted to the rock domains RSMG01 (Götemar granite) and RSMG02 (Uthammar granite). The Ävrö granite (RSMA01) is transparent. View from the northeast.

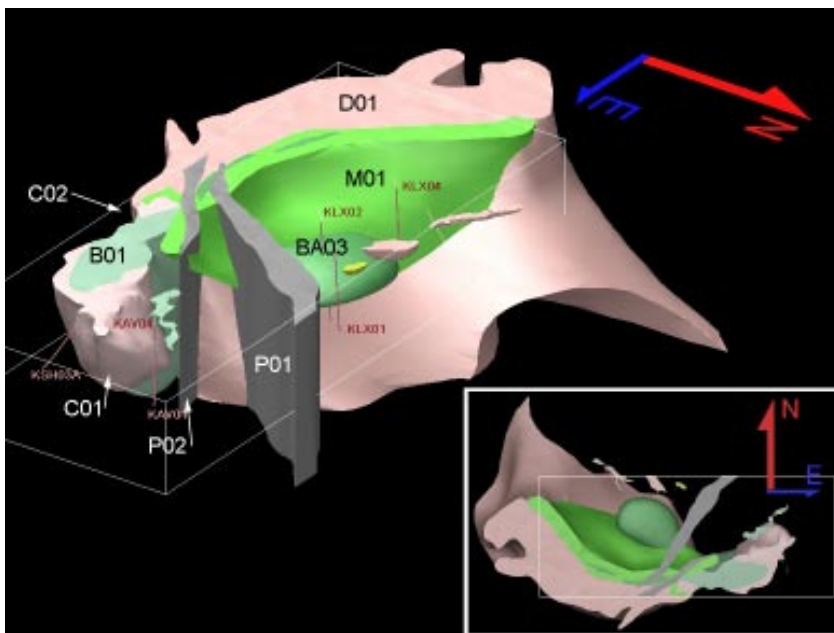


Figure 3-5. Close up of the rock domains in the local scale model volume. Note the northward extension at depth of the RSMMD01 and RSMMD01 domains. The RSMA01 domain is transparent. View from the northeast.

In the cored borehole KLX02, major segments between 540 and 960 metres are composed of fine-grained dioritoid. This section in the borehole has been defined as rock domain RSMBA03. The orientation and spatial extent of this lens-shaped domain is based on a subhorizontal seismic reflector that is interpreted to be caused by the lithological variations /Juhlin et al. 2002/. Note that this domain only occurs at depth (Figure 3-6) and is not visible in the 2D rock domain model.

The rock domain RSMB03 at the Ävrö island, northeast of the rock domain RSMB01 in the Simpevarp peninsula, was modelled already in the Simpevarp SDM 1.2. In the two cored boreholes KAV01 and KAV04A, minor sections of fine-grained dioritoid occur. However,

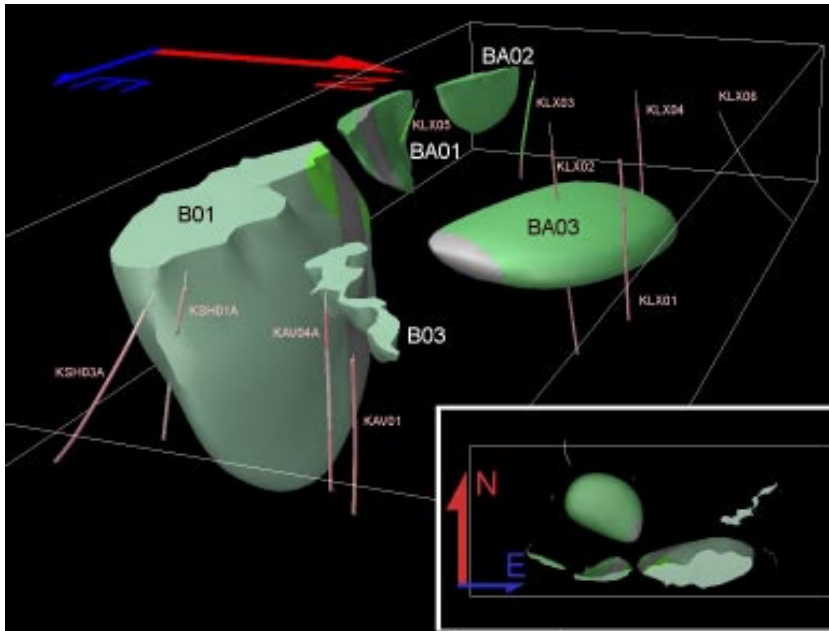


Figure 3-6. RSMB and RSMBA rock domains in the local scale model volume.

to incorporate these to be part of the rock domain RSMB03 is not reasonable. Corresponding isolated small bodies of fine-grained dioritoid were observed at the surface during the bedrock mapping and, hence, these are considered as small separate bodies in the RSMA01 and RSMC01 domains. Apart from the discussed intercepts, there is no new data concerning the RSMB03 domain. Conclusively, the RSMB03 has the same shape as in the Simpevarp SDM 1.2.

At the surface, the high frequency of diorite to gabbro that defines the rock domain RSMM01 is spatially related to the contact between Ävrö granite in the RSMA01 domain and the quartz monzodiorite in the RSMD01 domain. However, there are indications in the bedrock map that the diorite to gabbro is more spatially related to the Ävrö granite than to the quartz monzodiorite. This is also indicated at depth in the cored boreholes KLV03 and KLV05, and in the modelling of the gravity and magnetic data. Altogether, this indicates that the extension at depth of the rock domain RSMM01 does not follow the domain boundary between RSMA01 and RSMD01, but rather enters the RSMA01 domain with increasing depth.

The RSMP01 and RSMP02 domains are based on a high frequency of subvertically to vertically dipping, low-grade ductile shear zones and are modelled vertically to the bottom of both the local scale and regional model volume. The modelling of the RSMP01 and RSMP02 domains have been restricted to the local scale model area due to the uncertain continuation and extension of the low-grade ductile shear zones outside the local scale model area.

In the Simpevarp subarea, the geometry of rock domain RSMC01 has been modified since a segment between 289 and 690 metres in the cored borehole KAV04A has been identified as part of the domain.

3.5 Property of rock domains

3.5.1 Assignment of properties

Each rock domain has been assigned a set of properties (Table 3-3), including, for example, the dominant and subordinate rock types in the domain. All properties are presented in tabular format in Appendix 3.

For the rock domains situated within the Laxemar and Simpevarp subareas, the properties of the rock domains (Table 3-3) have been extracted from the outcrop databases and complementary mineralogical, geochemical and petrophysical data (see Section 2.2 and 2.2.7). Additional information is available in the data from the Boremap mapping of the cored boreholes KSH01A/B, KSH02, KSH03A/B, KAV01, KAV04A/B, KLX01, KLX02, KLX04A/B and preliminary/simplified mapping of the cored boreholes KLX05 and KLX06 (see Section 2.4). Only limited information is available from the bedrock compilation for rock domains or those parts of rock domains that are situated outside the Laxemar and Simpevarp subareas.

An example of the property tables presented in Appendix 3 is displayed for rock domain RSMA01 in Table 3-4.





Table 3-3. Properties assigned to each rock domain.

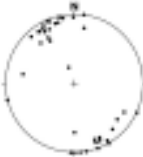

Rock domain ID (RSM***, according to the nomenclature recommended by SKB).
Property
Dominant rock type.
Mineralogical composition
Grain size
Age (million years)
Structure
Texture
Density
Porosity
Magnetic susceptibility (SI units)
Electric resistivity in fresh water (ohm m)
Uranium content based on gamma ray spectrometric data (ppm)
Natural exposure ($\mu\text{R/h}$)
Subordinate rock types.
Degree of inhomogeneity.
Metamorphism/alteration (%).
Mineral fabric (type/orientation).

Table 3-4. Property table for rock domain RSMA01.

RSMA01 Property	Character	Quantitative estimate	Confidence	Comment
Dominant rock type (%)	Ävrö granite (501044)	54–92	High	The quantitative estimate is based on occurrence in KSH03A, KAV01, KAV04A/B, KLX02, KLX04 and the Äspö tunnel (section 2,265–2,874 m).
Mineralogical composition (%) (dominant minerals)	Quartz	18.8±6.3	High	N=61. The quantitative estimate is based on modal analyses of surface samples from the Simpevarp and Laxemar subareas and samples from KSH01A, KSH03A, KAV01. Mean value ± std
	K-feldspar	17.6±8.5		
	Plagioclase	46.5±8.4		
	Biotite	10.5±4.9		
Grain size	Medium-grained		High	Based on outcrop database for the Simpevarp and Laxemar subareas and its immediate surroundings.

RSMA01 Property	Character	Quantitative estimate	Confidence	Comment
Age (million years)		1,800±4	High	U-Pb zircon-titanite dating of Ävrö granite
Structure	Isotropic to weakly foliated. Scattered mesoscopic, ductile shear zones		High	Based on outcrop database for the Simpevarp and Laxemar subareas and its immediate surroundings.
Texture	Unequigranular to porphyritic		High	Based on outcrop database for the Simpevarp and Laxemar subareas and its immediate surroundings.
Density (kg/m ³)		2,716±40	High	N=81. The quantitative estimate is based on surface samples from the Simpevarp and Laxemar subareas and samples from KAV01, KAV04A and KLX01. Mean value ± std
Porosity (%)		0.44±0.19	High	N=79. The quantitative estimate is based on surface samples from the Simpevarp and Laxemar subareas and samples from KAV01, KAV04A and KLX01. Mean value ± std
Magnetic susceptibility (SI units)		3.390±0.29	High	N=81. The quantitative estimate is based on surface samples from the Simpevarp and Laxemar subareas and samples from KAV01, KAV04A and KLX01. Average value in logarithmic scale ± std
Electric resistivity in fresh water (ohm m)		3.98±0.20	High	N=79. The quantitative estimate is based on surface samples from the Simpevarp and Laxemar subareas and samples from KAV01, KAV04A and KLX01. Average value in logarithmic scale ± std
Uranium content based on gamma ray spectrometric data (ppm)		4.0±1.4	High	N=67. The quantitative estimate is based on measurements on outcrops from the Simpevarp and Laxemar subareas, and a few measurements from the remaining part of the regional model area. Mean value ± std
Natural exposure (microR/h)		11.4±2.2	High	N=67. The quantitative estimate is based on measurements on outcrops from the Simpevarp and Laxemar subareas, and a few measurements from the remaining part of the regional model area. Mean value ± std
Subordinate rock types (%)	Fine- to medium-grained granite (511058)	1–22	High	The quantitative estimate is based on occurrence in KSH03A, KAV01, KAV04A, KLX02, KLX04, outcrop ASM000208 and the Äspö tunnel (section 2,265–2,874 m)
	Pegmatite (501061)	0–1		
	Fine-grained dioritoid (501030)	2–21		
	Diorite to gabbro (501033)	0–12		
	Fine-grained diorite to gabbro (505102)	0–5		
	Quartz monzodiorite (501036)	1–14		

RSMA01 Property	Character	Quantitative estimate	Confidence	Comment
Dykes of fine- to medium-grained granite (511058)	Orientation	Mean pole=338/12 K=1.5	High	N=72. Measurements from the local model area west of RSMP01 and RSMP02 and north of ZSMEW007A. Based on outcrop database for the Laxemar subarea and immediate surroundings. Mean pole is marked with a star.
				
		Mean pole=336/7 K=4.6	High	N=8. Measurements from the local model area west of RSMP01 and RSMP02 and south of ZSMEW007A. Based on outcrop database for the Laxemar subarea and immediate surroundings. Mean pole is marked with a star.
				
Pegmatite (501061)	Orientation	Mean pole=325/12 K=0.8	High	N=20. Measurements from the local model area west of RSMP01 and RSMP02 and north of ZSMEW007A. Based on outcrop database for the Laxemar subarea and immediate surroundings. Mean pole is marked with a star.
				
		Mean pole=297/9 K=0.4	High	N=5. Measurements from the local model area west of RSMP01 and RSMP02 and south of ZSMEW007A. Based on outcrop database for the Laxemar subarea and immediate surroundings. Mean pole is marked with a star.
				
Degree of inhomogeneity	Low		High	Based on outcrop database for the Simpevarp and Laxemar subareas and KSH03A, KAV01, KAV04A/B, KLX01, KLX02 and KLX04. The degree of inhomogeneity may locally be higher.
Metamorphism/alteration (%)	Inhomogeneous hydrothermal alteration (secondary red staining)	14–59	High	The quantitative estimate is based on faint to weak, including subordinate medium and strong, oxidation in KSH03A, KAV01, KAV04A, KLX01, KLX02 and KLX04 outside interpreted deformation zones in the single-hole interpretation. Epidotization, saussuritization, sericitization and chloritization also occur in subordinate amounts, varying between 0 and 3%.

RSMA01 Property	Character	Quantitative estimate	Confidence	Comment
Mineral fabric (type/orientation)	Weak magmatic to tectonic foliation	Mean pole = 337/3 K= 3.6 	High	N=41. Measurements from the local model area <i>east of</i> rock domains RSMP01 and RSMP02. Based on outcrop database for the Simpevarp and Laxemar subareas and immediate surroundings. The stereogram includes poles to all foliation measurements irrespective of rock domain. Mean pole is marked with a star.
		Mean pole = 24/3 K= 0.8 	High	N=105. Measurements from the local model area <i>west of</i> rock domain RSMP01 and RSMP02. Based on outcrop databases for the Laxemar subarea and immediate surroundings. The stereogram includes poles to all foliation measurements irrespective of rock domain. Mean pole is marked with a star.

Important properties for the construction of rock domains are composition, grain size and texture of the different rock types. In addition, structure is of vital importance for the characterization of the RSMP domains.

By using the information in the outcrop database from the Laxemar subarea, it has been possible to estimate qualitatively the relative amounts of the different rock types in each domain. For similar qualitative estimate for the Simpevarp subarea, see the Simpevarp SDM 1.2 /SKB 2005a/.

For example, in rock domain RSMA01, the lithology that forms the dominant rock type is the Ävrö granite, i.e. medium-grained, porphyritic granite to quartz monzodiorite (Figure 3-7). However, fine- to medium-grained granite, medium- to coarse-grained granite, pegmatite, fine-grained dioritoid, diorite to gabbro, fine-grained diorite to gabbro and quartz monzodiorite form subordinate rock types (Figure 3-7). Similar semi-quantitative information concerning the proportions of dominant and subordinate rock types in most of the remaining rock domains within the Laxemar subarea is presented in Appendix 4.

Based on the mapping of rock types in the cored boreholes KLX01, KLX02, KLX03, KLX04A, KLX05 and KLX06 in the Laxemar subarea, an estimate of the proportion of different rock types in the rock domains has been performed by quantifying the total occurrence in terms of borehole length in metres and the percentage of the total length of the core for the different rock types (Figure 3-8, Figure 3-10 and Figure 3-12). The same quantification has been carried out for the cored boreholes KSH01A, KSH02, KSH03A, KAV01 and KAV04A in the Simpevarp subarea (Figure 3-9, Figure 3-11 and Figure 3-13). A corresponding quantification was presented in the Simpevarp SDM 1.2 report, but the quantification has been updated in connection with the Laxemar 1.2 modelling work and the mapping of the cored borehole KAV04A has been added. This quantification is another estimate of the proportions of different rock types in the rock domains that complements the estimate based on the outcrop database.

An estimation of the percentage proportion of rock types in the RSMM01 domain (Figure 3-14) has been carried out as interpreted from the preliminary mapping of the cored borehole KLX05, the detailed bedrock map of the outcrop ASM000209 (outcrop for detailed fracture mapping, Figure 2-28) and the distribution of rock types in the bedrock map.

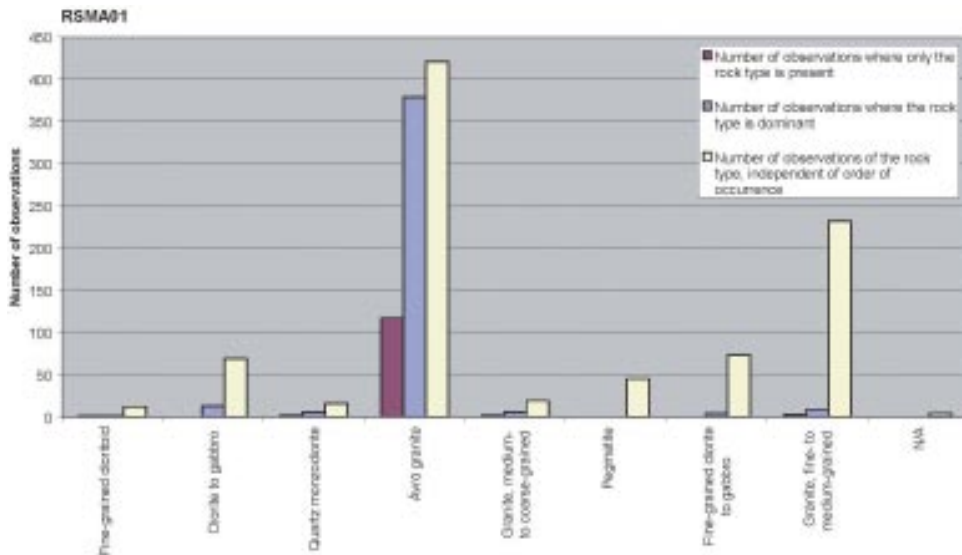


Figure 3-7. Qualitative assessment of dominant and subordinate rock types in rock domain RSMA01 (Ävrö granite) based on surface outcrop data from the bedrock mapping of the Laxemar subarea. Note that in the outcrop database, rocks are stored in relation to their order of occurrence at the observation point,

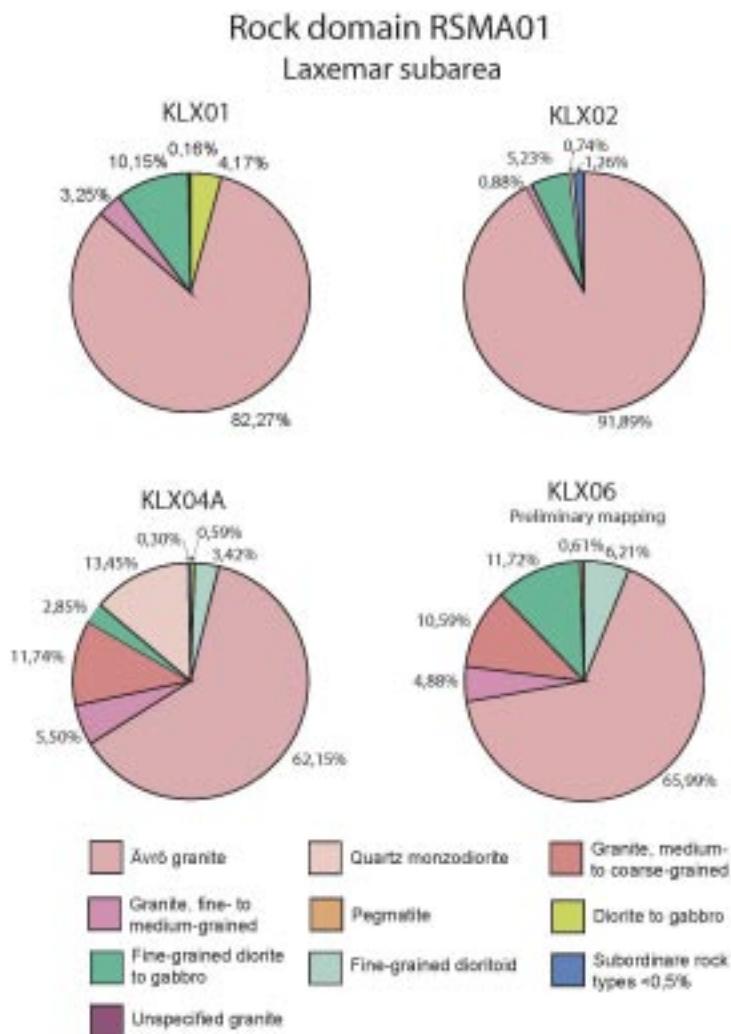


Figure 3-8. The proportion of different rock types in the rock domain RSMA01 in the Laxemar subarea, as interpreted in the cored boreholes KLX01, KLX02, KLX04 and KLX06.

Rock domain RSMA01
Simpevarp subarea

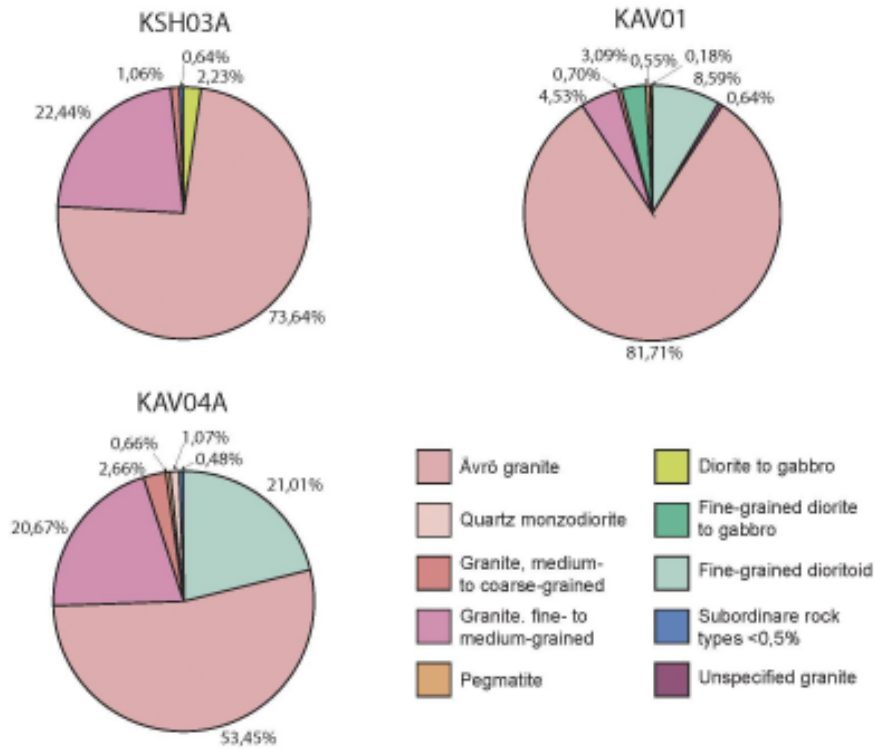


Figure 3-9. The proportion of different rock types in the rock domain RSMA01 in the Simpevarp subarea, as interpreted in the cored boreholes KSH03A, KAV01 and KAV04A.

Rock domains RSMBA
Laxemar subarea

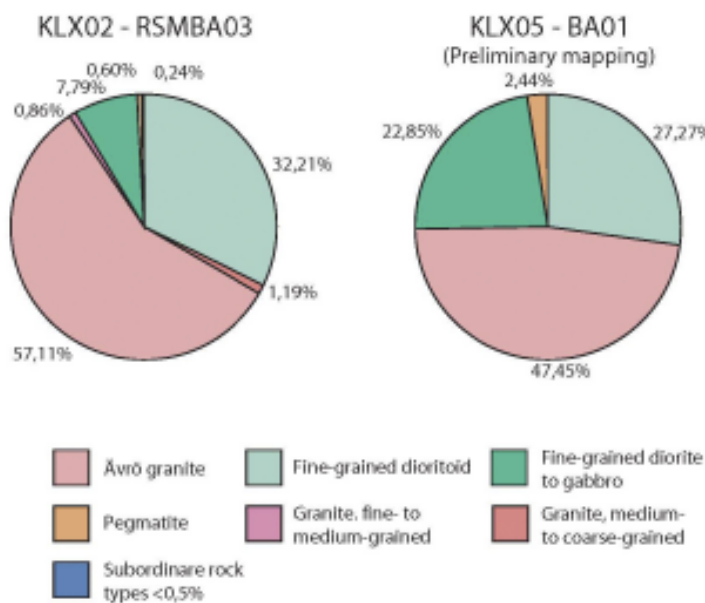


Figure 3-10. The proportion of different rock types in RSMBA rock domains in the Laxemar subarea, as interpreted in the cored boreholes KLX02 and KLX05.

Rock domain RSMC01
Simpevarp subarea

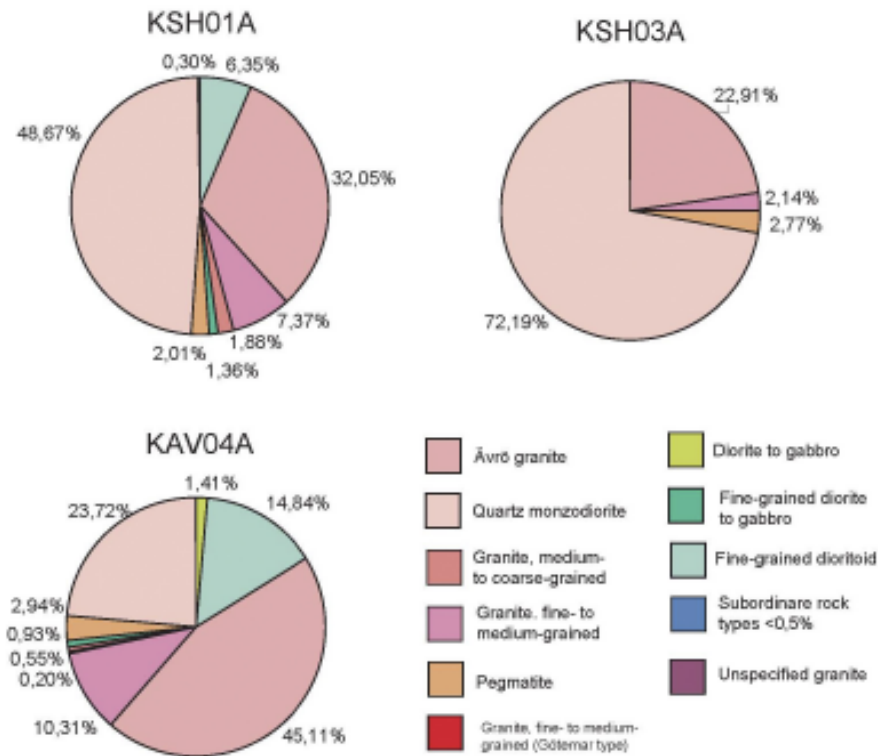


Figure 3-11. The proportion of different rock types in rock domain RSMC01 in the Simpevarp subarea, as interpreted in the cored boreholes KSH01A, KSH03A and KAV04A.

Rock domain RSMD01
Laxemar subarea

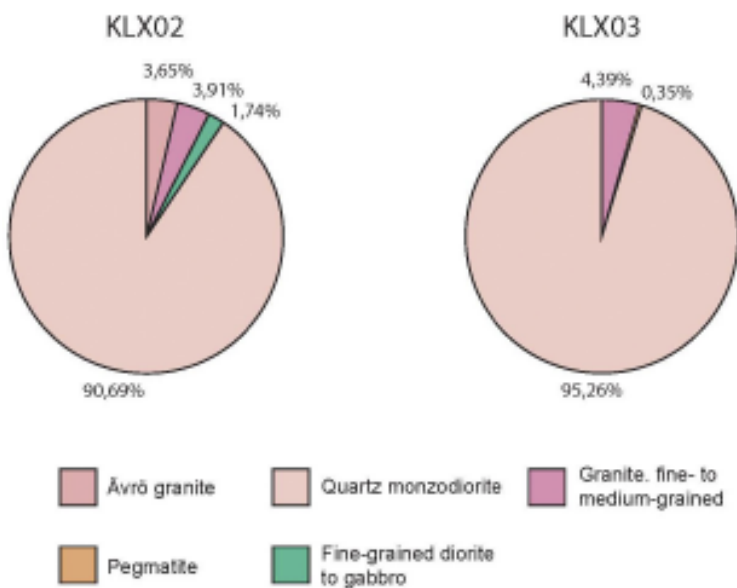


Figure 3-12. The proportion of different rock types in rock domain RSMD01 in the Laxemar subarea, as interpreted in the cored boreholes KLX02 and KLX03.

Rock domain RSMB01

Simpevarp subarea

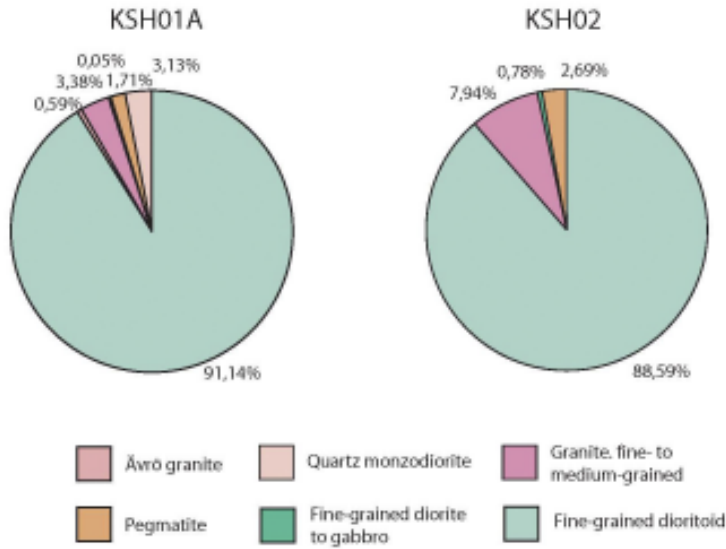


Figure 3-13. The proportion of different rock types in rock domain RSMB01 in the Simpevarp subarea, as interpreted in the cored boreholes KSH01A and KSH02.

Rock domain RSMM01

Laxemar subarea

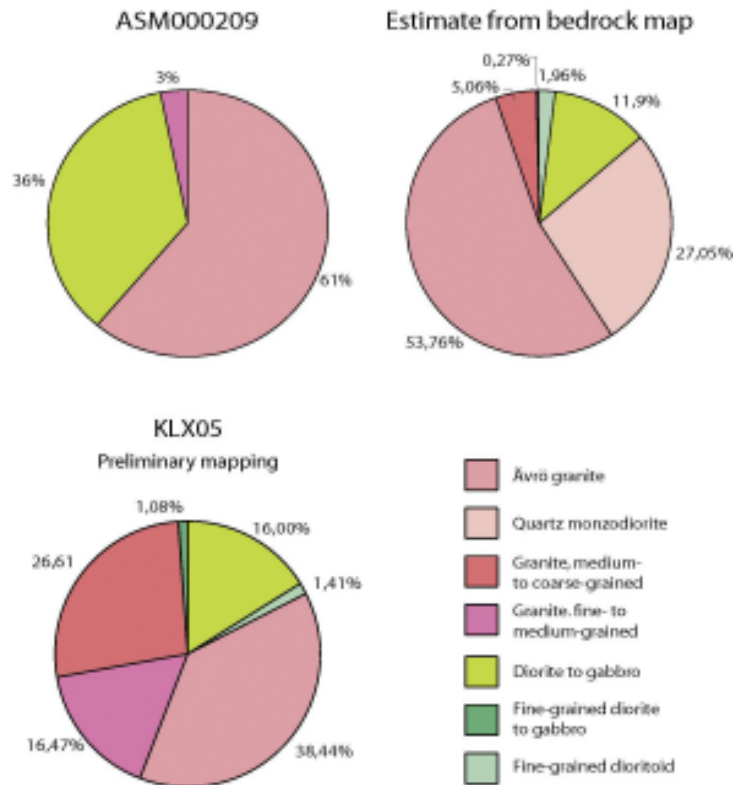


Figure 3-14. The proportion of different rock types in rock domain RSMM01 in the Laxemar subarea, as interpreted from the outcrop ASM000209, bedrock map and preliminary mapping of the drill core from KLX05.

Another property of the bedrock that are of importance, in particular for the thermal modelling, is the compositional variation of the rock types, particularly the Ävrö granite, that display a compositional variation from quartz monzodiorite to granite (see Section 2.2.5.1). In Figure 3-15, the variation in quartz content in the quartz monzodiorite and the Ävrö granite between different domains is displayed. As can be seen the quartz content is generally low and the variation between the domains is obvious. This has implications for the thermal conductivity and thereby thermal modelling

Furthermore, the orientation of the granitic and pegmatitic dykes (see Section 2.2.5.8) is an important anisotropy that might affect the thermal conductivity in the bedrock.

Another factor of inhomogeneity that has to be considered is an inhomogeneously distributed hydrothermal alteration (faint to strong), i.e. secondary red staining but also saussuritization, by using the data from the Boremap mapping of cored boreholes, but excluding the interpreted deformation zones. An estimate for rock domain RSMA01 in the Laxemar subarea is displayed in Figure 3-16. Estimates of the hydrothermal alteration in RSMM01 and RSMD01 in the southern part of Laxemar, based on KLX03, are presented in Figure 3-17. As can be seen in Figure 3-16 and Figure 3-17, the alteration is generally low to weak in character.

The estimate of alteration in the rock domains RSMA01, RSMB01 and RSMC01 in the Simpevarp subarea is presented in the Simpevarp SDM 1.2 report.

3.6 Evaluation of ore potential

The Simpevarp regional model area is dominated by intrusive rocks, i.e. dioritoids-syenitoids and granites that belong to the c. 1,810–1,760 Ma generation of the Transscandinavian Igneous Belt (TIB), which by experience is more or less devoid of metallic mineralisations. The only candidate for metallic mineralisations in the Simpevarp regional model area is the c. 1,450 Ma old Götömar type granite, that is judged to have a potential for tin (Sn) and tungsten (W), although no mineralisations of this type have so far been found. Consequently, the Simpevarp regional model area may be considered as sterile what concern ores and metallic mineralisations. Furthermore, there is no potential for industrial minerals /Lindroos 2004/.

Exploration of commercial stones, predominantly ornamental stones, has from time to time been extensive in southeastern Sweden, but has gradually declined and is of limited extent nowadays. However, the Götömar type granites have a potential for exploration of ornamental stones and one quarry is in operation in the Götömar granite.

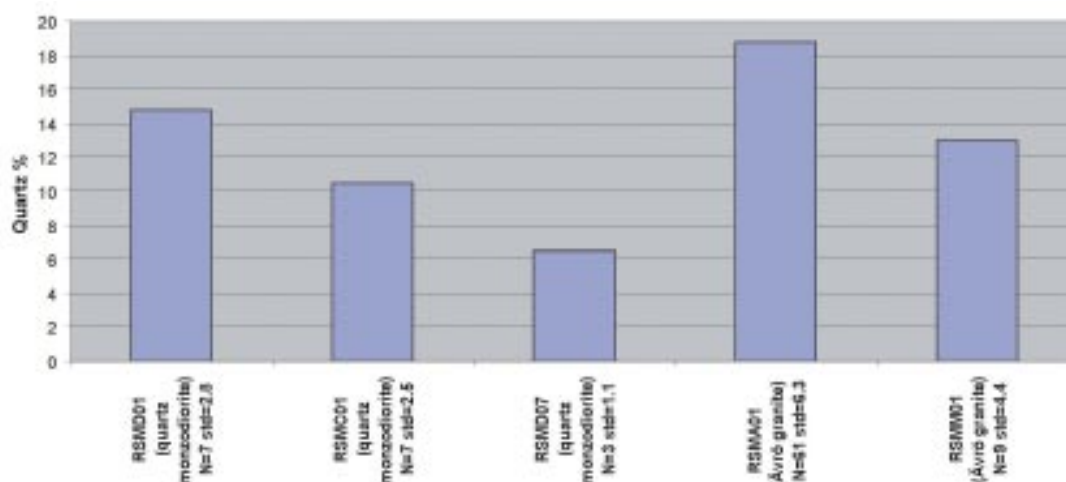


Figure 3-15. Quartz content (mean value) in quartz monzodiorite in RSMD01, RSMC01 and RSMD07 and in Ävrö granite in RSMA01 and RSMM01.

RSMA01 - alteration (mainly oxidation)
Laxemar subarea

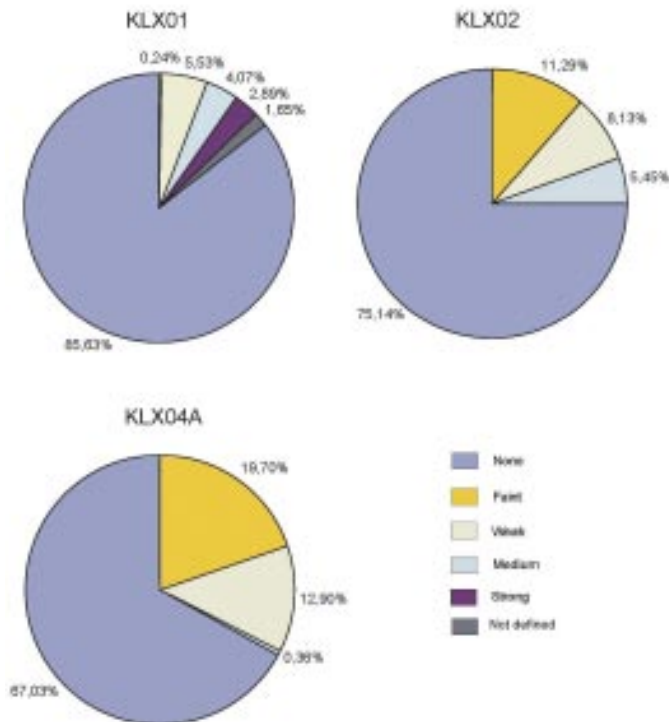


Figure 3-16. Estimate of alteration (mainly oxidation) in rock domain RSMA01, based on length of altered sections in the cored boreholes KLX01, KLX02 and KLX04A.

KLX03 - Alteration
Laxemar subarea

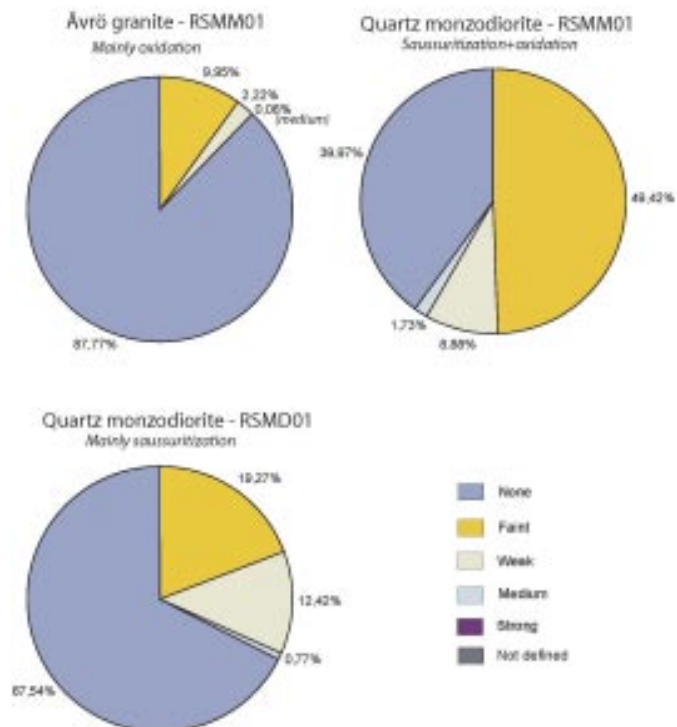


Figure 3-17. Estimate of alteration in rock domains RSMM01 and RSMD01, based on length of altered sections in the cored borehole KLX03.

3.7 Evaluation of uncertainties

The variation in the quality of the surface geological data across the regional model area (cf. Section 2.2) is important to consider in the modelling procedure. Since only surface information of point character was generated during the bedrock mapping of the regional model area the summer 2004 /Persson Nilsson et al. 2004/, the uncertainties described in the Simpevarp SDM version 1.2 for the regional model area will remain valid also for the Laxemar 1.2 site descriptive model. The uncertainties in the regional model area is obvious since, 1) only provisional bedrock map exist and, 2) the almost complete lack of subsurface information. Since all investigations during the complete site investigation phase will be focused to the local scale model area, these uncertainties will remain throughout the site investigation.

Although the Laxemar 1.2 modelling work is based on the new detailed bedrock map of the Laxemar and Simpevarp subareas and that the bedrock is generally well exposed, the location of the boundaries between the different rock units in the local scale model area is a matter of interpretation and must be considered as an uncertainty. An important uncertainty is the insufficient information what concerns the character of the inhomogeneity of the rock domains. In particular, this concerns the frequency and spatial distribution of subordinate rock types. The estimates of the proportion of subordinate rock types presented above (Section 3.5) indicate that the local variation may be high, i.e. specific parts of a rock domain may contain a high frequency, while other parts may be more or less devoid of subordinate rocks. Accordingly, the estimate of the degree of inhomogeneity is scale dependent. If for instance the entire rock domain RSMA01 is considered it may be judged to contain a fairly moderate amount of subordinate rock types, while specific parts of the rock domain may contain a large amount of subordinate rock types.

As there is a limited amount of subsurface lithological data, there remain considerable uncertainties concerning the extension at depth of the rock domains, apart from:

- The dominating rock domain RSMA01 (Ävrö granite), which constitutes the “matrix” in the rock domain model.
- The rock domain RSMB01 (fine-grained dioritoid) that has been verified between c. 320 and 630 metre along the cored borehole KSH01, and to a depth of 1,000 metres in the cored borehole KSH02.
- The rock domain RSMC01 (mixture of Ävrö granite and quartz monzodiorite), which has been verified to a depth of 1,000 metres in the cored borehole KSH01A, to a borehole length of c. 270 metres in the cored borehole KSH03 and between 290 and 690 metres in the cored borehole KAV04A.
- The rock domain RSMD01 (quartz monzodiorite) which is documented between c. 1,450 and 1,700 metres in the cored borehole KLX02, between c. 800 and 1,000 metres in the cored borehole KLX03 and between c. 465 and 1,000 metres in the cored borehole KLX05A (preliminary mapping).
- The rock domains RSMP01 and RSMP02 which are based on consistent structural data and magnetic anomalies

The depth extensions of the remaining rock domains are uncertain due to lack of information at depth from cored boreholes. Even though rock domains, including the above mentioned, have been verified to a certain depth, the geometrical relationships between most rock domains are considered uncertain. This problem will presumably persist throughout the site investigation programme for most of the rock domains, especially in the regional model area. The geometrical relationships between rock domains RSMP01 and RSMP02 and the surrounding rock domains are judged to be well constrained due to the consistency in the orientation of the mylonitic to protomylonitic foliation on which these domains are based. The general geometrical relationship between the two dominating rock domains RSMA01 and RSMD01, and the intervening RSMM01 rock domain in the Laxemar subarea is judged to be fairly well constrained.

However, local geometrical variations are anticipated and the geometry of the southern contact of the RSMD01 rock domain is uncertain. Reduction of this and remaining uncertainties what concern geometrical relationships between rock domains may be achieved particularly from information collected from cored boreholes, but also by future modelling of airborne and/or surface geophysical data. However, the uncertainty in the geometrical relationships between the rock domains primarily relates to the Simpevarp subarea and the remaining part of the regional model area.

With the above considerations in mind, an attempt has been made to assess, at least qualitatively, the confidence for the existence and geometry of the interpreted 34 rock domains (Table 3-5). Confidence is expressed at three levels; “high”, “medium” and “low”. It should be noted that the table of confidence for the existence and geometry of interpreted rock domains (Table 3-5) has been modified compared to the Simpevarp SDM 1.2. The new version more explicitly distinguishes between confidence of existence and uncertainty of geometry both at the surface and at depth. This is motivated by the circumstance that, for instance, the confidence of existence of a rock domain at depth may be high, but the uncertainty of geometry may be medium to high as well.

Table 3-5. Table of confidence for the existence and uncertainty of geometry of interpreted rock domains in the regional and local scale model volume employed for the Laxemar 1.2 site descriptive model.

Domain ID	Basis for interpretation	Confidence of existence at the surface	Confidence of existence at depth	Uncertainty of geometry at the surface	Uncertainty of geometry at depth	Comment
RSMA01	Bedrock geological map of the Simpevarp and Laxemar subareas and version 0 in the remaining area, KSH03A, KAV01, KAV04 A/B, KLX01, KLX02, KLX04, HAV09, HAV10, HLX21, HLX22, HLX23, HLX24, HLX25	High	High	Low	Medium	The uncertainty of geometry at both the surface and at depth is higher in the regional model area due lack of detailed information
RSMA02	Bedrock geological map, version 0	Medium	Medium	High	High	
R SMB01	Bedrock geological map the Simpevarp and Laxemar subareas, KSH01A, KSH02, HSH02	High	High	Low	Medium	
R SMB03	Bedrock geological map of the Simpevarp and Laxemar subareas	High	High	Low	High	
R SMBA01 (a–b)	Bedrock geological map of the Simpevarp and Laxemar subareas and KLX05 (preliminary mapping)	High	High	Medium	Medium	
R SMBA02	Bedrock geological map of the Simpevarp and Laxemar subareas	High	High	Medium	Medium	
R SMBA03	KLX02	–	High	–	Medium	This domain only occurs at depth
R SMC01	Bedrock geological map of the Simpevarp and Laxemar subareas, KSH01A, KSH01B, KSH03A, KSH03B, KAV04A, HSH01, HSH03	High	High	Low	Medium	

Domain ID	Basis for interpretation	Confidence of existence at the surface	Confidence of existence at depth	Uncertainty of geometry at the surface	Uncertainty of geometry at depth	Comment
RSMC02	Bedrock geological map of the Simpevarp and Laxemar subareas	High	High	Medium	Medium	
RSMD01 (a–b)	Bedrock geological map of the Simpevarp and Laxemar subareas, KLX02, KLX03 and KLX05 (preliminary mapping), HLX15, HLX26, HLX28	High	High	Low	Medium	
RSMD02	Bedrock geological map, version 0	Medium	Medium	High	High	
RSMD03	Bedrock geological map, version 0	Medium	Medium	High	High	
RSMD04	Bedrock geological map, version 0	Medium	Medium	High	High	
RSMD05	Bedrock geological map, version 0	Medium	Medium	High	High	
RSMD06	Bedrock geological map, version 0	Medium	Medium	High	High	
RSMD07	Bedrock geological map of the Simpevarp and Laxemar subareas	High	High	Low	Medium	
RSMD08	Bedrock geological map of the Simpevarp and Laxemar subareas	High	High	Low	Medium	
RSME01	Bedrock geological map of the Simpevarp and Laxemar subareas	High	High	Low	Medium	
RSME11	Bedrock geological map, version 0	High	High	Medium	High	
RSME12	Bedrock geological map, version 0	High	High	Medium	High	
RSME13	Bedrock geological map, version 0	High	High	Medium	High	
RSME14	Bedrock geological map, version 0	High	High	Medium	High	
RSME15	Bedrock geological map, version 0	High	High	Medium	High	
RSME16	Bedrock geological map, version 0	High	High	Medium	High	
RSME17	Bedrock geological map, version 0	High	High	Medium	High	
RSME18	Bedrock geological map, version 0	High	High	Medium	High	
RSMF01	Bedrock geological map, version 0	High	High	Medium	High	
RSMF02	Bedrock geological map of the Simpevarp and Laxemar subareas	High	High	Low	Medium	
RSMF03	Bedrock geological map, version 0	High	High	Medium	High	
RSMG01	Bedrock geological map, version 0	High	High	Low	Medium	
RSMG02	Bedrock geological map, version 0	High	High	Low	Medium	

Domain ID	Basis for interpretation	Confidence of existence at the surface	Confidence of existence at depth	Uncertainty of geometry at the surface	Uncertainty of geometry at depth	Comment
RSMM01 (a–d)	Bedrock geological map of the Simpevarp and Laxemar subareas, KLX03, KLX05 (preliminary mapping)	High	High	Low	Medium	
RSMP01	Bedrock geological map of the Simpevarp and Laxemar subareas, magnetic anomaly map, KAS04, KA1755A	High	High	Low	Low	
RSMP02	Bedrock geological map of the Simpevarp and Laxemar subareas, magnetic anomaly map	High	High	Low	Low	

The information concerning the properties of the different rock domains (Table 3-3) originates primarily from the surface outcrop data from the Laxemar and Simpevarp subareas (cf. Section 2.2). Subsurface data are available for rock domains RSMA01, RSMB01, RSMBA01, RSMBA03, RSMC01, RSMD01 and RSMM01. Despite the fact that it has been possible to estimate the proportions of different rock types in a specific rock domain from both surface and subsurface (borehole) data, there remains an uncertainty concerning the quantitative proportions of the different rock types, i.e. how much of a specific rock domain is occupied by subordinate rock types and furthermore, are the subordinate rock types homogeneously distributed or do they cluster in specific parts of the domain. This characteristic is a basis for the uncertainty assessment related to the bedrock heterogeneity in the rock domains. Based on a qualitative estimation at the present stage of the site investigation, subordinate rock types, particularly the frequently occurring fine- to medium-grained granite, is judged to occur in more or less the same amounts both in individual rock domains and between the various rock domains. However, local variations in the frequency of subordinate rock types are to be expected.

An uncertainty that is connected to the thermal modelling is the spatial distribution of the compositional varieties of the Ävrö granite, i.e. the quartz monzodioritic and the granitic to granodioritic varieties in rock domain RSMA01. As shown in Section 2.2.5.1, there are indications that the different varieties are spatially separated at the surface. However, the restricted amount of existing cored boreholes does not allow the division of the rock domain RSMA01 into two separate domains at depth that are characterized by different compositional varieties of the Ävrö granite. In forthcoming modelling work, when data from more cored boreholes are available, this possibility will be evaluated. Another factor of uncertainty that is of importance for the thermal properties and modelling is the degree and spatial distribution of hydrothermal alteration of the bedrock.

Due to the lack of data from the regional model area, the assigned properties of most rock types are incomplete and if necessary, have to be inherited from corresponding rock types in the Laxemar and Simpevarp subareas. Whether the properties of the rock types in the Laxemar and Simpevarp subareas are also valid for the rock types outside the local scale model area is uncertain. However, this is not considered to be of great importance, since the focus during the complete site investigation is to obtain a better resolution and improve the understanding of the bedrock within the local scale model area.

4 Deterministic deformation zone modelling

4.1 Modelling assumptions and input from other disciplines

A set of fundamental assumptions underlying the deformation zone model are made. It is assumed that:

- Deformation zones can be interpreted through both indirect sources of data such as geophysical maps (magnetics, VLF, slingram, gravimetric), topography, seismic reflections and refractions.
- Lineaments can provide the necessary detailed information about the location and extent at the surface of possible deformation zones.
- Deformation zones can further be interpreted through direct data in boreholes, tunnels and from surface field observations. The certitude in geological character and possible extent (length and thickness) of deformation zones inferred from indirect data sources is lower than for zones identified from direct observations.
- Different sources of data can complement each other and increase the confidence in the interpreted deformation zone. Several types of observations, both indirect and direct, also increase the degree of detail in which the zone can be described.
- Interpreted deformation zones can be interpolated between points of observation, if there are reasonable data to suggest the validity of such interpolation.
- Deformation zones are variable in their thickness and can be modelled honouring the inferred thickness, cf. Figure 2-94, or can be modelled as surfaces without thickness if no relevant data exist.
- Within the limits of the regional, or local model volumes, deformation zones interpreted at the ground surface can be extended toward depth with a depth extent equal to the interpreted length of the mapped surface trace. This means, for example, that deformation zones longer than 1 km at the surface are extended to the bottom of the local model volume (1,100 m).
- Each interpreted deformation zone has been ranked according to the confidence of its existence being high, medium or low. Zones that have high confidence ratings have, in addition to lineament indications, also supportive information from other sources of indirect data such as geo-physics and from sources of direct data, such as boreholes or tunnels.
- Deformation zones ranked with medium confidence show clear topographic, magnetic and/or surface geophysical anomalies which cannot be disregarded as being other linear structures in the landscape, such as Quaternary deposits, ditches, power lines, roads, forest fire lanes, or other man-made constructions.
- Interpreted zones with assigned low confidence are only supported by indirect sources of information such as lineament indications of lesser strength, either from topography, magnetics or electromagnetic methods.

The local scale model of deformation zones has made use of:

- the deformation zone model presented in Simpevarp 1.2 site descriptive model /SKB 2005a/,
- the interpretation of lineaments completed during the ongoing site investigation programme (see Section 2.2.9),
- the regional structural model presented in version 0 of the site descriptive model /SKB 2002/,
- the structural model of Äspö HRL (Äspö 96 model), /Rhén et al. 1997/,
- GEOMOD structural model /Berglund et al. 2003/,

- Ävrö RVS model /Markström et al. 2001/,
- measurements of mainly ductile structures, as well as some brittle structures and bedrock contacts at 91 of the 353 observation points documented during the bedrock mapping carried out during 2003 /Wahlgren et al. 2004/,
- measurements of mainly ductile structures, as well as some brittle structures and bedrock contacts deduced from the bedrock mapping carried out during 2004 /Persson Nilsson et al. 2004/,
- a variety of old structural geological data covering the Simpevarp peninsula and the islands of Hålö and Ävrö, as compiled by /Curtis et al. 2003ab/,
- data from percussion boreholes HLX13, HLX15, HLX21–28,
- seismic reflection data compiled in conjunction with the ongoing site investigation programme (see Sections 2.3 and 2.4.4).

The lineament map used in the Simpevarp 1.2 modelling /SKB 2005a/ has been updated and forms the basis for the surface interpretation of deformation zones (see Section 5.2.5). Interpretations that are related to the new lineament map are always preferred, unless there is other additional supporting information from geophysics, boreholes or tunnels.

The Laxemar 1.2 deformation zone model addresses deformation zones in the regional and local model areas on the same basis to that employed for Simpevarp version 1.2 model /SKB 2005a/. The local scale model contains deformation zones that are inferred to be of length 1 km or longer, i.e. local major and regional deformation zones according to the terminology of /Andersson et al. 2000/.

The surface data coverage in parts of the area outside the local model area has a lower resolution, which limits the possibilities to modelling zones of 1 km length or more. Parts of the offshore and north-western parts of the regional model area are covered only by the lineament map from the version 0 model of relatively low resolution /SKB 2002/. In order to provide a regional model based on an even resolution of data, inferred deformation zones outside the local model area have, therefore, been limited to be of length 1.6 km or longer. This approach produces a model which has an increased level of resolution around the area of highest interest, i.e. the local model area. The consequences of variable data resolution inside the regional model volume are addressed in connection with the presentation of alternative models (see Section 4.2).

Structures that are considered to be shorter than the modelled deformation zones in the local and regional areas are handled in a statistical way and are presented as part of the fracture statistical description in /Hermanson et al. 2005/. Hence, all lineaments shorter than 1 km are treated as part of the stochastic fracture network.

For the modelling of deformation zones, it is assumed that lineaments can provide the necessary detailed information about the location and extent at the surface of possible deformation zones and are regarded as the preferred surface information in comparison with existing older surface deduced lineament data.

The lineament map used in the Simpevarp 1.2 model /SKB 2005a/ has been updated and forms the basis for the surface interpretation of deformation zones. Interpretations that are related to the new lineament map are always preferred, unless there is other additional supporting information from geophysics, boreholes or tunnels.

In the cases where a deformation zone can be tied to both a lineament and a borehole, the strike of the zone is assumed to be the same as the trend of the matching lineament. The dip inferred from the borehole intercept is interpreted as the average dip angle of the zone, along its entire extent. Deformation zones observed only at the surface, which lack information on their subsurface extents, are assumed to be dipping vertical.

The steeply dipping zones are assumed to truncate, along their strike direction, against zones that have a higher order of significance. Generally, the order of significance is controlled by the classification of zones into regional and local major size classes or to best fit with the underlying data. The extension of deformation zones towards depth is assumed equal to the length of the surface lineaments. This assumption implies that the frequency of steeply dipping deterministically modelled deformation zones decreases with depth.

Gently dipping zones have been detected by an integration of data from boreholes and with the interpretation of seismic reflectors. The gently dipping zones are assumed to truncate, both along their strike and in the down-dip direction, against regional or local major, vertical and steeply dipping zones. In the working conceptual model, these zones have a higher order of significance in the structural hierarchy (see Section 4.2).

Each interpreted deformation zone has also been ranked according to the confidence of its existence being high, medium or low. Zones that have high confidence ratings have, in addition to lineament indications, also supportive information from other sources of indirect data such as geophysics *and* from sources of direct data, such as boreholes or tunnels.

Deformation zones ranked with medium confidence show clear topographic, magnetic and/or surface geophysical anomalies which cannot be disregarded as other linear structures in the landscape, such as quaternary deposits, ditches, power lines, roads, forest fire lanes or other man made constructions.

Interpreted zones with assigned low confidence are only supported by indirect sources of information such as lineament indications of lesser strength, either from topography, magnetics or EM.

4.2 Conceptual model of the kinematic evolution of deformation zones

The regional stress field at the time of formation of the deformation zones has had a major impact on the kinematics of deformation zones. The direction of the maximum compressive stress has shifted considerably during the geological evolution from being approximately N-S during the waning stages of the Svecokarelian orogeny, to approximately E-W during the Sveconorwegian orogeny, to approximately NW-SE during the Caledonian orogeny and the present day.

Deformation zones that were formed in the ductile regime are inferred to be related to the waning stages of the Svecokarelian orogeny. Consequently, E-W oriented deformation zones that are ductile, or exhibit a ductile component, are inferred to have formed in response to compression, whereas zones oriented in NE-SW and NW-SE direction would be characterised by sinistral and dextral components of movement, respectively. However, the inferred E-W maximum compression during the Sveconorwegian orogeny imply that E-W oriented zones, if reactivated, were exposed to extensional forces, whereas the NE-SW and NW-SE oriented zones would reverse and be characterised by dextral and sinistral movements, respectively. The latter deformation zones subsequently were exposed to compressional forces during the Caledonian orogeny. A conceptual model for the sense of movement in deformation zones with different orientations is displayed in Figure 4-1.

In an attempt to unravel the kinematic history, and to test the model summarised above, there are ongoing studies, in conjunction with the complete site investigation phase, that aim to characterise both the ductile and brittle deformation zones kinematically. The results of these studies, both at the surface and in boreholes, will be evaluated in forthcoming site descriptive modeling.

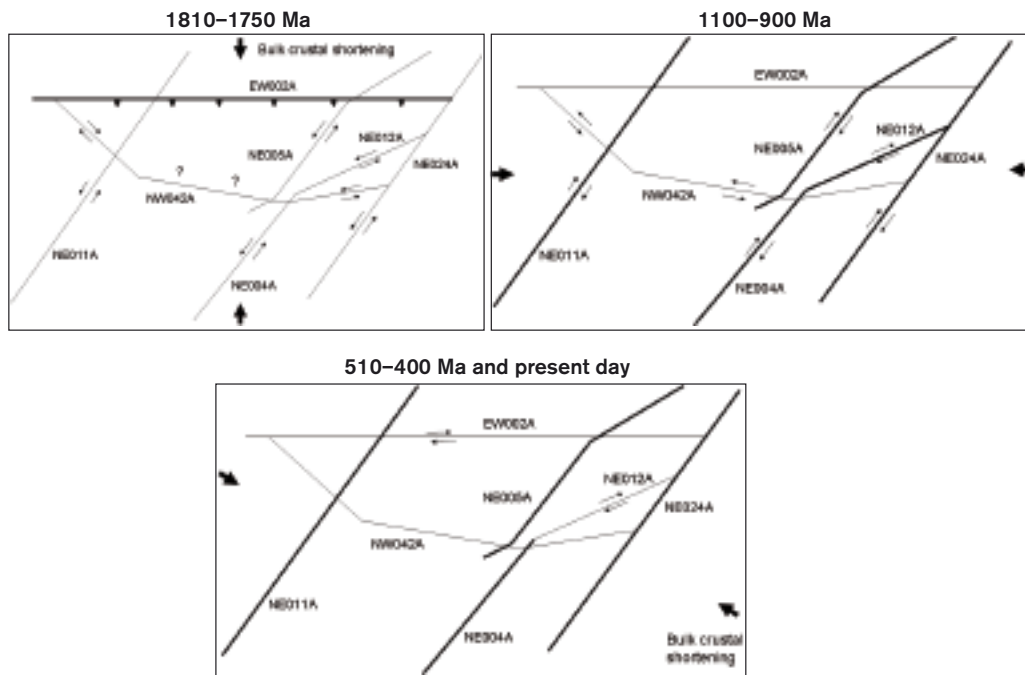


Figure 4-1. A conceptual model for the sense of movement in deformation zones with different orientations. Plan view with maximum compressive stress indicated by arrows.

4.3 Conceptual deformation zone model with potential alternatives

4.3.1 Conceptual base case deformation zone model

The modelling procedure used for establishing the deformation zone model follows the methodology presented in /Munier et al. 2003/. An initial step in the modelling procedure made use of the Sim-pevarp 1.2 model, established with a special focus on the Simpevarp subarea /SKB 2005a/. Each deformation zone in this previous model was checked against the updated lineament map (see Section 2.2.9), topographic and magnetic background maps, and against new information from surface geophysics, seismics, as well as relative to new borehole data acquired for this model version.

To further enhance the classification of deformation zones, the ensuing modelling work includes introduction of the following groups of deformation zones in the regional model volume, in the order indicated below:

- Regional deformation zones which are supported by direct data observations through new boreholes, ground geophysics, seismics, lineament support, and which have been included in older existing structural models, *i.e. regional high confidence zones*,
- Regional deformation zones which have lineament support and have been included in older existing structural models, *i.e. regional medium confidence zones*,
- Local major deformation zones supported by direct data and observations in new boreholes, lineament support and which have been included in older structural models, or are supported by new ground geophysics, seismics or borehole data, *i.e. local major high confidence zones*,
- Local major deformation zones, which are supported by lineament data and have been included in older structural models, *i.e. local major medium confidence zones*,
- Low confidence deformation zones that have been inferred solely on the basis of the interpretation of lineaments (topographic, magnetic or EM), *i.e. local major low confidence zones*.

The modelling procedure has made use of the key assumptions concerning relationships between dip and the along-strike and down-dip extents of individual deformation zones, as outlined in the previous section.

Thirty-five deformation zones (modelled in 38 segments) have been interpreted with a high confidence in their existence. Each one is observed both indirectly, through lineament or geophysical data, and directly through field mapping, borehole or tunnel observations. Exceptions are the Mederhult zone (ZSMEW002A), and zones ZSMNS009, -10 and -11, which have not been observed in boreholes or tunnels but in field mapping, or has such a major regional imprint in the topography, magnetic map or through clear anomalies in geophysical profiles that their existences are considered as being of high confidence. Also, a few high confidence zones have been based solely on indirect surface observations in combination with strong evidence from seismic refraction or reflections surveys.

The high confidence deformation zones are illustrated in plan surface view (2D) in Figure 4-2 and Figure 4-3 and are summarised in Table 4-1 where each zone is classified based on its estimated length to either regional (> 10 km) or local major (> 1 km) deformation zones. The estimation of geological length is based on the surface impression from indirect data sources such as topography and magnetics. However, for regional deformation zones which substantially extend outside the regional model domain, length estimates are based on published geological material from the Geological Survey of Sweden and on general geological understanding of south-eastern Sweden.

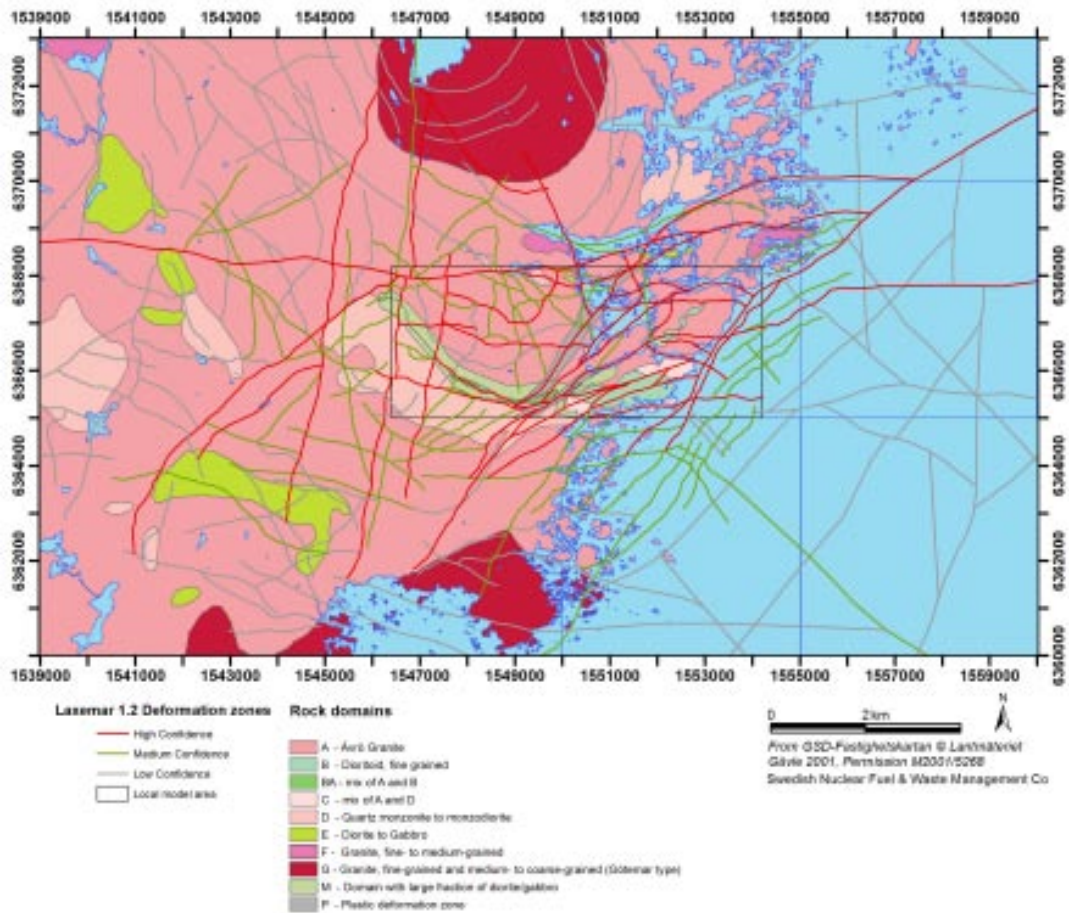


Figure 4-2. The interpreted thirty-four high confidence deformation zones in the Laxemar 1.2 regional model domain (red) together with interpreted medium and low confidence deformation zones in the regional and local model domains (green and gray respectively).

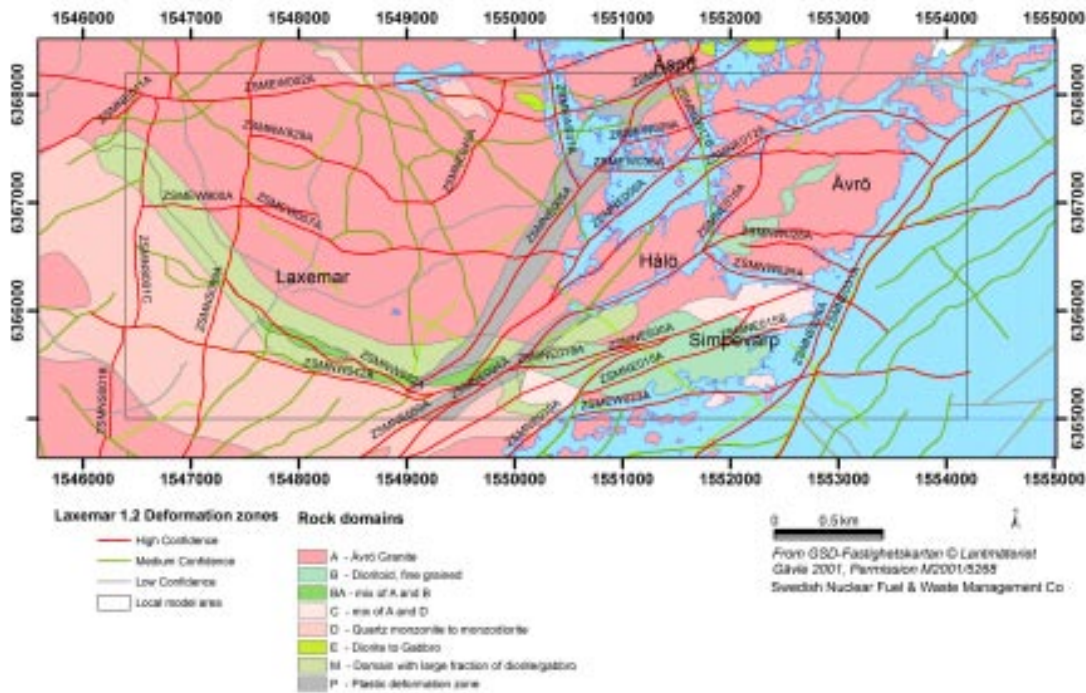


Figure 4-3. The interpreted high, medium and low confidence deformation zones in the Laxemar 1.2 regional model domain (red). The small box outlines the local scale model volume also including medium and low confidence zones in the local scale (green and gray respectively).

The average dips of the thirty-five high confidence zones have been estimated using existing observations from geophysical profiles, seismic refractions, seismic reflections, borehole or tunnel observations, where available. A vertical dip has been assumed for zones with no conditional information available on dip.

The observations are in several cases identical to observations used in the Simpevarp 1.2 modeling, but the redefined lineaments on the surface combined with new ground geophysics results, and new borehole data, have sometimes resulted in changes of the position and has therefore affected the attributed dip of a given deformation zone.

One hundred and fifty-five (N=155) medium and low confidence zones have also been included in the deformation zone model. Of these, sixty-two (N=62) are of medium confidence.

Table 4-1. Summary of high confidence deformation zones (N=34) included in the Laxemar 1.2 deterministic deformation zone model.

Zone ID	Alternative name or common name	Occurrence in older models	Approx length	Class	Basis for interpretation	Detailed description provided
ZSMEW002A	Mederhult zone	Simpevarp 1.2, v. 0, updated.	30 km	Regional	Airborne geophysics, topography, VLF, seismic refraction. Ground geology, boreholes.	Yes
ZSMEW007A		Simpevarp 1.2, updated.	3 km	Local Major	Airborne geophysics (magnetic 100% along the length, electrical data, low uncertainty), topography, borehole.	Yes

Zone ID	Alternative name or common name	Occurrence in older models	Approx length	Class	Basis for interpretation	Detailed description provided
ZSMEW009A		Simpevarp 1.2, not updated.	2 km	Local Major	Topography, ground geology, tunnel, borehole.	Yes
ZSMEW013A	EW1A	Simpevarp 1.2, updated.	2–4 km	Local Major	Airborne geophysics (magnetic) 100% along the length, electrical data, low uncertainty), topography, boreholes.	Yes
ZSMEW023A		In Simpevarp 1.2 modelled as low confidence zones ZSMEW023A and ZSMEW026X, respectively. Updated.	4 km	Local Major	Airborne geophysics, topography, seismic refraction profiling; OKG tunnel intercept.	Yes
ZSMEW038A		New.	3 km	Local Major	Airborne geophysics, topography, tunnel mapping and BHs. Potentially involves a series of narrow mylonites in a number of BHs and the tunnel, with potential interference from other zones including ZSMNE006A. The current modelled geometry is an over simplification.	Yes
ZSMEW900		In Simpevarp 1.2 modelled as ZSMEW005A and ZSMEW007A, now remodelled under new name.	2 km	Local Major	Airborne geophysics, topography, field mapping and geophysical ground survey.	Yes
ZSMNE004A		In Simpevarp 1.2 modelled as ZSMEW004A. Updated.	> 15 km	Regional	Airborne geophysics (magnetic 100% along the length, low uncertainty), tunnel.	Yes
ZSMNE005A	Äspö shear zone	Modelled in Simpevarp 1.2. Updated.	> 10 km	Local Major	Airborne geophysics (magnetic 100% along the length, low to medium uncertainty), ground geology, ground geophysics, borehole, Äspö HRL data.	Yes
ZSMNE006A	NE1	Simpevarp 1.2, updated.	2–4 km	Local Major	Airborne geophysics (magnetic 100% along the length, low to medium uncertainty), tunnel, boreholes, Äspö HRL data.	Yes
ZSMNE010A		Simpevarp 1.2, not updated.	3 km	Local Major	Airborne geophysics, topography, field control.	Yes
ZSMNE011A		Simpevarp 1.2, not updated.	8 to 12 km	Local Major	Airborne geophysics, topography, ground geophysics.	Yes
ZSMNE012A	NE4	In Simpevarp 1.2 modelled as ZSMNE012A and ZSMNW004A. Updated.	5 km	Local Major	Airborne geophysics, topography, seismic reflector, BH and tunnel (Äspö) intercepts	Yes

Zone ID	Alternative name or common name	Occurrence in older models	Approx length	Class	Basis for interpretation	Detailed description provided
ZSMNE015A		New.	2 km	Local Major	Airborne geophysics, topography, field mapping, along with Clab 1, Clab 2 and OKG excavation mapping.	Property table only
ZSMNE015B		New.	1 km	Local Major	Airborne geophysics, topography, field mapping, along with OKG excavation mapping.	Property table only
ZSMNE016A		Simpevarp 1.2, updated.	1 km	Local Major	Linked lineaments, seismic refraction, BH and tunnel (Äspö) intercepts	Property table only
ZSMNE018A		Simpevarp 1.2, updated.	1 km	Local Major	Airborne geophysics, extensive field mapping.	Property table only
ZSMNE019A		Simpevarp 1.2 ZSMNE019A and ZSMNE021A, northern part, updated.	4 km	Local Major	Airborne geophysics, topography, ground geophysical profiling.	Property table only
ZSMNE024A		Simpevarp 1.2, not updated.	> 10 km	Regional	Airborne geophysics, seismic reflector, seismic refractor, BHs and OKG cold water intake tunnel. This zone should be considered together with ZSMNE031A. Together they define a broad complex structural belt of deformation off the coast of Ävrö.	Property table only
ZSMNE031A		Simpevarp 1.2, updated.	5 km	Local Major	Airborne geophysics, seismic reflector, seismic refractor, BHs and OKG cold water intake tunnel. This zone should be considered together with ZSMNE024A. Together they define a broad complex structural belt of deformation off the coast of Ävrö.	Property table only
ZSMNE040A		In Simpevarp 1.2 modelled as eastern part of ZSMNE040A. Updated.	> 1 km	Local Major	Airborne geophysics, resistivity and seismic refraction profiling.	Yes
ZSMNE050A		Simpevarp 1.2, updated.	2 km	Local Major	Airborne geophysics, topography, field mapping.	Property table only
ZSMNE930A		New.	4 km	Local Major	Airborne geophysics, topography, extensive field mapping, excavation (OKG).	Property table only
ZSMNS001A–D		Simpevarp 1.2, not updated.	10 to > 11 km	Regional (A–D)	Airborne geophysics, ground geophysics, topography, refraction seismics.	Yes

Zone ID	Alternative name or common name	Occurrence in older models	Approx length	Class	Basis for interpretation	Detailed description provided
ZSMNS009A		Simpevarp 1.2, not updated.	10–12 km	Regional	Airborne geophysics, topography, ground magnetic and VLF.	Property table only
ZSMNS017A–B	NNW4	Simpevarp 1.2, updated.	3 km	Local Major	Topography, borehole and tunnel evidence.	Property table only
ZSMNS059A		Simpevarp 1.2, updated.	5 km	Local Major	Airborne geophysics, topography, field mapping and geophysical ground survey, seismic reflector.	Property table only
ZSMNW025A		Simpevarp 1.2, updated.	2 km	Local Major	Airborne geophysics, seismic refraction, borehole evidence.	Property table only
ZSMNW028A		In Simpevarp 1.2 modelled as ZSMEW028A. Updated.	1 km	Local Major	Airborne geophysics and borehole evidence.	Property table only
ZSMNW042A		Simpevarp 1.2, updated.	3 km	Local Major	Airborne geophysics, resistivity, magnetic and seismic refraction profiling.	Yes
ZSMNW928A		New.	1 km	Local Major	Seismic reflection and borehole evidence.	Yes
ZSMNW929A		In Simpevarp 1.2 modelled as western part of ZSMNE040A. Updated.	2 km	Local Major	Airborne geophysics, topography, boreholes.	Yes
ZSMNW931A		Simpevarp 1.2, updated.	4 km	Local Major	Airborne geophysics, topography, ground magnetic and VLF profiles.	Property table only
ZSMNW932A		In Simpevarp 1.2 modelled as ZSMNW006A. Updated Updated only from refined lineaments. No subsurface data.	3 km	Local Major	Airborne geophysics, topography, ground magnetic and VLF profiles.	Property table only
ZSMNW933A		New.	4 km	Regional	Airborne geophysics, topography, ground magnetic and VLF profiles.	Property table only

Twenty-nine of the high confidence deformation zones were already identified in the Simpevarp 1.2 model /SKB 2005a/. In the current model version, five new high confidence deformation zones, not previously identified, have been identified through geological field observations, borehole intersections in combination with ground geophysics or seismics, cf. Table 4-1. Most of the new material originates from Laxemar, although new submarine topography from the coast along Simpevarp and Ävrö have greatly improved the knowledge in the sea close to shore.

A few deformation zones from the Simpevarp 1.2 model have been removed on the basis of results from new data or new interpretations of existing topographic, bathymetric and airborne geophysical data, cf. Table 4-2.

Table 4-2. Deformation zones that have been removed from the Laxemar 1.2 deformation zone model since the last model version (Simpevarp 1.2).

Zone name	Reason for removal	Result
ZSMNW035A	New bathymetric data	Split into several shorter lineaments which are not possible to tie up to a deformation zone > 1 km
ZSMNW296A	New bathymetric data	Lack of evidence in the new data for a lineament
ZSMNE024A	New bathymetric data	Lack of evidence in the new data for a lineament
ZSMNE136	Length limitation	Lineament only 915 m (below truncation level of 1,000 m)
ZSMNW234A, B	Length limitation, offset between lineament segments to large	Segments 385 and 620 m each (below truncation level of 1,000 m)
ZSMNE138B	Length limitation, offset between lineament segments to large	Lineament segment 780 m (below truncation level of 1,000 m)
ZSMNE239A	Length limitation	Lineament only 971 m (below truncation level of 1,000 m)
ZSMNW016A	Length limitation	Lineament segment only 664 m (below truncation level of 1,000 m)
ZSMNE044A	Length limitation	Lineament only 411 m (below truncation level of 1,000 m)
ZSMEW013C	Length limitation, offset between lineament segments to large	Lineament segment only 647 m (below truncation level of 1,000 m)

4.3.2 Alternative deformation zone model

An alternative representation of the deformation zone model is to include only high and medium confidence deformation zones. These are deformation zones where evidence through direct observations, and strong seismic or geophysical profile anomalies certify their existence. Deformation zones of lower confidence may exist, but are in this case, not treated as part of the deterministic deformation zone model.

However, the high confidence deformation zones are almost all located inside the local model area, although several extend into the regional model area. Only three high confidence zones are defined completely within the regional model area and outside the local model area; NE010A, NE011A and NW933A. Therefore it is rather pointless and also misleading to present an alternative model in the regional model area.

The alternative deformation zone model consequently only exists in the local model domain as is shown in Figure 4-4, and consists of the thirty-two (N=32) high confidence zones that have at least some part originating from within the local model area together with thirty-four (N=34) medium confidence zones. This alternative model contains all the high confidence zones presented for the base case model with the exception of zones NE010A, NE011A and NW933A which fall outside the local model area.

The presented alternative deformation zone model is based on confidence levels. Other alternatives based on the geological characterisation, such as dividing zones into ductile and brittle, or on the basis of thickness or other geological means is preferable in future model versions. However, at the current level of understanding, data do not provide enough information for such alternatives. The vision is to provide better, geologically based, alternatives for model version 2.2.

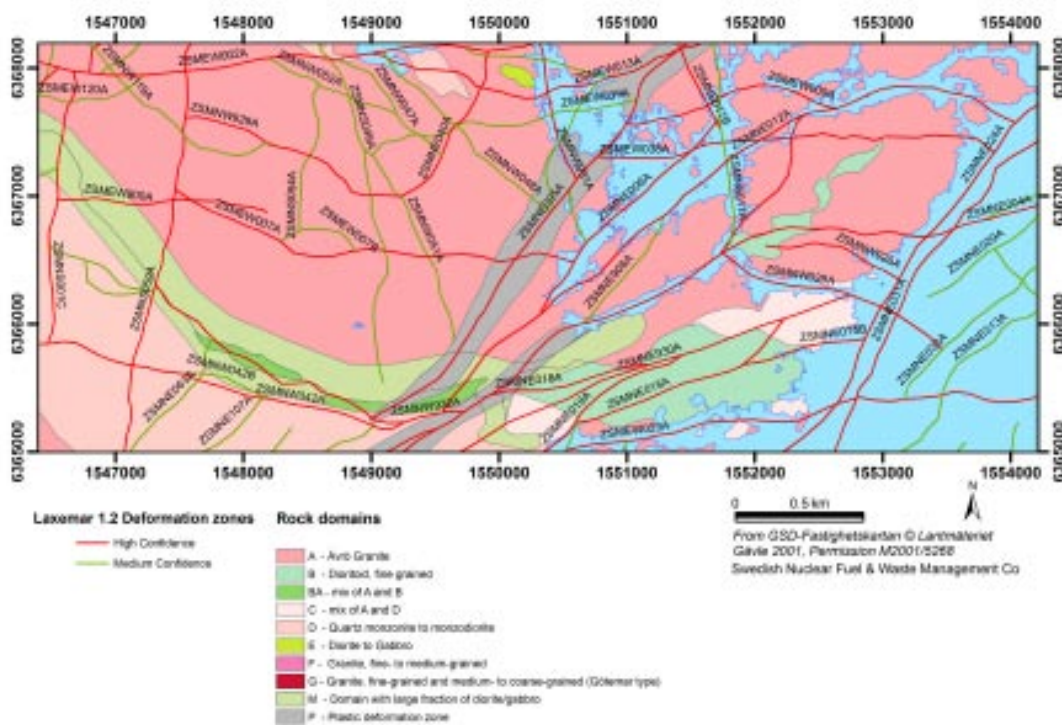


Figure 4-4. Alternative deformation zone model including high and medium confidence deformation zones within the local model area.

4.4 Laxemar and Simpevarp subareas – divided by regional shear zones

The Simpevarp peninsula, Ävrö and Hälö together with the eastern part on Äspö is intersected by regional NE trending shear zones with ductile-brittle behaviour. The magnetic map of the eastern part of Småland shows regional scale deformation zones with a major NE trend through the Simpevarp peninsula (Figure 4-5) where the western boundary is formed by ZSMNE006 together with the Äspö shear zone. This NE trending belt of regional zones encapsulates the Simpevarp peninsula which is dominated by anastomosing local major NE to ENE deformation zones throughout Simpevarp, Ävrö, Äspö and Hälö (Figure 4-6). The difference in degree of deformation between Laxemar and Simpevarp is also visible in the relatively higher fracture frequencies /Hermanson et al. 2005/ and more developed alteration of the bedrock (see Section 2.2.10.5) on the Simpevarp side. The Äspö island is partly within this tectonic belt of deformation zones where the Äspö HRL is located just on the eastern side of Äspö Shear zone.

Laxemar is influenced by the Mederhult Shear zone and other smaller EW trending deformation zones as well as by NS trending deformation zones in the western part. The NE set of regional deformation zones visible in Simpevarp is absent in this area. The southern part of the Laxemar subarea as well as the Simpevarp subarea also has an additional lithological coupling between the lithological boundary and parallel EW and SE trending deformation zones along the boundary of the dioritoid and quartz monzodiorite (B, BA and D domains) and the Ävrö granite (A domain) (see also Section 3.3).

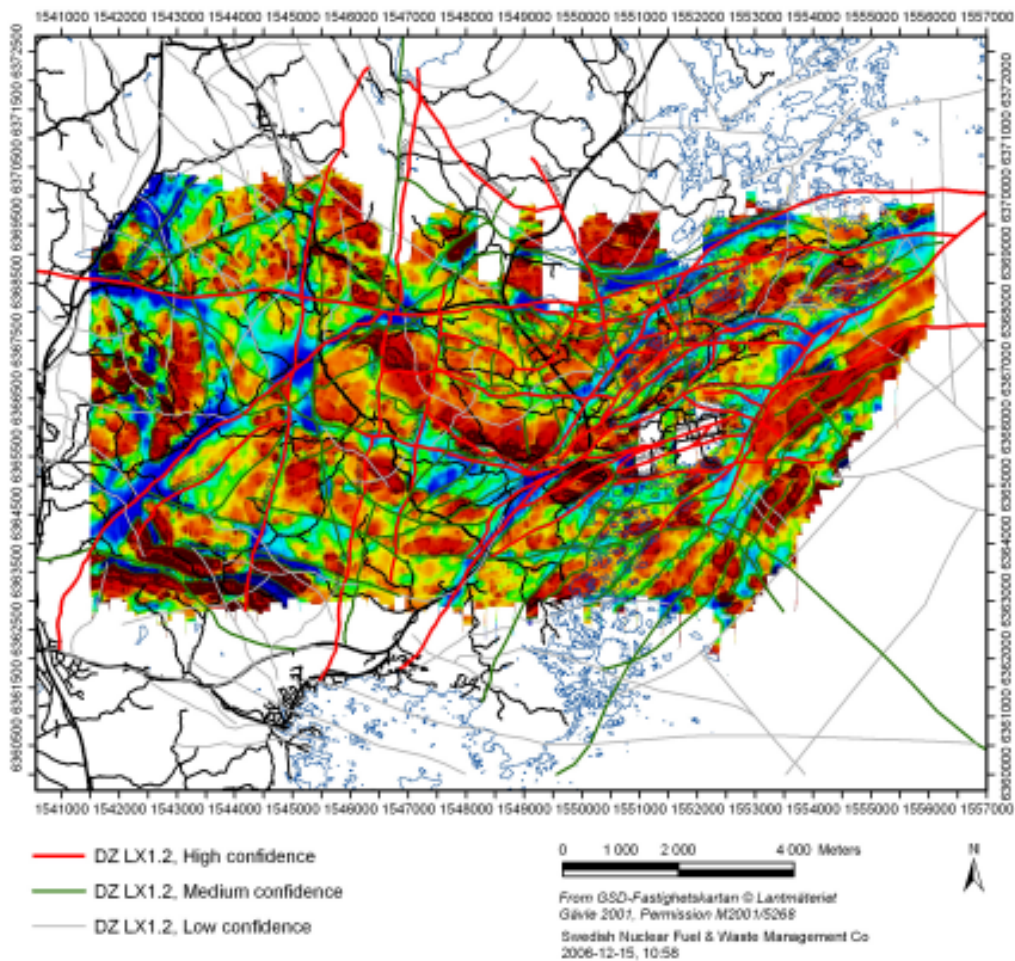


Figure 4-5. Magnetic map showing regional scale deformation zones over the Simpevarp and Laxemar subareas.

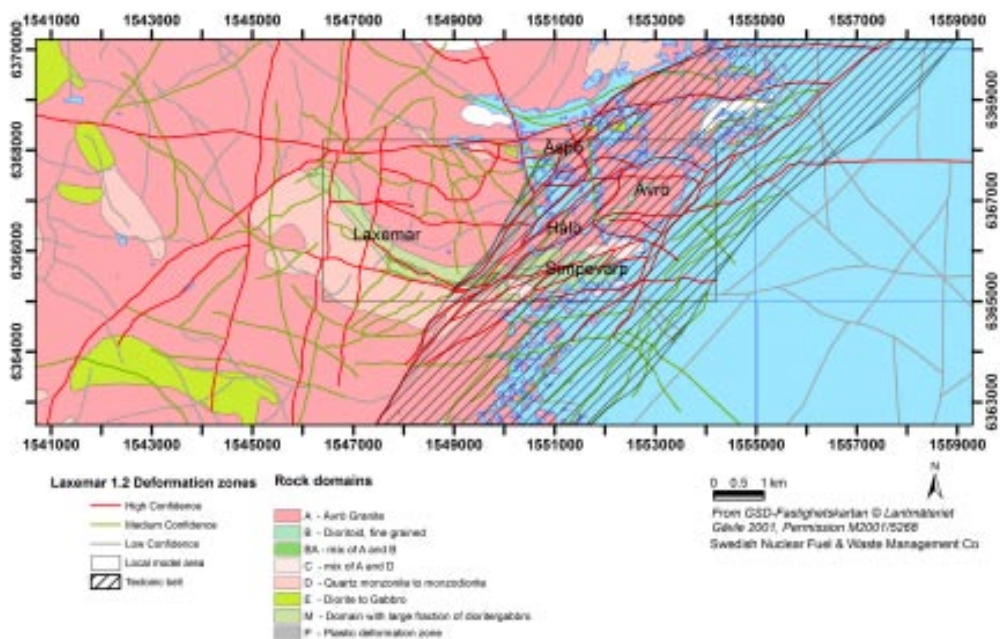


Figure 4-6. Increased tectonic influence east of NE005A (Äspö Shear zone) (hatched area). The tectonic deformation continues into the sea east of Simpevarp and is clearly visible in both the bathymetric and magnetic maps and in the core drilled borehole KSH03.

4.5 Property assignment to the base case model with specification of high confidence zones within the local model volume

Key properties, and numerical estimates of the uncertainty in some of these parameters, have been attributed to each of the thirty-two high confidence deformation zones that are based on a variety of geological and geophysical information, or deduced from older models (Table 4-3) within the local model volume. The properties of the deformation zones are presented in tabular format in the description of the high confidence deformation zones (Section 4.6).

There are few data available at present relating the properties (including numerical estimates of uncertainty) of the interpreted medium and low confidence deformation zones, which are based solely on the interpretation of linked lineaments.

4.6 High confidence deformation zones – detailed descriptions

Below follows a detailed description of interpreted high confidence deformation zones in the Laxemar 1.2 local model volume as specified in Table 4-1.

Property tables for the interpreted high confidence zones that have not been covered by a detailed description in this section can be found in Appendix 5. These zones have either not been updated since Simpevarp model version 1.2, because of no or limited amounts of new data, or have had limited change in their modelled geological geometry or a limited change in the level of knowledge about their character.

4.6.1 ZSMEW007A and ZSMEW900

The deformation zone ZSMEW007A (Figure 4-7) is based on a topographic and magnetic EW-lineament, seismics, ground geophysics and borehole intersections. The zone has been updated from Simpevarp version 1.2 with new borehole intersections as well as new ground geophysics. The previous interpretation extended from zone NS001C in the west to NE006A in the east. However, the western interpretation was not conclusive with regards to the dip. The eastern and central part of the zone was defined by the northerly dipping seismic reflector A /Juhlin et al. 2004a/ and a borehole intersection in KLX02.

Table 4-3. Properties assigned to the high confidence deformation zones of the Laxemar 1.2 model, along which there are, to variable extents, supporting geological and geophysical data.

Property	Comment
Deformation zone ID	ZSM*****, in two places with additional letter A, B, C, D and E (according to the nomenclature recommended by SKB).
Position	With numerical estimate of uncertainty.
Strike and dip	With numerical estimate of uncertainty.
Thickness	With numerical estimate of uncertainty.
Length	With numerical estimate of uncertainty.
Ductile deformation	Indicated if present along the zone.
Brittle deformation	Indicated if present along the zone.
Alteration	Indicated if present along the zone.
Fracture orientation	In places, with numerical estimate of uncertainty.
Fracture frequency	With numerical estimate of uncertainty.
Fracture filling	Mineral composition.

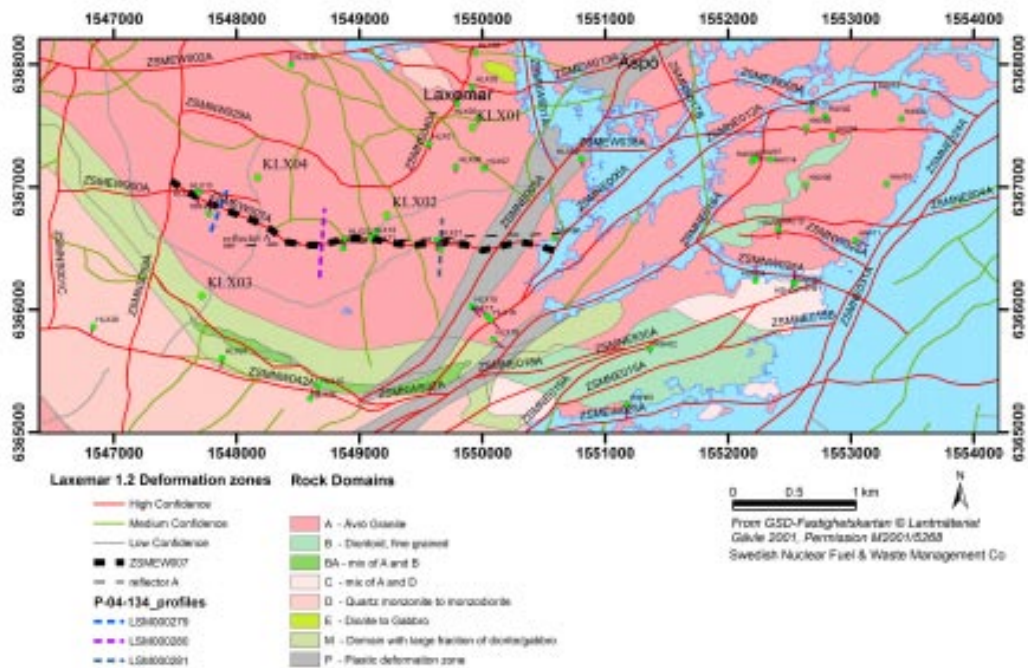


Figure 4-7. Illustration of EW007 together with all high, medium and low confidence zones identified in the local model domain. The surface intersection of seismic reflector A /Juhlin et al. 2004a/ crops out parallel to the central and east part of EW007.

New interpretations in the west and new data suggest a southerly dip based on a seismic reflector (L) /Juhlin et al. 2004a/, geophysical profiling /Lindqvist 2004b/ (Figure 4-9 to Figure 4-11) and from field observations. Also, HLX25 shows a low resistivity and low sonic section which corresponds with a southerly dip.

However, alternative interpretations are available through the new borehole KLX04 which together with resistivity profiles indicate also a northerly dip of the central and eastern part of the zone as shown in Figure 4-12. The magnetic map over EW007 shows a wide, complex anomaly with variable thickness that is pronounced in the central part of Laxemar (Figure 4-8) and is also supporting a split of EW007 into two separate structures (along its extent); one gently dipping structure in the central/east and one steeply dipping towards the south (in the west).

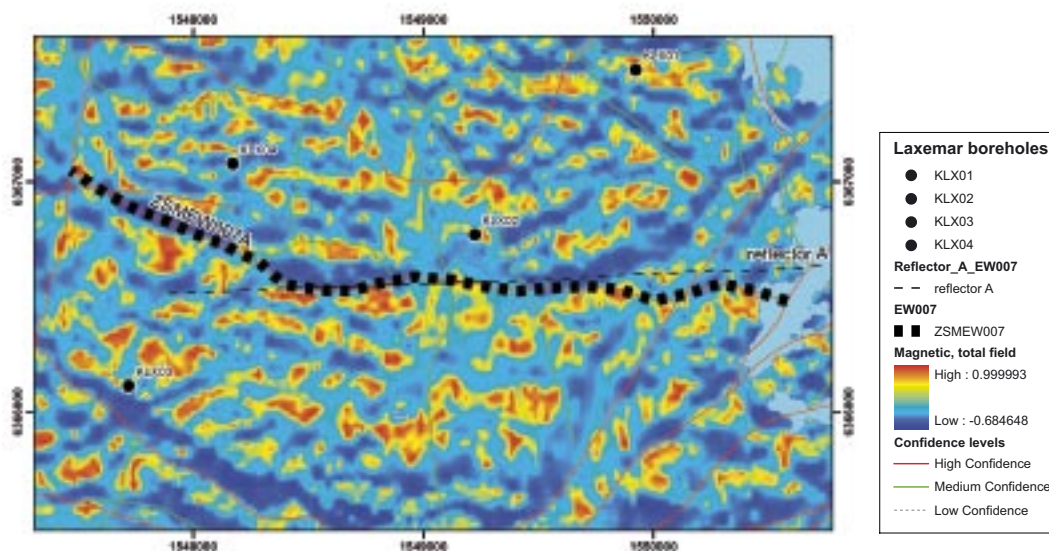


Figure 4-8. Interpolated magnetic map (total field) showing the low magnetic anomaly of EW007 /Triumpf et al. 2003/.

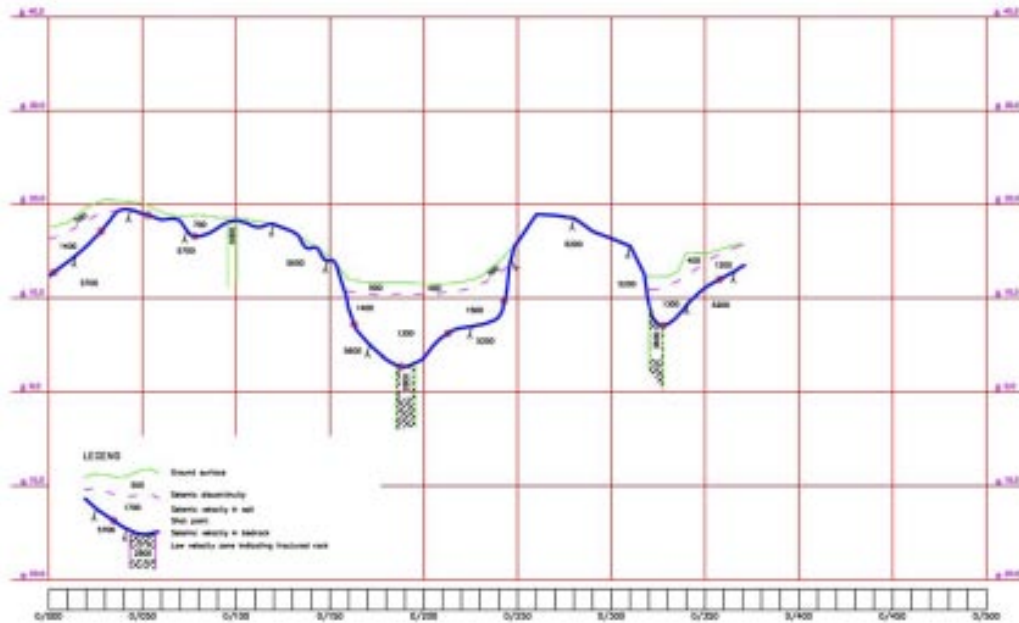


Figure 4-9. Refraction seismic along profile 279 (westernmost part of EW007) /Lindqvist 2004b/. For location of the profile, see Figure 4-7. South is to the left in the figure.

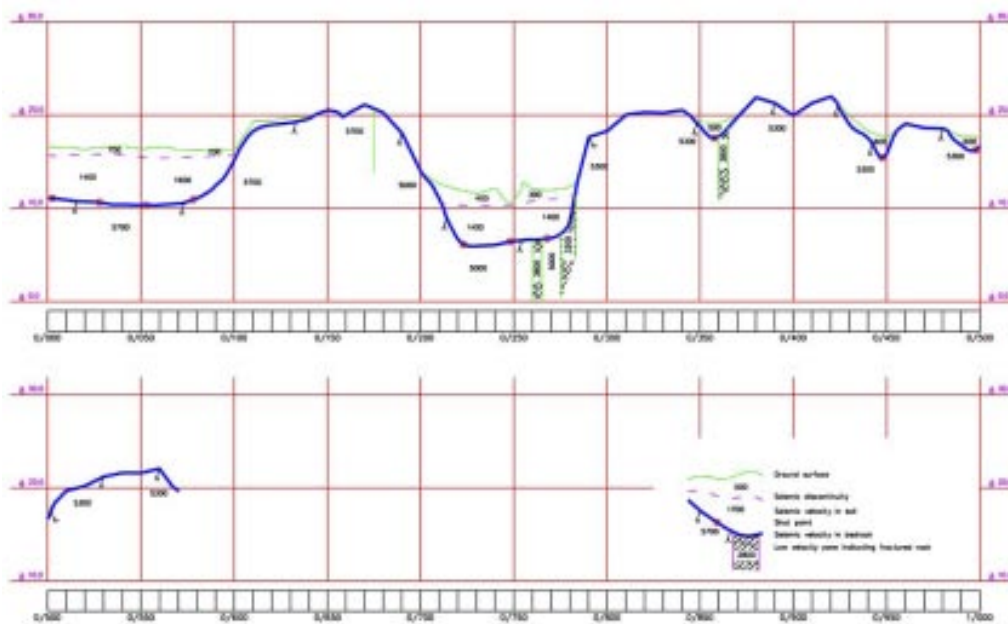


Figure 4-10. Refraction seismic along profile 280 (central part of EW007) /Lindqvist 2004b/. For location of the profile, see Figure 4-7. South is to the left in the figure.

In this model version, it was therefore decided to terminate EW007 against NS059A in the west and create a new deformation zone, EW900 extending from NS001C to just south of KLX04. EW900 is interpreted to dip south about 70 degrees, whereas EW007 dips north 43 degrees as shown in Figure 4-13.

Refraction profiling over EW007, shown in Figure 4-9 to Figure 4-11, shows a zone that has a thickness of at least 10 m, and possibly several neighbouring splay structures. Resistivity sections over the central profile, cf. Figure 4-12, indicates a thickness of about 60 m and the section possibly shows both the northerly dipping EW007 as well as a south dipping zone that could be interpreted as EW900.

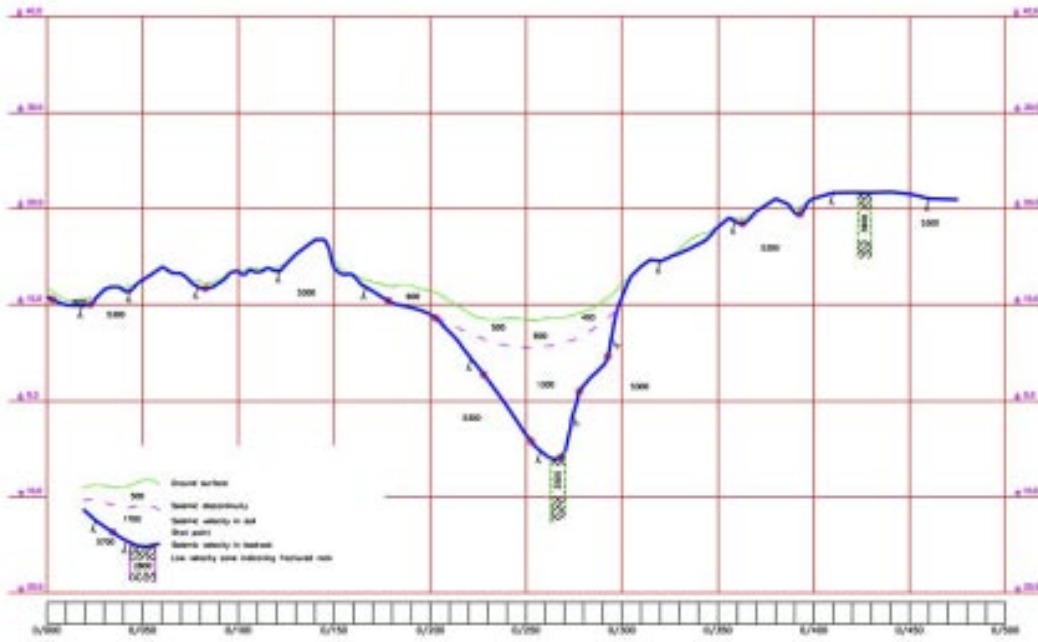


Figure 4-11. Refraction seismic along profile 281 (eastern part of EW007) /Lindqvist 2004b/. For location of the profile, see Figure 4-7. South is to the left in the figure.

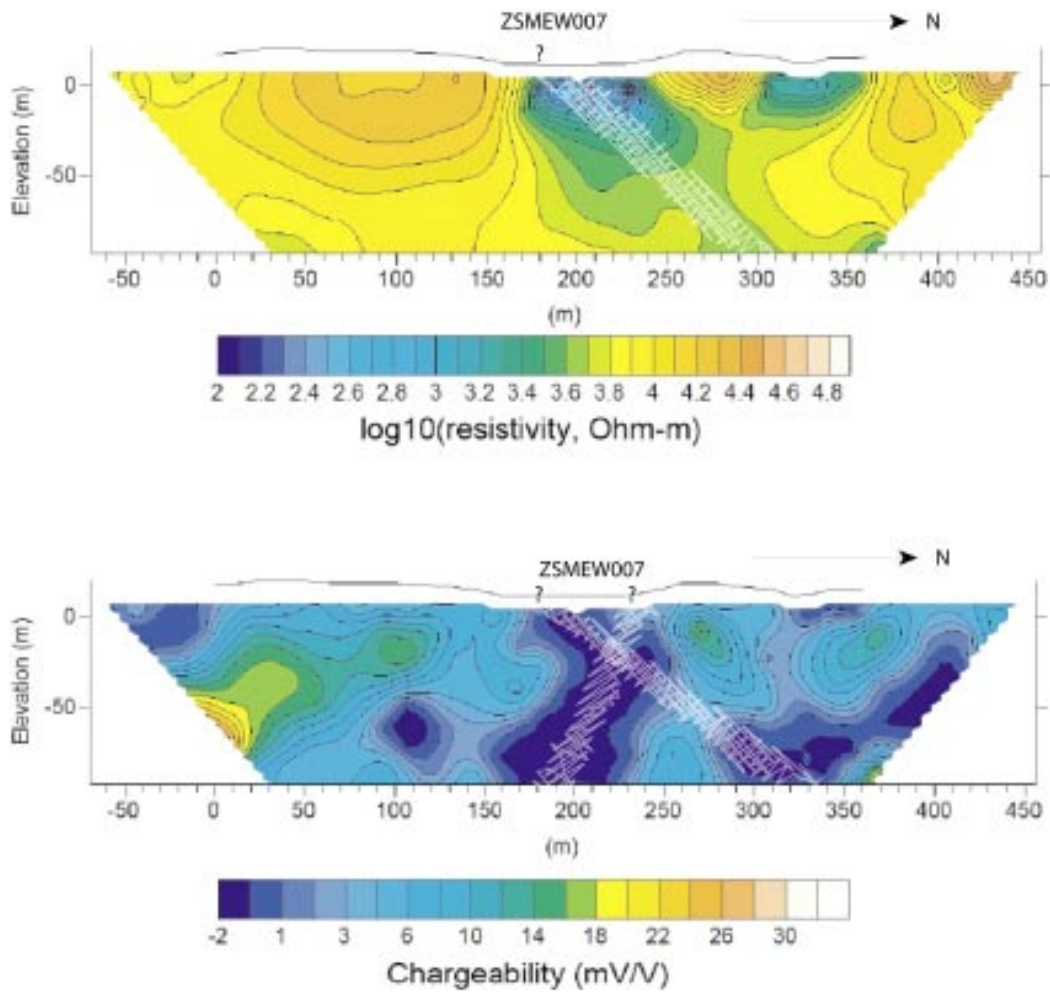


Figure 4-12. Vertical sections of resistivity and chargeability across profiles 279, 310 and 311 /Thunehed et al. 2004/.

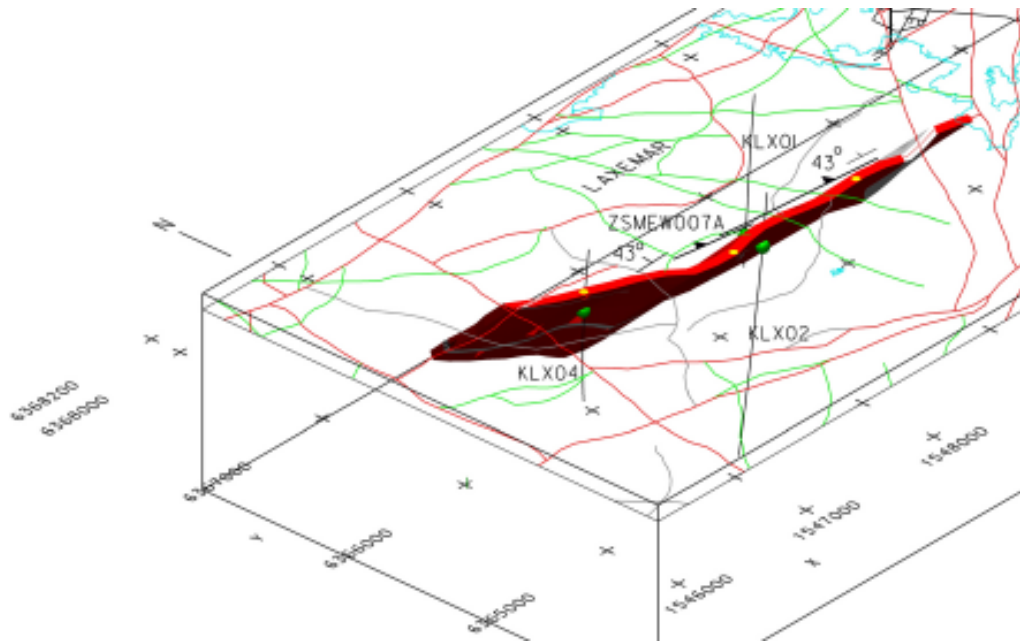


Figure 4-13. EW007 is interpreted to dip northwards (43°) and brittle deformation zones or increased fracturing is observed in KLX01, KLX02 and KLX04. The interpreted dip is parallel to the seismic reflector A /Juhlin et al. 2004a/.

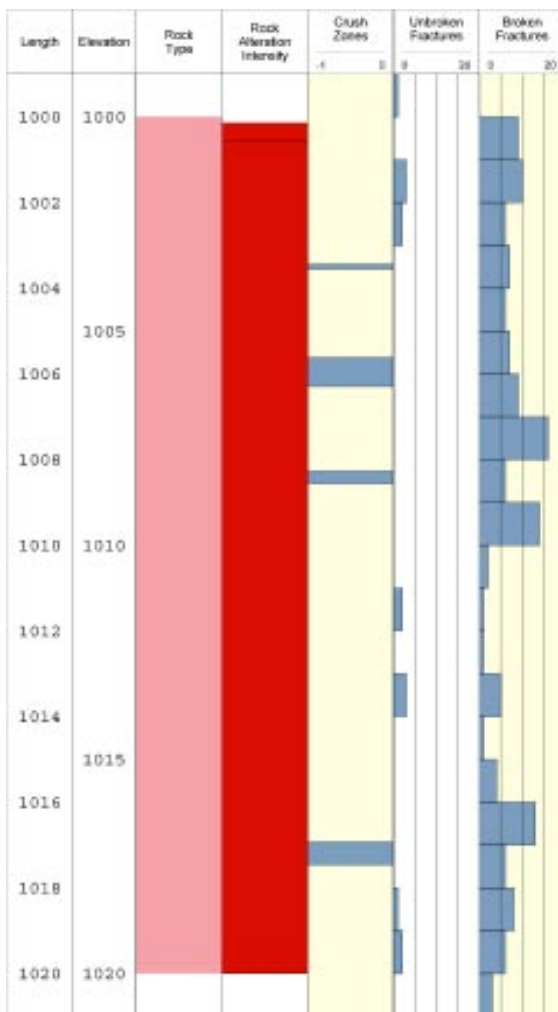


Figure 4-14. The interpreted intersection depth in KLX01, section 1,000 to 1,020 m. Increased fracturing and crush is dominating most of this section together with altered host rock.

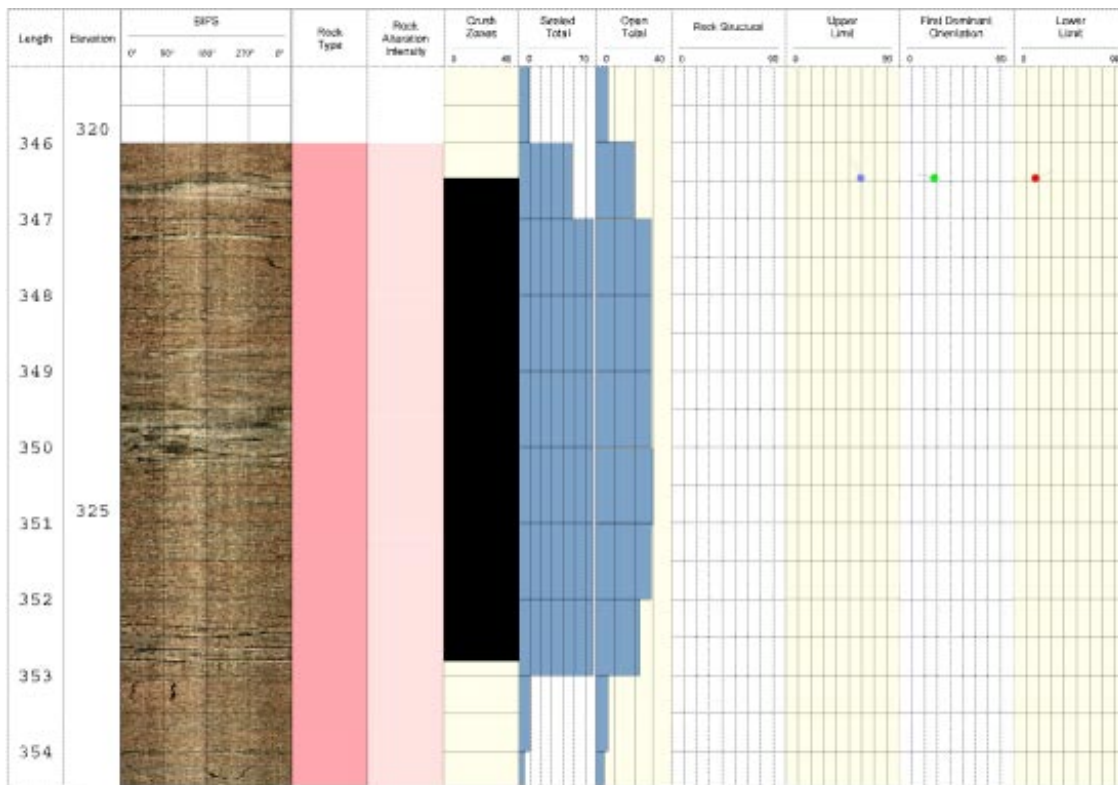


Figure 4-15. The interpreted intersection depth of EW007 in KLX04, section 346 to 354 is dominated by crush and increased fracturing as well as intense alteration. The dominant rock structure in this section is E-W.

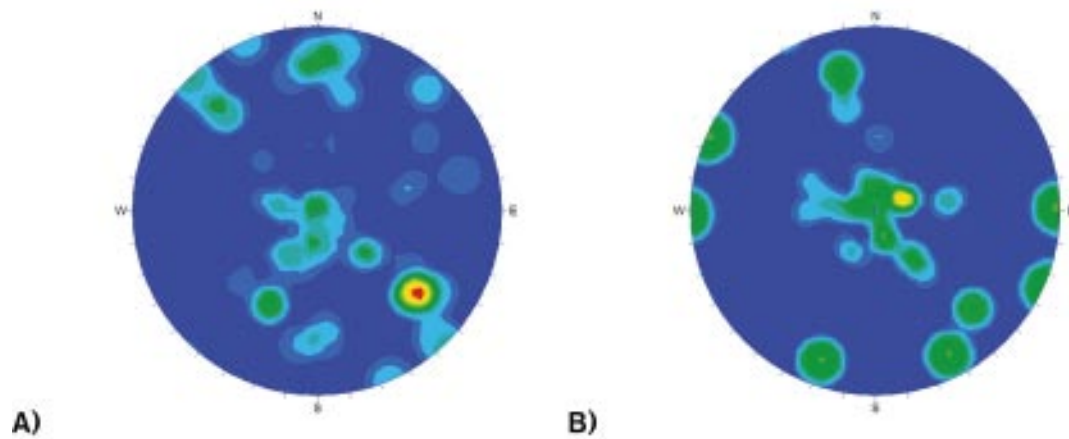


Figure 4-16. Fracture orientations in the target sections of KLX02 (255–265 m), and KLX04 (346–354 m).

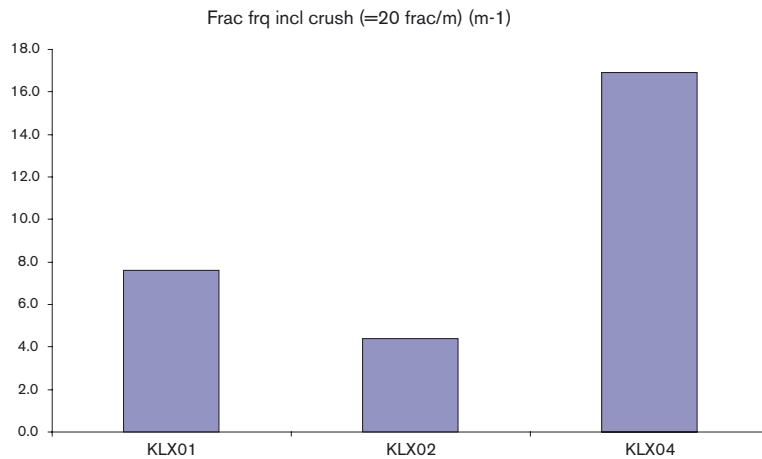


Figure 4-17. Fracture frequency observed in target sections of KLX01, KLX02 and KLX04. Frequency include crush, calculated as 20 fractures per meter.

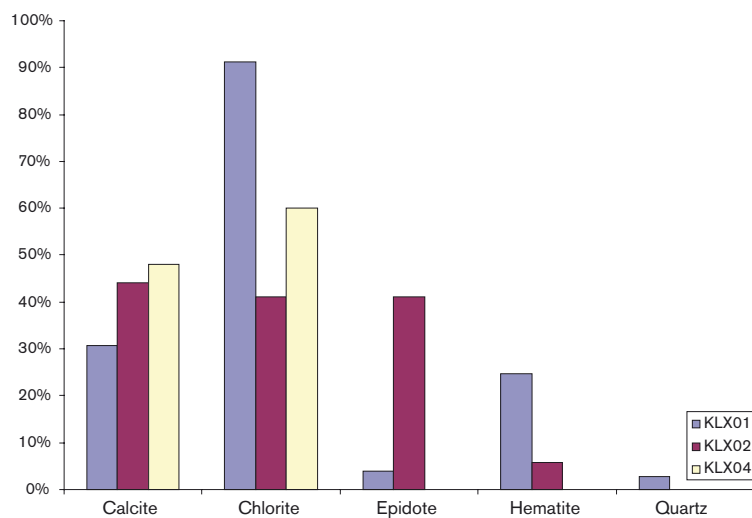


Figure 4-18. Observed fracture minerals in target sections of KLX01, KLX02 and KLX04.

Figure 4-13 illustrates the interpreted northerly dip of EW007 and the borehole intersections with KLX01, KLX02 and KLX04. At the intersection depth in KLX01 fracture frequency is increased as well as several crush sections and increased alteration of the host rock, cf. Figure 4-14. The section in KLX04 (314–391 m), cf. Figure 4-15, shows a altered, highly fractured rock and with a foliation in an E-W orientation parallel to EW007, which indicates not only a brittle component but also an older, ductile deformation along the zone (Figure 4-16).

Fracture frequency in the KLX01, KLX02 and KLX04 sections range between 4 to 18 fractures per meter which is dominated by chlorite and calcite filled fractures as shown in Figure 4-17 and Figure 4-18.

The assembled properties and interpreted borehole intercepts for EW007 and for EW900 is presented in Table 4-4 to Table 4-7.

Table 4-4. Property table for ZSMEW007A.

ZSMEW007A				
Property	Estimate	Span	Basis for interpretation	Comments
Confidence in existence	High		Linked lineament, BH and geophysical ground survey	
Strike (regional scale)	278	± 20	Strong magnetic and topographic lineament	
Dip (regional scale)	43	± 10	Seismic reflector and BH indicators	Seismic reflector survey (P-04-215) reflector A, good agreement with strike and dip 43° N. Geophysical profiling; resistivity, magnetic; all suggest northern dip 40–55°.
Thickness, (including transition zones, regional scale)	50 m	20 to 60 m	Lineament, BH and geophysical ground survey	Complex zone. 50 m, based on inclusion of estimated likely transition zones. 10 m wide 'core' of more highly fractured rock based on general ref: geophysical profiling -refraction (P-04-134)
Length (regional scale)	3.3 km	± 200 m	Linked lineaments	
Ductile deformation	–			Brittle deformation zone
Brittle deformation	Yes		Rare field indicators, high fracture frequency in BH's	
Alteration	Oxidation		BH's	Red colouration
Water	Water bearing		BH's	No analysis available
Fracture orientation	Not yet assessed			
Fracture frequency m ⁻¹	10		KLX01, KLX02, KLX04	Frac' frq' incl' crush (= 20 frac/m) (m ⁻¹)
Fracture filling	Ca 41%, Chl 64%, Ep 23%, He 10%, Qtz 1%		KLX01, KLX02, KLX04	

Table 4-5. EW007 borehole intercepts.

BH	Geometrical intercept	Target intercept	Comment
KLX01	972–1,044	1,000–1,020	Oxidation, high fracture frequency, narrow sections with crushed rock, several chlorite or calcite sealed fractures. Uncertainty = 3
KLX02	234–311	265–275	Orientated open fracture sets between BH length 260–280 m show good agreement.
KLX04	314–391	346–355	Brittle deformation with brecciation (sealed network). Low resistivity, variable sonic, very low susceptibility and small caliper anomaly. Radar reflectors at 350.7 m with the angle 70° to borehole axis and at 352.1 m with the angle 20° to borehole axis. Uncertainty = 3
HLX23	0–39		No results available – will require remodelling at a higher resolution with local lineament adjustment to include results

BH	Geometrical intercept	Target intercept	Comment
HLX24			No results available – will require remodelling at a higher resolution with local lineament adjustment to include results
HLX21	1–52		No results available – will require remodelling at a higher resolution with local lineament adjustment to include results
HLX22			No results available – will require remodelling at a higher resolution with local lineament adjustment to include results

Table 4-6. Property table for ZSMEW900A.

ZSMEW900A				
Property	Estimate	Span	Basis for interpretation	Comments
Confidence in existence	High		Linked lineament, field mapping and geophysical ground survey	
Strike (regional scale)	100	± 20	Magnetic and topographic lineaments	Lineament interpretation needs further review.
Dip (regional scale)	70	± 20	Seismic reflector, field mapping and geophysical profiling.	Based generally on field measurements, seismic reflector L (P-04-215), geophysical profiling (P-04-134)
Thickness, (including transition zones, regional scale)	20 m	± 10	Lineament, geophysical ground survey	Based on inclusion of estimated likely transition zones. 10 m wide 'core' of more highly fractured rock based on general ref: geophysical profiling – refraction (P-04-134)
Length (regional scale)	1.7 km	1 to 2 km	Linked lineaments	Clear alternative lineament tie-ups are possible.
Ductile deformation	Yes		Single field indicator	Ductile-brittle deformation zone
Brittle deformation	Yes		Field indicators, inferred from seismic refraction survey	
Alteration	–		await results	
Water	–		await results	
Fracture orientation	–		await results	
Fracture frequency	–		await results	
Fracture filling	–		await results	

Table 4-7. EW900 borehole intercepts.

BH	Geometrical intercept	Target intercept	Comment
HLX25	169–182	166–185	Low resistivity, low sonic, variable density and low susceptibility.
HLX14	11–29	–	await results

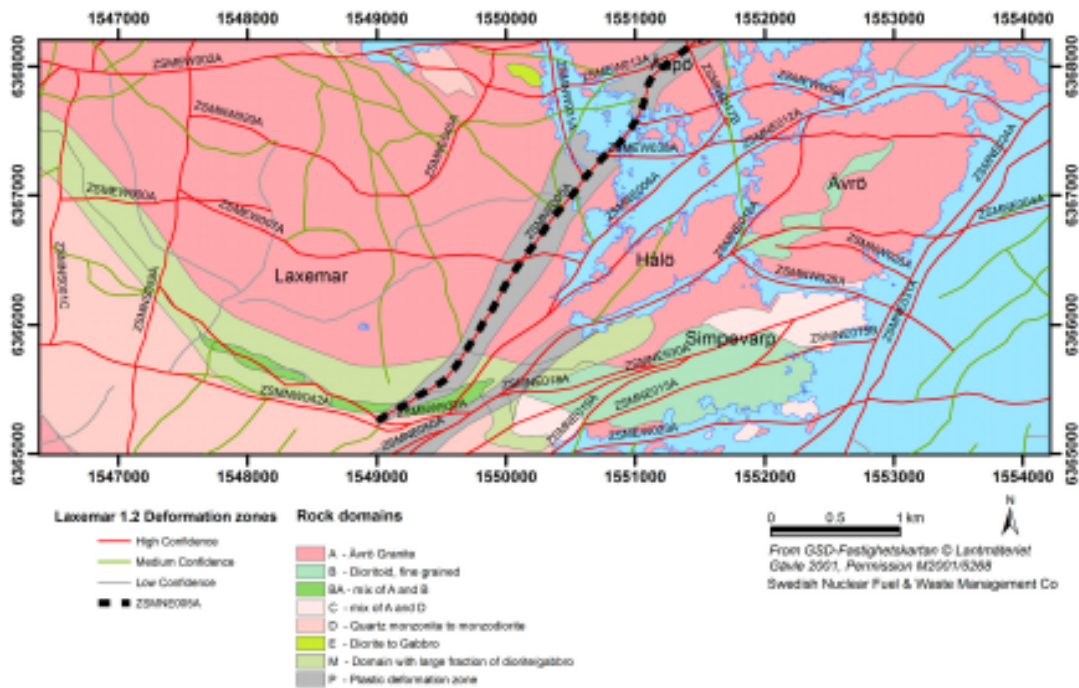


Figure 4-19. ZSMNE005A (Äspö shear zone).

4.6.2 ZSMNE005A (Äspö Shear zone)

ZSMNE005A, Äspö shear zone forms the boundary between the more tectonically influenced rock mass in the Simpevarp subarea from Laxemar (see Section 4.4). The deformation zone is a complex and dominantly ductile zone with smaller sections of brittle deformation, cf. Figure 4-19.

At Äspö, where it is best known, /Rhén et al. 1997/ describes its character as a primarily ductile shear zone with mylonites and epidotic anastomosing shear zones which are interpreted to control the orientation of later brittle deformation, evident in the form of increased fracturing and brecciation. Hydrothermal alteration and formation of different fracture filling minerals probably had an important sealing effect on the main core of the zone. The most hydraulically conductive parts appears to coincide with some narrow highly fractured sections, or single open fractures, which are probably not connected along the entire extent of the zone.

Significant modifications have been made to the zone geometry in this model version compared to Simpevarp 1.2 /SKB 2005a/. An envelope thickness of 250 m was used for the zone to contain the indicators from the geological field mapping, these inferred from the total magnetic field and the results from a reassessment of Äspö data and the existing Geomod model /Berglund et al. 2003/. The Geomod modelled deformation zones EW01b, NEHQ3(top) and NEHQ3(bottom), cf. Figure 4-20, have been interpreted as being associated with the Äspö shear zone (ZSMNE005A) whilst EW1b is interpreted as having a closer association with the Mederhult zone (ZSMNE002A). The 250 m wide envelope contains the trench and borehole indications from EW1b and NEHQ3, cf. Table 4-8 and Table 4-9.

The southern termination to the zone is based on the magnetic anomalies which forms the basis for the surface lineament for Äspö shear zone, cf. Figure 4-21. The narrowing geometry of the zone in the south has been created to more closely conform to the ductile domain P in the rock domain model, cf. Figure 4-3. The northern extension of the zone has been developed in conjunction with a reassessment of the Mederhult zone. Both zones have been reassessed based on the tectonic patterns indicated by the underlying data to the lineament map, particularly the field mapping and the magnetic map, including an estimated thickness and possible continuity in lateral extent of both zones.

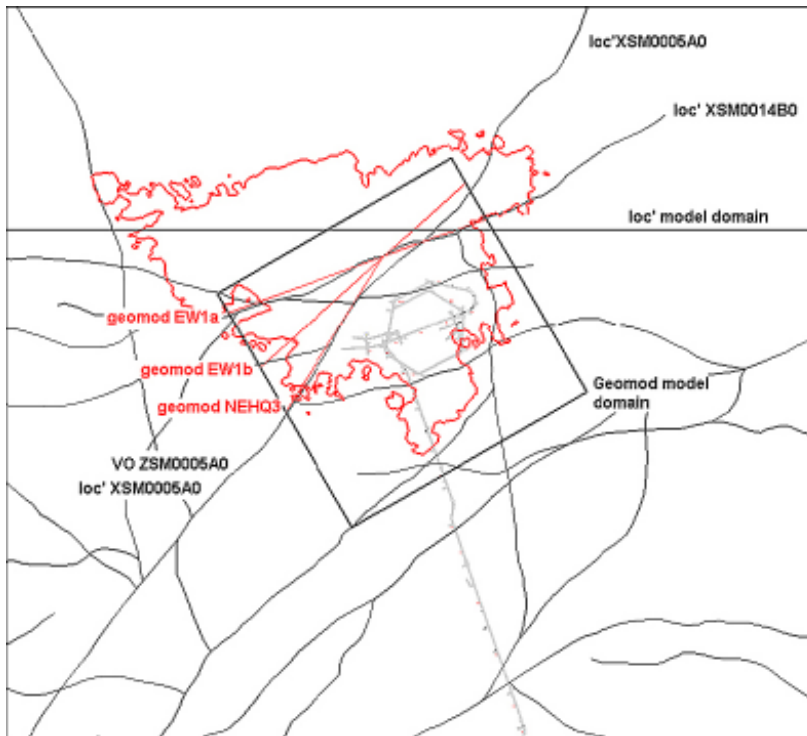


Figure 4-20. Interpretation of Äspö shear zone over Äspö /Berglund et al. 2003/.

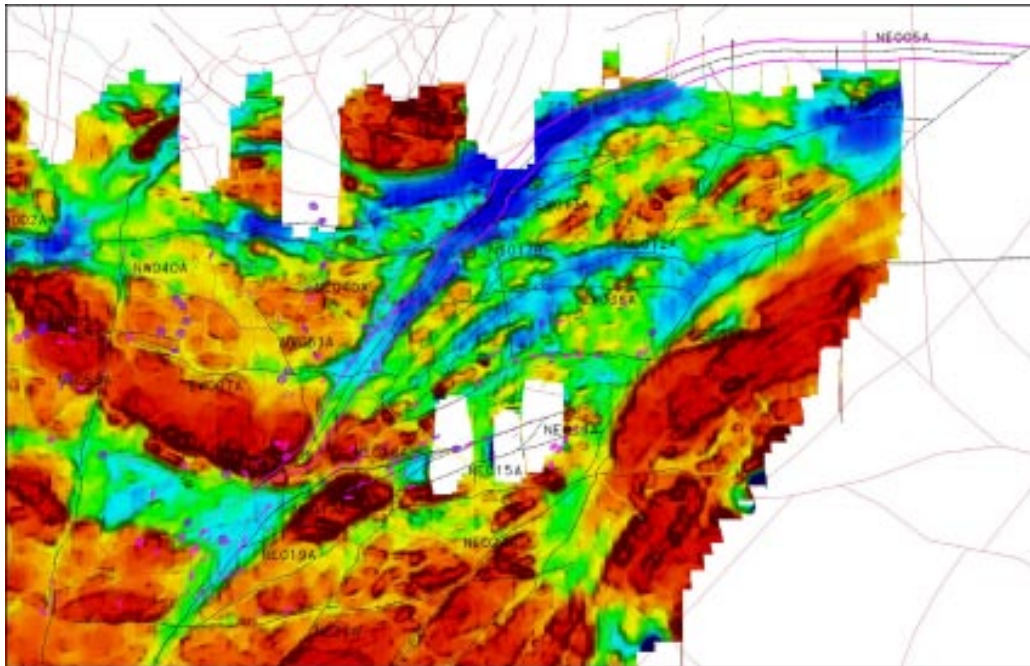


Figure 4-21. Total magnetic field showing the depression along ZSMNE005A.

The north-eastern termination of the zone into ZSMNE024A is uncertain and similar to other zones, it may terminate more to the NE to conform to a more typical sigmoidal pattern. The zone has been modelled vertical, as shown in Figure 4-22, rather than steeply dipping towards the south as in the Simpevarp 1.2 model. The current stand is considered more reasonable considering the complexity and dominating ductile nature of the zone and the lack of well constrained data to support a certified dip direction for the whole deformation zone.

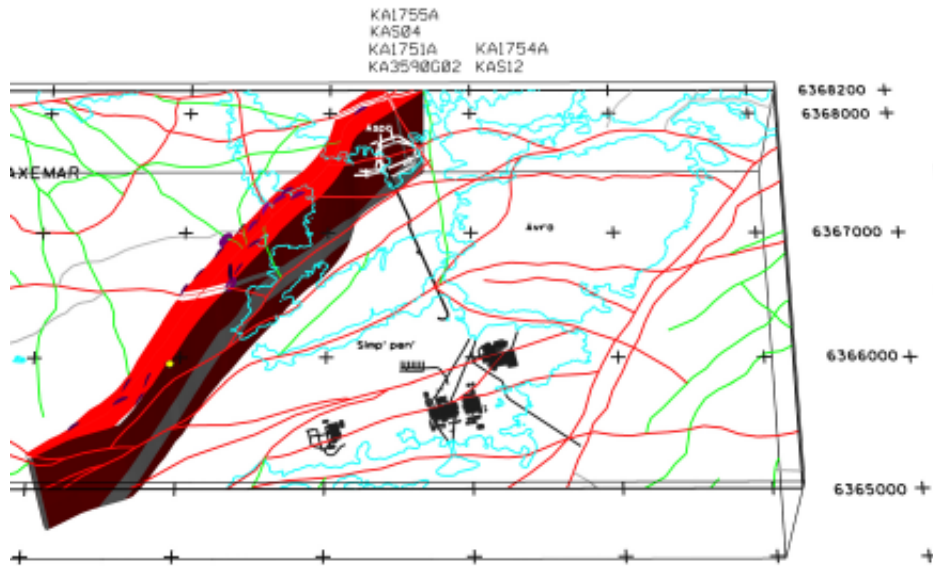


Figure 4-22. ZSMNE005A (Äspö shear zone) is modelled as a 250 m thick deformation zone with a vertical dip based on its complex brittle and ductile nature. Discs at surface intersections represent field observations. The list of boreholes (top) have been used as direct observations of NE005 during the three dimensional modeling process (see also Table 4-9).

A seismic refraction survey /Lindqvist 2004a/ and Äspö data suggest that while 250 m may be a reasonable thickness to use for representing the zone from a geological standpoint, such a thickness should not be taken to infer the extent of poor rock conditions or rock mass quality /Rhen et al. 1997/. For much of this thickness the rock mass quality is likely to be 'Fair' (based on the RMR system).

Boreholes KA1755A, KA1754A, KA1751A, KAS04, KA3590G02, KAS02, KAS12, KAS17 has been interpreted by /Berglund et al. 2003/ to indicate the position and character of Äspö shear zone at Äspö. In Laxemar, preliminary interpretation of percussion drilling indicates that HLX09 and HLX16 confirm the character inferred from interpretations made from Äspö data, cf. Table 4-9.

Table 4-8. Property table for ZSMNE005A (Äspö shear zone).

ZSMNE005A (Äspö shear zone)				
Property	Estimate	Span	Basis for interpretation	Comments
Confidence in existence	High		Linked lineaments – particularly magnetic. Field mapping results. BHs	
Strike (regional scale)	060	030 to 90	Linked lineaments	030 within the local model area, curving to 090 further north.
Dip (regional scale)	90	± 10	Field mapping	Modelled as vertical to allow for local variations. However, a dip of 90 to 80 SE is considered most probable.
Thickness, (including transition zones, regional scale)	250 m	50 to 300 m	aerial magnetic survey, topography and field mapping	Complex zone, inferred anastomosing geometry.
Length (regional scale)	10.5 km	± 200 m	Linked lineaments	

ZSMNE005A (Äspö shear zone)				
Property	Estimate	Span	Basis for interpretation	Comments
Ductile deformation	Yes		Frequent evidence from field mapping	Ductile-brittle zone.
Brittle deformation	Yes		Weak evidence from field mapping. However, BHs show increased fracturing and brecciation.	Ductile clearly dominates but there has been clear brittle reactivation.
Alteration Water				/Rhen et al. 1997/: report the most conductive parts coincide with some narrow highly fractured sections or single open fractures which are probably not connected along the entire zone.
Fracture orientation	Not yet assessed			
Fracture frequency m ⁻¹	9		KA1755A, KA1754A, KA1751A, KAS04, KA3590G02, KAS02, KAS12	Frac' frq' incl' crush (= 20 frac/m) (m ⁻¹)
Fracture filling	Ca 45%, Chl 69%, Ep 14%, He 14%, Qtz 3%		KA1755A, KA1754A, KA1751A, KAS04, KA3590G02, KAS02, KAS12	

Table 4-9. Borehole indications for ZSMNE005A (Äspö shear zone).

BH	Geometrical intercept	Target intercept	Comment
KA1755A	22–288	95–140	At core length 95–140 m generally > 10 fract./m, at nine sites > 20 fract./m. This wide zone coincides geometrically with EW-1b. Most of the zone is developed in fine-grained granite and partly in granodiorite. Only a thin zone of true mylonite, with a medium tectonized area of 2–4 m around it. RQD is less than 25 at several locations in the zone. At core length 203–213 m ca 10 fract/m except for a 1–2 m wide, /Berglund et al. 2003/.
KA1754A	26–160 (Base)	90–115	A crush zone and surrounding tectonization at ca 90–115 m fits geometrically with EW-1b. The area has a very high fracture frequency and the rock is fine-grained granite, granodiorite and “greenstone” /Berglund et al. 2003/.
KA1751A	45–150 (Base)	110–114	The rock is fine-grained granite, granodiorite and greenstone. No major indications of deformation in the database. However, in /Stanfors et al. 1994/ a section between core length 140 and 150 m coincides with this area and is mapped as a fracture zone and as tectonized. At approximately 110 m there is a crush zone and a tectonized area developed in fine-grained granite and “greenstone”, /Berglund et al. 2003/.
KAS04	2–464	131–437	Two mylonites. Also four areas with weak to intermediate tectonization. The rock is granodiorite and fine-grained granite, /Berglund et al. 2003/.
KA3590G02	20–30 (Base)	19–30	Intermediate tectonization. /Berglund et al. 2003/.
KAS02	–	795–924	No longer geometrical intercept but keep indicator for review
KAS12	0 (Top)–269	19–286	
HLX09	99–151 (Base)	–	mapping not available at the time of modelling
HLX16	0–83	–	mapping not available at the time of modelling
KAS17	86–360	–	Only summary preliminary mapping available.

4.6.3 ZSMEW002A (Mederhult shear zone)

The regional Mederhult deformation zone, ZSMEW002A, follows, in the western part, the interpretation made in model version 0 and in the eastern part a topographic and magnetic lineament running along the northern coastline of Äspö (see Figure 4-23 and Figure 4-24). The continuation of the zone along this alignment fits well with the trends indicated by seismic reflector projections /Juhlin et al. 2002, 2004a/, the resistivity measurements from the airborne geophysical surveys (Figure 4-25), /Thunehed et al. 2004/, topographical map /Wiklund 2002/, ground geophysics /Stenberg and Sehlstedt 1989/ and the interpretation for the extension of Äspö shear zone (ZSMNE005A) /Berglund 2004/.

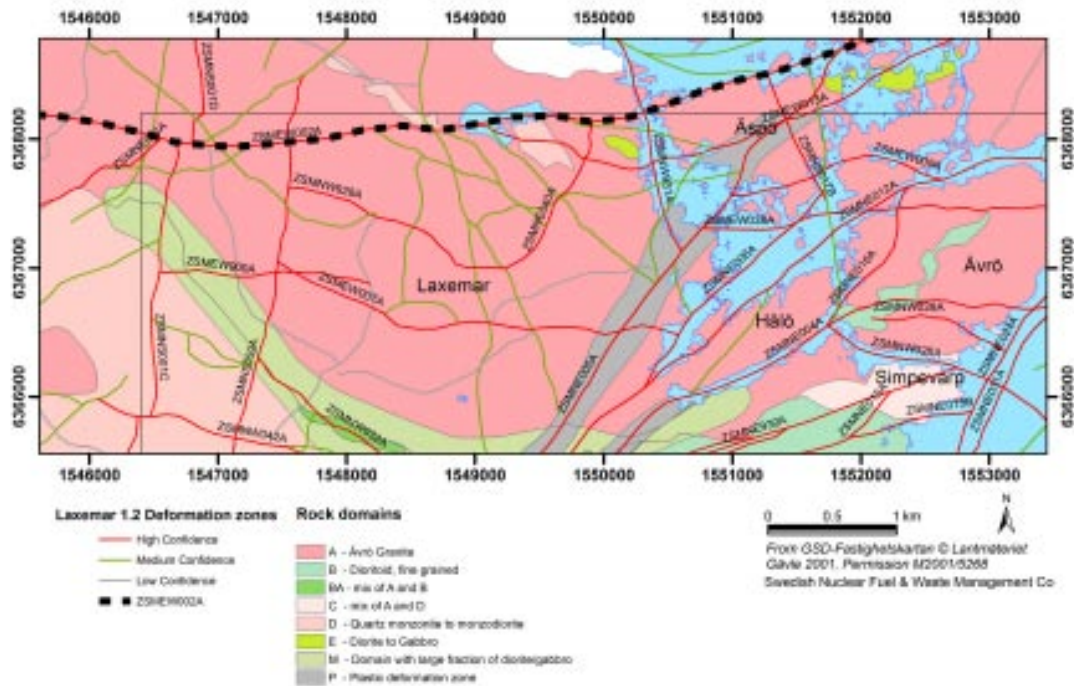


Figure 4-23. Location of the surface trace of ZSMEW002A (Mederhult shear zone).

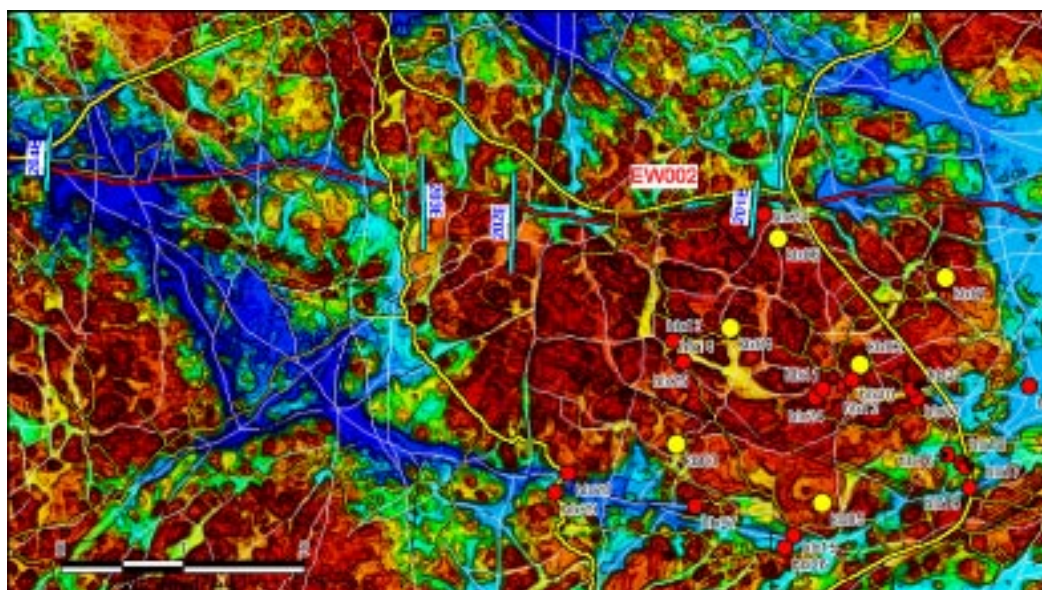


Figure 4-24. Topographical terrain model /Wiklund 2002/ indicates that ZSMEW002A follows a topographical depression with a width typically around 40 to 150 m. Blue lines represents geophysical profiles by /Stenberg and Sehlstedt 1989/.

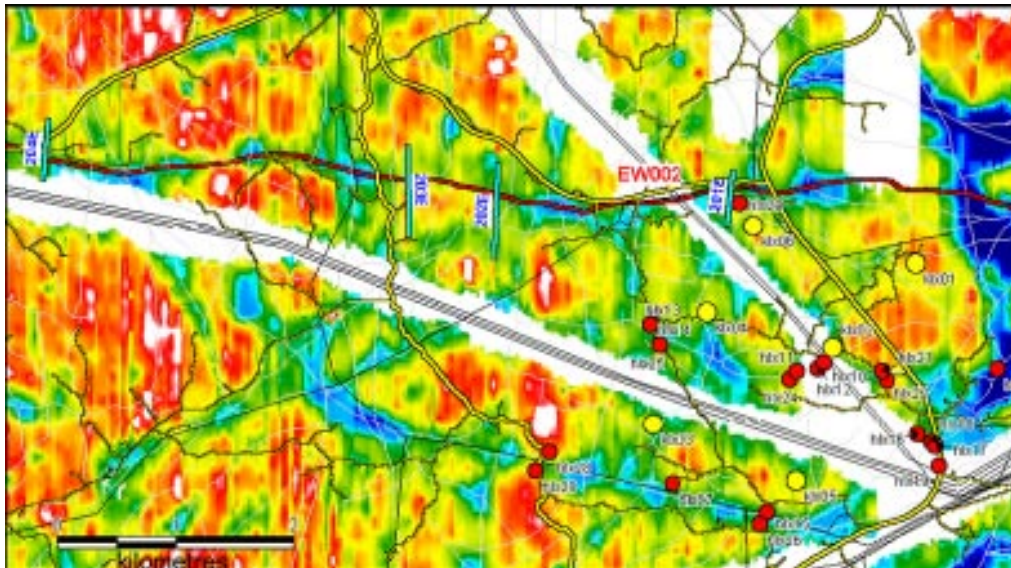


Figure 4-25. Resistivity from helicopter measurements, /Thunehed et al. 2004/, where blue represents low relative resistivity which confirms the EW trend of Mederhult shear zone. Blue lines represents geophysical profiles by /Stenberg and Sehlstedt 1989/.

The zone has previously been verified by ground magnetic and VLF measurements /Stenberg and Sehlstedt 1989/, a refraction seismic survey /Rydström and Gereben 1989/, reflection seismics /Bergman et al. 2001/ and surface geology /Stanfors and Erlström 1995/. Results from the VLF measurements indicate that the zone has a steep southerly dip, whereas observations on the surface suggest a more gentle dip to the southeast, cf. Figure 4-26.

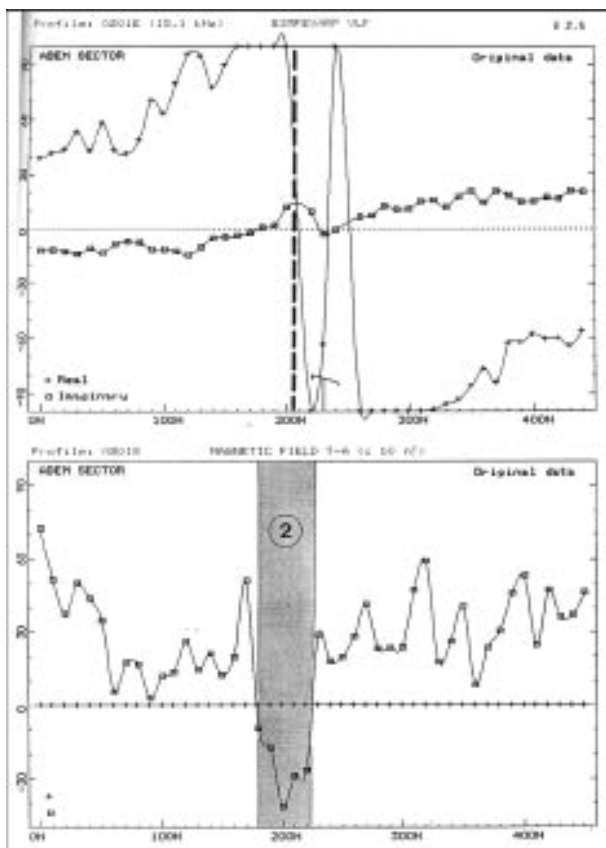


Figure 4-26. Ground geophysical (VLF) profile 201E from /Stenberg and Sehlstedt 1989/ showing a low magnetic anomaly, approximately 40 m wide.

The interpreted mean geometry in terms of strike and dip of the zone within the local model volume is 90/65. The conclusion in the version 0 model regarding dextral movements during the Phanerozoic has not been verified and remains an open issue. The Mederhult deformation zone is considered to have formed under ductile conditions, but have been reactivated under brittle conditions, presumably during several events.

Changes in model version 1.2 are summarised below:

Strike:

Modelled as an EW deformation zone (90°) along a modified lineament trace. This alternative interpretation for the eastern part of the zone has been examined based on a lineament running along the northern coastline of Äspö (see Figure 4-23 and Figure 4-24). The continuation of the zone along this alignment allows a better fit with the trends indicated by the seismic reflector projections, the results from the airborne geophysical surveys, topography and an alternative interpretation for the extension of the Äspö shear zone (ZSMNE005A). Variations of this approximate alignment, locally around Äspö, exist in other reports ex. /Berglund et al. 2003/ and /Rhen et al. 1997/.

Dip:

Seismic reflection results /Juhlin et al. 2002, 2004a/ indicating a steeper dip than in model version Simpevarp 1.2, cf. Figure 4-27. Previously dip was modelled towards the south (55°). However, seismic reflections indicate a steeper southerly dip of 70°S. Dip is modelled as 65° to fit also with borehole intersections.

Thickness (modelled):

The zone is modelled with a total thickness of 100 m (based on an attempt to provide a representative value over the entire zone length), cf. Figure 4-28 and Table 4-10. This thickness, like others, should be interpreted as an envelope, containing the zone indicators, multiple inferred splays etc. Further, the estimated thickness is based on a combination of ‘hard’ data from field mapping, boreholes and tunnel intercepts along with ‘fuzzy’ data from the various background data sets to the original lineament interpretations-magnetic maps etc.

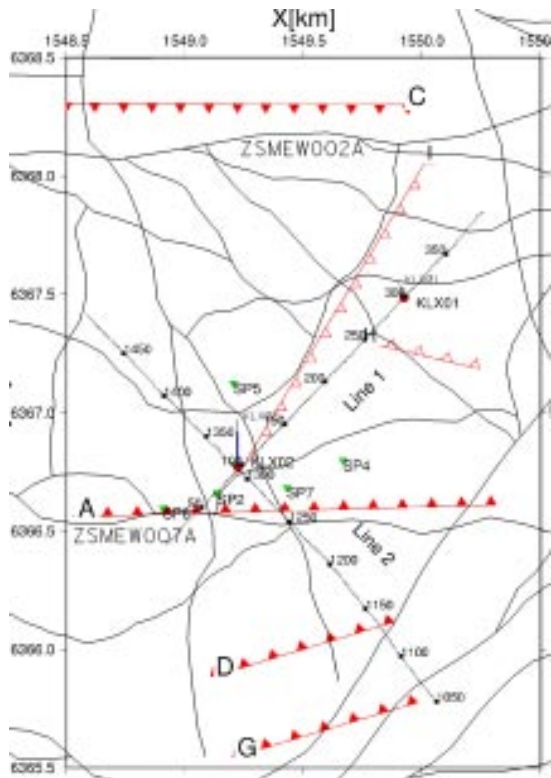


Figure 4-27. Seismic reflector study performed by /Juhlin et al. 2002, 2004a/ show a southerly dip of the Mederhult shear zone.

The zone has been identified in KAS03 (modelled geometrical intersections: 307–495 m, KAS log: around 280–480 m). KLX06 also contains an interpreted intersection as shown in Figure 4-29 (modelled geometrical intersection: 300–430 m, KLX06 log: around 300–400 m, only preliminary mapping available). KAS17 and HLX20 are potentially also intersecting the zone, but no complete information was available at this model version. The zone is not interpreted to intersect borehole KLX02, but to pass underneath the bottom of this borehole.

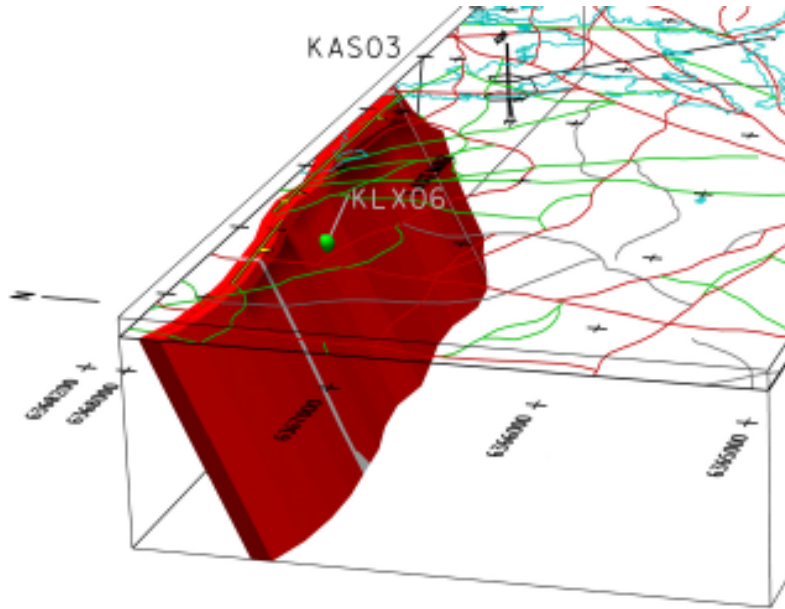


Figure 4-28. ZSMEW002A (Mederhult shear zone) is modelled as a 100 m thick geological shear zone with an orientation of 90/65. The intersection with KLX06 is indicated in green.

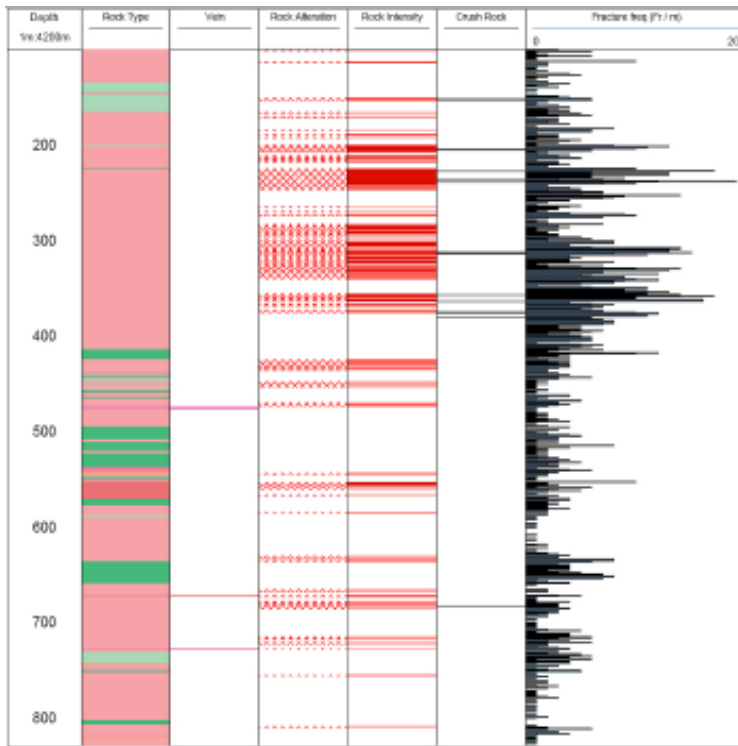


Figure 4-29. Borehole log from KLX06 showing the anticipated intercept of the Mederhult zone in section 300–400 m.

Table 4-10. Property table for ZSMEW002A (Mederhult shear zone).

ZSMEW002A				
Property	Estimate	Span	Basis for interpretation	Comments
Confidence in existence	High		Linked lineament, BH and geophysical ground survey	
Strike (regional scale)	090	± 20	Strong magnetic and topographic lineament	
Dip (regional scale)	65	± 10	Seismic relector and BH indicators	
Thickness, (including transition zones, regional scale)	100 m	20 to 200 m	Lineament, BH and geophysical ground survey	Complex zone, inferred anastomosing geometry.
Length (regional scale)	17.8 km	± 5 km	Linked lineaments	30 km, including extension outside the regional model area
Rock type	Ävrö granite dominates, with fine grained diorite gabbro		KAS03 and KLX06	
Ductile deformation	Yes		Mylonite KAS17. Field mapping	Brittle-ductile zone. Dominantly brittle.
Brittle deformation	Yes		Field indicators. Multiple crush zones KLX06 (only preliminary mapping available). Breccia and crush zones KAS03	
Alteration	Oxidation			
Water				
Fracture orientation	Not yet assessed			
Fracture frequency m ⁻¹	9		KAS03	Frac' frq' incl' crush (= 20 frac/m) (m ⁻¹)
Fracture filling	Ca 66%, Chl 67%, Ep 6%, He 46%, Qtz 5%		KAS03	

Table 4-11. Borehole indications for ZSMEW002A.

BH	Geometrical intercept	Target intercept	Comment
KAS03	307–495	280–480	Brittle and ductule indicators.
KAS17	249–360		Only incomplete preliminary mapping available.
KLX06	300–430	300–400	only preliminary mapping available
HLX20	60–185		No results available

4.6.4 ZSMNW042A

The local major zone ZSMNW042A is located along the southern boundary of the local model area and extends between ZSMNE004A in the east to ZSMNE065A (a medium confidence zone) in the west, cf. Figure 4-30. The extent of the zone is well indicated in the topographical map, cf. Figure 4-31, as well as by a relatively strong magnetic anomaly, Figure 4-32. Two geophysical profiles indicate a subvertical deformation zone /Thunehed et al. 2004/,

cf. Figure 4-33, whereas seismic refractions indicates a 20 m thick core of more highly fractured rock dipping 75 degrees either to the north or to the south /Lindqvist 2004b/, cf. Figure 4-34.

A series of percussion boreholes have been drilled on ZSMNW042A in conjunction with the geophysical profiles /Ask et al. 2005/. However, the locations of these percussion holes are mostly completely within the zone limits and therefore are results from these holes inconclusive with regards to the geological character and thickness of the zone. Several intervals of increased fracturing are observed in HLX15 and HLX26, as can be seen in Figure 4-35 paired with significant water bearing structures in HLX27 and HLX28. This indicates that the hydraulic conductivity of the zone appears to be greater in the west than in the east.

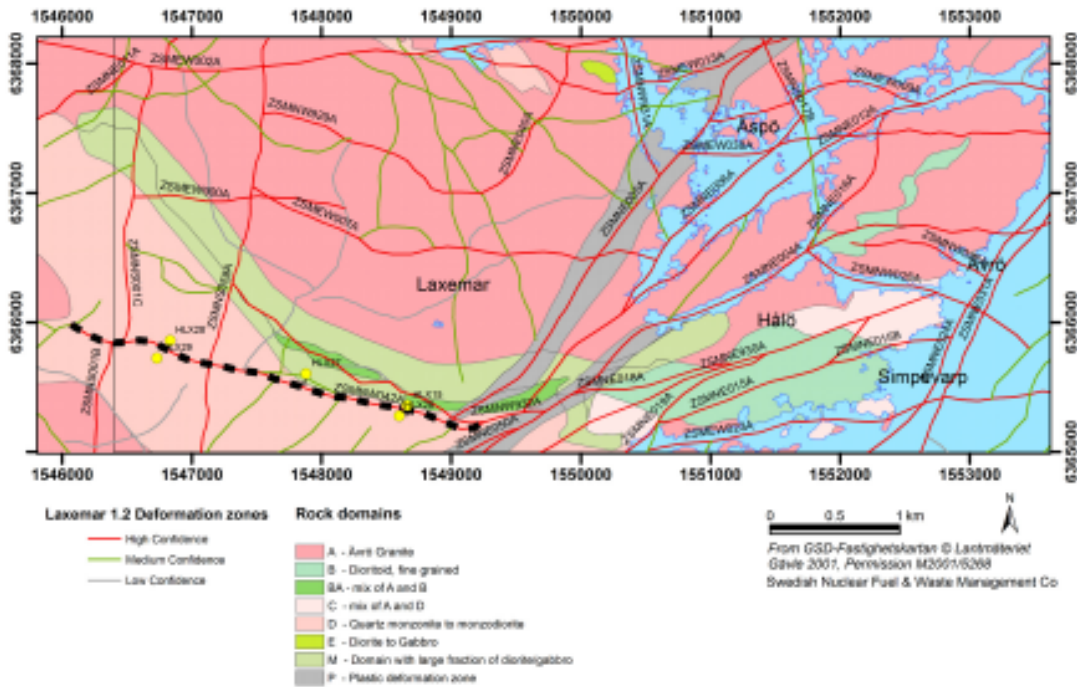


Figure 4-30. Location of ZSMNW042A.

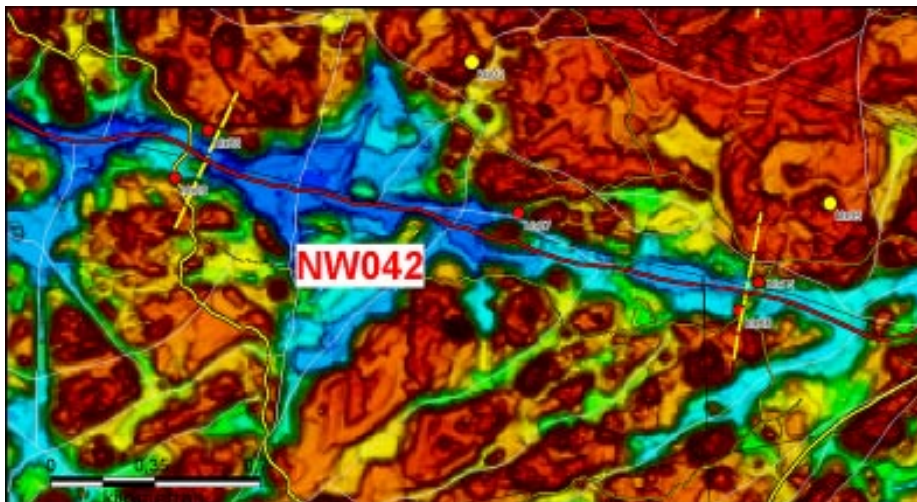


Figure 4-31. Topographical map indicating the two geophysical profiles 276 and 277 across ZSMNW042A /Thunehed et al. 2004/.

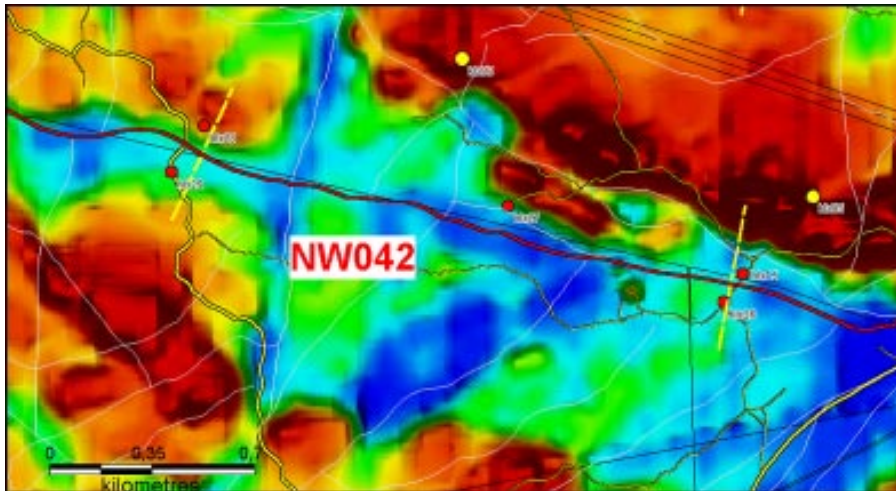


Figure 4-32. Magnetic map indicating the two geophysical profiles 276 (left) and 277 (right) across ZSMNW042A /Thunehed et al. 2004/.

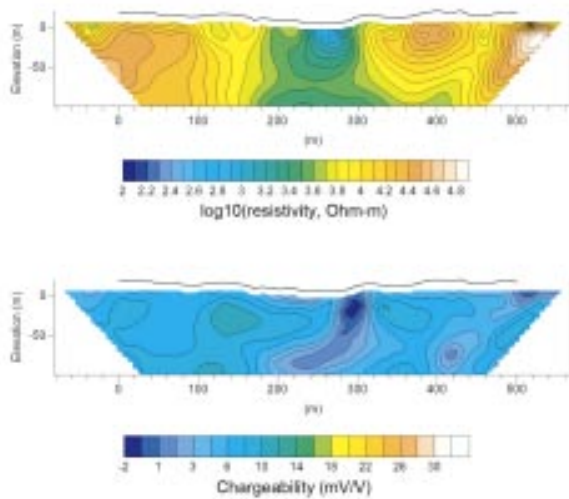


Figure 4-33. Geophysical profile 276 indicating a vertical to southerly dip of ZSMNW042A /Thunehed et al. 2004/.

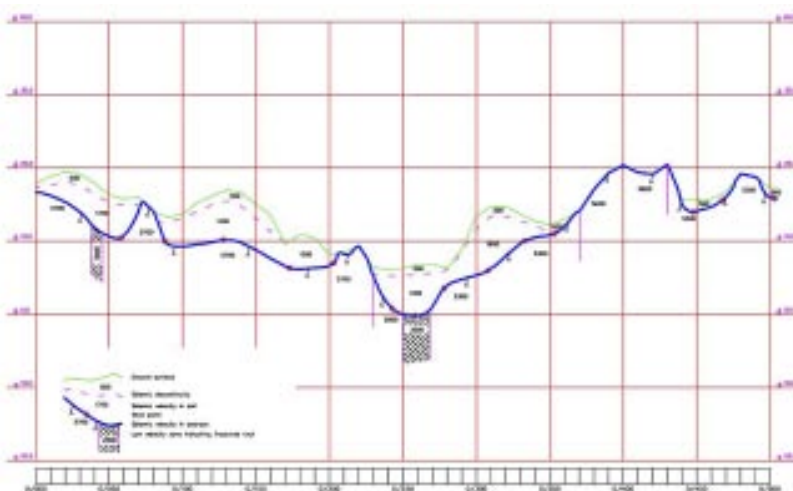


Figure 4-34. Refraction seismic profile 276 across ZSMNW042A /Lindqvist 2004b/. South is to the left in the figure.

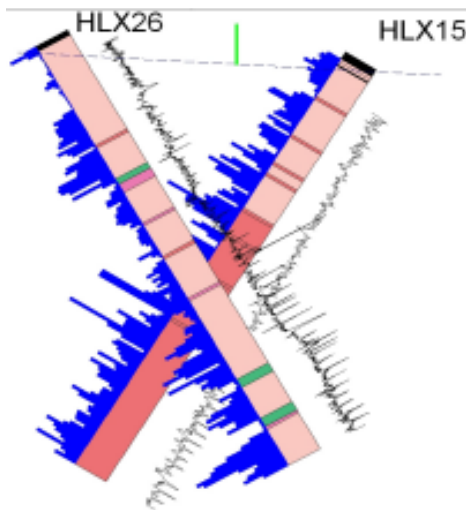


Figure 4-35. Percussion borehole log of HLX15 and HLX26 through ZSMNW042A /Ask et al. 2004c/.

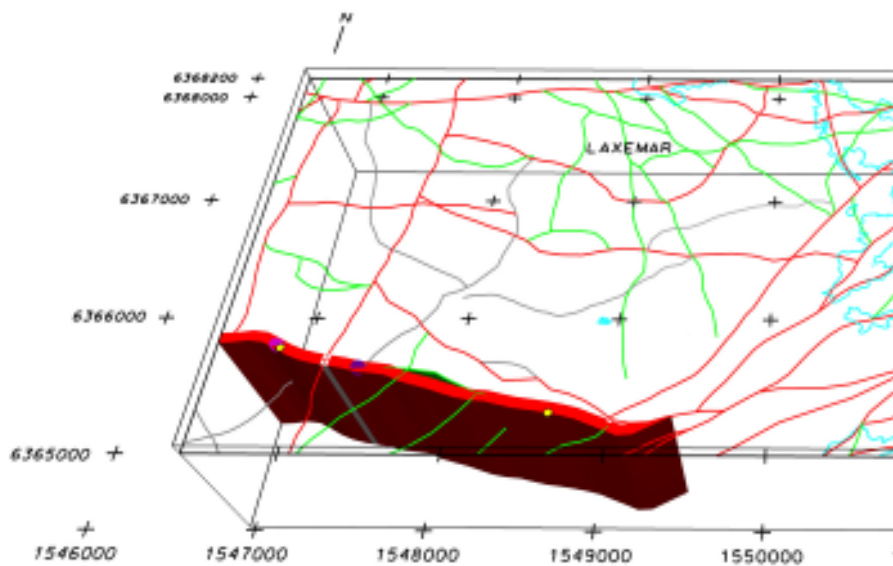


Figure 4-36. ZSMNW042A is modelled with a thickness of 80 m and a vertical dip.

Results from the percussion drillings were only preliminary at the time of modeling and further data are necessary to confirm the character of this zone.

The zone is modelled with a thickness of 80 m which represents an envelope including narrower inferred splays, cf. Figure 4-36.

Table 4-12 and Table 4-13 present the properties and the available borehole indications for ZSMNW042A.

Table 4-12. Property table for ZSMNW042A.

ZSMNW042A				
Property	Estimate	Span	Basis for interpretation	Comments
Confidence in existence	High		Linked lineaments, magnetic, resistivity and seismic refraction profiling	
Strike (regional scale)	105	± 10	Linked lineaments	
Dip (regional scale)	90	± 20	Linked lineaments. Dip-field mapping suggests dip to south, HLX15 orientated fractures suggest 75° to S or N. Surface geophysics suggest subvertical.	
Thickness, (including transition zones, regional scale)	80 m	30 to 80 m	Magnetic and topographic lineament widths.	Model width of 80 m represents an envelope width containing narrower inferred splays. Seismic refraction results indicate a narrower, 20 m wide fractured core.
Length (regional scale)	3.3 km	± 100 m	Linked lineaments	ZSMNW042A,B,C together = 8.3 km
Ductile deformation	Yes		Weak field indicators	Await BH results. current weak evidence suggests a ductile-brittle zone.
Brittle deformation	Yes		Weak field indicators	
Alteration				
Water				
Fracture orientation				
Fracture frequency				
Fracture filling				

Table 4-13. Borehole indications for ZSMNW042A.

BH	Geometrical intercept	Target intercept	Comment
HLX15	0–143		Await results
HLX26	40–151 (Base)		Await results
HLX27	136–165 (Base)		Await results
HLX28	72–154 (Base)		Await results
HLX29			Await results- no current geometrical intercept
KLX05			Await results- no current geometrical intercept

4.6.5 ZSMNS001A–D

The north-south trending regional deformation zone ZSMNS001A–D is divided into four segments which seem to be off set by E-W deformation zones in a right-lateral movement, cf. Figure 4-37. The segments are indicated both in topographic and airborne geophysical data and have been verified through ground magnetic measurements /Stenberg and Sehlstedt 1989/. Furthermore, the northern segment has also been verified in a refraction seismic survey /Rydström and Gereben 1989/ and by increased small-scale fracturing, locally sealed by epidote, and mesoscopic brittle-ductile shear zones along or close to the marked zone.

A steep to vertical dip is indicated by the results of the ground VLF measurements. The thickness of the zone core is estimated to be 5–10 m and the modelled thickness including a transition zone is 100 m, cf. Figure 4-38. This deformation zone has not been studied since version 0 /SKB 2002/ and needs further confirmation through drilling and possibly excavation. Available properties are given in Table 4-14.

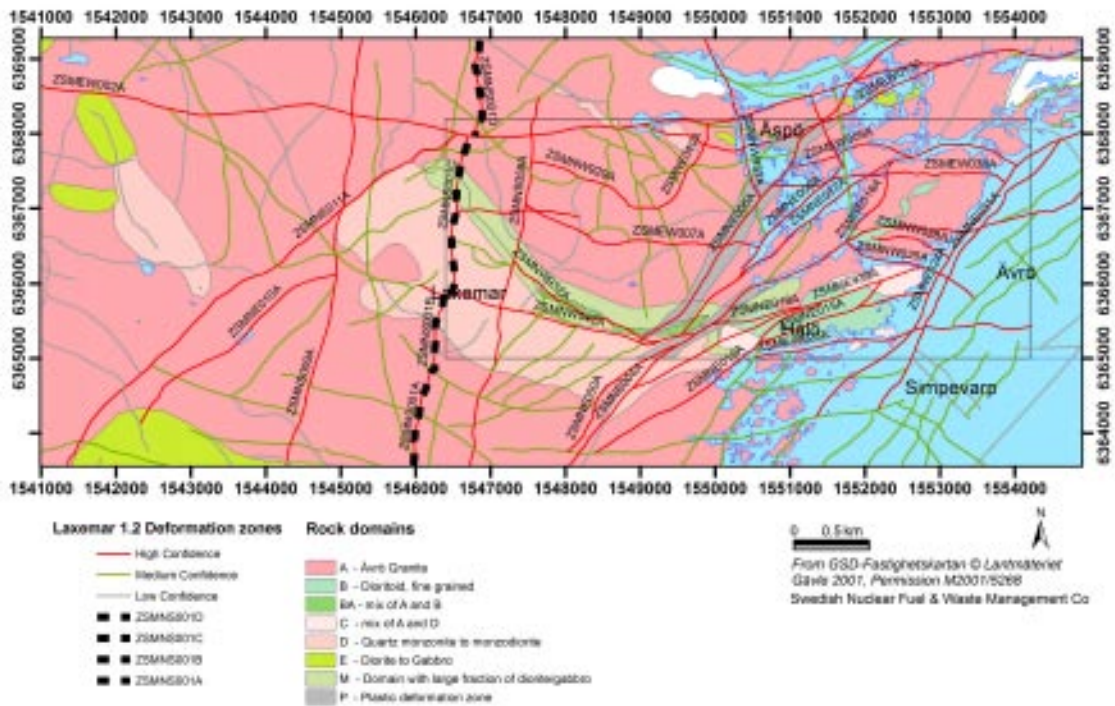


Figure 4-37. Location of ZSMNS001A–D.

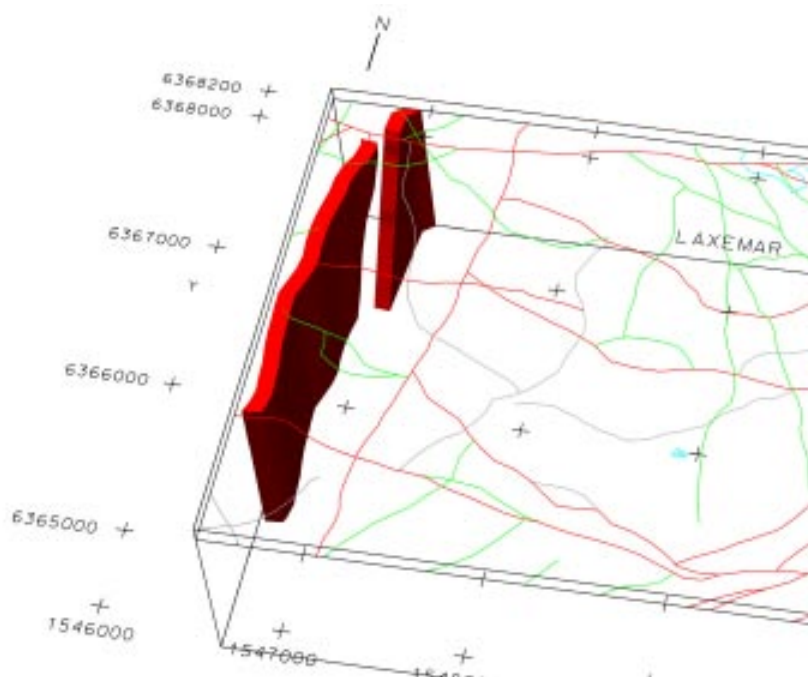


Figure 4-38. ZSMNS001A–D is modelled with a thickness of 100 m and a vertical dip.

Table 4-14. Property table for ZSMNS001A–D.

ZSMNS001A–D				
Property	Estimate	Span	Basis for interpretation	Comments
Confidence in existence	High		Linked lineaments. Ref: v. 0. Verified by field control - ground magnetic and VLF measurements. The northern segment has also been verified by a refraction seismic survey /Rydström and Gereben 1989/	This zone has not been reviewed in Laxemar v1.2. Eastern side down thrown. Ref: /Kresten and Chyssler 1976/.
Strike (regional scale)	010	± 15	Linked lineaments	
Dip (regional scale)	90	± 15	Steep to vertical dip -VLF	
Thickness, (including transition zones, regional scale)	100 m	± 50 m	Linked lineaments	Ref: v0, 10 m 'cores' of highly fractured rock. 50–150 m wide transition envelope.
Length (regional scale)	A_3.4 km B_1.1 km C_2.2 km D_4.4 km	10 to > 11 km	Linked lineaments	Possible southward and northward extension beyond the regional model boundary
Ductile deformation	Yes		Field evidence, Ref: v.0.	Ductile-brittle zone.
Brittle deformation	Yes		Field control.Ref: v. 0. Mesoscopic brittle-ductile shear zones along or close to the marked fracture zone	
Alteration			No data	
Water			No data	
Fracture orientation			No data	
Fracture frequency			No data	
Fracture filling	Ep		Field control.Ref: v. 0.	

4.6.6 ZSMEW009A (EW3 at Äspö)

The deformation zone ZSMEW009A is based on a topographic and magnetic lineament, tunnel and borehole intersections at Äspö HRL, and surface observations in one of the trenches cutting over the Äspö Island /Berglund et al. 2003/. ZSMEW009A is a ductile-brittle zone extending from Äspö shear zone in the west to ZSMNE012A in the east, cf. Figure 4-39.

The orientation, 85/76, is estimated from tunnel observations (TASA ch. 1/407 m), see stereogram in Figure 4-40, and corresponds to zone EW3 at Äspö HRL, /Berglund et al. 2003/. This deformation zone is recognised as a re-activated ductile zone with a crushed and altered mylonitic core as observed in the tunnel and in borehole KAS06 at 66 m borehole length (Table 4-15 and Table 4-16). The thickness, estimated to 12 m from the tunnel, exhibits a variability in thickness between 5 m to 20 m. The tunnel intersection shows a 1–2 m wide central zone of clay alteration.

It is also a major hydraulic conductor with reported inflows to the tunnel in the order of 90 litres per minute, cf. Table 4-15.

The modelled geometry is essentially unchanged from Simpevarp model version 1.2.

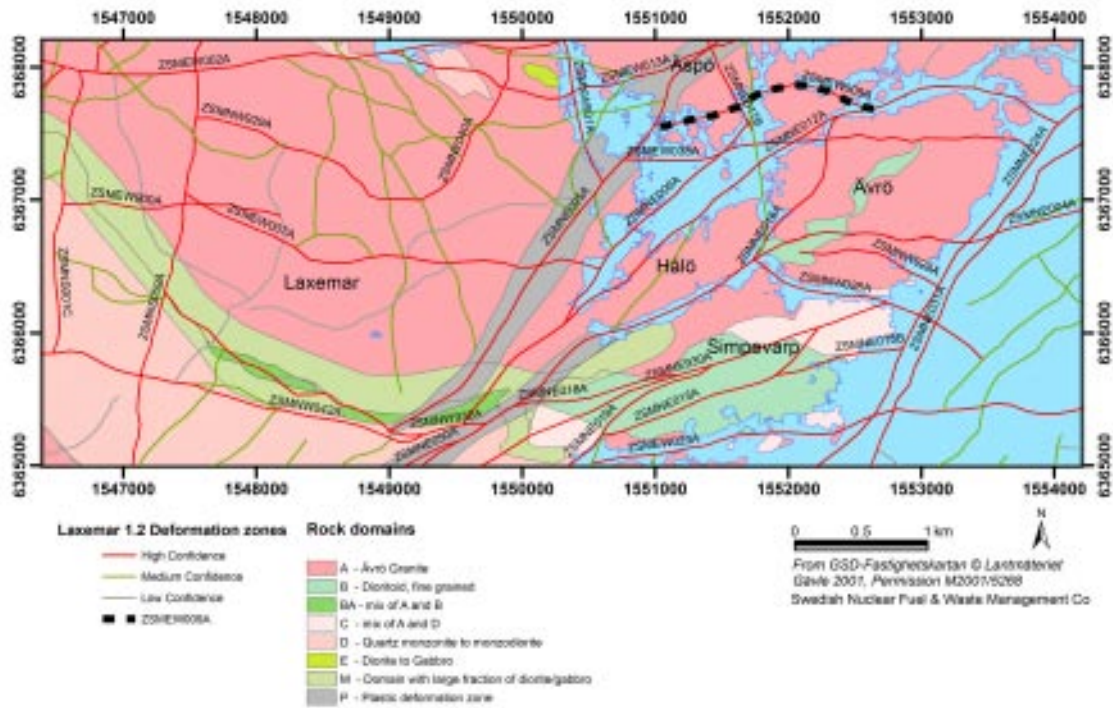


Figure 4-39. Location of ZSMEW009A.

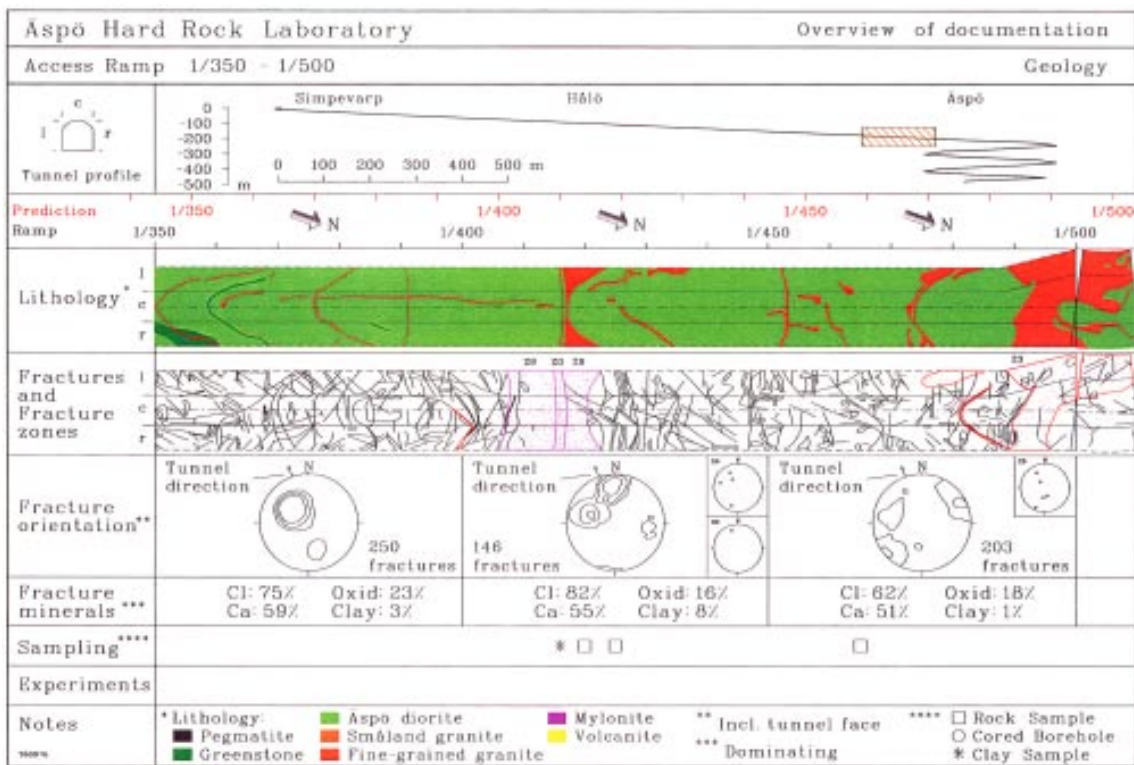


Figure 4-40. Tunnel mapping along the Äspö HRL tunnel, chainage 1/407 m, /PR-HRL-96-19/.

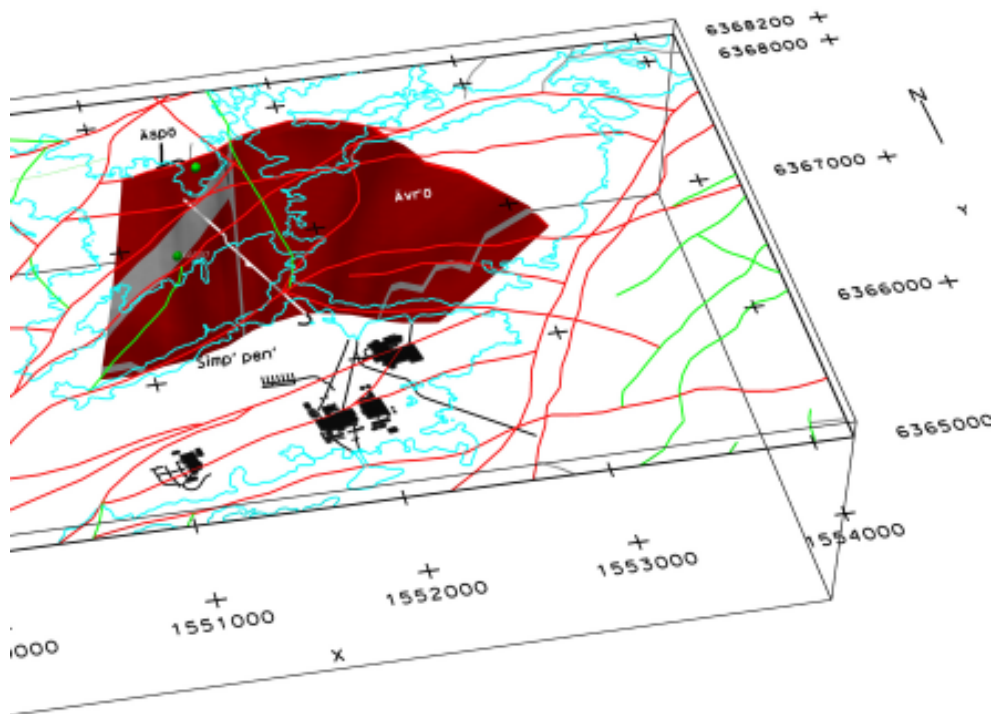


Figure 4-41. ZSMEW900 modelled with a thickness of 12 m. The zone is currently terminated against Äspö shear zone in the west and towards ZSMNE012A in the east.

Table 4-15. Property table for ZSMEW009A.

ZSMEW009A (EW3 at Äspö)				
Property	Estimate	Span	Basis for interpretation	Comments
Confidence in existence	High		Linked lineaments; Surface mapping; BHs; TASA (Äspö) tunnel intercept.	
Strike (regional scale)	085	± 15	Linked lineaments	
Dip (regional scale)	76	± 10	linked lineaments, TASA	
Thickness, (including transition zones, regional scale)	12 m	5 to 20 m	Linked lineaments; BHs; TASA (Äspö) tunnel intercept.	
Length (regional scale)	1.7 km	± 100 m	Linked lineaments	
Ductile deformation	Yes		KAS06 (66 m) mylonitic	Ductile-brittle zone
Brittle deformation	Yes		TASA (Äspö)	
Alteration	1.5 to 2 m thick central clay zone.		TASA (Äspö)	
Water	90 l/min		Inflow into TASA	Ref: PR 25-95-20
	$1.7 \cdot 10^{-5} \text{ m}^2/\text{s}$		Inflow into TASA	Ref: PR HRL96-19
Fracture orientation	Not analysed			
Fracture frequency m^{-1}	14		KAS06	Frac' frq' incl' crush (= 20 frac/m) (m^{-1})
Fracture filling	Ca 65%, Chl 79%, Ep 6%, He 21%, Qtz 1%		KAS06	

Table 4-16. Borehole indications for ZSMEW009A.

BH	Geometrical intercept	Target intercept	Comment
HAS14	0.2–49		Await results
HAS21	25–57		Await results
KAS06	59–76	60–75	Strong tectonization and several sections of crushed core. 1 m thick mylonitic section.
KAS07	562–604 (Base)		Not used in the current model to define geometry. (tectonization recorded /Berglund et al. 2003/)
TASA		1,407–1,421	Figure 4-40. Tunnel mapping along the Äspö HRL tunnel, chainage 1/407 m, /Berglund et al. 2003/.
Surface trench (Äspö)		x = 6367638 y = 1551412 z = 2.5	1.5 m thick mylonite

4.6.7 ZSMEW013A (EW1a on Äspö)

The local major zone ZSMEW013A extends EW along a magnetic and topographic lineament across the Äspö island and is interpreted as being a brittle-ductile zone, cf. Figure 4-42 and Table 4-17. This zone is interpreted as EW1a at Äspö /Berglund et al. 2003, Rhén et al. 1997/, and is also supported by field mapping and borehole intersections and can be considered as a large scale splay structure between Äspö shear zone and Mederhult shear zone. The magnetic map, Figure 4-43, shows weak indication of a low magnetic zone along its extent. The topographic map, Figure 4-44, show a well developed depression west of Äspö which is interpreted as being the extension of EW1a towards the west.

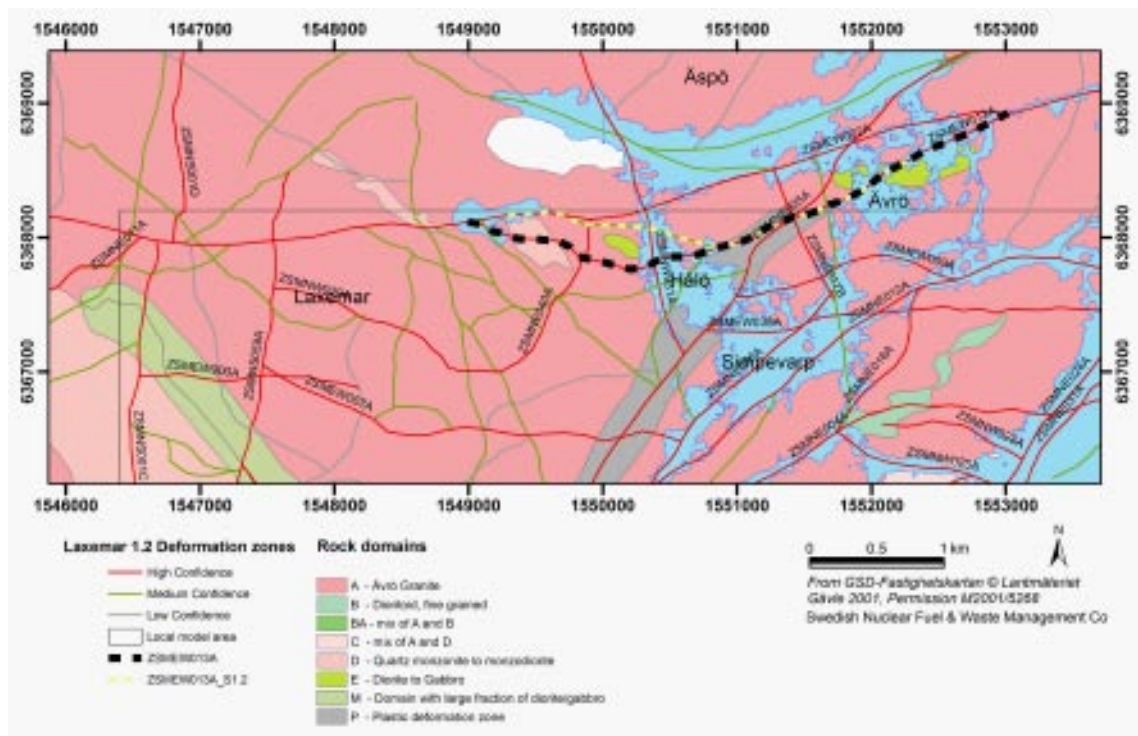


Figure 4-42. Location of ZSMEW013A (black) and the old interpretation in Simpevarp 1.2 (yellow).

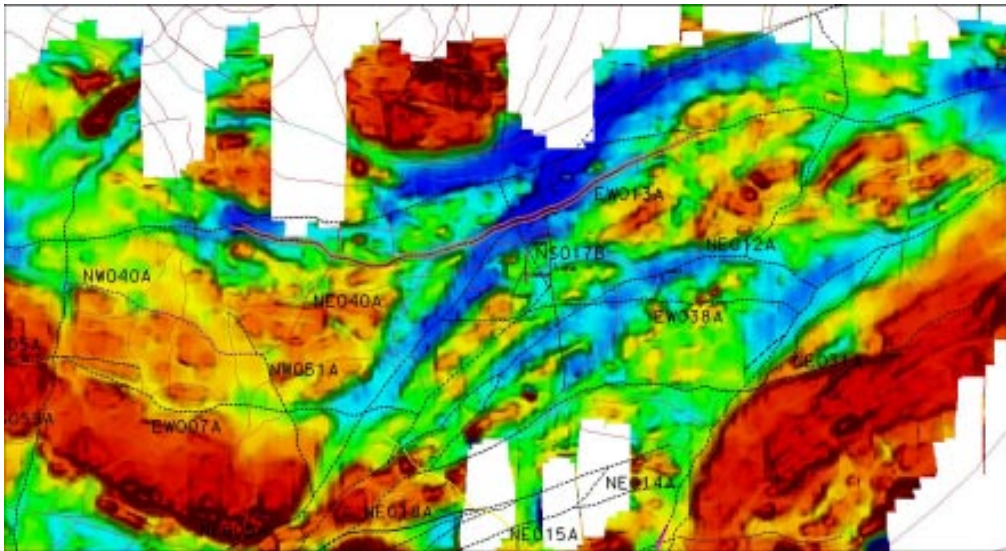


Figure 4-43. Magnetic map over the extension of ZSMEW013A (red) shows a weak anomaly along the extent of the zone.

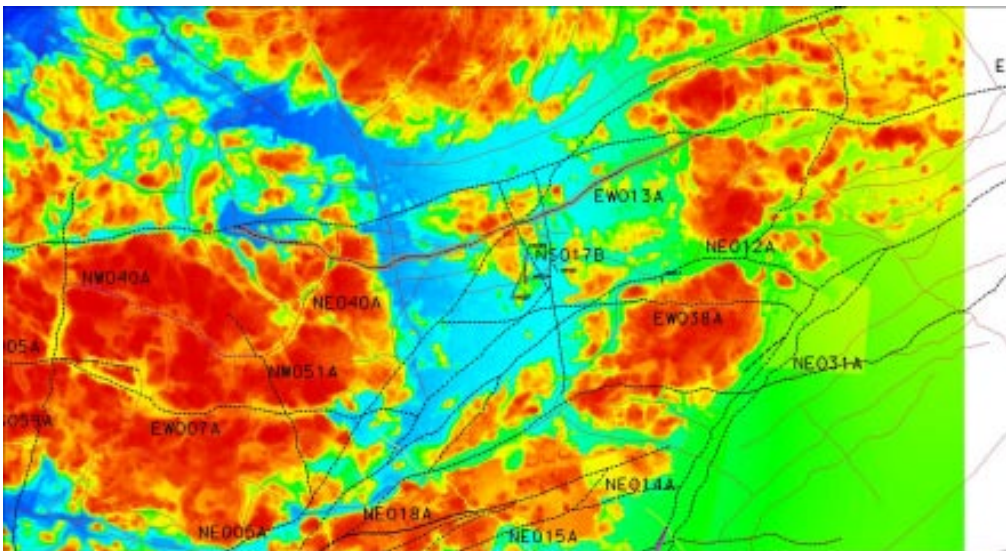


Figure 4-44. Topographical map show a narrow depression along the extent of ZSMEW013A (red).

The zone is described as a crush zone, with enhanced fracture frequency in KA1755A /Stanfors et al. 1994/, also containing a thin breccia/mylonite and a ca 5–7 m wide zone of tectonization, cf. Table 4-17 and Table 4-18. KAS04 is reported to have five thin mylonites in connection with the zone.

ZSMEW013A have been updated in its western extension to correlate better with the Mederhult deformation zone and have been modelled with an orientation of 85/90 and a 45 m thickness, cf. Figure 4-45.

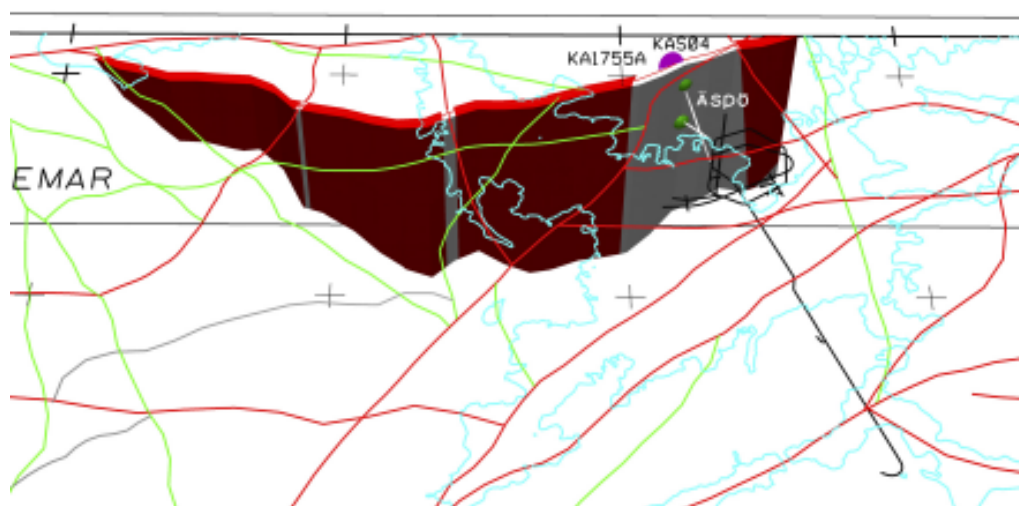


Figure 4-45. ZSMEW013A has been modelled with a thickness of 45 m based on observations at Äspö (EW1a).

Table 4-17. Property table for ZSMEW013A.

ZSMEW013A (EW1a)				
Property	Estimate	Span	Basis for interpretation	Comments
Confidence in existence	High		Linked lineaments, field mapping and BHs.	
Strike (regional scale)	85	105 to 065	Linked lineaments	105 in the west curving round to 065 in the east
Dip (regional scale)	90	± 10	Linked lineaments and BHs.	Ref: Geomod EW1a
Thickness, (including transition zones, regional scale)	45 m	20 to 50 m	Linked lineaments and BHs.	
Length (regional scale)	4.4 km	2.5 to 4.4 km	Linked lineaments.	An alternative interpretation is to terminate the zone against ZSMNE005A
Ductile deformation	Yes		Field mapping and BH (mylonite)	Brittle-ductile zone
Brittle deformation	Yes		BH breccia and crush zones.	
Alteration	Epidotized			
Water				
Fracture orientation	Not yet assessed			
Fracture frequency m ⁻¹	5		KAL755A, KAS04	Frac' frq' incl' crush (= 20 frac/m) (m ⁻¹)
Fracture filling	Ca 57%, Chl 46%, Ep 23%, He 1%, Qtz 3%		KAL755A, KAS04	

Table 4-18. Borehole indications for ZSMEW013A.

BH	Geometrical intercept	Target intercept	Comment
KA1755A	188–234	180–230	A crush zone, with enhanced fracture frequency. A thin breccia/ mylonite and a ca 5–7 m wide zone of tectonization have been recorded. The area as interpreted as EW-1a in /Stanfors et al. 1994/.
KAS04	100–185	87–158	Five thin mylonites at depths: 87, 140, 147, 153 and 158 m. Intense tectonization around the mylonite at 147 m. Ref:Geomod.
HLX03	0–19	–	Awaiting results
HAS01	4–100	–	No information

4.6.8 ZSMEW023A

ZSMEW023A is interpreted to be essentially a brittle zone extending from ZSMNE021A in the west to the local model boundary in the east, cf. Figure 4-46 and Table 4-19.

The geometry, extent and confidence level of this zone has been significantly changed from Simpevarp model version 1.2.

At the western end of the previously interpreted medium confidence zone (Simpevarp 1.2) the surface lineament divided into two branches with the chosen main ‘a’ branch continuing overland on the peninsula. However, a review has led to this being modified with the southerly ‘b’ branch being retained and the more northerly ‘a’ branch being completely removed from the model. This was based on a reassessment of the refraction seismic data /Lindqvist 2004a/ and topographic background data to the lineament map and taking into account the latest field mapping results. Seismic refraction profiles (182 and 184) south of the Simpevarp peninsula show a relatively vertical structure parallel to the bay, cf. Figure 4-47 and Figure 4-48).

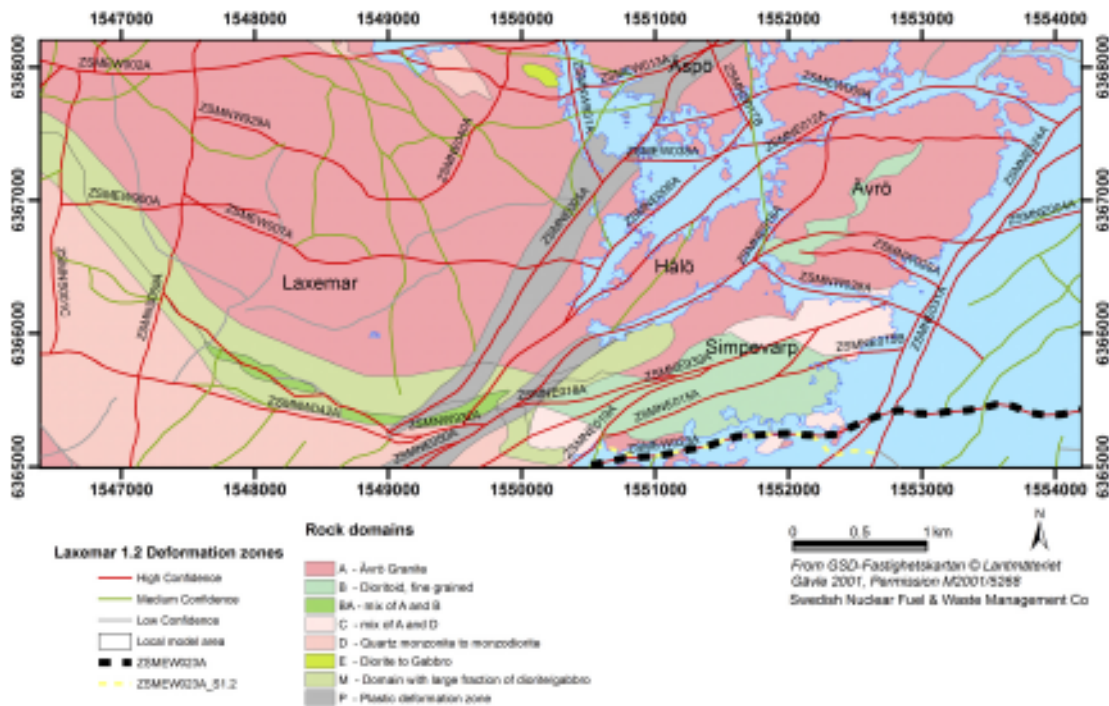


Figure 4-46. Location of ZSMEW023A (black) and the previous interpretation from Simpevarp 1.2 (yellow).



Figure 4-47. Seismic refraction studies on the Simpevarp peninsula and Ävrö island /Lindqvist 2004a/.

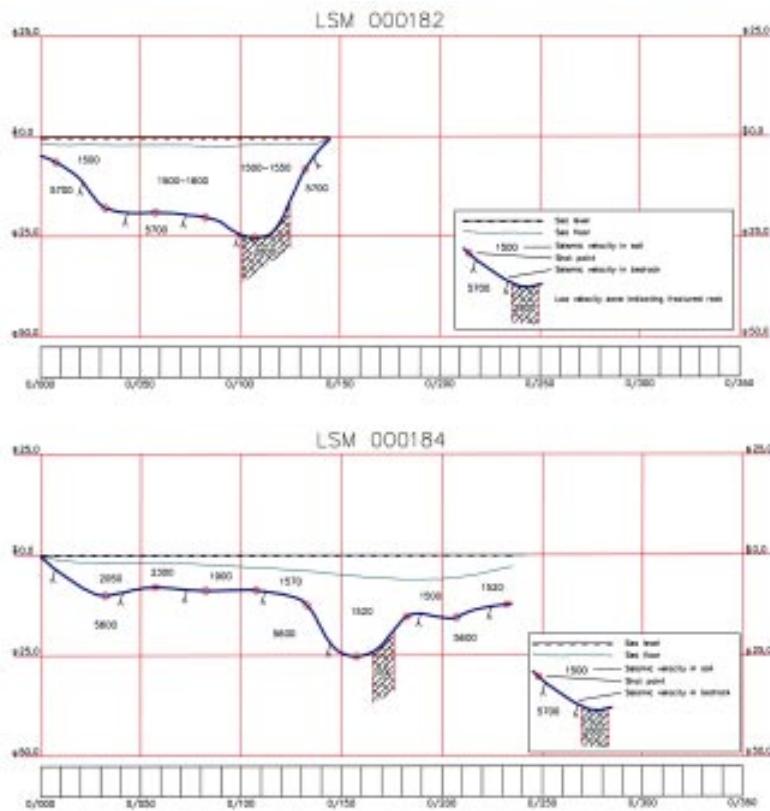


Figure 4-48. Seismic refraction profile LSM000182 (north to the left in the figure) and LSM000184 (south to the left in the figure). See Figure 4-47 for location /Lindqvist 2004a/.

The eastern extension of this zone has also been significantly revised. It was considered that the construction of the man made harbour area for OKG had unduly influenced the ‘natural’ lineaments in this area and suggested that the zone did not intersect the harbour. The geometry has been subsequently modified to reflect bathymetric and magnetic information further east of the harbour, cf. Figure 4-49. An intercept with a brittle structure has been recorded in the OKG water intake tunnel, Figure 4-50, with a ENE, steeply inclined orientation. Observations in the tunnel, Table 4-20, indicated a more diffuse zone consisting of increased fracturing and only minor shears. Preliminary indications also exist in HSH05 at 191–200 m borehole length.

The zone has been modelled as vertical and with an envelope thickness of 20 m based on the background data for the lineament map and seismic refraction survey, cf. Figure 4-51.

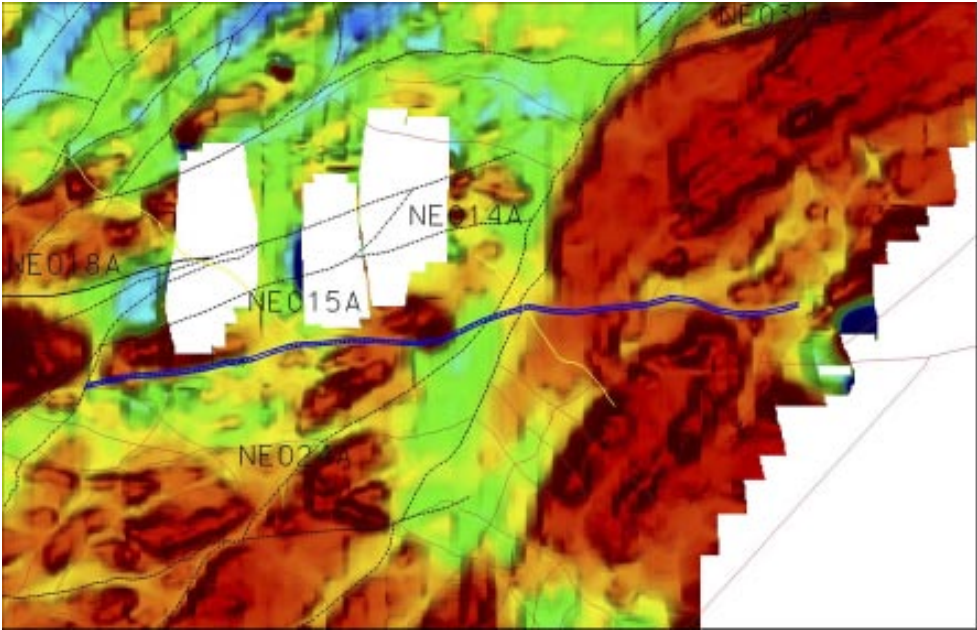


Figure 4-49. Magnetic map showing the interpreted extent of ZSMEW023A.

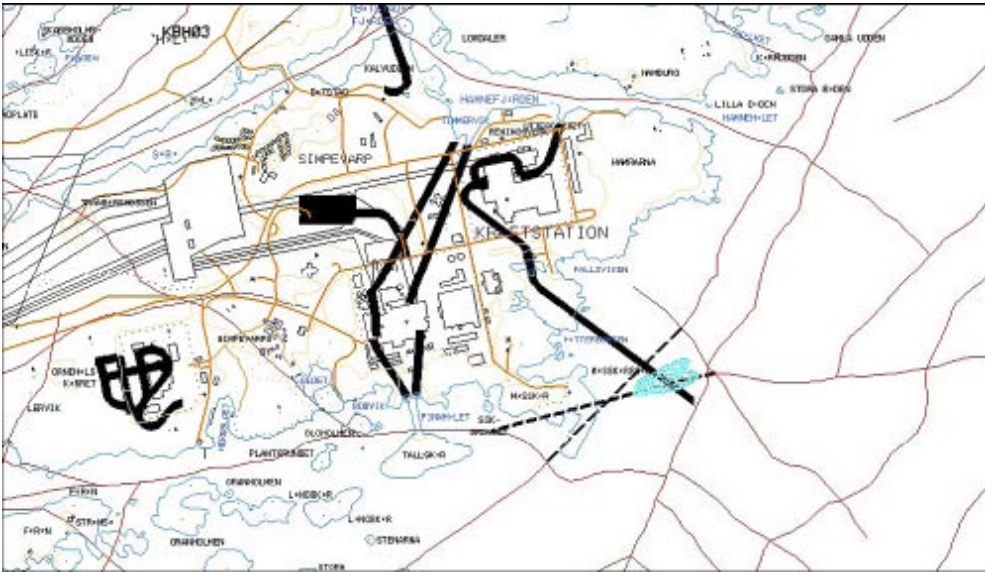


Figure 4-50. OKG water intake tunnel observations that match with a more easterly interpretation of ZSMEW023A.

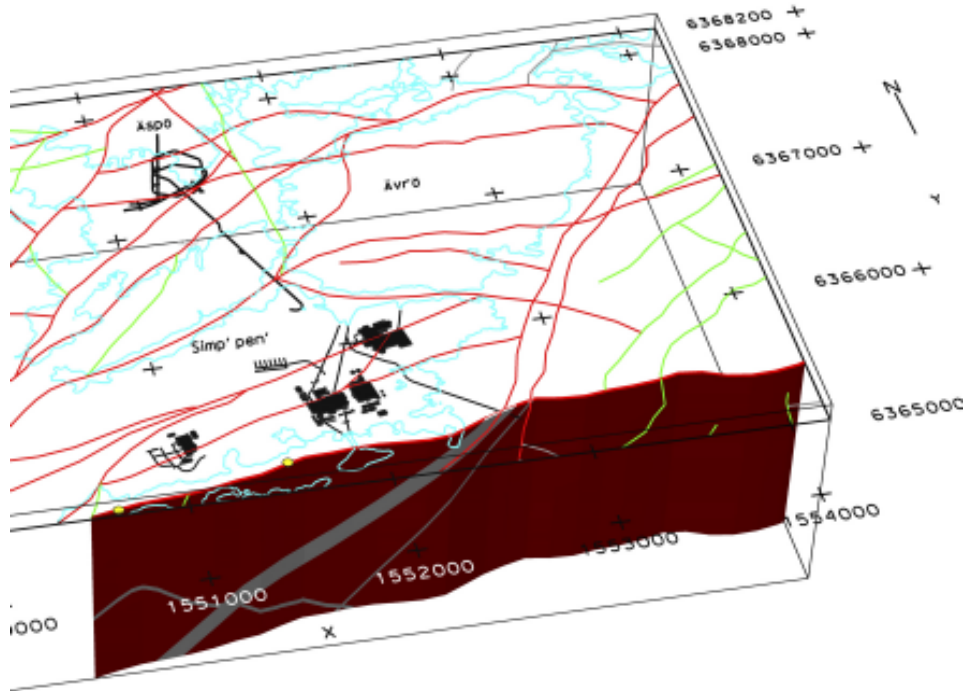


Figure 4-51. ZSMEW023A is modelled with an orientation of 275/90 and a thickness of 20 m.

Table 4-19. Property table for ZSMEW023A.

ZSMEW023A Property	Estimate	Span	Basis for interpretation	Comments
Confidence in existence	High		Linked lineaments; seismic refraction profiling; OKG tunnel intercept.	
Strike (regional scale)	275	± 15	Linked lineaments	
Dip (regional scale)	90	± 20	OKG	
Thickness, (including transition zones, regional scale)	20 m	5 to 50 m	Linked lineaments, seismic refraction profiling and field mapping	The upper 50 m limit is based on indications from OKG that suggest locally a more diffuse zone consisting of increased fracturing and only minor shears.
Length (regional scale)	3.8 km	± 200 m	Linked lineaments	
Ductile deformation	–		No indicators	Brittle zone
Brittle deformation	Yes		OKG	
Alteration	Chlorite and clay			Clay may be depth dependent and be associated with the weathering profile considering the relatively shallow intercept position.
Water	Low transmissivity		Local 'dripping' reported in OKG excavation mapping.	
Fracture orientation	Not analysed			
Fracture frequency	Not analysed			
Fracture filling	CHI, Ca, Clay		OKG	

Table 4-20. Borehole and tunnel indications for ZSMEW023A.

BH	Geometrical intercept	Target intercept	Comment
OKG		Cold water intake ch. 065–110 m	OKG cold water intake ch 065–110 m increased fracturing with up to 1 m wide chlorite and clay filled shear zone.
HSH05	191–200 (Base)	–	await results

4.6.9 ZSMEW038A

ZSMEW038A is interpreted as a ductile structure with a split geometry extending eastward from Äspö shear zone to ZSMNE024A off the coast of Ävrö, cf. Figure 4-52. The zone is interpreted to involve a series of narrow mylonites in a number of boreholes as well as the Äspö tunnel, with potential interference from other zones including ZSMNE006A, cf. Table 4-21 and Table 4-22.

The zone has been extended in both easterly and westerly directions from Simpevarp model version 1.2 based on a review of the topographical and magnetic background material to the lineament map. Previously this medium confidence deformation zone was subdivided into two isolated, widely separate sections leading to one branch being outside of the local Simpevarp 1.2 model. The remaining arm in the local model of Simpevarp 1.2 continued eastwards under Ävrö. The topographic map in Figure 4-53 shows a topographic depression along the extension over Ävrö as well as a weak magnetic anomaly, cf. Figure 4-54 which is now interpreted as being one continuous deformation zone.

This zone is only considered to be a local major deformation zone and intercepts the Äspö access tunnel at 1/180 m where it is visible as a minor mylonite, cf. Figure 4-55. The intercept in the tunnel shows sub-parallel steeply inclined ENE fault orientations, Figure 4-56.

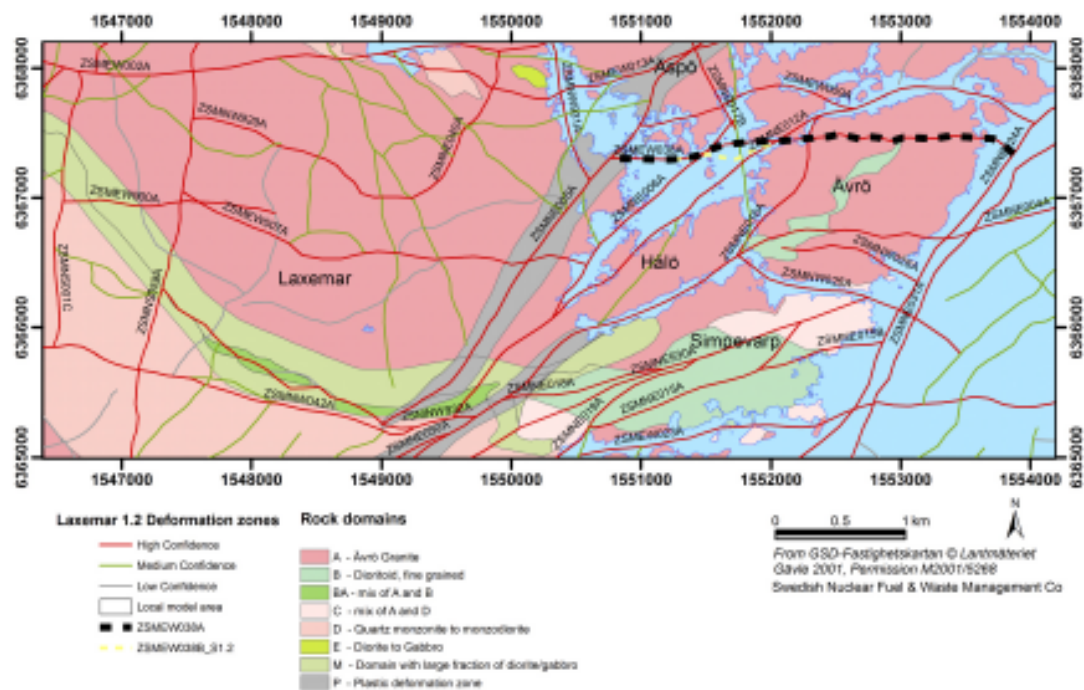


Figure 4-52. Location of ZSMEW038A (black) and the previous interpretation in Simpevarp 1.2 (yellow)

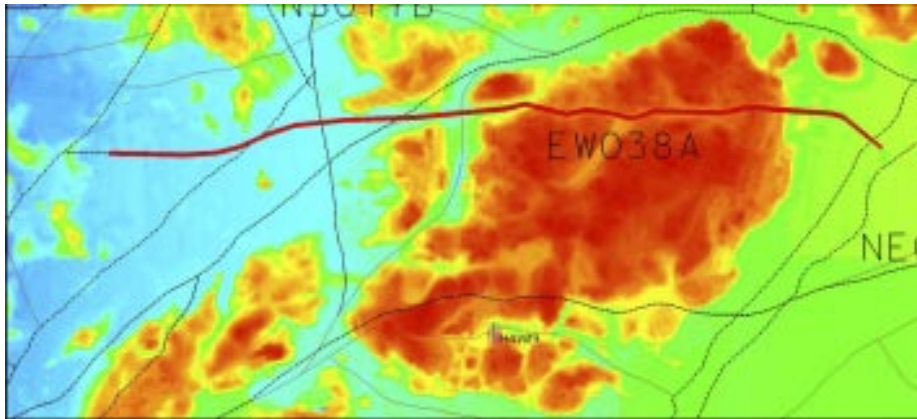


Figure 4-53. Topographic map in the area of ZSMEW038A. Indications of a weak depression is shown over Ävrö.

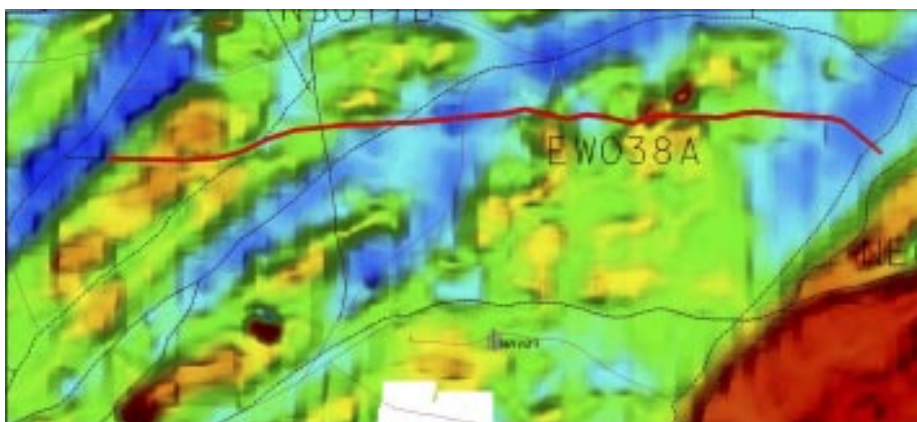


Figure 4-54. Magnetic map in the area of ZSMEW038A shows magnetic anomalies over sections of the extent of the zone.

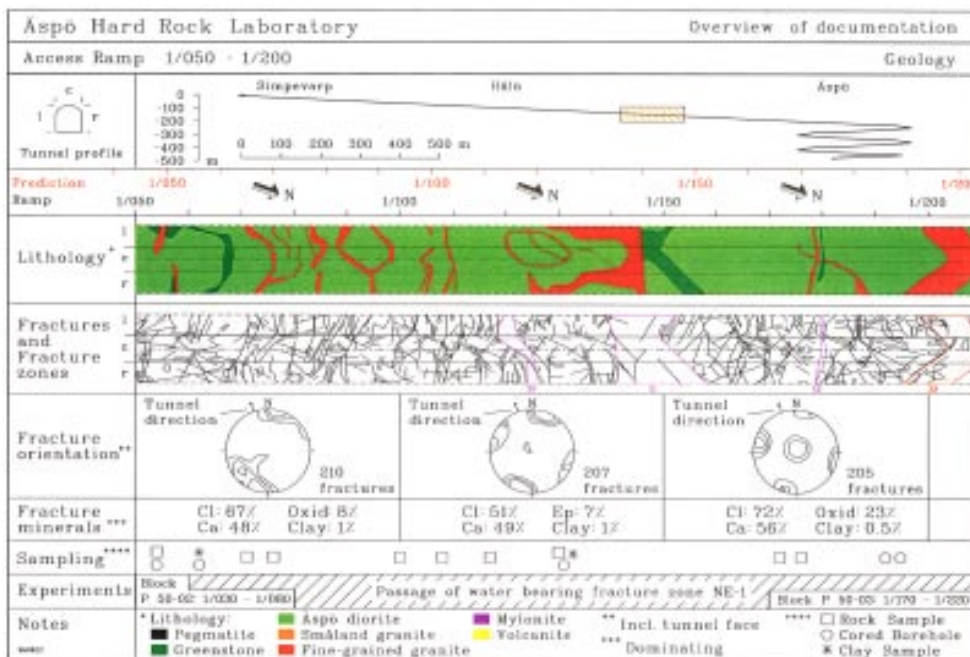


Figure 4-55. Interpreted intercept of ZSMEW038A in the Äspö tunnel at 1/180 m. /PR-HRL-96-19/.

It is also associated with a series of mylonites in KAS09, KBH02, KA1131B and KA1061, cf. Figure 4-57. However, the borehole intersections have not been used to constrain the exact geometry in RVS.

A seismic reflector, B2, shown in Figure 4-58, /Juhlin et al. 2004b/ indicates that the zone may extend parallel to the surface lineament over Ävrö, although it may also be related to the nearby deformation zone ZSMNE012A. A further indicator is a low velocity zone identified from the seismic refraction survey by /Lindqvist 2004a/, cf. Figure 4-59.

The current modelled surface position and dip is considered reasonable with a $\pm 15^\circ$ uncertainty. The geometry can be further clarified by a detailed examination of the tunnel and borehole data. The zone has been modelled as a vertical deformation zone with a thickness of 10 m, cf. Figure 4-60.

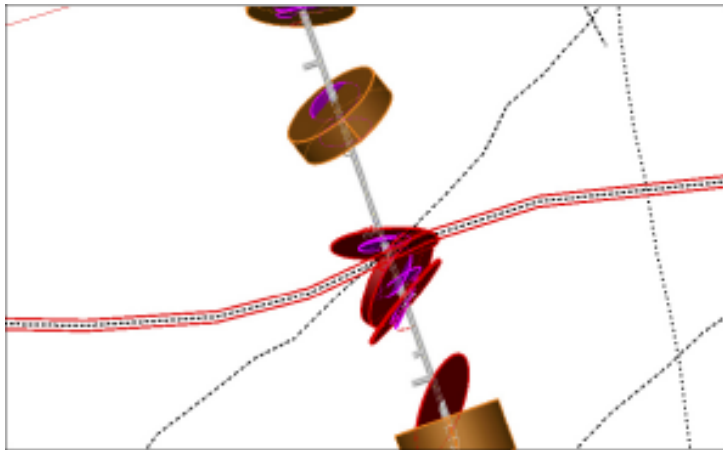


Figure 4-56. Visualisation of tunnel mapping results (at chainage 1/180 m) show several sub-parallel structures with sub-vertical inclinations.

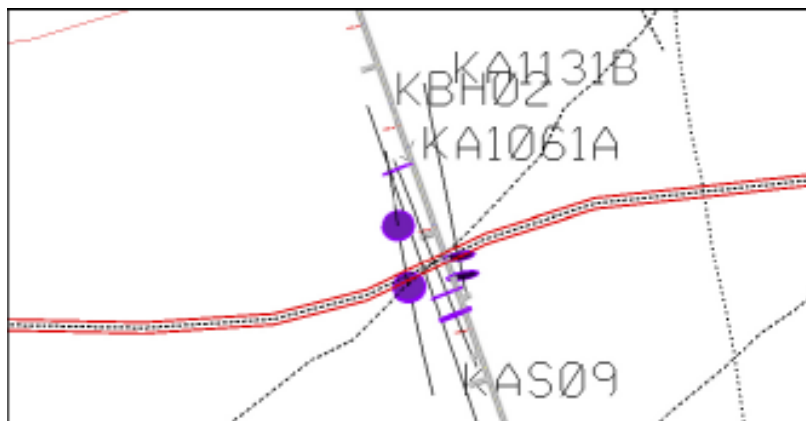


Figure 4-57. Visualised mylonites in the boreholes KAS09, KBH02, KA1131B and KA1061 surrounding the tunnel intercept at 1/180 m.



Figure 4-58. Seismic reflector B2 /Juhlin et al. 2004b/ indicates the extension of ZSMEW038A over Ävrö.

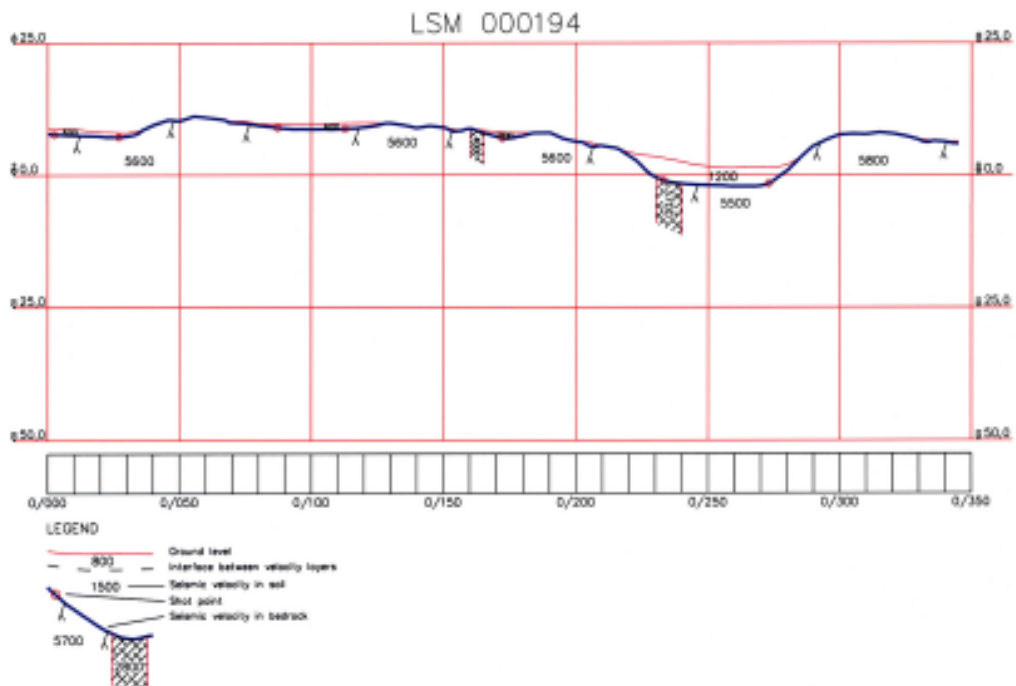


Figure 4-59. Refraction seismic profile LSM000194 shows a low velocity zone interpreted as ZSMEW038A with essentially a vertical inclination /Lindqvist 2004a/. South is to the left in the figure. See Figure 4-47 for location of profile.

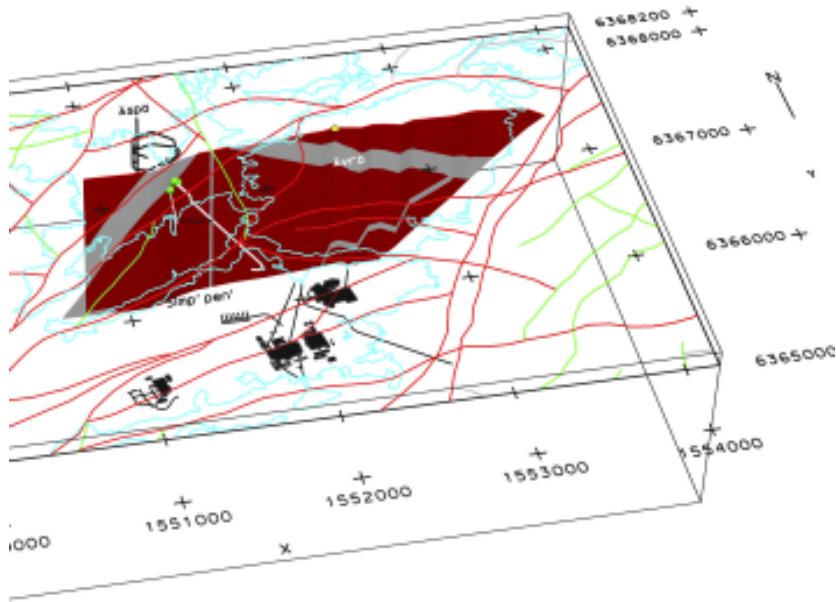


Figure 4-60. ZSMEW038A has been modelled with an orientation of 90/90 and with a thickness of 10 m. Äspö tunnel and borehole (KAS09) indications are shown with green dots and field observations on Ävrö in yellow.

Table 4-21. Property table for ZSMEW038A.

ZSMEW038A				
Property	Estimate	Span	Basis for interpretation	Comments
Confidence in existence	High		Linked lineaments, tunnel mapping and BHs.	Considered a minor structure.
Strike (regional scale)	090	± 10	Linked lineaments and tunnel	Complex split geometry. Potentially involves a series of narrow mylonites in a number of BHs and the tunnel, with potential interference from other zones including ZSMNE006A. The current modelled geometry is an over simplification.
Dip (regional scale)	90	± 15	Linked lineaments, BHs and tunnel intercepts	
Thickness, (including transition zones, regional scale)	10 m	1 to 15 m	Linked lineaments, BHs and tunnel intercepts.	1 m thick in TASA; 10 m represents an envelope thickness.
Length (regional scale)	3.2 km	± 100 m	Linked lineaments.	
Ductile deformation	Yes		Tunnel mapping (mylonite) TASA ch. 1,180 A minor mylonite, alternative intercepts exist.	Dominantly ductile zone. Possible brittle reactivation. Requires further review of Äspö data.
Brittle deformation	Yes		Inferred from tunnel mapping, transmissivity and seismic refraction profiling. Requires further study. Tunnel brittle evidence maybe associated with the development of other zones.	
Alteration				
Water	T= 1.3·10 ⁻⁶ m ² /s		TASA ch. 1,180	

ZSMEW038A				
Property	Estimate	Span	Basis for interpretation	Comments
Fracture orientation	Not yet assessed			
Fracture frequency m ⁻¹	13		KA1131B	Frac' frq' incl' crush (= 20 frac/m) (m ⁻¹)
Fracture filling	Ca 95%, Chl 70%, Ep 20%, He 0%, Qtz 0%		KA1131B	

Table 4-22. Borehole and tunnel indications for ZSMEW038A.

BH	Geometrical intercept	Target intercept	Comment
HAV05	20–38	–	Awaiting results.
KAS09	220–239	249–253	Possible associated mylonite
KBH02	538–547		
KA1131B	35–44	34–36	Mylonite
KA1061	100–109	74–75	Possible associated mylonite
TASA		1,180	(0.5–1 m thick)

4.6.10 ZSMNE004A

ZSMNE004A is one of the larger regional deformation zones in the mainland area, and together with Äspö shear zone, forms the tectonic structure in the regional model area, cf. Figure 4-61. This is mainly a ductile deformation zone with an anastomosing geometry, probably involving smaller subparallel deformation zones and splay structures, especially in the south central part of the local model close to Äspö shear zone. However, the complexity is not well known with only a few detailed observations from field mapping and from the Äspö tunnel, cf. Table 4-23.

The southern part of ZSMNE004A extends far beyond the regional model boundary and is observed in several outcrops as can be seen in Figure 4-62 /Persson Nilsson et al. 2004/. At the southern border of the local model the zone is interpreted to flex east and away from the southern termination of Äspö shear zone based mainly on the airborne magnetic map in Figure 4-63. The area is characterized by a mix of different rock types, intense ductile deformation and few surface outcrops. Two separate plastic rock domains for ZSMNE004A and Äspö shear zone are proposed for this area, cf. Figure 4-62. The whole section where ZSMNE004A and the Äspö shear zone are in close proximity may be well connected, but information is not conclusive with regards to zone terminations and geological character. The northern part of ZSMNE004A turns eastwards over Ävrö and is interpreted (with lower confidence) to extend eastwards out in the Baltic sea.

A 70 degree dip towards the southeast is observed in the Äspö tunnel at chainage 0/318 m, cf. Figure 4-64 and Table 4-24. The section of ZSMNE004A across Ävrö is also indicated by seismic reflector B4 by /Juhlin et al. 2004b/ although the reflector is interpreted as being shallow dipping (28°) towards the south, cf. Figure 4-58. Refraction seismics show a low velocity zone along one of the profiles over Ävrö, cf. Figure 4-65. Dip measurements from field mapping vary between 75N to 65S /Wahlgren et al. 2004/.

ZSMNE004A is modelled with a vertical dip to accommodate the variable dips from observations in the field, tunnel and from seismics. A 100 m thickness is suggested to incorporate an envelope of inferred sub-parallel splays. The current model of the three dimensional geometry is shown in Figure 4-66.

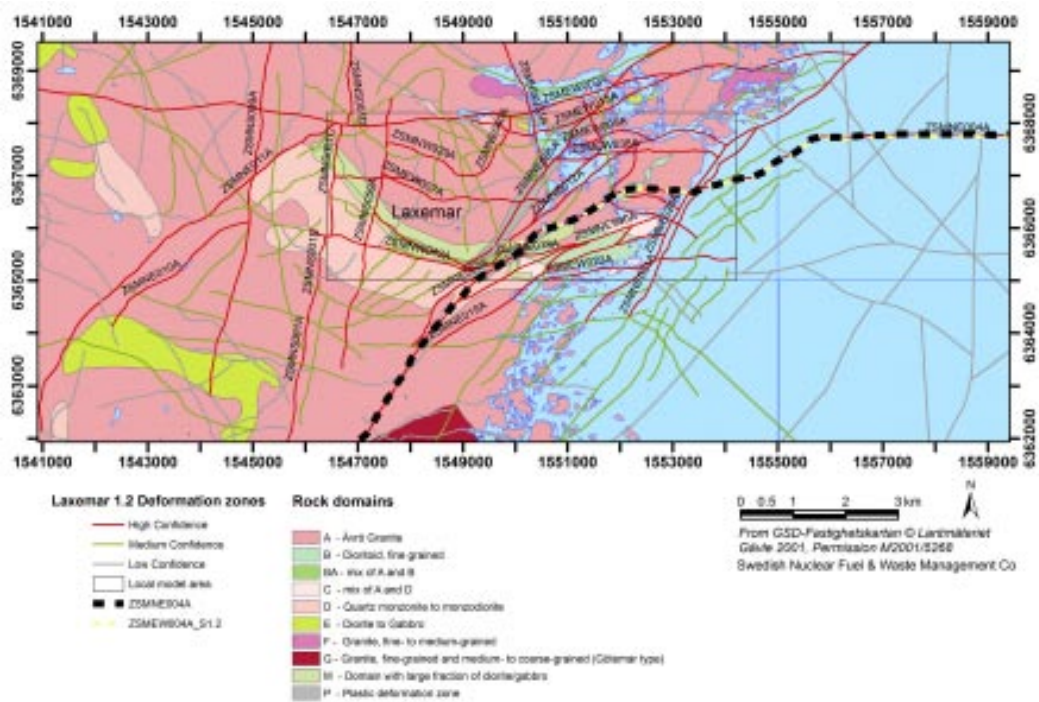


Figure 4-61. Location of ZSMNE004A (black) and the previous interpretation in the Simpevarp model version 1.2.

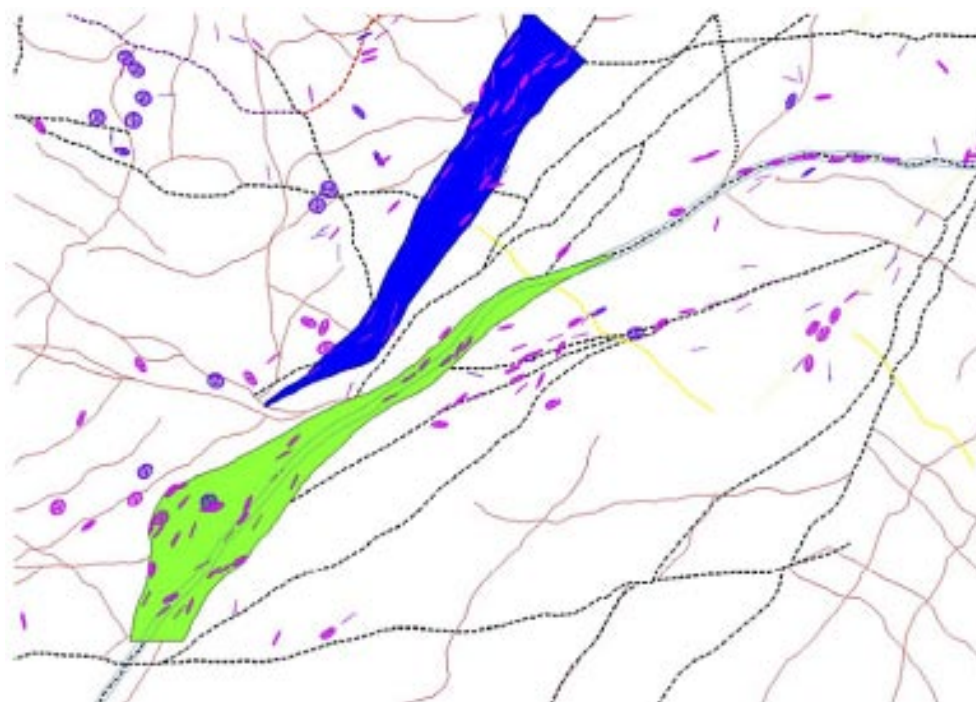


Figure 4-62. Orientation measurements along ZSMNE004A from field observations visualized as discs. The green and blue areas indicate the two P domains in the rock domain model.

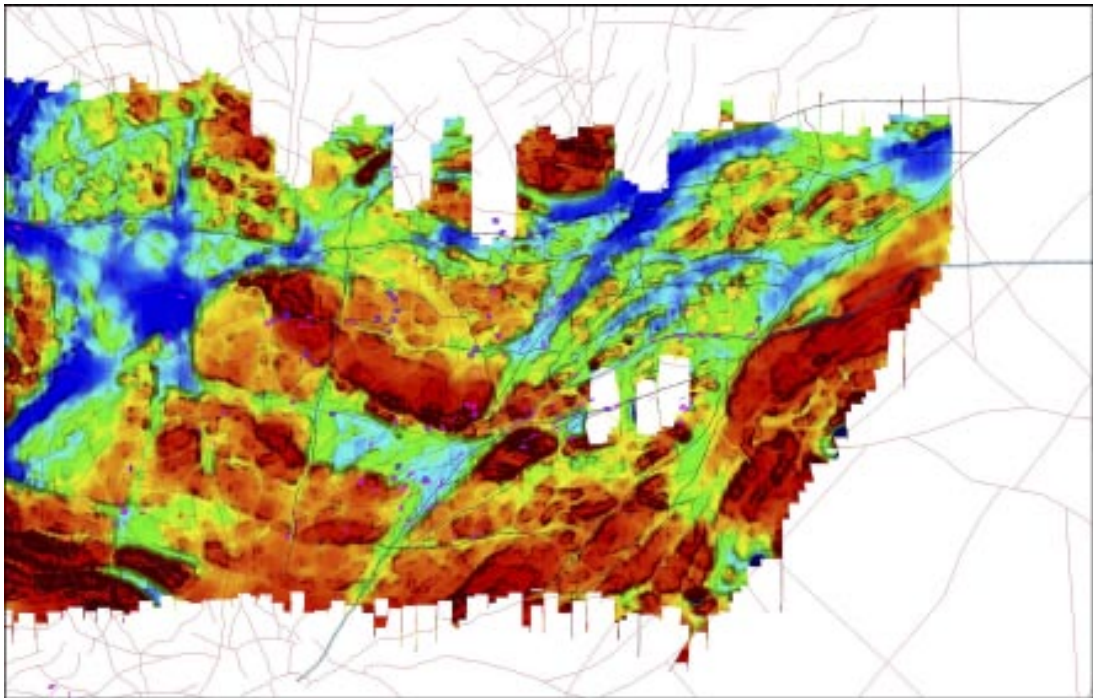


Figure 4-63. Magnetic map showing the regional impact of ZSMNE004A.

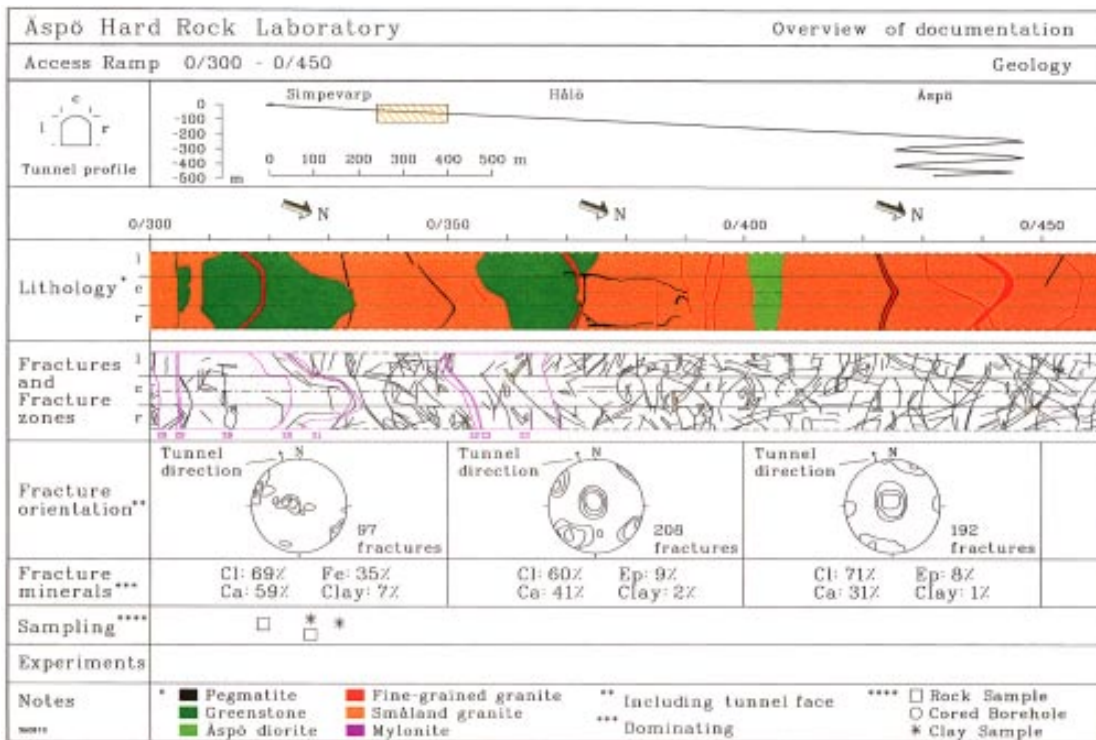


Figure 4-64. Äspö tunnel observation of ZSMNE004A at chainage 0/302–0/334 m /PR-HRL-96-19/.

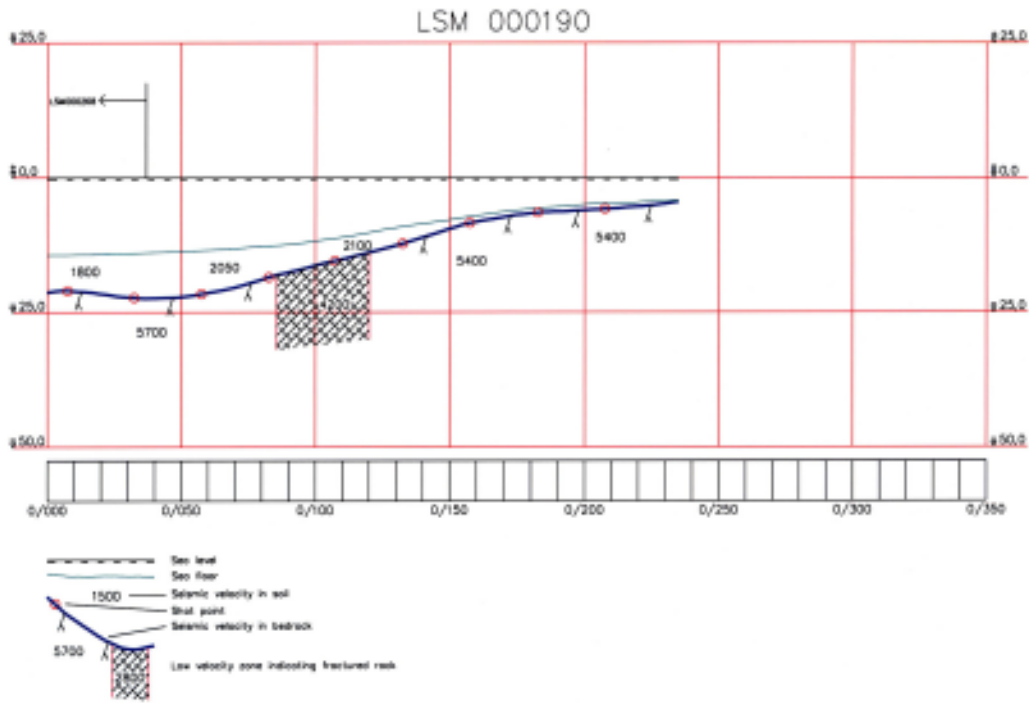


Figure 4-65. ZSMNE004A is indicated by a low velocity zone in seismic refraction profile LSM000190 /Lindqvist 2004a/. Southeast is to the left in the figure. See Figure 4-47 for location.

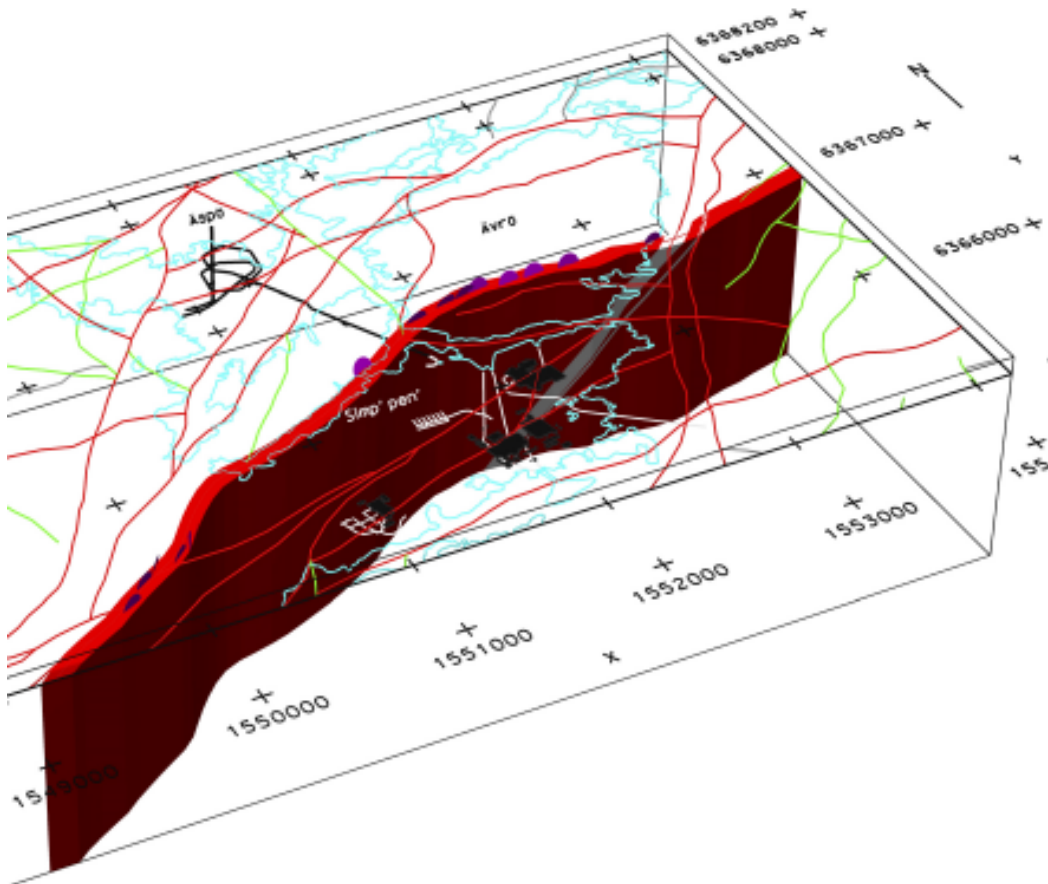


Figure 4-66. ZSMNE004A is modelled with an orientation of 050/90 and a thickness of 100 m including the transition zone.

Table 4-23. Property table for ZSMNE004A.

ZSMEW038A				
Property	Estimate	Span	Basis for interpretation	Comments
Confidence in existence	High		Linked lineament, Extensive field mapping and tunnel (Åspö) intercept. Seismic refraction.	
Strike (regional scale)	050	generally 030–070	Strong magnetic and topographic lineament; extensive field mapping	Curving geometry. However, the 090 trending eastwards extension has high uncertainty.
Dip (regional scale)	90	± 20	Extensive field mapping and tunnel (Åspö) intercept.	The vertical dip has been modified from Simp V1.2 (70°S) to vertical + 20° to allow for variations along entire zone length. It may be preferable to model the zone with a steep dip to the S in the N and a vertical to N dip in the south with a smooth change over.
Thickness, (including transition zones, regional scale)	100 m	20 to 120 m	Linked lineament, tunnel and field mapping.	A plastic complex zone, inferred anastomosing geometry. The 100 m thickness is an envelope thickness containing the inferred splays.
Length (regional scale)	15.6 km	8 to > 15 km	Linked lineaments	Possible termination at ZSMNE024A or NE extension outside the regional model area. Limited data.
Ductile deformation	Yes		Extensive field mapping evidence.	Ductile-brittle zone.
Brittle deformation	–		TASA -highly fractured rock: see engineering comment below. Possible general association with KAV04 raised fracture frequency, though this is not clearly supported by fracture orientations.	
Alteration				
Water	2.8·10 ⁻⁶ m ² /s		TASA ch. 300	
Fracture orientation	Not yet assessed			
Fracture frequency	Not yet assessed			
Fracture filling	Chl, Ca, Cy, Fe, Qz; clay		TASA ch. 302–334	

Table 4-24. Borehole and tunnel indications for ZSMEW039A.

BH	Geometrical intercept	Target intercept	Comment
HLX19	174–202	–	Awaiting results
KAV04	–	–	No geometrical intersection but the BH lies on the border of the modelled transition zone and may be responsible for the relatively high fracture frequency and degree of alteration throughout much of the BH though this is not clearly supported by fracture orientations.
TASA		302–334	

4.6.11 ZSMNE006A (NE1 on Äspö)

ZSMNE006A is directly observed through boreholes and tunnels at Äspö and indirectly in the magnetic map and is characterized mainly as a brittle deformation zone with at least three branches intermingled with minor mylonites, clay and brecciations, cf. Figure 4-67. The zone is highly conductive and is a potential engineering difficulty /Chang et al. 2005/.

The intercept with the Äspö tunnel occur at chainage 1/300 m and is described by /Rhén et al. 1997/ as a highly water-bearing brittle zone approximately 15 m thick with a highly fractured, brecciated 5 m thick core, cf. Table 4-25. The central part of the core contains a 1 m thick sequence of crush and fault gouge. More or less tectonized granite and mylonites occur with older fracture formations found as fragments indicating that gouge formation is a reactivation of earlier deformations. The intensive core of the zone with centimeter wide fractures and cavities is surrounded by 10–15 m wide sections of more or less fractured rock. The zone intersection with the tunnel extends over 30 m. A set of highly water-bearing structures gently dipping towards the north contributes to the complex character of the zone.

The mylonite is quartzo-feldspatic with accessories of chlorite and corroded magnetite. The precursor to this rock could be either fine-grained granite or a coarser granitoid. The mylonite is penetrated by fractures sealed with quartz and iron hydroxides, with some fluorite and pyrite. The gouge samples consist of angular fragments of tectonized rock, which are oxidized. Late overgrowth of calcite indicates that the zone has been reactivated. Smaller fractions contain large portions of clay minerals. The clay mineralogy is dominated by mixed layer illite/smectite.

No geometrical updates have been performed for this deformation zone compared to model version Simpevarp 1.2. The deformation zone is modelled with a 130 m thickness in order to envelope all borehole and tunnel indications. Borehole and tunnel indications are listed in Table 4-26.

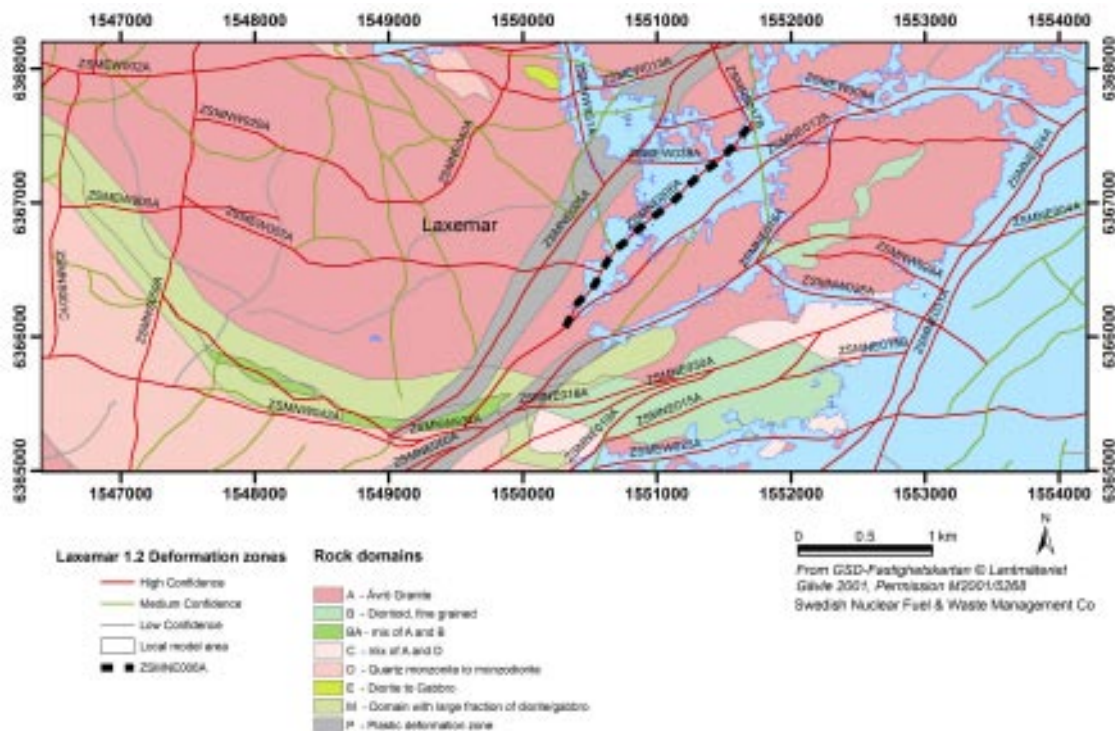


Figure 4-67. Location of ZSMNE006.

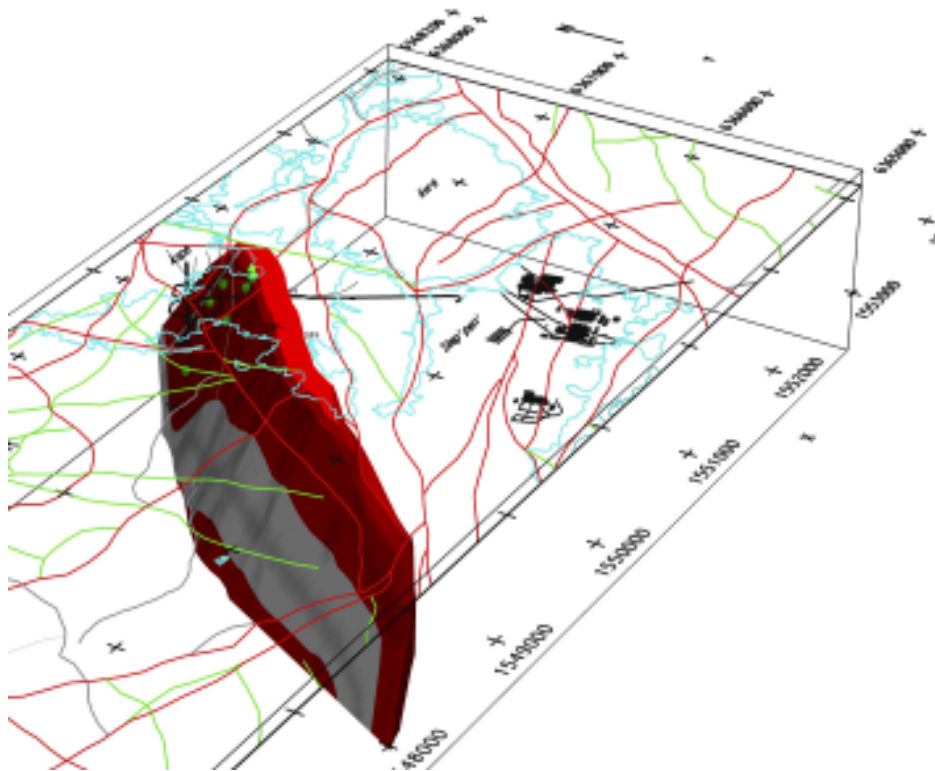


Figure 4-68. ZSMNE006A is modelled with an orientation of 215/65 and a thickness of 130 m, including the transition zone.

Table 4-25. Property table for ZSMNE006A.

ZSMNE006A Property	Estimate	Span	Basis for interpretation	Comments
Confidence in existence	High		Linked lineaments, BH and tunnel (Äspö) intercepts	
Strike (regional scale)	215	± 10	Linked lineaments	
Dip (regional scale)	65	± 20	Linked lineaments, BH and tunnel (Äspö) intercepts	
Thickness, (including transition zones, regional scale)	130 m	60 to 130 m	Linked lineaments, BH and tunnel (Äspö) intercepts	Model thickness of 130 m represents an envelope thickness containing narrower inferred splays. At Äspö NE1 is considered to consist of 3 main branches totaling 85 m as intercepted in the tunnel.
Length (regional scale)	2.1 km	2 to 4 km	Linked lineaments	An alternative interpretation allows the zone to continue further north eastwards.
Ductile deformation	Yes		Multiple 1cm thick Mylonite bands, tunnel mapping.	Dominantly brittle zone with minor plastic indicators
Brittle deformation	Yes		Breccia and fault gauge	
Alteration	1 m wide central completely altered clay core			5–8 m wide partially clay altered.
Water				All 3 branches are water bearing

ZSMNE006A				
Property	Estimate	Span	Basis for interpretation	Comments
Fracture orientation	230/35, 341/45, 284/90, 045/30, 050/60, 094/60, 120/35, 310/38, 310/75			The first two sets are water bearing. The analysis did not include the 933 fractures in the 1 m core. See text for details.
Fracture frequency m ⁻¹	11		KA1131B, KAS07, KAS08, KAS11, KAS14, KBH02, KAS02	Frac' frq' incl' crush (= 20 frac/m) (m ⁻¹)
Fracture filling	Ca 60%, Chl 49%, Ep 27%, He 23%, Qtz 1%		KA1131B, KAS07, KAS08, KAS11, KAS14, KBH02, KAS02	

Table 4-26. Borehole and tunnel indications for ZSMNE006A.

BH	Geometrical intercept	Target intercept	Comment
KA1061	94–209 (Base)	198–209	/Berglund et al. 2003/
KA1131B	47–203 (Base)	173–203	/Berglund et al. 2003/
KAS07	402–602 (Base)	497–602	/Berglund et al. 2003/
KAS08	440–590 (Base)	537–601	/Berglund et al. 2003/
KAS09	53–225	50–112	/Berglund et al. 2003/
KAS11	115–249	156–220	/Berglund et al. 2003/
KAS14	38–194	51–91	/Berglund et al. 2003/
KBH02	543–706 (Base)	667–706	/Berglund et al. 2003/
KAS02	740–924 (Base)	806–914	/Berglund et al. 2003/
KAS16	228–439	380–430	/Berglund et al. 2003/
TASA		1,240–1,325	/Berglund et al. 2003/

4.6.12 ZSMNE010A and ZSMNE011A

The local major deformation zone ZSMNE010A is a NE trending, probably steeply dipping deformation zone based on a topographic and magnetic lineament, cf. Figure 4-69 and verified by geological field control where epidote-healed fractures were found, cf. Table 4-27. The geometry has not been changed in this model version. The thickness is set to a default value of 10 m.

The local major fracture zone ZSMNE011A is indicated by both topographic and airborne magnetic data, cf. Figure 4-69. The positional accuracy of the zone is ± 50 m. It is verified by ground magnetic and VLF measurements /Stenberg and Sehlstedt 1989/, and by field observation of increased small-scale fracturing, mesoscopic brittle and brittle-ductile deformation zones and epidote-healed fractures /Bergman et al. 2000/, cf. Table 4-28. The fracture zone strikes 050–065° and extends over 5 km. However, the lineament identification during the feasibility study indicates that the fracture zone possibly continues to the southwest where it is truncated by a NW-trending lineament. Consequently, this zone is possibly of regional character.

ZSMNE011A has not been reviewed since model version 0 and has been given lower priority since it lies west of the local model area. It has been modelled with a geological thickness of 100 m including a transition zone and splay structures.

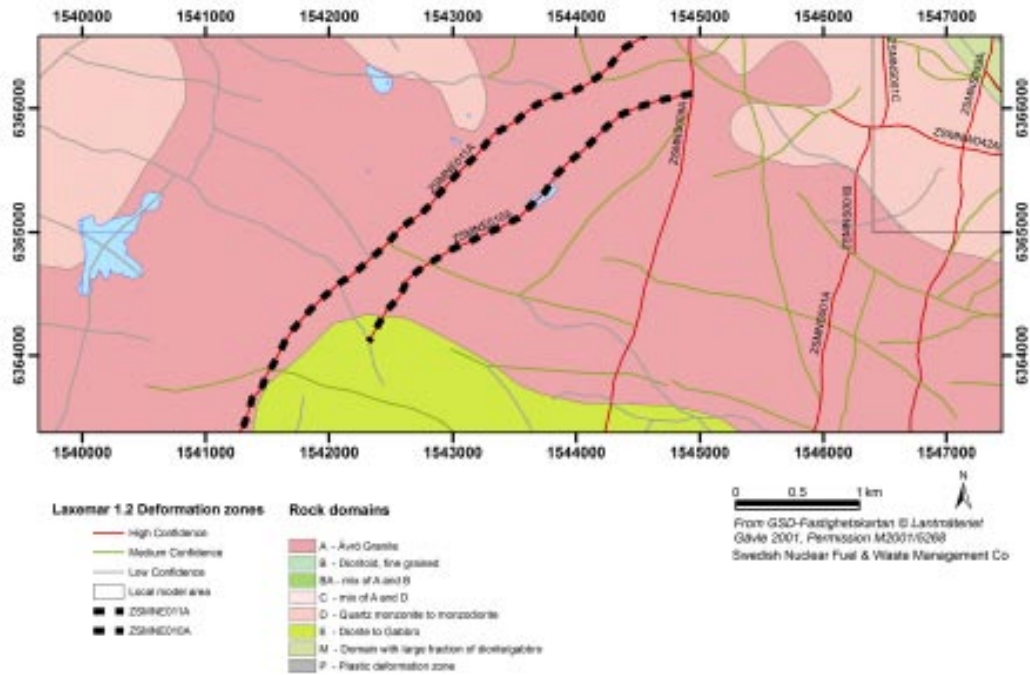


Figure 4-69. Location of ZSMNE010A.

Table 4-27. Property table for ZSMNE010A.

ZSMNE010A				
Property	Estimate	Span	Basis for interpretation	Comments
Confidence in existence	High		Linked lineaments. Ref: v. 0. Verified by field control- epidote healed fractures	This zone has not been reviewed in Laxemar v1.2.
Strike (regional scale)	055	± 15	Linked lineaments	
Dip (regional scale)	90		Assumed. No information	
Thickness, (including transition zones, regional scale)	10 m	2 to 10 m	Ref: v. 0. Verified by field control- epidote healed fractures	
Length (regional scale)	3.4 km	± 200	Linked lineaments	
Ductile deformation	–		No data	Brittle zone.
Brittle deformation	Yes		Field control.Ref: v. 0.	
Alteration			No data	
Water				
Fracture orientation				
Fracture frequency				
Fracture filling	Ep		Field control.Ref: v. 0.	

Table 4-28. Property table for ZSMNE011A.

ZSMNE011A Property	Estimate	Span	Basis for interpretation	Comments
Confidence in existence	High		Linked lineaments. Ref: v. 0. Verified by field control- ground magnetic and VLF measurements.	This zone has not been reviewed in Laxemar v1.2.
Strike (regional scale)	055	± 15	Linked lineaments	
Dip (regional scale)	90		Assumed. No information	
Thickness, (including transition zones, regional scale)	100 m	± 50	Linked lineaments	Ref: v0, 5–10 m 'cores' of highly fractured rock. 50–150 m wide transition envelope.
Length (regional scale)	8.5 km	8 to 12 km	Linked lineaments	Possible extension to SW.
Ductile deformation	Yes		Field evidence, Ref: v.0.	Ductile-brittle zone.
Brittle deformation	Yes		Field control. Ref: v. 0. increased small scale fracturing, mesoscopic brittle and ductile-brittle deformation zones and epidote healed fractures	
Alteration			No data	
Water			No data	
Fracture orientation			No data	
Fracture frequency			No data	
Fracture filling	Ep		Field control. Ref: v. 0.	

4.6.13 ZSMNE012A

The local major zone ZSMNE012A extends from ZSMNW932A in the south to ZSMNE024A in northeast and is tectonically related to the deformation zones ZSMNE004A and Äspö shear zone, cf. Figure 4-70. The position and orientation of the zone is based on magnetic and topographic lineaments, seismic reflectors /Juhlin et al. 2004b/, refractions /Lindqvist 2004a/, boreholes and tunnel intercepts /Rhen et al. 1997/. The geological character is interpreted as a reactivated brittle-ductile shear zone with increased fracturing, alteration, breccias and mylonites, cf. Table 4-29.

ZSMNE012A intersects the Äspö access tunnel at chainage 0/827 m and is locally named EW-7 and NE-4 at Äspö. The tunnel intercept, Figure 4-71, is characterized by an 80 m thick inhomogeneous brittle-ductile deformation with cataclasites, crush, high alteration, clay filled faults and high transmissivity /Rhen et al. 1997/. Borehole intercepts at Äspö, Ävrö, Simpevarp and Laxemar indicate similar geology as well as increased transmissivity, cf. Table 4-30.

Seismic reflector B1 and B2 /Juhlin et al. 2004b/ north of Ävrö corresponds with the easterly extent of ZSMNE012A. This section of the zone was previously interpreted as ZSMNE004A, but has been re-assessed in this model version to be part of ZSMNE012A based on an alternative lineament interpretation. This is further indicated by refraction seismics by /Lindqvist 2004a/ which shows low velocity zones in profiles LSM00192 and 193, cf. Figure 4-72.

The orientation derives from the surface lineament trend whereas the dip comes from the Äspö tunnel and from borehole intercepts at Äspö, Ävrö and Simpevarp. A modelled thickness of 120 m represents an envelope containing inferred sub-parallel splays. At Äspö this zone incorporates both EW-7 and NE-4, cf. Figure 4-73.

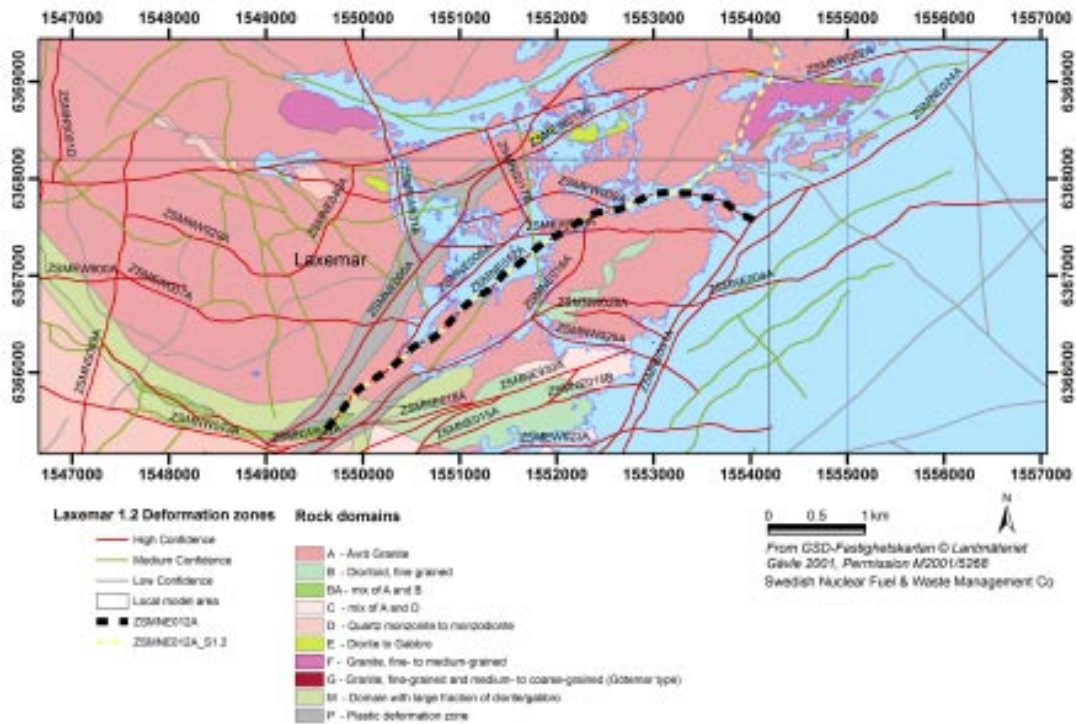


Figure 4-70. Location of ZSMNE012A (black) and the previous interpretation in Simpevarp model version 1.2 (yellow).

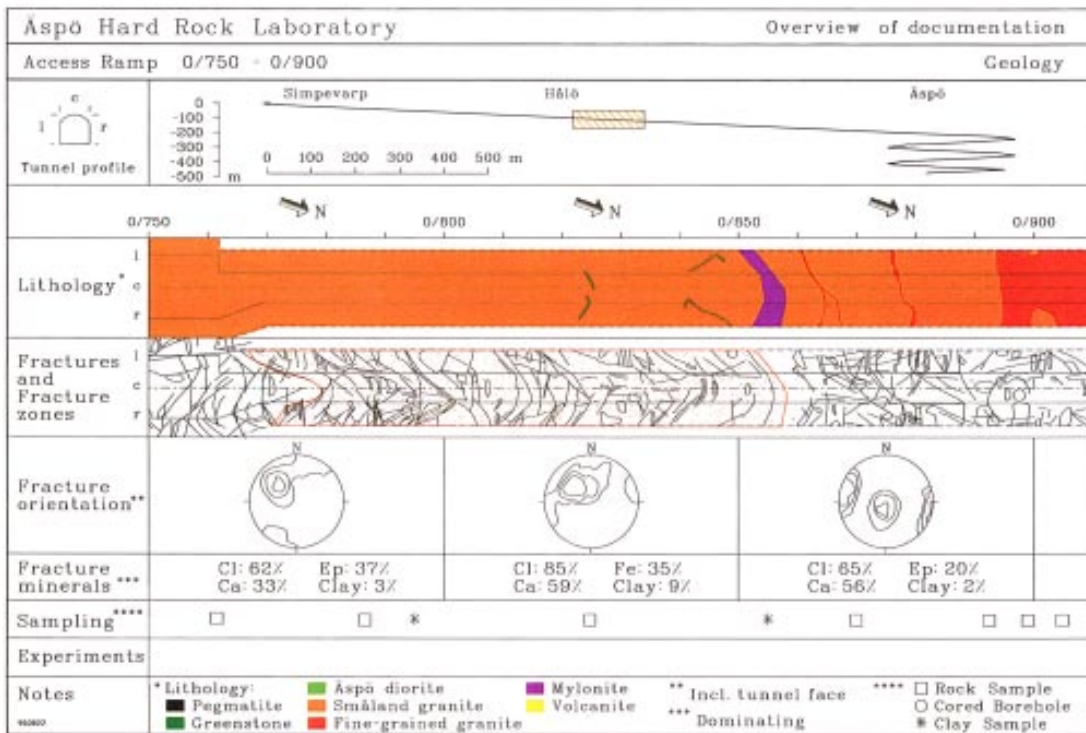


Figure 4-71. Intercept in Åspö access tunnel at chainage 0/827 m /PR-HRL-96-19/.

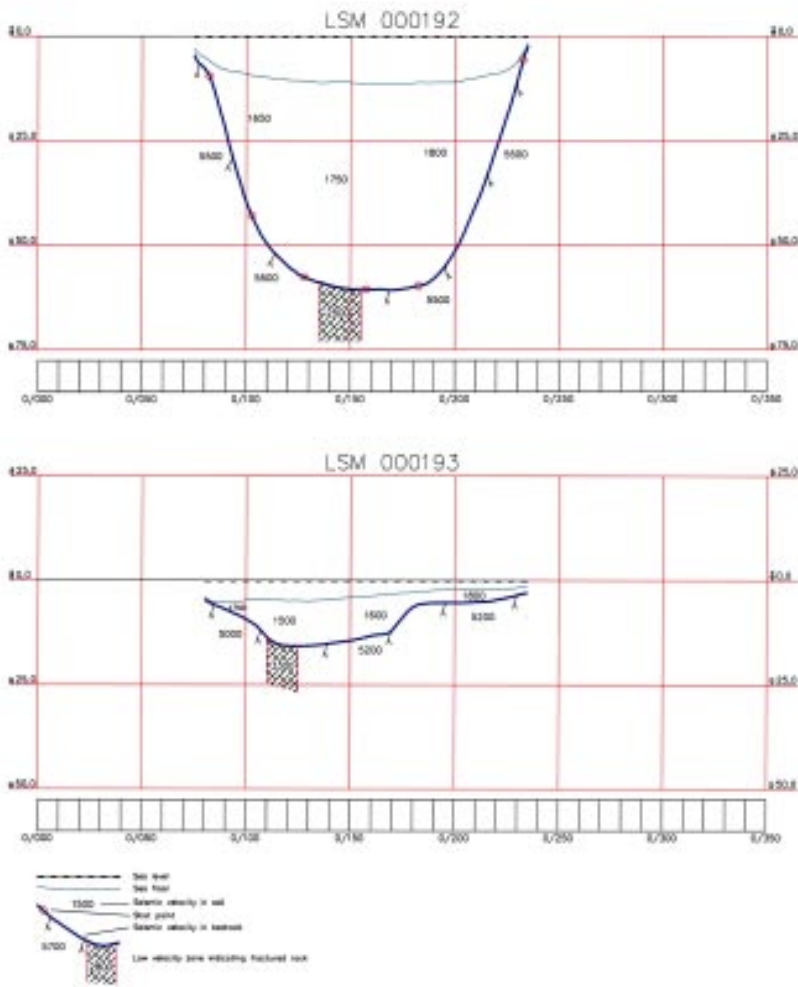


Figure 4-72. Seismic refraction profiles LSM00192 and LSM00193 /Lindqvist 2004a/. South is to the left in the figures. See Figure 4-47 for location.

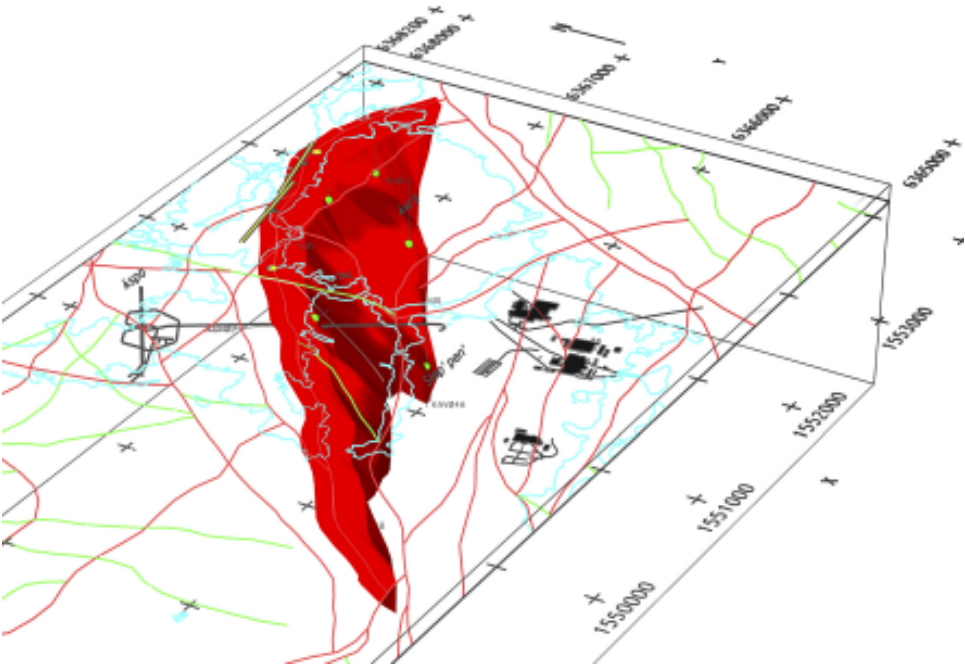


Figure 4-73. ZSMNE012A is modelled with a orientation of 060/45 and with a thickness of 120 m representing an envelope containing narrower inferred splays.

Table 4-29. Property table for ZSMNE012A.

ZSMNE012A (EW7-NE4)				
Property	Estimate	Span	Basis for interpretation	Comments
Confidence in existence	High		Linked lineaments, seismic reflector, BH and tunnel (Äspö) intercepts	
Strike (regional scale)	060	050 to 110	Linked lineaments	
Dip (regional scale)	45	± 10	Linked lineaments, BH and tunnel (Äspö) intercepts	
Thickness, (including transition zones, regional scale)	120 m	60 to 120 m	Linked lineaments, BH and tunnel (Äspö) intercepts	Model thickness of 120 m represents an envelope thickness containing narrower inferred splays. At Äspö this zone potentially incorporates both EW7 and NE4. Seismic refraction profiling indicate cores of fractured or altered rock with thicknesses of 15 to 20 m and velocities of 2,500–3,300 m/s
Length (regional scale)	5.5 km	± 200 m	Linked lineaments	
Ductile deformation	Yes		Mylonite on northern boundary (TASA)	Ductile-brittle zone
Brittle deformation	Yes		Breccia and crushed mylonite.	
Alteration	Clay. Fracture fillings chlorite and epidote		TASA	
Water	Transmissivity 10 ⁻⁴ to 10 ⁻⁵ m ² /s		TASA	
Fracture orientation	Not yet assessed			
Fracture frequency m ⁻¹	9		KAV01, KAV04A, KBH02	Frac' frq' incl' crush (= 20 frac/m) (m ⁻¹)
Fracture filling	Ca 64%, Chl 48%, Ep 20%, He 14%, Qtz 3%		KAV01, KAV04A, KBH02	

Table 4-30. Borehole and tunnel indications for ZSMNE012A.

BH	Geometrical intercept	Target intercept	Comment
HAV02	90–163 (Base)	90–150	Penetration rate indicates fractured or weak rock from ca. 89–149 m depth.
HAV12	18–136	51–127	Penetration rate and BIPS indicate fractured or weak rock from ca.51–76 m with possible extension to 93 m. Low permeability. Between ca. 100–127 m is water bearing. (only preliminary results available)
HAV13	0–121		Await results
HLX018	0–181(Base)	16–181	Penetration rate indicates fractured or weak rock between 16–115 m, ca. 147–151 m and ca. 160–181 m. Water inflows at ca. 53 m (1.5 l/min), ca.57 m (20l/min), ca. 67 m (21l/min), ca. 110 m (37–70 l/min) and ca. 150 m (> 130 l/min). (only preliminary results available)
HMJ01	0–46(Base)		No information

BH	Geometrical intercept	Target intercept	Comment
KAV01	401–630	400–580	Increased fracturing; alteration; low susceptibility and resistivity; low density. Mapped minor shear zones, breccias and mylonites.
KAV03	188–248	164–232	SICADA: 183–185 m brittle-ductile shear zone.
KAV04A	745–947	840–900	Increased number of crush zones. The deformation zone is characterized by an inhomogeneous brittle-cataclastic deformation. The focused resistivity (300) is markedly low along the section c. 860–900 m, but no other geophysical logging methods indicate significant anomalies.
KBH02	107–245	140–194	SICADA; 140.18 m–194.01 m code 42= Brittle-ductile shear zone

4.6.14 ZSMNW928A

ZSMNW928A is based on the interpreted subhorizontal seismic reflector N /Juhlin et al. 2004b/ and through possible intercepts with boreholes KLX02 and KLX04. The seismic reflector is strongly supported not to extend through the Mederhult zone in the north, which implies no surface intersection (Figure 4-74). Lateral extent in other directions is currently limited to the nearest high confidence regional or local major deformation zone but needs further evaluation through borehole data, hydraulic tests and/or seismics.

The possible intersection point in KLX02 (at 770–960 m) is indicated in the single-hole interpretation as a generally increased frequency of open fractures with increased oxidation. The most intensely fractured part of the zone is located between 845–880 m, which is indicated by distinct low p-wave velocity and partly by a somewhat reduced resistivity. Nine radar reflectors from directional antenna have been attributed to the zone. The geometry of the reflectors is strike 94 to 133 degrees and dip 29 to 56 degrees. Most of them are dipping around 50°. A number of sections with increased fracturing may indicate associated minor deformation zones currently of unknown orientation.

The interpreted possible intersection point in KLX04 (at 873 to 973 m) is indicated in the single-hole interpretation as repetitive sections of crush and sealed networks. Alteration is evident in the upper part of the section, cf. Figure 4-75.

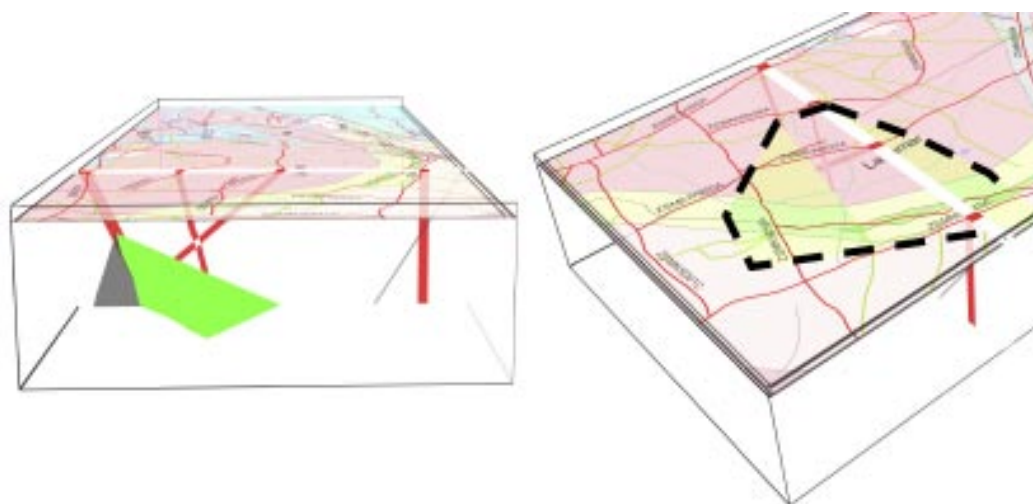


Figure 4-74. ZSMNW928 (green in the left illustration and hatched black line in the right) is modelled with a geometry of 120/28 and currently with no attributed geological thickness.

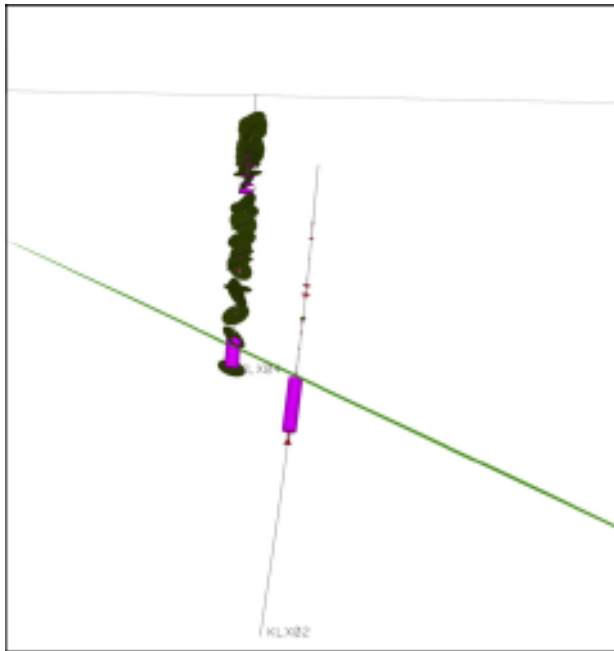


Figure 4-75. Possible intersection points with KLX04 (left) and KLX02 (right). ZSMNW928A is illustrated by the green line intersecting the boreholes.

The frequency of open fractures is relatively high, but variable throughout the section with a core zone characterised by strong inhomogeneous brittle deformation. The most intensely deformed part of the zone is found between c. 930 and 973 m. An intensely crushed part, between 936–946 m, correlates well with the seismic reflector N /Juhlin et al. 2004b/ at 940 m. Low resistivity, variable sonic, very low susceptibility and minor caliper anomalies are found in the sections 875–895 m and 935–971 m of KLX04.

Several radar reflectors are found within the zone, one at 877.5 m with the orientation 071/25, and one at 970.7 m with the orientation 046/20 or alternatively 270/07. Eleven radar reflectors have angles between 52–88° to the borehole axis, whereas one at 915.7 m has an angle of 31° to the borehole axis and one at 888.5 m has an angle of 21° to the borehole axis. The rock type is interpreted to be granite to quartz monzodiorite, generally porphyritic (Ävrö granite).

4.6.15 ZSMNE040A and ZSMNW929A

The local major zones ZSMNE040A and ZSMNW929A have been modified since the Simpevarp 1.2 version in such a way that the original zone (ZSMNE040A) has been divided into two separate branches with ZSMNE040A in the east and ZSMNW929A in the west, cf. Figure 4-76.

ZSMNW929A is indicated by field observations /Wahlgren et al. 2005/, topographic and airborne geophysical lineaments and borehole intersections in KLX02A (at 845–880 m) and in KLX04 (at 870–970 m). The borehole intercepts are characterised by a general increase in the frequency of open fractures and a higher degree of oxidation. The zone is also characterised by distinctly low P-wave velocity and partly by a somewhat reduced resistivity. A number of borehole sections with increased fracturing, crush, sealed networks and altered host rock may indicate a more complex zone consisting of a number of minor deformation zones. This generally brittle zone has been modelled with a thickness of 50 m representing an envelope thickness containing smaller narrow inferred splays, illustrated in Figure 4-77. Property table and borehole indications for ZSMNW929A is displayed in Table 4-31 and Table 4-32, respectively.

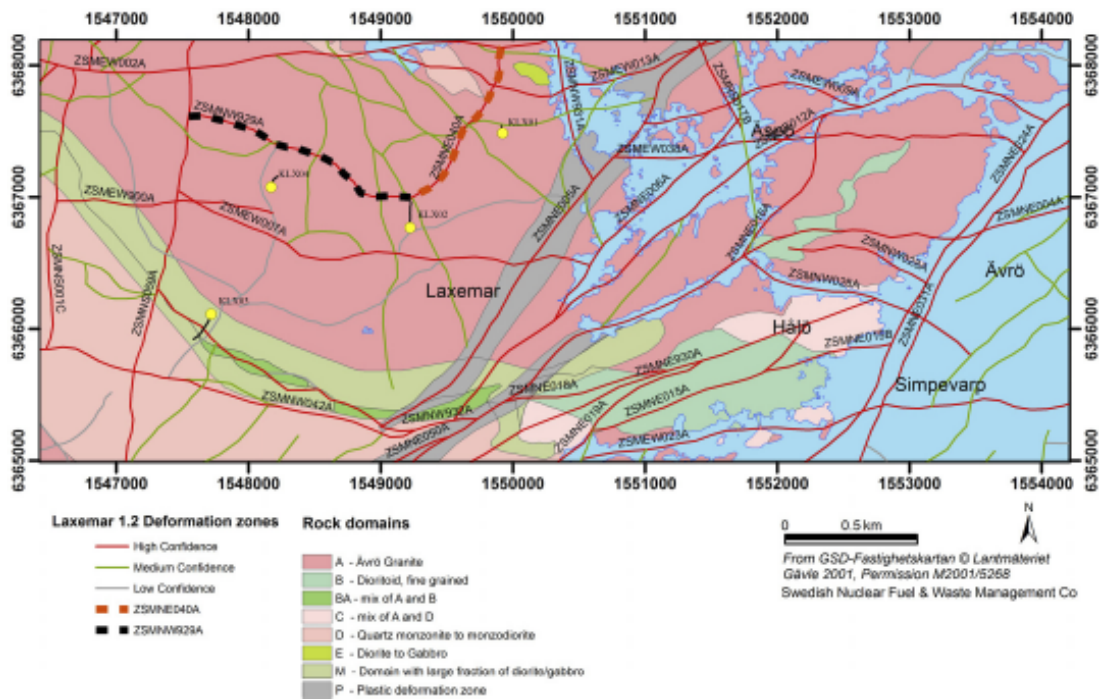


Figure 4-76. Location of ZSMNW929A and ZSMNE040A

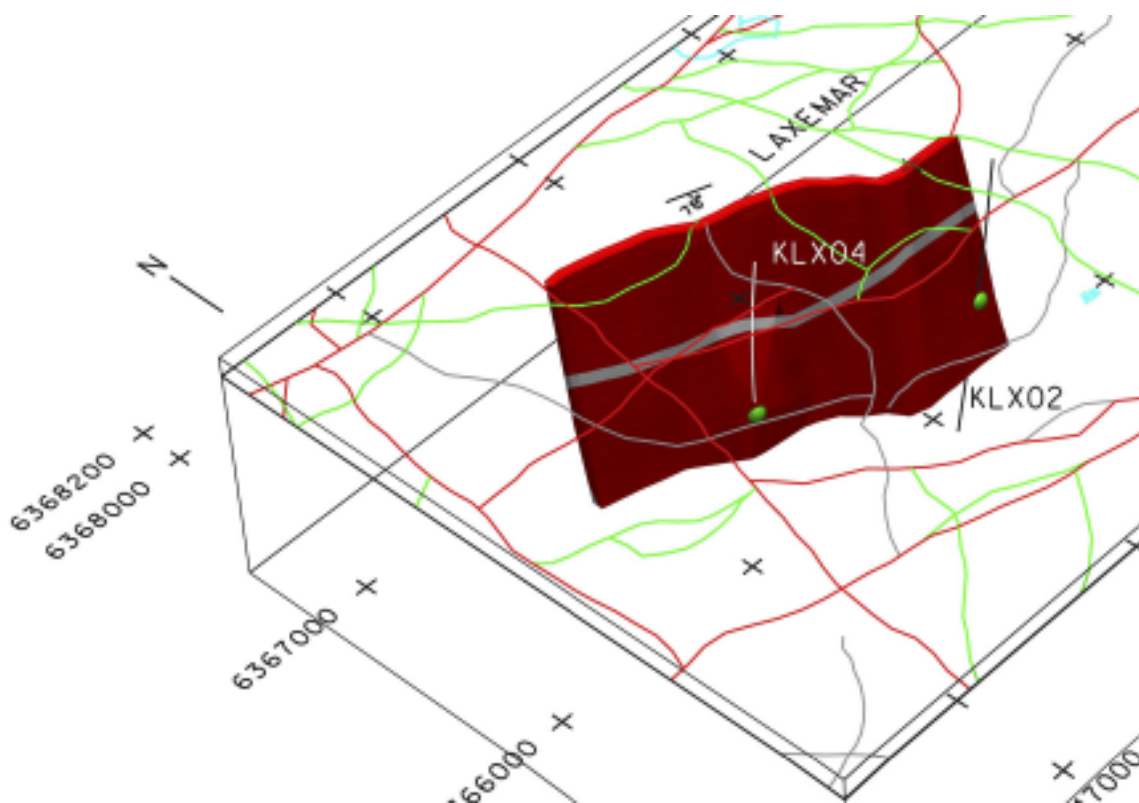


Figure 4-77. ZSMNW929A is modelled with a geometry of 113/79 and a geological thickness of 50 m including its transition zone.

Table 4-31. Property table for ZSMNW929A.

ZSMNW929A				
Property	Estimate	Span	Basis for interpretation	Comments
Confidence in existence	High		Linked lineament and BH intercepts.	
Strike (regional scale)	113	± 10	Magnetic and topographic lineaments	Lineament interpretation needs further review.
Dip (regional scale)	79	± 10	Lineament trace coupled with KLX02 and KLX04 single hole interpretations and orientated fractures in KLX04 between 870–970 Bhl.	
Thickness, (including transition zones, regional scale)	50 m	20 to 50 m	Magnetic and topographic lineaments	Model width of 50 m represents an envelope width containing narrower inferred splays.
Length (regional scale)	1.9 km	± 100 m	Linked lineaments	
Ductile deformation	–		No indicators	Brittle deformation zone
Brittle deformation	Yes		BHs, increased fracture frequency and crush zones	Brittle deformation zone
Alteration	Oxidation			
Water	–			Not yet analysed
Fracture orientation	Not yet assessed			
Fracture frequency m ⁻¹	10		KLX02, KLX04	Frac' frq'incl' crush (= 20 frac/m) (m ⁻¹)
Fracture filling	Ca 51%, Chl 57%, Ep 13%, He 7%, Qtz 10%		KLX02, KLX04	.

Table 4-32. Borehole indications for ZSMNW929A.

BH	Geometrical intercept	Target intercept	Comment
KLX02	778–935	770–960	Generally increased frequency of open fractures and higher oxidation. The most intensive part of the zone is located between 845–880 m, which is indicated by distinct low p-wave velocity and partly somewhat lower resistivity. A number of sections with increased fracturing may indicate minor deformation zones.
KLX04	861–986	873–973	Repeated crush and sealed network. Alteration in upper part, but missing in the central part. High frequency of open fractures. Zone centre with strong inhomogeneous brittle deformation. The most intensely deformed part in this section is between c. 930 and 973 m. A radar reflector at 915.7 m has an angle of 31° to borehole axis and one reflector at 888.5 m has the angle 21° to borehole axis. Rock type is interpreted to be granite to quartz monzodiorite, generally porphyritic (Åvrö granite). Note: An intensely crushed part at 936–946 m may correlate with a seismic reflector (ZSMNE928A) with the orientation 120/30.

ZSMNE040A is indicated through topographic and airborne geophysical lineaments, a borehole intersection in KLX01A (at 610 m) and is also weakly supported by anomalies in geophysical profiles /Thunehed et al. 2004/. A seismic reflection survey by /Bergman et al. 2001/ suggests a reflector with a matching surface intercept to the lineament but with weak indications for an intercept with KLX01A. The generally brittle zone has been modeled with a thickness of 20 m representing an envelope thickness inferred to contain discontinuous splays with thicknesses of c. 5 m of fractured rock as inferred from seismic refraction profiling, cf. Figure 4-78. Property table and borehole indications for ZSMNE040A is displayed in Table 4-33 and Table 4-34, respectively.

Table 4-33. Property table for ZSMNE040A.

ZSMNE040A Property	Estimate	Span	Basis for interpretation	Comments
Confidence in existence	High		Linked lineaments; magnetic, resistivity and seismic refraction profiling-	
Strike (regional scale)	030	± 10	Linked lineaments	
Dip (regional scale)	90	± 10	Magnetic and resistivity profiling.	Modelled as vertical to allow for local variations. However, resistivity profiling weakly indicates a steep (80°) dip to SE
Thickness, (including transition zones, regional scale)	20 m	5 to 20 m	Magnetic, resistivity and seismic refraction profiling	20 m represents an envelope width, inferred to contain discontinuous splays with widths of c. 5 m of fractured rock as inferred from seismic refraction profiling.
Length (regional scale)	1.4 km	± 100 m	Linked lineaments	
Ductile deformation	–			Brittle zone (preliminary assessment- but based on extremely weak evidence)
Brittle deformation	Yes		Inferred from seismic refraction low velocity. Possible associated field mapping indicators.	Brittle zone (preliminary assessment- but based on extremely weak evidence)
Alteration				
Water				
Fracture orientation				
Fracture frequency				
Fracture filling				

Table 4-34. Borehole indications for ZSMNE040A.

BH	Geometrical intercept	Target intercept	Comment
HLX01	0–30		Awaiting BH results
HLX04	21–82		Awaiting BH results

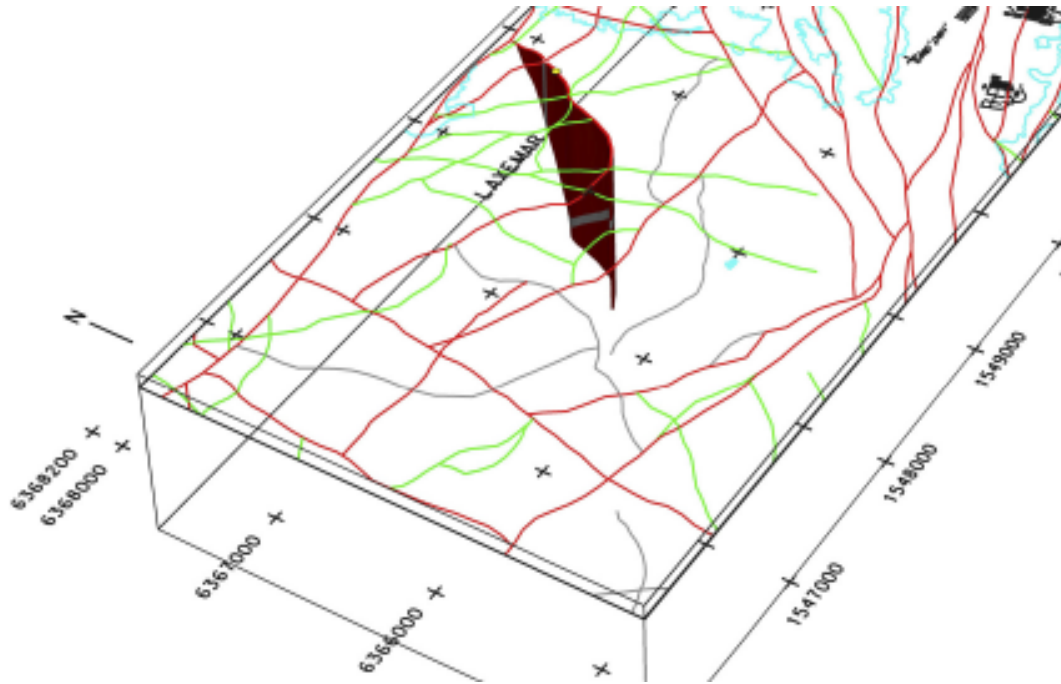


Figure 4-78. ZSMNE040A is modelled with a geometry of 030/90 and a geological thickness of 20 m including its transition zone.

4.7 Evaluation of uncertainties

At present, thirty-five (N=35) deformation zones are attributed a high confidence of occurrence. One hundred and fifty-five (N=155) deformation zones are interpreted with medium or low confidence of occurrence, of which sixty-two (N=62) are of medium confidence.

The uncertainties in the deformation zone model in the regional model area are dependent on the lineament map, which gives the fundamental surface information regarding the zones. Since there is considerable uncertainty concerning the interpretation of the geological significance of the lineaments, the 155 deformation zones that are based solely on indirect interpretation of lineaments (and their underlying data) are judged to have a lower degree of confidence. The majority of the latter zones are found in the western part of the local model area and in the regional model area.

Uncertainties also depend on the almost complete lack of subsurface information outside the local model area. Since all investigations during the complete site investigation will be focused to the local model area, these uncertainties are likely to remain throughout the site investigation.

As there is a limited amount of subsurface data, there remain considerable uncertainties concerning the extension at depth of all zones. It is assumed that zones extend as deep as their interpreted surface length although there are limited possibilities to check this assumption at present. Borehole intersections are relatively few in each deformation zone and are used to confirm its existence and indicate the geometry and geological character of selected zones. Even though deformation zones have been verified at some specific depths, the detailed geometrical relationships such as termination and connectivity are still considered uncertain for most deformation zones. This uncertainty is likely to persist throughout the site investigation programme, especially in the regional model area.

Deformation zones interpreted with low and medium confidence are observed through indirect lineament interpretations at the surface and are modelled with a vertical dip. High confidence zones have dip angles according to information from boreholes, tunnels or through seismics.

Not all deformation zones identified with a high degree of confidence have direct observations. In fact, only twenty-four out of thirty-five high confidence zones have been identified in boreholes, tunnels and through seismics, as is shown in Table 4-35.

Four deformation zones; NE010A, EW900A, NE018A and NE050A have been identified through field observations in combination with several indirect data sources but generally lack confirmation from boreholes (EW900A may have indications from percussion boreholes, but the data are inconclusive).

Seven deformation zones; NE011A, NE019A, NE040A, NS009A, NW931A, NW932A and NW933A have been identified based only on strong support from geophysical profiles in combination with other sources of indirect data. The confidence that these deformation zones indeed exist is high, but confidence in their orientation, geological character and extent at depth is of course lower than for zones that have been penetrated by boreholes.

In addition, an alternative study of lineaments was conducted by an independent geological team using the same underlying topographic and airborne geophysical data /Korhonen et al. 2005/. A preliminary assessment of this independent analysis shows that there are few deviations from the lineament interpretations and the resulting lineament map used in the current model version. This preliminary assessment adds confidence that the lineament map in itself is rather stable, i.e. linear anomalies in the underlying data are interpreted in the same way by independent geological teams.

In summary, the confidence that all thirty-five high confidence deformation zones exist is high although the uncertainty with regards to extent at depth, dip angle and geological character is variable depending on the amount of available data.

In addition to these uncertainties, each property table specifies the estimated span in orientation, surface length and thickness of each high confidence zone. For well known deformation zones mineralisations and internal fracture orientations give further indication on the character and the observed variability of properties.

Table 4-35. High confidence deformation zones (N=24) which have been verified by borehole, tunnel or through seismics at depth.

Zone ID	Alternative name	Class	Zone ID	Alternative name	Class
ZSMEW002A	Mederhult zone	Regional	ZSMNE015A		Local Major
ZSMEW007A		Local Major	ZSMNE015B		Local Major
ZSMEW009A		Local Major	ZSMNE016A		Local Major
ZSMEW013A	EW1A	Local Major	ZSMNE024A		Regional
ZSMEW023A		Local Major	ZSMNE031A		Local Major
ZSMEW038A		Local Major	ZSMNE930A		Local Major
ZSMNE004A		Regional	ZSMNS001A-D		Regional (A–D)
ZSMNE005A	Äspö shear zone	Local Major	ZSMNS017A-B	NNW4	Local Major
ZSMNE006A	NE1	Local Major	ZSMNS059A		Local Major
ZSMNE012A	NE4	Local Major	ZSMNW025A		Local Major
ZSMNW928A		Local Major	ZSMNW028A		Local Major
ZSMNW929A		Local Major	ZSMNW042A		Local Major

5 References

Andersson J, Ström A, Svemar C, Almén K-E, Ericsson L O, 2000. What requirements does the KBS-3 repository make on the host rock? Geoscientific suitability indicators and criteria for siting and site evaluation. SKB TR-00-12, Svensk Kärnbränslehantering AB.

Andersson J, Berglund J, Follin S, Hakami E, Halvarson J, Hermanson J, Laaksoharju M, Rhén I, Wahlgren C-H, 2002a. Testing the methodology for site descriptive modelling. Application for the Laxemar area. SKB TR-02-19, Svensk Kärnbränslehantering AB.

Andersson P, Byegård J, Dershowitz B, Doe T, Hermanson J, Meier P, Tullborg E-L, Winberg A, 2002b. Final report of the TRUE Block Scale. 1. Characterisation and model development. SKB TR-02-13, Svensk Kärnbränslehantering AB.

Ask H, Samuelsson L-E, Zetterlund M, 2005. Oskarshamn site investigation. Percussion drilling of boreholes HLX15, HLX26, HLX27, HLX28, HLX29 and HLX32 for investigation of lineament NW042. SKB P-04-235. Svensk Kärnbränslehantering AB.

Berglund J, Curtis P, Eliasson T, Ohlsson T, Starzec P, Tullborg E-L, 2003. Äspö Hard Rock Laboratory – Update of the geological model 2002. SKB IPR-03-34, Svensk Kärnbränslehantering AB.

Berglund J, 2004. Oskarshamn site investigation. Scan line fracture mapping. Subarea Laxemar and passage for tunnel. SKB P-04-244, Svensk Kärnbränslehantering AB.

Bergman T, Isaksson H, Johansson R, Lindén A H, Lindgren J, Lindroos H, Rudmark L, Wahlgren C-H, 1998. Förstudie Oskarshamn. Jordarter, bergarter och deformationszoner. SKB R-98-56, Svensk Kärnbränslehantering AB.

Bergman T, Follin S, Isaksson H, Johansson R, Lindén A H, Lindroos H, Rudmark L, Stanfors R, Wahlgren C-H, 1999. Förstudie Oskarshamn. Erfarenheter från geovetenskapliga undersökningar i nordöstra delen av kommunen. SKB R-99-04, Svensk Kärnbränslehantering AB.

Bergman T, Rudmark L, Wahlgren C-H, Johansson R, Isaksson H, 2000. Förstudie Oskarshamn. Kompletterande geologiska studier. SKB R-00-45, Svensk Kärnbränslehantering AB.

Bergman B, Juhlin C, Palm H, 2001. Reflektionsseismiska studier inom Laxemarområdet. SKB R-01-07, Svensk Kärnbränslehantering AB.

Bergman B, Juhlin C, Palm H, 2002. Reflection seismic imaging of the upper 4 km of crust using small charges (15–75 grams) at Laxemar, southeastern Sweden. *Tectonophysics* 355, 201–213.

BFS, 1990. Nybyggnadsregler ändringar. Boverkets författningssamling. BFS 1990:28, Nr. 2, Stockholm, ISBN 91-38-12510-2.

Chang Y, Swindell R, Bogdanoff I, Lindström B, Termén J, Starzec P, 2005. Study of tunnelling through water-bearing fracture zones. Baseline study on technical issues with NE-1 as reference. SKB R-05-25, Svensk Kärnbränslehantering AB.

Curtis P, Elfström M, Stanfors R, 2003a. Oskarshamn site investigation. Compilation of structural geological data covering the Simpevarp peninsula, Ävrö and Hälö. SKB P-03-07, Svensk Kärnbränslehantering AB.

Curtis P, Elfström M, Stanfors R, 2003b. Oskarshamn site investigation. Visualization of structural geological data covering the Simpevarp peninsula, Ävrö and Hälö. SKB P-03-36, Svensk Kärnbränslehantering AB.

- Cronquist T, Forssberg O, Hansen L, Jonsson A, Koyi S, Leiner P, Sävås J, Vestgård J, 2004.** Oskarshamn site investigation. Detailed fracture mapping of two outcrops at Laxemar. SKB P-04-274, Svensk Kärnbränslehantering AB.
- Debon F, Le Fort P, 1983.** A chemical-mineralogical classification of common plutonic rocks and associations. Transactions of Royal Society of Edinburgh, Earth Sciences 73, 135–149.
- Drake H, Tullborg E-L, 2004.** Fracture mineralogy and wall rock alteration, results from drill core KSH01A+B. SKB P-04-250, Svensk Kärnbränslehantering AB.
- Drake H, Savolainen M, Tullborg E-L, 2004.** Fracture filling and wall rock alteration – results from borehole KSH01, Simpevarp and KFM01, Forsmark. GFF 126, 170.
- Drake H, Tullborg E-L, 2006.** Oskarshamn site investigation. Fracture mineralogy of the Götömar granite. Results from drill cores KKR01, KKR02 and KKR03. SKB P-06-04. Svensk Kärnbränslehantering AB.
- Ehrenborg J, Stejskal V, 2004a.** Oskarshamn site investigation. Boremap mapping of core drilled boreholes KSH01A and KSH01B. SKB P-04-01. Svensk Kärnbränslehantering AB.
- Ehrenborg J, Stejskal V, 2004b.** Oskarshamn site investigation. Boremap mapping of core drilled borehole KLX02. SKB P-04-129. Svensk Kärnbränslehantering AB.
- Ehrenborg J, Stejskal V, 2004c.** Oskarshamn site investigation. Boremap mapping of core drilled borehole KAV01. SKB P-04-130. Svensk Kärnbränslehantering AB.
- Ehrenborg J, Stejskal V, 2004d.** Oskarshamn site investigation. Boremap mapping of core drilled borehole KSH02. SKB P-04-131. Svensk Kärnbränslehantering AB.
- Ehrenborg J, Stejskal V, 2004e.** Oskarshamn site investigation. Boremap mapping of core drilled boreholes KSH03A and KSH03B. SKB P-04-132. Svensk Kärnbränslehantering AB.
- Ehrenborg J, Stejskal V, 2005.** Oskarshamn site investigation. Boremap mapping of core drilled boreholes KAV04A and KAV04B. SKB P-05-22 (in press). Svensk Kärnbränslehantering AB.
- Ehrenborg J, Dahlin P, 2005a.** Oskarshamn site investigation. Boremap mapping of core drilled borehole KLX04. SKB P-05-23. Svensk Kärnbränslehantering AB.
- Ehrenborg J, Dahlin P, 2005b.** Oskarshamn site investigation. Boremap mapping of core drilled borehole KLX03. SKB P-05-24. Svensk Kärnbränslehantering AB.
- Elhammer A, Sandkvist Å, 2005.** Oskarshamn site investigation. Detailed marine geological survey of the sea bottom outside Simpevarp. SKB P-05-35, Svensk Kärnbränslehantering AB. In press.
- Eliasson T, 1993.** Mineralogy, geochemistry and petrophysics of red coloured granite adjacent to fractures. SKB TR-93-06, Svensk Kärnbränslehantering AB.
- Hermanson J, Hansen L, Wikholm M, Cronquist T, Leiner P, Vestgård J, Sandahl K-A, 2004.** Detailed fracture mapping of four outcrops at the Simpevarp peninsula and Ävrö. SKB P-04-35. Svensk Kärnbränslehantering AB.
- Hermanson J, Forsberg O, Fox A, La Pointe P, 2005.** Statistical model of fractures and deformation zones. Preliminary site description, Laxemar subarea, version 1.2. SKB R-05-45, Svensk Kärnbränslehantering AB.
- Hultgren P, Stanfors R, Wahlgren C-H, Carlsten S, Mattsson H, 2004.** Oskarshamn site investigation. Geological single-hole interpretation of KSH03A, KSH03B, KLX02, HAV09 and HAV10. SKB P-04-231, Svensk Kärnbränslehantering AB.
- Högdahl K, Andersson U B, Eklund O, (Editors) 2004.** The Transscandinavian Igneous Belt (TIB) in Sweden: a review of its character and evolution. Geological Survey of Finland, Special Paper 37, 1–125.

- Jonsson, S, 2004.** Djupförvarsteknik. Relation between fine-grained granitic dykes and structures at the Äspö Hard Rock Laboratory, north of Oskarshamn, Sweden. SKB TD-04-11, Svensk Kärnbränslehantering AB.
- Juhlin C, Palm H, 1999.** 3D structure below Ävrö island from high resolution reflection seismic studies, southeastern Sweden. *Geophysics* 64, 662–667.
- Juhlin C, Bergman B, Cosma C, Keskinen J, Enescu, 2002.** Vertical seismic profiling and integration with reflection seismic studies at Laxemar, 2000. SKB TR-02-04, Svensk Kärnbränslehantering AB.
- Juhlin C, Bergman B, Palm H, 2004a.** Oskarshamn site investigation. Reflection seismic studies performed in the Laxemar area during 2004. SKB P-04-215, Svensk Kärnbränslehantering AB.
- Juhlin C, Bergman B, Palm H, Tryggvason A, 2004b.** Oskarshamn site investigation. Reflection seismic studies on Ävrö and Simpevarpshalvön, 2003. SKB P-04-52, Svensk Kärnbränslehantering AB.
- Kresten P, Chyssler J, 1976.** The Götömar massif in south-eastern Sweden: A reconnaissance survey. *Geologiska Föreningens i Stockholm Förhandlingar* 98, 155-161.
- Kornfält K-A, Wikman H, 1988.** The rocks of the Äspö island. Description to the detailed maps of solid rocks including maps of 3 uncovered trenches. SKB PR-25-88-12, Svensk Kärnbränslehantering AB.
- Kornfält K-A, Persson P-O, Wikman H, 1997.** Granitoids from the Äspö area, southeastern Sweden – geochemical and geochronological data. *GFF* 119, 109–114.
- Korhonen K, Kuivamäki A, Ruotoistenmäki T, Paananen M, 2005.** Interpretation of lineaments from airborne geophysical and topographic data. An alternative model within version Laxemar 1.2 of the Oskarshamn modelling project. SKB P-05-247, Svensk Kärnbränslehantering AB.
- LeMaitre R W (Editor), 2002.** A classification of igneous rocks and glossary of terms: Recommendations of the International Union of Geological Sciences, Subcommittee on the Systematics of Igneous Rocks, 2nd edition, Blackwell, Oxford.
- Lindqvist, G, 2004a.** Oskarshamn site investigation. Refraction seismic measurements in the water outside Simpevarp and Ävrö and on land on Ävrö. SKB P-04-201, Svensk Kärnbränslehantering AB.
- Lindqvist, G, 2004b.** Oskarshamn site investigation. Refraction seismic measurements in Laxemar. SKB P-04-134, Svensk Kärnbränslehantering AB.
- Lindroos H, 2004.** The potential for ore, industrial minerals and commercial stones in the Simpevarp area. SKB R-04-72, Svensk Kärnbränslehantering AB.
- Markström I, Stanfors R, Juhlin C, 2001.** Äspölaboratoriet. RVS-modellering, Ävrö. Slutrapport. SKB R-01-06, Svensk Kärnbränslehantering AB.
- Mattsson H, Triumf C-A, Wahlgren C-H, 2002.** Prediktering av förekomst av finkorniga granitgångar i Simpevarpsområdet. SKB P-02-05, Svensk Kärnbränslehantering AB.
- Mattsson H, Thunehed H, Triumf C-A, 2003.** Oskarshamn site investigation. Compilation of petrophysical data from rock samples and in situ gamma-ray spectrometry measurements. SKB P-03-97, Svensk Kärnbränslehantering AB.
- Mattsson H, Thunehed H, Triumf C-A, 2004a.** Oskarshamn site investigation. Compilation of petrophysical data from rock samples and in situ gamma-ray spectrometry measurements. Stage 2 – 2004 (including 2002). SKB P-04-294, Svensk Kärnbränslehantering AB.

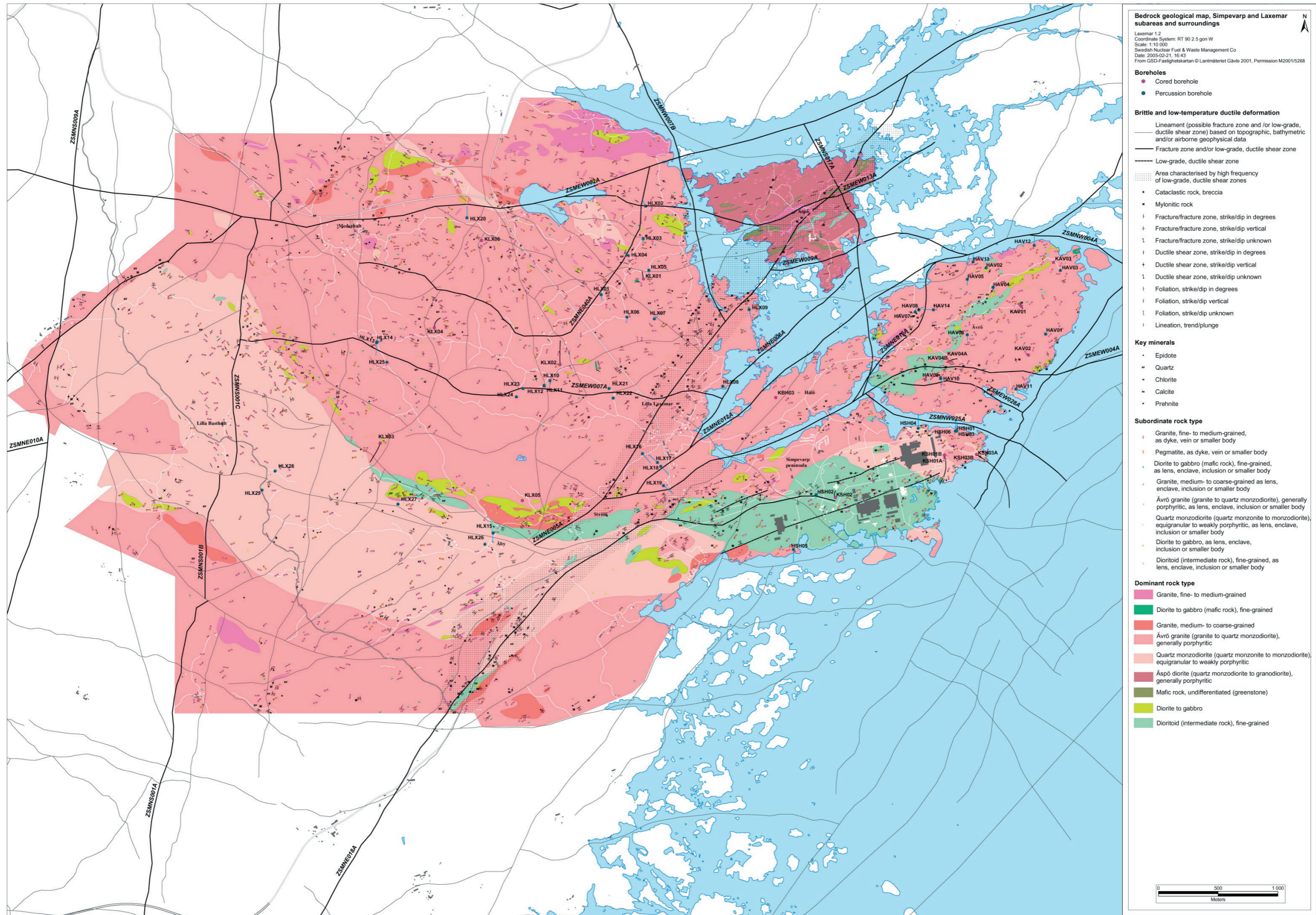
- Mattsson H, Stanfors R, Wahlgren C-H, Carlsten S, Hultgren P, 2004b.** Oskarshamn site investigation. Geological single-hole interpretation of KSH01A, KSH01B, HSH01, HSH02 and HSH03. SKB P-04-32, Svensk Kärnbränslehantering AB.
- Mattsson H, Stanfors R, Wahlgren C-H, Carlsten S, Hultgren P, 2004c.** Oskarshamn site investigation. Geological single-hole interpretation of KSH02 and KAV01. SKB P-04-133, Svensk Kärnbränslehantering AB.
- Middlemost E A K, 1994.** Naming materials in the magma/igneous rock system. *Earth-Science Reviews* 37, 215–224.
- Munier R, 1989.** Brittle tectonics on Äspö, SE Sweden. SKB PR 25-89-15. Svensk Kärnbränslehantering AB.
- Munier R, 1993.** Segmentation, fragmentation and jostling of the Baltic shield with time. Thesis, Acta Universitatis Upsaliensis 37.
- Munier R, Stanfors R, Milnes A G, Hermanson J, Triumf C-A, 2003.** Geological Site Descriptive Model. A strategy for the development during site investigations. SKB R-03-07, Svensk Kärnbränslehantering AB.
- Munier R, 2004.** Statistical analysis of fracture data, adapted for modelling Discrete Fracture Networks-Version 2. SKB R-04-66. Svensk Kärnbränslehantering AB.
- Nisca D, 1987.** Aerogeophysical interpretation. Bedrock and tectonic analysis. SKB PR 25-87-04, Svensk Kärnbränslehantering AB.
- Persson Nilsson K, Bergman T, Eliasson T, 2004.** Oskarshamn site investigation. Bedrock mapping 2004 – Laxemar subarea and regional model area. Outcrop data and description of rock types. SKB P-04-221, Svensk Kärnbränslehantering AB.
- Rhén I, Gustafson G, Stanfors R, Wikberg P, 1997.** Äspö HRL – Geoscientific evaluation 1997/5. Models based on site characterization 1986–1995. SKB TR 97-06, Svensk Kärnbränslehantering AB.
- Rydström H, Gereben L, 1989.** Regional geological study. Seismic refraction survey. SKB PR 25-89-23, Svensk Kärnbränslehantering AB.
- Rønning H J S, Kihle O, Mogaard J O, 2003.** Simpevarp site investigation. Helicopter borne geophysics at Simpevarp, Oskarshamn, Sweden. SKB P-03-25, Svensk Kärnbränslehantering AB
- Schmelzbach C, Juhlin C, 2004.** Oskarshamn site investigation. 3D processing of reflection seismic data acquired within and near the array close to KAV04A on Ävrö, 2003. SKB P-04-204, Svensk Kärnbränslehantering AB.
- SKB, 2002.** Simpevarp – site descriptive model version 0. SKB R-02-35, Svensk Kärnbränslehantering AB.
- SKB, 2004.** Preliminary site description. Simpevarp area – version 1.1. SKB R-04-25, Svensk Kärnbränslehantering AB.
- SKB, 2005a.** Preliminary site description. Simpevarp subarea – version 1.2. SKB R-05-08, Svensk Kärnbränslehantering AB.
- SKB, 2005b.** Preliminary site description. Forsmark area – version 1.2. SKB R-05-18, Svensk Kärnbränslehantering AB.
- SKB, 2006.** Hydrogeochemical evaluation. Preliminary site description Laxemar subarea – version 1.2. SKB R-06-12. Svensk Kärnbränslehantering AB.
- Stanfors R, Rhén I, Forsmark T, Wikberg P, 1994.** Evaluation of the fracture zone EW-1, based on the cored boreholes KA1755A, KA1751, KA1754A and KAS04. SKB PR 25-94-39, Svensk Kärnbränslehantering AB.

- Stanfors R, Erlström M, 1995.** SKB Palaeohydrogeological programme. Extended geological models of the Äspö area. SKB Arbetsrapport 95-20. Svensk Kärnbränslehantering AB.
- Stanfors R, Rhén I, Tullborg E-L, Wikberg P, 1999.** Overview of geological and hydrogeological conditions of the Äspö Hard Rock laboratory site. *Applied Geochemistry* 14, 819–834.
- Stenberg L, Sehlstedt S, 1989.** Geophysical profile measurements on interpreted regional aeromagnetic lineaments in the Simpevarp area. SKB PR 25-89-13, Svensk Kärnbränslehantering AB.
- Streckeisen A, 1976.** To each plutonic rock its proper name. *Earth Science Reviews* 12, 1–33.
- Sundblad K, Alm E, Huhma H, Vaasjoki M, Sollien D B, 2004.** Early Devonian tectonic and hydrothermal activity in the Fennoscandian Shield; evidence from calcite-fluorite-galena mineralization. In: Mertanen S (ed.), *Extended abstracts, 5th Nordic Paleomagnetic workshop. Supercontinents, remagnetizations and geomagnetic modelling.* Geological Survey of Finland, pp. 67–71
- Thunehed H, Triumf C-A, Pitkänen T, 2004.** Oskarshamn site investigation. Geophysical profile measurements over interpreted lineaments in the Laxemar area. SKB P-04-211, Svensk Kärnbränslehantering AB.
- Triumf C-A, 2003.** Oskarshamn site investigation. Geophysical measurements for the siting of a deep borehole at Ävrö and for investigations west of CLAB. SKB P-03-66, Svensk Kärnbränslehantering AB.
- Triumf C-A, Thunehed H, Kero L, Persson L, 2003.** Oskarshamn site investigation. Interpretation of airborne geophysical survey data. Helicopter borne survey data of gamma ray spectrometry, magnetics and EM from 2002 and fixed wing airborne survey data of the VLF-field from 1986. SKB P-03-100, Svensk Kärnbränslehantering AB.
- Triumf C-A, 2004a.** Oskarshamn site investigation. Joint interpretation of lineaments. SKB P-04-49, Svensk Kärnbränslehantering AB.
- Triumf C-A, 2004b.** Oskarshamn site investigation. Gravity measurements in the Laxemar model area with surroundings. SKB P-04-128, Svensk Kärnbränslehantering AB.
- Wahlgren C-H, Persson L, Danielsson P, Berglund J, Triumf C-A, Mattsson H, Thunehed H, 2003.** Oskarshamn site investigation. Geologiskt underlag för val av prioriterad plats inom området väster om Simpevarp. SKB P-03-06, Svensk Kärnbränslehantering AB.
- Wahlgren C-H, Ahl M, Sandahl K-A, Berglund J, Petersson J, Ekström M, Persson P-O, 2004.** Oskarshamn site investigation. Bedrock mapping 2003 – Simpevarp subarea. Outcrop data, fracture data, modal and geochemical classification of rock types, bedrock map, radiometric dating. SKB P-04-102, Svensk Kärnbränslehantering AB.
- Wahlgren C-H, Bergman T, Persson Nilsson K, Eliasson T, Ahl M, Ekström M, 2005.** Oskarshamn site investigation. Bedrock map of the Laxemar subarea and surroundings. Description of rock types, modal and geochemical analyses. SKB P-05-180, Svensk Kärnbränslehantering AB.
- Wiklund S, 2002.** Digitala ortofoton och höjdmodeller. Redovisning av metodik för platsundersökningsområdena Oskarshamn och Forsmark samt förstudieområdet Tierp Norra. SKB P-02-02, Svensk Kärnbränslehantering AB.
- Wikman H, Kornfält K-A, 1995.** Updating of a lithological model of the bedrock of the Äspö area, SKB PR 25-95-04, Svensk Kärnbränslehantering AB.
- Åhäll K-I, 2001.** Åldersbestämning av svårdaterade bergarter i sydöstra Sverige. SKB R-01-60, Svensk Kärnbränslehantering AB.

Nomenclature of rock types (in English and Swedish), including rock codes applied in the site investigation at Oskarshamn

Nomenclature of rock types applied in the site investigation in Oskarshamn.





Rock code	Rock nomenclature (names within parenthesis refer to nomenclature used in the the Äspö Hard Rock Laboratory and related studies)	Descriptive nomenclature of rock type	R	G	B
501027	Dolerite Diabas	Dolerite Diabas	152	83	161
531058	Fine-grained Götemar granite Finkornig Götemargranit	Granite, fine- to medium-grained, ("Götemar granite") Granit, fin- till medelkornig, ("Götemargranit")	255	0	0
521058	Coarse-grained Götemar granite Grovkornig Götemargranit	Granite, coarse-grained, ("Götemar granite") Granit, grovkornig, ("Götemargranit")	200	24	56
511058	Fine-grained granite Finkornig granit	Granite, fine- to medium-grained Granit, fin- till medelkornig	235	122	179
501061	Pegmatite Pegmatit	Pegmatite Pegmatit	241	157	86
501058	Granite Granit	Granite, medium- to coarse-grained Granit, medel- till grovkornig	237	113	116
501044	Ävrö granite (<i>Småland-Ävrö granite</i>) Ävrögranit (<i>Småland-Ävrögranit</i>)	Granite to quartz monzodiorite, generally porphyritic Granit till kvartsmonzodiorit, vanligtvis porfyrisk	246	162	168
501036	Quartz monzodiorite (<i>Äspö diorite, tonalite</i>) Kvartsmonzodiorit (<i>Äspödiorit, tonalit</i>)	Quartz monzonite to monzodiorite, equigranular to weakly porphyritic Kvartsmonzonit till monzodiorit, jämnkornig till glest porfyrisk	250	199	193
501033	Diorite/gabbro Diorit/Gabbro	Diorite to gabbro Diorit till gabbro	193	221	53
501030	Fine-grained dioritoid (<i>Metavolcanite, volcanite</i>) Finkornig dioritoid (<i>Metavulkanit, vulkanit</i>)	Intermediate magmatic rock Intermediär magmatisk bergart	168	216	183
505102	Fine-grained diorite-gabbro (<i>Greenstone</i>) Finkornig diorit-gabbro (<i>Grönsten</i>)	Mafic rock, fine-grained Mafisk bergart, finkornig	69	185	124
509010	Sulphide mineralization Sulfidmineralisering	Sulphide mineralization Sulfidmineralisering	204	204	204
506007	Sandstone Sandsten	Sandstone Sandsten	217	192	106



Property tables for rock domains

Average values for Magnetic susceptibility and Electric resistivity are given in logarithmic scale \pm std (base 10).

RSMA01 Property	Character	Quantitative estimate	Confidence	Comment
Dominant rock type (%)	Ävrö granite (501044)	54–92	High	The quantitative estimate is based on occurrence in KSH03A, KAV01, KAV04A/B, KLX02, KLX04 and the Äspö tunnel (section 2,265–2,874 m).
Mineralogical composition (%) (dominant minerals)	Quartz	18.8 \pm 6.3	High	N=61. The quantitative estimate is based on modal analyses of surface samples from the Simpevarp and Laxemar subareas and samples from KSH01A, KSH03A, KAV01. Mean value \pm std.
	K-feldspar	17.6 \pm 8.5		
	Plagioclase	46.5 \pm 8.4		
	Biotite	10.5 \pm 4.9		
Grain size	Medium-grained		High	Based on outcrop database for the Simpevarp and Laxemar subareas and its immediate surroundings.
Age (million years)		1,800 \pm 4	High	U-Pb zircon-titanite dating of Ävrö granite.
Structure	Isotropic to weakly foliated. Scattered mesoscopic, ductile shear zones		High	Based on outcrop database for the Simpevarp and Laxemar subareas and its immediate surroundings.
Texture	Unequigranular to porphyritic		High	Based on outcrop database for the Simpevarp and Laxemar subareas and its immediate surroundings.
Density (kg/m ³)		2,716 \pm 40	High	N=81. The quantitative estimate is based on surface samples from the Simpevarp and Laxemar subareas and samples from KAV01, KAV04A and KLX01. Mean value \pm std.
Porosity (%)		0.44 \pm 0.19	High	N=79. The quantitative estimate is based on surface samples from the Simpevarp and Laxemar subareas and samples from KAV01, KAV04A and KLX01. Mean value \pm std.
Magnetic susceptibility (SI units)		3.390 \pm 0.29	High	N=81. The quantitative estimate is based on surface samples from the Simpevarp and Laxemar subareas and samples from KAV01, KAV04A and KLX01. Average value in logarithmic scale \pm std.
Electric resistivity in fresh water (ohm m)		3.98 \pm 0.20	High	N=79. The quantitative estimate is based on surface samples from the Simpevarp and Laxemar subareas and samples from KAV01, KAV04A and KLX01. Average value in logarithmic scale \pm std.

RSMA01 Property	Character	Quantitative estimate	Confidence	Comment
Uranium content based on gamma ray spectrometric data (ppm)		4.0±1.4	High	N=67. The quantitative estimate is based on measurements on outcrops from the Simpevarp and Laxemar subareas, and a few measurements from the remaining part of the regional model area. Mean value ± std.
Natural exposure (microR/h)		11.4±2.2	High	N=67. The quantitative estimate is based on measurements on outcrops from the Simpevarp and Laxemar subareas, and a few measurements from the remaining part of the regional model area. Mean value ± std.
Subordinate rock types (%)	Fine- to medium-grained granite (511058) Pegmatite (501061) Fine-grained dioritoid (501030) Diorite to gabbro (501033) Fine-grained diorite to gabbro (505102) Quartz monzodiorite (501036)	1–22 0–1 2–21 0–12 0–5 1–14	High	The quantitative estimate is based on occurrence in KSH03A, KAV01, KAV04A, KLX02, KLX04, outcrop ASM000208 and the Äspö tunnel (section 2,265–2,874 m).
Dykes of fine- to medium-grained granite (511058)	Orientation	Mean pole=338/12 K=1.5 	High	N=72. Measurements from the local model area west of RSMP01 and RSMP02 and north of ZSMEW007A. Based on outcrop database for the Laxemar subarea and immediate surroundings. Mean pole is marked with a star.
		Mean pole=336/7 K=4.6 	High	N=8. Measurements from the local model area west of RSMP01 and RSMP02 and south of ZSMEW007A. Based on outcrop database for the Laxemar subarea and immediate surroundings. Mean pole is marked with a star.
Pegmatite (501061)	Orientation	Mean pole=325/12 K=0.8 	High	N=20. Measurements from the local model area west of RSMP01 and RSMP02 and north of ZSMEW007A. Based on outcrop database for the Laxemar subarea and immediate surroundings. Mean pole is marked with a star.
		Mean pole=297/9 K=0.4 	High	N=5. Measurements from the local model area west of RSMP01 and RSMP02 and south of ZSMEW007A. Based on outcrop database for the Laxemar subarea and immediate surroundings. Mean pole is marked with a star.

RSMA01 Property	Character	Quantitative estimate	Confidence	Comment
Degree of inhomogeneity	Low		High	Based on outcrop database for the Simpevarp and Laxemar subareas and KSH03A, KAV01, KAV04A/B, KLX01, KLX02 and KLX04. The degree of inhomogeneity may locally be higher.
Metamorphism/ alteration (%)	Inhomogeneous hydrothermal alteration (secondary red staining)	14–59	High	The quantitative estimate is based on faint to weak, including subordinate medium and strong, oxidation in KSH03A, KAV01, KAV04A, KLX01, KLX02 and KLX04 outside interpreted deformation zones in the single-hole interpretation. Epidotization, saussuritization, sericitization and chloritization also occur in subordinate amounts, varying between 0 and 3%.
Mineral fabric (type/orientation)	Weak magmatic to tectonic foliation	Mean pole=337/3 K= 3.6	High	N=41. Measurements from the local model area <i>east of</i> rock domains RSMP01 and RSMP02. Based on outcrop database for the Simpevarp and Laxemar subareas and immediate surroundings The stereogram includes poles to all foliation measurements irrespective of rock domain. Mean pole is marked with a star.
		Mean pole=24/3 K= 0.8	High	N=105. Measurements from the local model area <i>west of</i> rock domain RSMP01 and RSMP02. Based on outcrop databases for the Laxemar subarea and immediate surroundings The stereogram includes poles to all foliation measurements irrespective of rock domain. Mean pole is marked with a star.

RSMA02 Property	Character	Quantitative estimate	Confidence	Comment
Dominant rock type (%)	Ävrö granite (501044)		Medium	
Mineralogical composition (%) (dominant minerals)				No data; inferred to be comparable to RSMA01.
Grain size				No data; inferred to be comparable to RSMA01.
Age (million years)		c. 1,800	High	No data; inferred to be comparable to RSMA01.
Structure				No data; inferred to be comparable to RSMA01.
Texture				No data; inferred to be comparable to RSMA01.
Density (kg/m ³)				No data; inferred to be comparable to RSMA01.
Porosity (%)				No data; inferred to be comparable to RSMA01.
Magnetic susceptibility (SI units)				No data; inferred to be comparable to RSMA01.
Electric resistivity in fresh water (ohm m)				No data; inferred to be comparable to RSMA01.
Uranium content based on gamma ray spectrometric data (ppm)				No data; inferred to be comparable to RSMA01.
Natural exposure (microR/h)				No data; inferred to be comparable to RSMA01.
Subordinate rock types (%)				No data; inferred to be comparable to RSMA01.
Degree of inhomogeneity				No data; inferred to be comparable to RSMA01.
Metamorphism/alteration (%)				No data; inferred to be comparable to RSMA01.
Mineral fabric (type/orientation)				No data; inferred to be comparable to RSMA01.

RSMB01 Property	Character	Quantitative estimate	Confidence	Comment
Dominant rock type (%)	Fine-grained dioritoid (501030)	89–91	High	The quantitative estimate is based on occurrence in KSH01A and KSH02.
Mineralogical composition (%) (dominant minerals)	Quartz	7.4±5.0	High	N=21. The quantitative estimate is based on modal analyses of surface samples from the Simpevarp subarea, KSH01A and KSH02. Mean value ± std.
	K-feldspar	11.3±6.4		
	Plagioclase	51.4±8.7		
	Biotite	14.7±7.6		
	Amphibole	0–14		
	Pyroxene	0–22		
Grain size	Fine-grained		High	Based on outcrop database for the Simpevarp and Laxemar subareas and its immediate surroundings.

RSMB01 Property	Character	Quantitative estimate	Confidence	Comment
Age (million years)		c. 1,800	High	Not dated. Based on U-Pb zircon age of the Ävrö granite (cf. RSMA01) and the quartz monzodiorite (cf. RSMC01). Field relationships strongly indicate that the fine-grained dioritoid is formed during the same magmatic event.
Structure	Isotropic to weakly foliated. Scattered mesoscopic, ductile shear zones		High	Based on outcrop database for the Simpevarp and Laxemar subareas and its immediate surroundings.
Texture	Equigranular to unequigranular		High	Based on outcrop database for the Simpevarp and Laxemar subareas and its immediate surroundings.
Density (kg/m ³)		2,786±20	High	N=9. The quantitative estimate is based on surface samples and KSH02. Mean value ± std.
Porosity (%)		0.33±0.08	High	N=9. The quantitative estimate is based on surface samples and KSH02. Mean value ± std.
Magnetic susceptibility (SI units)		3.39±0.55	High	N=9. The quantitative estimate is based on surface samples and KSH02. Average value in logarithmic scale ± std.
Electric resistivity in fresh water (ohm m)		4.54±0.37	High	N=9. The quantitative estimate is based on surface samples and KSH02. Average value in logarithmic scale ± std.
Uranium content based on gamma ray spectrometric data (ppm)		4.0±1.7	High	N=9. The quantitative estimate is based on measurements on outcrops. Mean value ± std.
Natural exposure (microR/h)		11.6±3.4	High	N=9. The quantitative estimate is based on measurements on outcrops. Mean value ± std.
Subordinate rock types (%)	Quartz monzodiorite (501036) 0–3 Fine-to medium-grained granite (511058) 3–8 Pegmatite (501061) 2–3 Fine-grained mafic rock (505102) 0–1 Ävrö granite (501044) 0–1		High	Quantitative estimate based on occurrence in KSH01A and KSH02.
Degree of inhomogeneity	Low		High	Based on outcrop database for the Simpevarp subarea, KSH01A and KSH02.
Metamorphism/alteration (%)	Inhomogeneous hydrothermal alteration (secondary red staining)	10–38	High	The quantitative estimate is based on faint to weak, including subordinate medium and strong, oxidation in KSH01A and KSH02 outside interpreted deformation zones in the single-hole interpretation.
Mineral fabric (type/orientation)				No data

RSMB03 Property	Character	Quantitative estimate	Confidence	Comment
Dominant rock type (%)	Fine-grained dioritoid (501030)	90.6–94.2	High	The quantitative estimate refers to RSMB01.
Mineralogical composition (%) (dominant minerals)	Quartz	7.4±5.0	High	N=21. The quantitative estimate is based on modal analyses of surface samples from the Simpevarp subarea, KSH01A and KSH02. Mean value ± std.
	K-feldspar	11.3±6.4		
	Plagioclase	51.4±8.7		
	Biotite	14.7±7.6		
	Amphibole	0–14		
	Pyroxene	0–22		
Grain size	Fine-grained		High	Based on outcrop database for the Simpevarp subarea.
Age (million years)		c. 1,800	High	Cf. RSMB01.
Structure	Isotropic to weakly foliated. Scattered mesoscopic, ductile shear zones		High	Based on outcrop database for the Simpevarp subarea.
Texture	Unequigranular		High	Based on outcrop database for the Simpevarp subarea.
Density (kg/m ³)		2,786±20	High	N=9. The quantitative estimate refers to RSMB01. Mean value ± std.
Porosity (%)		0.33±0.08	High	N=9. The quantitative estimate refers to RSMB01. Mean value ± std.
Magnetic susceptibility (SI units)		3.39±0.55	High	N=9. The quantitative estimate refers to RSMB01. Average value in logarithmic scale ± std.
Electric resistivity in fresh water (ohm m)		4.54±0.37	High	N=9. The quantitative estimate refers to RSMB01. Average value in logarithmic scale ± std.
Uranium content based on gamma ray spectrometric data (ppm)		4.0±1.7	High	N=9. The quantitative estimate refers to RSMB01. Mean value ± std.
Natural exposure(microR/h)		11.6±3.4	High	N=9. The quantitative estimate refers to RSMB01. Mean value ± std.
Subordinate rock types (%)	Fine- to medium-grained granite (511058) Pegmatite (501061) Diorite to gabbro (501033) Ävrö granite (501044)		High	Based on outcrop database for the Simpevarp subarea. No quantitative estimate is available.
Degree of inhomogeneity	Low		High	Based on outcrop database for the Simpevarp subarea.
Metamorphism/alteration (%)	Inhomogeneous hydrothermal alteration (secondary red staining)		High	Based on outcrop database for the Simpevarp subarea.
Mineral fabric (type/ orientation)				No data

RSMBA01(a-b) Property	Character	Quantitative estimate	Confidence	Comment
Dominant rock type (%)	Fine-grained dioritoid (501030) 27 Ävrö granite (501044) 47		Medium	Mixture of fine-grained dioritoid (501030) and Ävrö granite (501044). Assumption of mixture based on sections in KLX02 and KLX05. The quantitative estimate is based on KLX05 (preliminary mapping).
Mineralogical composition (%) (dominant minerals)	–			Cf. data for RSMA01 and RSMB01.
Grain size				Cf. data for RSMA01 and RSMB01.
Age (million years)		c. 1,800	High	Cf. data for RSMA01 and RSMB01.
Structure				Cf. data for RSMA01 and RSMB01.
Texture				Cf. data for RSMA01 and RSMB01.
Density (kg/m ³)				Cf. data for RSMA01 and RSMB01.
Porosity (%)				Cf. data for RSMA01 and RSMB01.
Magnetic susceptibility (SI units)				Cf. data for RSMA01 and RSMB01.
Electric resistivity in fresh water (ohm m)				Cf. data for RSMA01 and RSMB01.
Uranium content based on gamma ray spectrometric data (ppm)		3.8±0.8		N=2 The quantitative estimate is based on measurements on outcrops. Mean value ± std.
Natural exposure (microR/h)		10.3±1.0		N=2. The quantitative estimate is based on measurements on outcrops. Mean value ± std.
Subordinate rock types (%)	Fine- to medium-grained granite (511058) 23 Fine-grained diorite to gabbro (505102) 2 Quartz monzodiorite (501036) 2 Pegmatite (501061) 2		High	Based on outcrop database for the Laxemar subarea and KLX05. The quantitative estimate is based on KLX05. Only existence but no quantitative estimate is available for fine- to medium-grained granite (511058) and quartz monzodiorite (501036).
Degree of inhomogeneity	Medium		Medium	Based on outcrop database for the Laxemar subarea.
Metamorphism/alteration (%)	Inhomogeneous hydrothermal alteration (secondary red staining)		Medium	Based on outcrop database for the Laxemar subarea. Alteration intensity unknown.
Mineral fabric (type/ orientation)				No data

RSMBA02				
Property	Character	Quantitative estimate	Confidence	Comment
Dominant rock type (%)	Fine-grained dioritoid (501030) Ävrö granite (501044)		Medium	Mixture of fine-grained dioritoid (501030) and Ävrö granite (501044). Assumption of mixture based on sections in KLX02 and KLX05.
Mineralogical composition (%) (dominant minerals)				Cf. data for RSMA01 and RSMB01.
Grain size				Cf. data for RSMA01 and RSMB01.
Age (million years)		c. 1,800	High	Cf. data for RSMA01 and RSMB01.
Structure				Cf. data for RSMA01 and RSMB01.
Texture				Cf. data for RSMA01 and RSMB01.
Density (kg/m ³)				Cf. data for RSMA01 and RSMB01.
Porosity (%)				Cf. data for RSMA01 and RSMB01.
Magnetic susceptibility (SI units)				Cf. data for RSMA01 and RSMB01.
Electric resistivity in fresh water (ohm m)				Cf. data for RSMA01 and RSMB01.
Uranium content based on gamma ray spectrometric data (ppm)		3.6		N=1 The quantitative estimate is based on measurement on outcrop.
Natural exposure (microR/h)		11.1		N=1 The quantitative estimate is based on measurement on outcrop.
Subordinate rock types (%)	Fine- to medium-grained granite (511058) Pegmatite (501061) Fine-grained diorite to gabbro (505102) Diorite to gabbro (501033)			Existence is based on outcrop database for the Laxemar subarea. No quantitative estimate is available.
Degree of inhomogeneity	Medium		Medium	Based on outcrop database for the Laxemar subarea.
Metamorphism/alteration (%)				No data
Mineral fabric (type/orientation)				No data



RSMBA03 (only occurs at depth)				
Property	Character	Quantitative estimate	Confidence	Comment
Dominant rock type (%)	Fine-grained dioritoid (501030) Ävrö granite (501044)	32 57	High	Mixture of fine-grained dioritoid (501030) and Ävrö granite (501044). The quantitative estimate is based on KLX02.
Mineralogical composition (%) (dominant minerals)				Cf. data for RSMA01 and RSMB01.
Grain size				Cf. data for RSMA01 and RSMB01.
Age (million years)		c. 1,800	Medium	Cf. data for RSMA01 and RSMB01.
Structure				Cf. data for RSMA01 and RSMB01.
Texture				Cf. data for RSMA01 and RSMB01.
Density (kg/m ³)				Cf. data for RSMA01 and RSMB01.
Porosity (%)				Cf. data for RSMA01 and RSMB01.
Magnetic susceptibility (SI units)				Cf. data for RSMA01 and RSMB01.
Electric resistivity in fresh water (ohm m)				Cf. data for RSMA01 and RSMB01.
Uranium content based on gamma ray spectrometric data (ppm)				Cf. data for RSMA01 and RSMB01.
Natural exposure (microR/h)				Cf. data for RSMA01 and RSMB01.
Subordinate rock types (%)	Fine-grained diorite to gabbro (505102)	8	High	The quantitative estimate is based on KLX02.
	Fine- to medium-grained granite (511058)	1		
	Granite (501058)	1		
	Pegmatite (501061)	1		
Degree of inhomogeneity	High		High	Based on KLX02.
Metamorphism/alteration (%)	Inhomogeneous hydrothermal alteration (secondary red staining)	22	High	The quantitative estimate is based on faint to weak oxidation in KLX02 outside interpreted deformation zones in the single-hole interpretation.
Mineral fabric (type/ orientation)				No data

RSMC01 Property	Character	Quantitative estimate	Confidence	Comment
Dominant rock type (%)	Quartz monzodiorite (501036) Ävrö granite (501044)	24–72 23–45	High	Mixture of quartz monzodiorite (501036) and Ävrö granite (501044). Quantitative estimate based on occurrence in KSH01A, KSH03A and KAV04A.
Mineralogical composition (%) (dominant minerals)	Quartz (501036) K-feldspar (501036) Plagioclase (501036) Biotite (501036) Amphibole (501036) Pyroxene (501036)	10.5±2.5 12.3±5.4 45.5±3.6 16.3±5.2 6.7±4.5 0–8.2	High	N=7. The quantitative estimate refers to the quartz monzodiorite and is based on modal analyses of surface samples from the Simpevarp subarea and KSH01A, B. For the composition of the Ävrö granite, cf. RSMA01.
Grain size	Medium-grained		High	Based on outcrop database for the Simpevarp subarea.
Age (million years)		1,802±4	High	U-Pb zircon dating of quartz monzodiorite. For the radiometric age of Ävrö granite, cf. RSMA01.
Structure	Isotropic to weakly foliated. Scattered mesoscopic, ductile shear zones		High	Based on outcrop database for the Simpevarp subarea.
Texture	Equigranular (501036) Unequigranular to porphyritic (501044)		High	Based on outcrop database for the Simpevarp subarea.
Density (kg/m ³)	Quartz monzodiorite (501036) Ävrö granite (501044)	2,837±57 2,724±72	High High	N=13. Quantitative estimate based on data from KSH01A/B and KSH03A. N=13. Quantitative estimate based on data from KSH01A/B and KSH03A.
Porosity (%)	Quartz monzodiorite (501036) Ävrö granite (501044)	0.44±0.14 0.64±0.42	High High	N=13. Quantitative estimate based on data from KSH01A/B and KSH03A. N=5. Quantitative estimate based on data from KSH01A/B and KSH03A.
Magnetic susceptibility (SI units)	Quartz monzodiorite (501036) Ävrö granite (501044)	3.171±0.758 3.153±0.295	High High	N=13. Quantitative estimate based on data from KSH01A/B and KSH03A. N=13. Quantitative estimate based on data from KSH01A/B and KSH03A.
Electric resistivity in fresh water (ohm m)	Quartz monzodiorite (501036) Ävrö granite (501044)	4.13±0.31 3.62±0.39	High High	N=13. Quantitative estimate based on data from KSH01A/B and KSH03A. N=5. Quantitative estimate based on data from KSH01A/B and KSH03A.
Uranium content based on gamma ray spectrometric data (ppm)				Cf. RSMA01 and RSMD01.

RSMC01 Property	Character	Quantitative estimate	Confidence	Comment
Natural exposure(microR/h)				Cf. RSMA01 and RSMD01.
Subordinate rock types (%)	Fine-grained dioritoid (501030)	0–15	High	The quantitative estimate is based on occurrence in KSH01A, KSH03A and KAV04A.
	Fine- to medium-grained granite (511058)	2–10		
	Granite (501058)	0–2		
	Fine-grained mafic rock (505102)	0–1		
	Pegmatite (501061)	2–3		
	Diorite to gabbro (501033)	0–1		
Degree of inhomogeneity	High		High	Based on outcrop database for the Simpevarp subarea, KSH01A, B, KSH03A, B and KAV04A.
Metamorphism/alteration (%)	Inhomogeneous hydrothermal alteration (secondary red staining)	13–86	High	Based on outcrop database for the Simpevarp subarea, KSH01A, B, KSH03A, B and KAV04A. The quantitative estimate is based on faint to weak, including subordinate medium and strong, oxidation in KSH01A, KSH03A and KAV04A outside interpreted deformation zones in the single-hole interpretation.
Mineral fabric (type/ orientation)				No data

RSMC02 Property	Character	Quantitative estimate	Confidence	Comment
Dominant rock type (%)	Quartz monzodiorite (501036) Ävrö granite (501044)		High	Cf. RSMC01.
Mineralogical composition (%) (dominant minerals)				Cf. RSMC01.
Grain size				Cf. RSMC01.
Age (million years)		c. 1,800	High	Cf. RSMC01.
Structure				Cf. RSMC01.
Texture				Cf. RSMC01.
Density (kg/m ³)	Quartz monzodiorite (501036) Ävrö granite (501044)			Cf. RSMC01.
Porosity (%)	Quartz monzodiorite (501036) Ävrö granite (501044)			Cf. RSMC01.
Magnetic susceptibility (SI units)	Quartz monzodiorite (501036) Ävrö granite (501044)			Cf. RSMC01.
Electric resistivity in fresh water (ohm m)	Quartz monzodiorite (501036) Ävrö granite (501044)			Cf. RSMC01.
Uranium content based on gamma ray spectrometric data (ppm)				Cf. RSMA01 and RSMD01.
Natural exposure (microR/h)				Cf. RSMA01 and RSMD01.
Subordinate rock types (%)	Fine-grained dioritoid (501030) Fine- to medium-grained granite (511058) Granite (501058) Fine-grained mafic rock (505102) Pegmatite (501061) Diorite to gabbro (501033)		High	Based on outcrop database for the Laxemar subarea and its immediate surroundings. No quantitative estimate available.
Degree of inhomogeneity	High		High	Based on outcrop database for the Laxemar subarea and its immediate surroundings.
Metamorphism/alteration (%)	Inhomogeneous hydrothermal alteration (secondary red staining)		Medium	Based on outcrop database for the Laxemar subarea and its immediate surroundings. Alteration frequency and intensity unknown.
Mineral fabric (type/orientation)				Very few data. Cf. stereogram in RSMA01 east of RSMP01.

RSMD01(a-b) Property	Character	Quantitative estimate	Confidence	Comment
Dominant rock type (%)	Quartz monzodiorite (501036)	95	High	The quantitative estimate is based on KLX03.
Mineralogical composition (%) (dominant minerals)	Quartz K-feldspar Plagioclase Biotite Amphibole	14.8±2.8 13.9±6.2 43.8±3.6 14.3±2.9 7.6±3.0	High	N=7. The quantitative estimate is based on modal analyses of surface samples from the Laxemar subarea and its immediate surroundings.
Grain size	Medium-grained		High	Based on outcrop database for the Laxemar subarea and its immediate surroundings.
Age (million years)		1,802±4	High	Based on U-Pb zircon dating of sample from RSMC01.
Structure	Isotropic to weakly foliated. Scattered mesoscopic, ductile shear zones		High	Based on outcrop database for the Laxemar subarea and its immediate surroundings.
Texture	Equigranular		High	Based on outcrop database for the Laxemar subarea and its immediate surroundings.
Density (kg/m ³)		2,767±19	High	N=12. The quantitative estimate is based on surface samples from the Laxemar subarea and its immediate surroundings. Mean value ± std.
Porosity (%)		0.54±0.11	High	N=12. The quantitative estimate is based on surface samples from the Laxemar subarea and its immediate surroundings. Mean value ± std.
Magnetic susceptibility (SI units)		3.33±0.22	High	N=12. The quantitative estimate is based on surface samples from the Laxemar subarea and its immediate surroundings. Average value in logarithmic scale ± std.
Electric resistivity in fresh water (ohm m)		4.12±0.14	High	N=12. The quantitative estimate is based on surface samples from the Laxemar subarea and its immediate surroundings. Average value in logarithmic scale ± std.
Uranium content based on gamma ray spectrometric data (ppm)		3.1±0.6	High	N=34. The quantitative estimate is based on measurements on outcrops in the Laxemar subarea and its immediate surroundings. Mean value ± std.
Natural exposure (microR/h)		9.5±1.2	High	N=34. The quantitative estimate is based on measurements on outcrops in the Laxemar subarea and its immediate surroundings. Mean value ± std.

RSMD01(a-b) Property	Character	Quantitative estimate	Confidence	Comment
Subordinate rock types (%)	Fine- to medium-grained granite (511058) Pegmatite (501061) Fine-grained diorite to gabbro (505102) Ävrö granite (501044) Fine-grained dioritoid (501030)	4 0.3	High	The existence is based on outcrop database for the Laxemar subarea and its immediate surroundings and KLX03. Quantitative estimate based on KLX03. No quantitative estimate is available for fine-grained diorite to gabbro (505102), Ävrö granite (501044) and fine-grained dioritoid (501030).
Dykes of fine- to medium-grained granite (511058)	Orientation	Mean pole=357/54 K=1.3 	High	N=31. Measurements from the local model area. Based on outcrop database for the Laxemar subarea and immediate surroundings. Mean pole is marked with a star.
Pegmatite (501061)	Orientation	Mean pole=341/31 K=1.4 	High	N=10. Measurements from the local model area. Based on outcrop database for the Laxemar subarea and immediate surroundings. Mean pole is marked with a star.
Degree of inhomogeneity	Low		High	Based on outcrop database for the Laxemar subarea and its immediate surroundings and KLX03.
Metamorphism/alteration (%)	Inhomogeneous hydrothermal alteration (saussuritization) Inhomogeneous hydrothermal alteration (secondary red staining)	25 7	High	The quantitative estimate is based on faint to weak and subordinate medium, saussuritization and oxidation in KLX03 outside interpreted deformation zones in the single-hole interpretation. The saussuritization is based on a slight greenish colouring of the plagioclase.
Mineral fabric (type/ orientation)	Weak magmatic to tectonic foliation			Cf. RSMA01 west of RSMP01 and RSMP02

RSMD02 Property	Character	Quantitative estimate	Confidence	Comment
Dominant rock type (%)	Quartz monzodiorite (501036)		Medium	Based on Simpevarp SDM v. 0.
Mineralogical composition (%) (dominant minerals)				No data
Grain size				No data
Age (million years)		c. 1,800	High	No data; inferred to be comparable to U-Pb zircon age of quartz monzodiorite in RSMC01.
Structure				No data
Texture				No data
Density (kg/m ³)				No data
Porosity (%)				No data
Magnetic susceptibility (SI units)				No data
Electric resistivity in fresh water (ohm m)				No data
Uranium content based on gamma ray spectrometric data (ppm)				No data
Natural exposure (microR/h)				No data
Subordinate rock types (%)				No data
Degree of inhomogeneity				No data
Metamorphism/alteration (%)				No data
Mineral fabric (type/ orientation)				No data

RSMD03 Property	Character	Quantitative estimate	Confidence	Comment
Dominant rock type (%)	Quartz monzodiorite (501036)		Medium	Based on Simpevarp SDM v. 0.
Mineralogical composition (%) (dominant minerals)				No data
Grain size				No data
Age (million years)		c. 1,800	High	No data; inferred to be comparable to U-Pb zircon age of quartz monzodiorite in RSMC01.
Structure				No data
Texture				No data
Density (kg/m ³)				No data
Porosity (%)				No data
Magnetic susceptibility (SI units)				No data
Electric resistivity in fresh water (ohm m)				No data
Uranium content based on gamma ray spectrometric data (ppm)				No data
Natural exposure (microR/h)				No data
Subordinate rock types (%)				No data
Degree of inhomogeneity				No data
Metamorphism/alteration (%)				No data
Mineral fabric (type/ orientation)				No data

RSMD04 Property	Character	Quantitative estimate	Confidence	Comment
Dominant rock type (%)	Quartz monzodiorite (501036)		Medium	Based on Simpevarp SDM v. 0.
Mineralogical composition (%) (dominant minerals)				No data
Grain size				No data
Age (million years)		c. 1,800	High	No data; inferred to be comparable to U-Pb zircon age of quartz monzodiorite in RSMC01.
Structure				No data
Texture				No data
Density (kg/m ³)				No data
Porosity (%)				No data
Magnetic susceptibility (SI units)				No data
Electric resistivity in fresh water (ohm m)				No data
Uranium content based on gamma ray spectrometric data (ppm)				No data
Natural exposure (microR/h)				No data
Subordinate rock types (%)				No data
Degree of inhomogeneity				No data
Metamorphism/alteration (%)				No data
Mineral fabric (type/ orientation)				No data

RSMD05 Property	Character	Quantitative estimate	Confidence	Comment
Dominant rock type (%)	Quartz monzodiorite (501036)		Medium	Based on Simpevarp SDM v. 0.
Mineralogical composition (%) (dominant minerals)				No data
Grain size				No data
Age (million years)		c. 1,800	High	No data; inferred to be comparable to U-Pb zircon age of quartz monzodiorite in RSMC01.
Structure				No data
Texture				No data
Density (kg/m ³)				No data
Porosity (%)				No data
Magnetic susceptibility (SI units)				No data
Electric resistivity in fresh water (ohm m)				No data
Uranium content based on gamma ray spectrometric data (ppm)				No data
Natural exposure (microR/h)				No data
Subordinate rock type(s)				No data
Degree of inhomogeneity				No data
Metamorphism/alteration				No data
Mineral fabric (type/ orientation)				No data

RSMD06 Property	Character	Quantitative estimate	Confidence	Comment
Dominant rock type (%)	Quartz monzodiorite (501036)		Medium	Based on Simpevarp SDM v. 0.
Mineralogical composition (%) (dominant minerals)				No data
Grain size				No data
Age (million years)		c. 1,800	High	No data; inferred to be comparable to U-Pb zircon age of quartz monzodiorite in RSMC01.
Structure				No data
Texture				No data
Density (kg/m ³)				No data
Porosity (%)				No data
Magnetic susceptibility (SI units)				No data
Electric resistivity in fresh water (ohm m)				No data
Uranium content based on gamma ray spectrometric data (ppm)				No data
Natural exposure (microR/h)				No data
Subordinate rock types (%)				No data
Degree of inhomogeneity				No data
Metamorphism/alteration (%)				No data
Mineral fabric (type/ orientation)				No data

RSM07 Property	Character	Quantitative estimate	Confidence	Comment
Dominant rock type (%)	Quartz monzodiorite (501036)		High	
Mineralogical composition (%) (dominant minerals)	Quartz	6.5±1.1	High	N=3. The quantitative estimate is based on modal analyses of surface samples.
	K-feldspar	3.1±2.4		
	Plagioclase	39.8±2.0		
	Biotite	15.5±6.5		
	Amphibole	28.1±9.4		
Grain size	Medium-grained		High	Based on outcrop database for the Laxemar subarea and its immediate surroundings.
Age (million years)		c. 1,800	High	No data; inferred to be comparable to U-Pb zircon age of quartz monzodiorite in RSMC01.
Structure	Isotropic to weakly foliated.		High	Based on outcrop database for the Laxemar subarea and its immediate surroundings.
Texture	Equigranular		High	Based on outcrop database for the Laxemar subarea and its immediate surroundings.
Density (kg/m ³)				No data
Porosity (%)				No data
Magnetic susceptibility (SI units)				No data
Electric resistivity in fresh water (ohm m)				No data
Uranium content based on gamma ray spectrometric data (ppm)				No data
Natural exposure (microR/h)				No data
Subordinate rock types (%)	Fine- to medium-grained granite (511058) Pegmatite (501061) Ävrö granite (501044) Diorite to gabbro (501033)		High	Based on outcrop database for the Laxemar subarea and its immediate surroundings. No quantitative estimate is available.
Degree of inhomogeneity	Medium		High	Based on outcrop database for the Laxemar subarea and its immediate surroundings.
Metamorphism/alteration (%)				No data
Mineral fabric (type/orientation)				Cf. RSMA01 west of RSMP01 and RSMP02.

RSMD08 Property	Character	Quantitative estimate	Confidence	Comment
Dominant rock type (%)	Quartz monzodiorite (501036)		High	
Mineralogical composition (%) (dominant minerals)	Quartz K-feldspar Plagioclase Biotite Amphibole			No data from this domain. Cf. quantitative estimate in RSMD07.
Grain size	Medium-grained		High	Based on outcrop database for the Laxemar subarea. and its immediate surroundings.
Age (million years)		c. 1,800	High	No data; inferred to be comparable to U-Pb zircon age of quartz monzodiorite in RSMC01.
Structure	Isotropic to foliated.		High	Based on outcrop database for the Laxemar subarea and its immediate surroundings.
Texture	Equigranular		High	Based on outcrop database for the Laxemar subarea and its immediate surroundings.
Density (kg/m ³)				No data
Porosity (%)				No data
Magnetic susceptibility (SI units)				No data
Electric resistivity in fresh water (ohm m)				No data
Uranium content based on gamma ray spectrometric data (ppm)		1.7		N=1. The quantitative estimate is based on measurement on outcrop.
Natural exposure (microR/h)		7.1		N=1. The quantitative estimate is based on measurement on outcrop.
Subordinate rock types (%)	Fine- to medium-grained granite (511058) Pegmatite (501061) Granite (501058) Ävrö granite (501044) Diorite to gabbro (501033)		High	Based on outcrop database for the Laxemar subarea and its immediate surroundings. No quantitative estimate is available.
Degree of inhomogeneity	Medium		High	Based on outcrop database for the Laxemar subarea and its immediate surroundings.
Metamorphism/alteration (%)				
Mineral fabric (type/ orientation)				Cf. RSMA01 west of RSMP01 and RSMP02.

RSME01 Property	Character	Quantitative estimate	Confidence	Comment
Dominant rock type (%)	Diorite to gabbro (501033)		High	
Mineralogical composition (%) (dominant minerals)	Quartz	4±0.6	Medium	N=4. The quantitative estimate is based on modal analyses of surface samples from corresponding rock types in the Simpevarp subarea. No data from this domain. Mean value ± std.
	Plagioclase	47.4±4.5		
	Biotite	10.8±3.8		
	Amphibole	29.4±5.3		
Grain size	Medium-grained		High	Based on outcrop database for the Laxemar subarea and its immediate surroundings.
Age (million years)		c. 1,800	High	Not dated. Based on U-Pb zircon age of the Ävrö granite (cf. RSMA01) and the quartz monzodiorite (RSMC01). Field relationships strongly indicate that the diorite to gabbro is formed during the same magmatic event.
Structure	Isotropic to weakly foliated		High	Based on outcrop database for the Laxemar subarea and its immediate surroundings.
Texture	Equigranular		High	Based on outcrop database for the Laxemar subarea and its immediate surroundings.
Density (kg/m ³)		2,960±43	High	N=11. The quantitative estimate is based on surface samples from corresponding rock types in the Laxemar subarea, KLX01 and KLX03. No data from this domain. Mean value ± std.
Porosity (%)		0.19±0.14	High	N=11. The quantitative estimate is based on surface samples from corresponding rock types in the Laxemar subarea, KLX01 and KLX03. No data from this domain. Mean value ± std.
Magnetic susceptibility (SI units)		2.694±0.733	High	N=11. The quantitative estimate is based on surface samples from corresponding rock types in the Laxemar subarea, KLX01 and KLX03. No data from this domain. Average value in logarithmic scale ± std.
Electric resistivity in fresh water (ohm m)		4.38±0.24	High	N=11. The quantitative estimate is based on surface samples from corresponding rock types in the Laxemar subarea, KLX01 and KLX03. No data from this domain. Average value in logarithmic scale ± std.
Uranium content based on gamma ray spectrometric data (ppm)		1.9±0.8	High	N=5. The quantitative estimate is based on surface samples from corresponding rock types in the Laxemar subarea. No data from this domain. Mean value ± std.
Natural exposure (microR/h)		5.7±1.2	High	N=5. The quantitative estimate is based on surface samples from corresponding rock types in the Laxemar subarea. No data from this domain. Mean value ± std.

RSME01 Property	Character	Quantitative estimate	Confidence	Comment
Subordinate rock types (%)	Fine- to medium-grained granite (511058)		High	Based on outcrop database for the Laxemar subarea and its immediate surroundings. No quantitative estimate is available.
Degree of inhomogeneity	Medium		High	Based on outcrop database for the Laxemar subarea and its immediate surroundings.
Metamorphism/alteration (%)				No data
Mineral fabric (type/orientation)				Cf. RSMA01 west of RSMP01 and RSMP02.

RSME11 Property	Character	Quantitative estimate	Confidence	Comment
Dominant rock type (%)	Diorite to gabbro (501033)		High	
Mineralogical composition (%) (dominant minerals)				No data
Grain size				No data
Age (million years)		c. 1,800	High	Not dated. Based on U-Pb zircon age of the Ävrö granite (cf. RSMA01) and the quartz monzodiorite (RSMC01). Field relationships strongly indicate that the diorite to gabbro is formed during the same magmatic event.
Structure				No data
Texture				No data
Density (kg/m ³)				No data
Porosity (%)				No data
Magnetic susceptibility (SI units)				No data
Electric resistivity in fresh water (ohm m)				No data
Uranium content based on gamma ray spectrometric data (ppm)				No data
Natural exposure (microR/h)				No data
Subordinate rock types (%)				No data
Degree of inhomogeneity				No data
Metamorphism/alteration (%)				No data
Mineral fabric (type/orientation)				No data

RSME12 Property	Character	Quantitative estimate	Confidence	Comment
Dominant rock type (%)	Diorite to gabbro (501033)		High	
Mineralogical composition (%) (dominant minerals)				No data
Grain size				No data
Age (million years)		c. 1,800	High	Not dated. Based on U-Pb zircon age of the Ävrö granite (cf. RSMA01) and the quartz monzodiorite (RSMC01). Field relationships strongly indicate that the diorite to gabbro is formed during the same magmatic event.
Structure				No data
Texture				No data
Density (kg/m ³)				No data
Porosity (%)				No data
Magnetic susceptibility (SI units)				No data
Electric resistivity in fresh water (ohm m)				No data
Uranium content based on gamma ray spectrometric data (ppm)				No data
Natural exposure (microR/h)				No data
Subordinate rock types (%)				No data
Degree of inhomogeneity				No data
Metamorphism/alteration (%)				No data
Mineral fabric (type/ orientation)				No data

RSME13 Property	Character	Quantitative estimate	Confidence	Comment
Dominant rock type (%)	Diorite to gabbro (501033)		High	
Mineralogical composition (%) (dominant minerals)				No data
Grain size				No data
Age (million years)		c. 1,800	High	Not dated. Based on U-Pb zircon age of the Ävrö granite (cf. RSMA01) and the quartz monzodiorite (RSMC01). Field relationships strongly indicate that the diorite to gabbro is formed during the same magmatic event.
Structure				No data
Texture				No data
Density (kg/m ³)				No data
Porosity (%)				No data
Magnetic susceptibility (SI units)				No data
Electric resistivity in fresh water (ohm m)				No data
Uranium content based on gamma ray spectrometric data (ppm)				No data
Natural exposure (microR/h)				No data
Subordinate rock types (%)				No data
Degree of inhomogeneity				No data
Metamorphism/alteration (%)				No data
Mineral fabric (type/ orientation)				No data

RSME14 Property	Character	Quantitative estimate	Confidence	Comment
Dominant rock type (%)	Diorite to gabbro (501033)		High	
Mineralogical composition (%) (dominant minerals)				No data
Grain size				No data
Age (million years)		c. 1,800	High	Not dated. Based on U-Pb zircon age of the Ävrö granite (cf. RSMA01) and the quartz monzodiorite (RSMC01). Field relationships strongly indicate that the diorite to gabbro is formed during the same magmatic event.
Structure				No data
Texture				No data
Density (kg/m ³)				No data
Porosity (%)				No data
Magnetic susceptibility (SI units)				No data
Electric resistivity in fresh water (ohm m)				No data
Uranium content based on gamma ray spectrometric data (ppm)				No data
Natural exposure (microR/h)				No data
Subordinate rock types (%)				No data
Degree of inhomogeneity				No data
Metamorphism/alteration (%)				No data
Mineral fabric (type/ orientation)				No data

RSME15 Property	Character	Quantitative estimate	Confidence	Comment
Dominant rock type (%)	Diorite to gabbro (501033)		High	
Mineralogical composition (%) (dominant minerals)				No data
Grain size				No data
Age (million years)		c. 1,800	High	Not dated. Based on U-Pb zircon age of the Ävrö granite (cf. RSMA01) and the quartz monzodiorite (RSMC01). Field relationships strongly indicate that the diorite to gabbro is formed during the same magmatic event.
Structure				No data
Texture		>		No data
Density (kg/m ³)				No data
Porosity (%)				No data
Magnetic susceptibility (SI units)				No data
Electric resistivity in fresh water (ohm m)				No data
Uranium content based on gamma ray spectrometric data (ppm)				No data
Natural exposure (microR/h)				No data
Subordinate rock types (%)				No data
Degree of inhomogeneity				No data
Metamorphism/alteration (%)				No data
Mineral fabric (type/ orientation)				No data

RSME16 Property	Character	Quantitative estimate	Confidence	Comment
Dominant rock type (%)	Diorite to gabbro (501033)		High	
Mineralogical composition (%) (dominant minerals)				No data
Grain size				No data
Age (million years)		c. 1,800	High	Not dated. Based on U-Pb zircon age of the Ävrö granite (cf. RSMA01) and the quartz monzodiorite (RSMC01). Field relationships strongly indicate that the diorite to gabbro is formed during the same magmatic event.
Structure				No data
Texture				No data
Density (kg/m ³)				No data
Porosity (%)				No data
Magnetic susceptibility (SI units)				No data
Electric resistivity in fresh water (ohm m)				No data
Uranium content based on gamma ray spectrometric data (ppm)				No data
Natural exposure (microR/h)				No data
Subordinate rock types (%)				No data
Degree of inhomogeneity				No data
Metamorphism/alteration (%)				No data
Mineral fabric (type/ orientation)				No data

RSME17 Property	Character	Quantitative estimate	Confidence	Comment
Dominant rock type (%)	Diorite to gabbro (501033)		High	
Mineralogical composition (%) (dominant minerals)				No data
Grain size				No data
Age (million years)		c. 1,800	High	Not dated. Based on U-Pb zircon age of the Åvrö granite (cf. RSMA01) and the quartz monzodiorite (RSMC01). Field relationships strongly indicate that the diorite to gabbro is formed during the same magmatic event.
Structure				No data
Texture				No data
Density (kg/m ³)				No data
Porosity (%)				No data
Magnetic susceptibility (SI units)				No data
Electric resistivity in fresh water (ohm m)				No data
Uranium content based on gamma ray spectrometric data (ppm)				No data
Natural exposure (microR/h)				No data
Subordinate rock types (%)				No data
Degree of inhomogeneity				No data
Metamorphism/alteration (%)				No data
Mineral fabric (type/ orientation)				No data

RSME18 Property	Character	Quantitative estimate	Confidence	Comment
Dominant rock type (%)	Diorite to gabbro (501033)		High	
Mineralogical composition (%) (dominant minerals)				No data
Grain size				No data
Age (million years)		c. 1,800	High	Not dated. Based on U-Pb zircon age of the Ävrö granite (cf. RSMA01) and the quartz monzodiorite (RSMC01). Field relationships strongly indicate that the diorite to gabbro is formed during the same magmatic event.
Structure				No data
Texture				No data
Density (kg/m ³)				No data
Porosity (%)				No data
Magnetic susceptibility (SI units)				No data
Electric resistivity in fresh water (ohm m)				No data
Uranium content based on gamma ray spectrometric data (ppm)				No data
Natural exposure (microR/h)				No data
Subordinate rock types (%)				No data
Degree of inhomogeneity				No data
Metamorphism/alteration (%)				No data
Mineral fabric (type/ orientation)				No data

RSMF01 Property	Character	Quantitative estimate	Confidence	Comment
Dominant rock type (%)	Fine- to medium-grained granite (511058)		Medium	
Mineralogical composition (%) (dominant minerals)	Quartz K-feldspar Plagioclase	25.8±4.2 33.8±3.3 29.8±3.3	Medium	N=5. The quantitative estimate is based on samples from the Laxemar subarea and KSH03. No data from this domain.
Grain size				No data
Age (million years)		c. 1,800	High	Based on /Wikman and Kornfält 1995/; U-Pb zircon dating of fine-grained granite in the access tunnel to ÄHRL.
Structure				No data
Texture				No data
Density (kg/m ³)				No data
Porosity (%)				No data
Magnetic susceptibility (SI units)				No data
Electric resistivity in fresh water (ohm m)				No data
Uranium content based on gamma ray spectrometric data (ppm)				No data
Natural exposure (microR/h)				No data
Subordinate rock types (%)				No data
Degree of inhomogeneity				No data
Metamorphism/alteration (%)				No data
Mineral fabric (type/ orientation)				No data

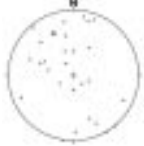

RSMF02 Property	Character	Quantitative estimate	Confidence	Comment
Dominant rock type (%)	Fine- to medium-grained granite (511058)		High	
Mineralogical composition (%) (dominant minerals)				Cf. RSMF01.
Grain size	Fine- to medium-grained			Based on outcrop database for the Laxemar subarea and its immediate surroundings.
Age (million years)		c. 1,800	High	Based on /Wikman and Kornfält 1995/; U-Pb zircon dating of fine-grained granite in the access tunnel to ÄHRL.
Structure	Isotropic to weakly foliated			Based on outcrop database for the Laxemar subarea and its immediate surroundings.
Texture	Equigranular			Based on outcrop database for the Laxemar subarea and its immediate surroundings.
Density (kg/m ³)				No data
Porosity (%)				No data
Magnetic susceptibility (SI units)				No data
Electric resistivity in fresh water (ohm m)				No data
Uranium content based on gamma ray spectrometric data (ppm)				No data
Natural exposure (microR/h)				No data
Subordinate rock types (%)	Diorite to gabbro (501033) Ävrö granite (501044) Pegmatite (501061) Fine-grained diorite to gabbro (505102)		High	Based on outcrop database for the Laxemar subarea and its immediate surroundings. No quantitative estimate is available.
Degree of inhomogeneity	Medium		Medium	Based on outcrop database for the Laxemar subarea and its immediate surroundings.
Metamorphism/alteration (%)				No data
Mineral fabric (type/ orientation)				No data

RSMF03 Property	Character	Quantitative estimate	Confidence	Comment
Dominant rock type (%)	Fine- to medium-grained granite (511058)		Medium	
Mineralogical composition (%) (dominant minerals)				Cf. RSMF01.
Grain size				No data
Age (million years)		c. 1,800	High	Based on /Wikman and Kornfält 1995/; U-Pb zircon dating of fine-grained granite in the access tunnel to ÄHRL.
Structure				No data
Texture				No data
Density (kg/m ³)				No data
Porosity (%)				No data
Magnetic susceptibility (SI units)				No data
Electric resistivity in fresh water (ohm m)				No data
Uranium content based on gamma ray spectrometric data (ppm)				No data
Natural exposure (microR/h)				No data
Subordinate rock types (%)				No data
Degree of inhomogeneity				No data
Metamorphism/alteration (%)				No data
Mineral fabric (type/ orientation)				No data


RSMG01 Property	Character	Quantitative estimate	Confidence	Comment
Dominant rock type (%)	Granite (521058) Fine-grained granite (531058)		High	
Mineralogical composition (%) (dominant minerals)	Quartz K-feldspar Plagioclase	31.3±5.6 36.7±7.1 24.1±6.3	High	N=10. Quantitative estimate based on modal analyses in /Wikman and Kornfält 1995/. Mean value ± std.
Grain size	Fine- to medium- and coarse-grained		High	Based on /Wikman and Kornfält 1995/.
Age (million years)		1,452±11/-9	High	U-Pb zircon dating. Based on /Åhäll 2001/.
Structure	Isotropic		High	Based on /Kresten and Chyssler 1976/ and /Wikman and Kornfält 1995/.
Texture	Equigranular and porphyritic		High	Based on /Kresten and Chyssler 1976/ and /Wikman and Kornfält 1995/.
Density (kg/m ³)		2,620±20	High	N=14. Based on /Nisca 1987/.
Porosity (%)				No data
Magnetic susceptibility (SI units)		1.80±0.90	High	N=14. Based on /Nisca 1987/. Average value in logarithmic scale ± std.
Electric resistivity in fresh water (ohm m)				No data
Uranium content based on gamma ray spectrometric data (ppm)		14.6±8.2	High	N=7. Based on geochemical analyses /Wikman and Kornfält 1995/.
Natural exposure (microR/h)				No data
Subordinate rock types (%)				Not assessed
Degree of inhomogeneity	Low		High	
Metamorphism/alteration (%)				Not assessed
Mineral fabric (type/ orientation)				

RSMG02 Property	Character	Quantitative estimate	Confidence	Comment
Dominant rock type (%)	Granite (521058)		High	
Mineralogical composition (%) (dominant minerals)	Quartz K-feldspar Plagioclase	34.6±5.5 37.4±7.2 21.6±3.8	High	N=5. Quantitative estimate based on modal analyses in /Wikman and Kornfält 1995/. Mean value ± std.
Grain size	Coarse-grained			
Age (million years)		1,441+5/-3	High	U-Pb zircon dating. Based on /Åhäll 2001/.
Structure	Isotropic		High	
Texture				
Density (kg/m ³)		2,620±10	High	N=10. Based on /Nisca 1987/.
Porosity (%)				No data
Magnetic susceptibility (SI units)		2.35±0.64	High	N=10. Based on /Nisca 1987/. Average value in logarithmic scale ± std.
Electric resistivity in fresh water (ohm m)				No data
Uranium content based on gamma ray spectrometric data (ppm)				No data
Natural exposure (microR/h)				No data
Subordinate rock type(s)				No data
Degree of inhomogeneity	Low		High	
Metamorphism/alteration				No data
Mineral fabric (type/ orientation)				


RSMM01 (a–d)				
Property	Character	Quantitative estimate	Confidence	Comment
Dominant rock type (%)	Ävrö granite (501044)	38–73	High	The rock domain is characterized by the high amount of diorite to gabbro (501033) mainly in the contact zone between the Ävrö granite (501044) and the quartz monzodiorite (501036) in RSMA01 and RSMD01, respectively. The quantitative estimate is based on KLX03, KLX05 (preliminary mapping), outcrop ASM000209 and the bedrock map of the Laxemar and Simpevarp subareas.
	Quartz monzodiorite (501036)	0–27		
	Diorite to gabbro (501033)	1–36		
Mineralogical composition (%) (dominant minerals)	Quartz (501044)	13.0±4.4	High	N=9. The quantitative estimate refers to Ävrö granite and is based on modal analyses of surface samples from the Laxemar subarea and KLX03. For the composition of the quartz monzodiorite and the diorite to gabbro, cf. RSMD01 and RSME01, respectively.
	K-feldspar (501044)	13.8±6.6		
	Plagioclase (501044)	52.3±5.3		
	Biotite (501044)	12.5±5.3		
	Amphibole (501044)	3.7±3.1		
Grain size				Cf. RSMA01, RSMD01 and RSME01.
Age (million years)		c. 1,800	High	Cf. RSMA01 and RSMC01.
Structure	Isotropic to weakly foliated. Scattered mesoscopic, ductile shear zones			Based on outcrop database for the Laxemar subarea and immediate surroundings.
Texture				Cf. RSMA01, RSMD01 and RSME01.
Density (kg/m ³)				Cf. RSMA01, RSMD01 and RSME01.
Porosity (%)				Cf. RSMA01, RSMD01 and RSME01.
Magnetic susceptibility (SI units)				Cf. RSMA01, RSMD01 and RSME01.
Electric resistivity in fresh water (ohm m)				Cf. RSMA01, RSMD01 and RSME01.
Uranium content based on gamma ray spectrometric data (ppm)				Cf. RSMA01, RSMD01 and RSME01.
Natural exposure (microR/h)				Cf. RSMA01, RSMD01 and RSME01.
Subordinate rock types (%)	Fine- to medium-grained granite (511058)	1–16	High	Based on outcrop database for the Laxemar subarea and immediate surroundings, KLX03, KLX05 and outcrop ASM000209. The quantitative estimate is based on KLX03, KLX05 (preliminary mapping), outcrop ASM000209 and the bedrock map of the Laxemar and Simpevarp subareas.
	Pegmatite (501061)	0–0.3		
	Fine-grained diorite to gabbro (505102)	0–3		
	Granite (501058)	0–26		
	Fine-grained dioritoid	1–3		

RSMM01 (a-d) Property	Character	Quantitative estimate	Confidence	Comment
Dykes of fine- to medium-grained granite (511058)	Orientation	Mean pole=335/29 K=0.8 	High	N=28. Measurements from the local model area. Based on outcrop database for the Laxemar subarea and immediate surroundings. Mean pole is marked with a star.
Pegmatite	Orientation	Mean pole=331/8 K=1.1 	High	N=14. Measurements from the local model area. Based on outcrop database for the Laxemar subarea and immediate surroundings. Mean pole is marked with a star.
Degree of inhomogeneity	High		High	Based on outcrop database for the Laxemar subarea and immediate surroundings, bedrock map, KLX03, KLX05 and outcrop ASM000209. The degree of inhomogeneity varies and may be low locally.
Metamorphism/ alteration (%)	Hydrothermal alteration (saussuritization in Ävrö granite (501044))	3	High	The quantitative estimate is based on faint to weak and subordinate medium, saussuritization and oxidation in KLX03 outside interpreted deformation zones in the single-hole interpretation. The saussuritization is based on a slight greenish colouring of the plagioclase.
	Hydrothermal alteration (saussuritization in quartz monzodiorite (501036))	43		
	Hydrothermal alteration (red staining in Ävrö granite(501044))	9		
	Hydrothermal alteration (red staining in quartz monzodiorite (501036))	17		
Mineral fabric (type/ orientation)	Weak magmatic to tectonic foliation			Cf. RSMA01 west and east of RSMP01 and RSMP02.

RSMP01 Property	Character	Quantitative estimate	Confidence	Comment
Dominant rock type (%)	Ävrö granite (501044)		High	Based on outcrop databases for the Laxemar subarea and immediate surroundings.
Mineralogical composition (%) (dominant minerals)				Cf. RSMA01 what concerns undeformed to weakly deformed varieties of the Ävrö granite. No quantitative data for mylonitic varieties.
Grain size	Fine- to medium-grained		High	Based on outcrop databases for the Laxemar subarea and immediate surroundings.
Age (million years)		c. 1,800	High	Age refers to rock types. Cf. RSMA01. Age of low-grade deformation is unknown, but is inferred to be close in time (c. 1,800–1,750 Ma) to the age of intrusion of the rock types.
Structure	Isotropic to mylonitic			Based on outcrop databases for the Laxemar subarea and immediate surroundings.
Texture	Unequigranular to porphyritic to porphyroclastic		High	Based on outcrop databases for the Laxemar subarea and immediate surroundings.
Density (kg/m ³)				Cf. RSMA01 for undeformed varieties. No data for mylonitic varieties.
Porosity (%)				Cf. RSMA01 for undeformed varieties. No data for mylonitic varieties.
Magnetic susceptibility (SI units)				Cf. RSMA01 for undeformed varieties. No data for mylonitic varieties.
Electric resistivity in fresh water (ohm m)				Cf. RSMA01 for undeformed varieties. No data for mylonitic varieties.
Uranium content based on gamma ray spectrometric data (ppm)				Cf. RSMA01 for undeformed varieties. No data for mylonitic varieties.
Natural exposure (microR/h)				Cf. RSMA01 for undeformed varieties. No data for mylonitic varieties.
Subordinate rock types (%)	Fine- to medium-grained granite (511058) Pegmatite (501061) Diorite to gabbro (501033) Fine-grained dioritoid (501030) Fine-grained diorite to gabbro (505102)		High	Existence is based on outcrop database for the Laxemar subarea. No quantitative estimate is available. The fine-grained dioritoid is predominantly occurring in the southernmost part of the domain. Otherwise the amount of subordinate rock types is presumably comparable to RSMA01.

RSMP01 Property	Character	Quantitative estimate	Confidence	Comment
Degree of inhomogeneity	Low		High	Based on outcrop databases for the Laxemar subarea and immediate surroundings. The degree of inhomogeneity based on subordinate rock types are judged to be comparable to RSMA01, but the degree of inhomogeneity what relates to the degree of ductile shear deformation is high.
Metamorphism/ alteration (%)	Low-grade metamorphic alteration		High	Based on outcrop databases for the Laxemar subarea and immediate surroundings.
Mineral fabric (type/ orientation)	Protomylonitic to mylonitic foliation	Mean pole=307/2 K=1.3	High	N=28. Based on outcrop databases for the Laxemar subarea and immediate surroundings. The foliation has a northeasterly orientation and a subvertical to vertical dip. The stereogram includes poles to all measurements of mylonitic foliation from RSMP01. Mean pole is marked with a star.
				

RSMP02 Property	Character	Quantitative estimate	Confidence	Comment
Dominant rock type (%)	Ävrö granite (501044) Quartz monzodiorite (501036)		Medium	Ävrö granite (501044) dominates in the northeastern and southwestern part of the domain, and quartz monzodiorite (501036) in the central part.
Mineralogical composition (%) (dominant minerals)				Cf. RSMA01 and RSMD01a for undeformed varieties. No data for mylonitic varieties.
Grain size				Cf. RSMA01 and RSMD01a for undeformed varieties. No data for mylonitic varieties.
Age (million years)		c. 1,800	High	Age refers to rock types. Cf. RSMA01 and RSMC01. Age of low-grade deformation is unknown, but is inferred to be close in time (c. 1,800–1,750 Ma) to the age of intrusion of the rock types.
Structure				Cf. RSMA01 and RSMD01a for undeformed varieties. No data for mylonitic varieties.
Texture				Cf. RSMA01 and RSMD01a for undeformed varieties. No data for mylonitic varieties.
Density (kg/m ³)				Cf. RSMA01 and RSMD01a for undeformed varieties. No data for mylonitic varieties.

RSMP02 Property	Character	Quantitative estimate	Confidence	Comment
Porosity (%)				Cf. RSMA01 and RSMD01a for undeformed varieties. No data for mylonitic varieties.
Magnetic susceptibility (SI units)				Cf. RSMA01 and RSMD01a for undeformed varieties. No data for mylonitic varieties.
Electric resistivity in fresh water (ohm m)				Cf. RSMA01 and RSMD01a for undeformed varieties. No data for mylonitic varieties.
Uranium content based on gamma ray spectrometric data (ppm)				Cf. RSMA01 and RSMD01a for undeformed varieties. No data for mylonitic varieties.
Natural exposure (microR/h)				Cf. RSMA01 and RSMD01a for undeformed varieties. No data for mylonitic varieties.
Subordinate rock types (%)	Fine-grained dioritoid (501030) Diorite to gabbro (501033) Granite (501058) Fine- to medium-grained granite (511058) Pegmatite (501061) Fine-grained diorite to gabbro (505102)		High	Existence is based on outcrop database for the Laxemar subarea. No quantitative estimate is available. The amount of subordinate rock types is presumably comparable to RSMA01 and RSMD01.
Degree of inhomogeneity	Medium		High	Based on outcrop databases for the Laxemar subarea and immediate surroundings.
Metamorphism/alteration (%)	Low-grade metamorphic alteration		High	Based on outcrop databases for the Laxemar subarea and immediate surroundings.
Mineral fabric (type/orientation)		Mean pole=313/0 K=2.8 	High	N=35. Based on outcrop databases for the Laxemar subarea and immediate surroundings. The foliation has a northeasterly orientation and a subvertical to vertical dip. The stereogram includes poles to all measurements of mylonitic foliation from RSMP02. Mean pole is marked with a star.

Dominant and subordinate rock type statistics

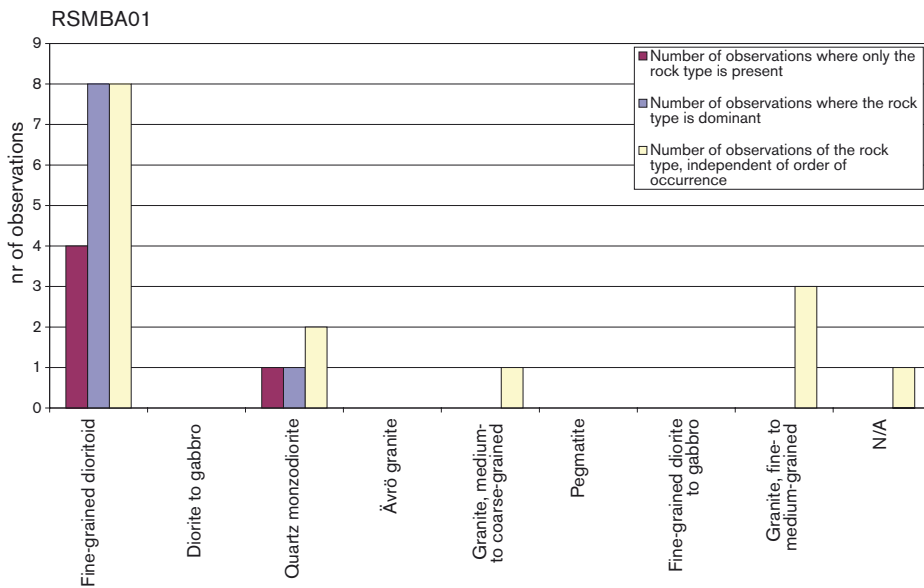
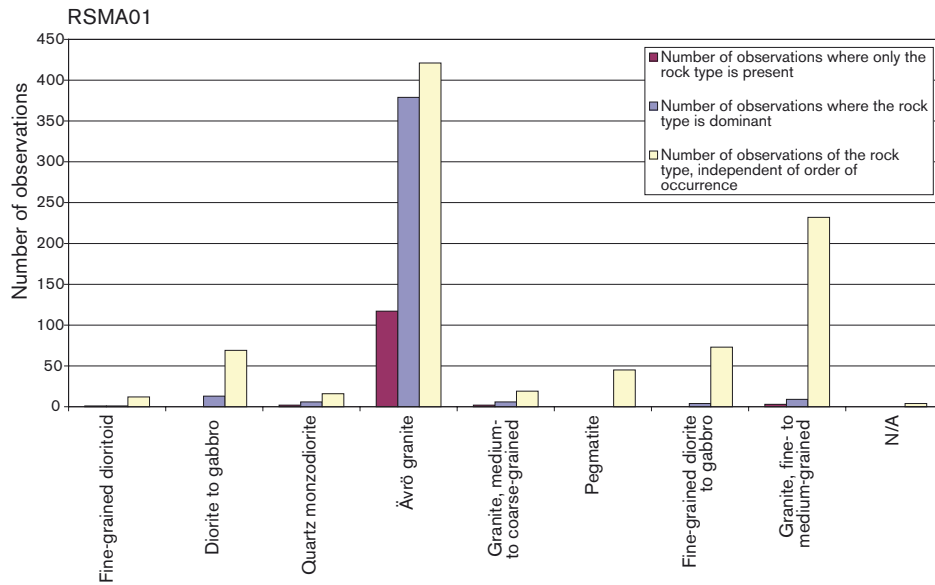


Figure A4-1. Qualitative assessment of dominant and subordinate rock types in rock domains based on surface outcrop data from the Laxemar subarea.

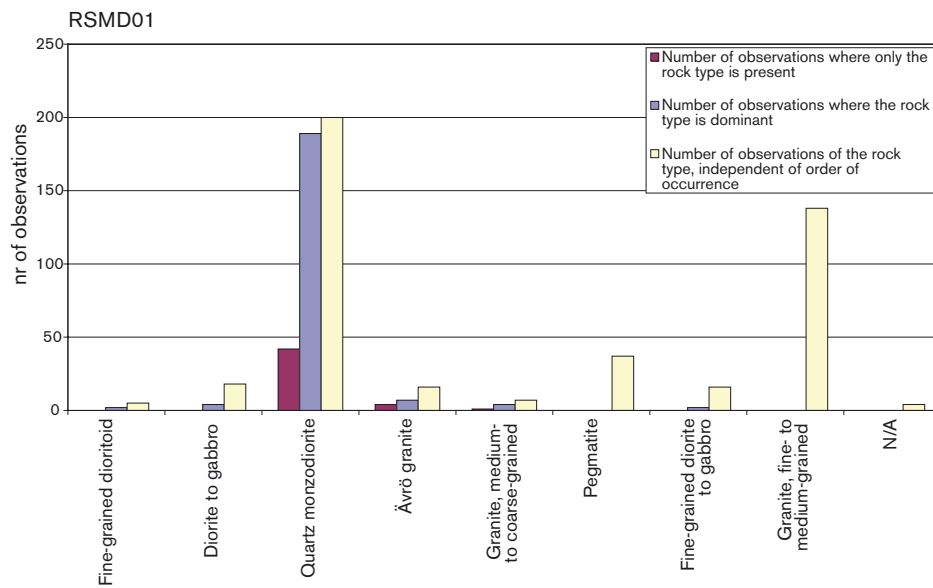
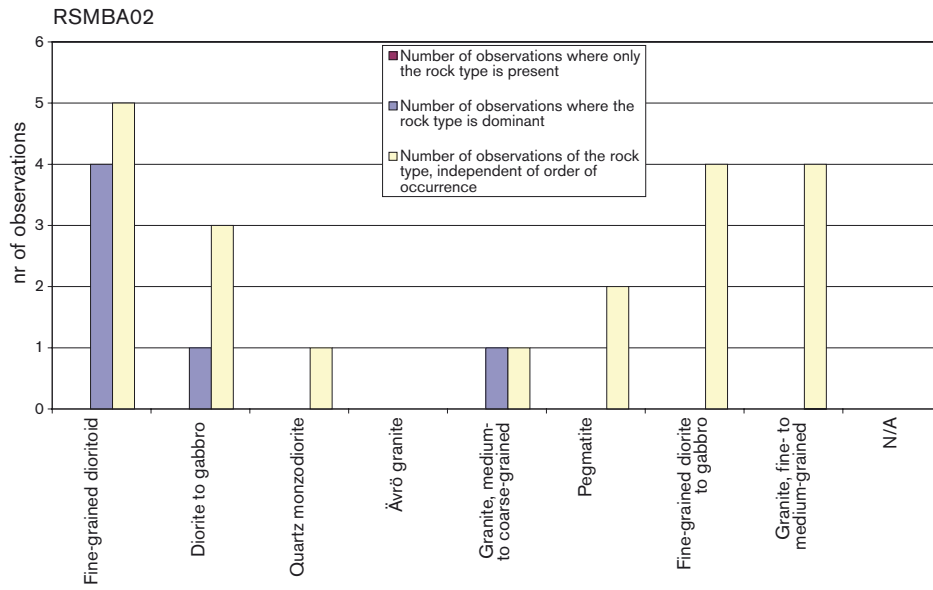


Figure A4-2. Qualitative assessment of dominant and subordinate rock types in rock domains based on surface outcrop data from the Laxemar subarea.

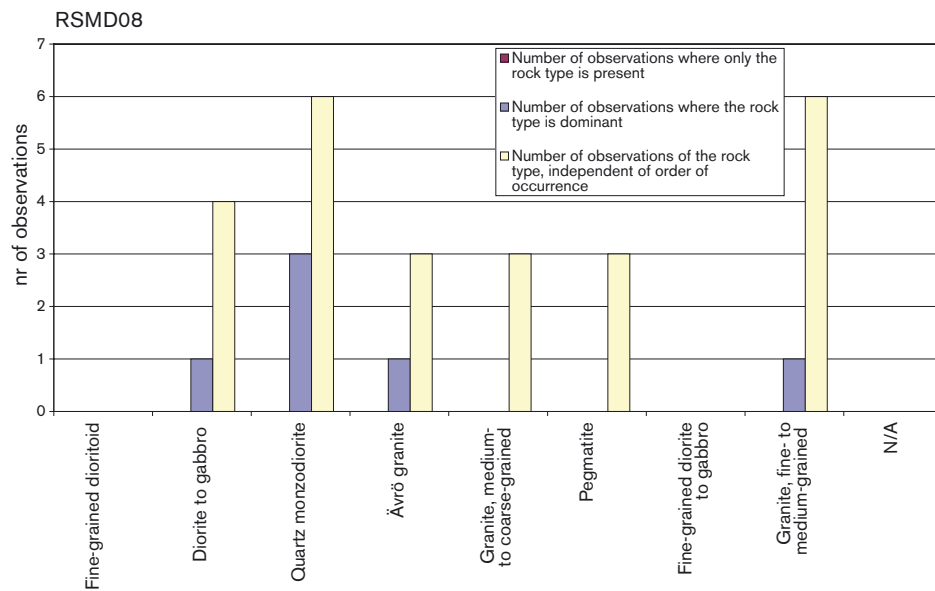
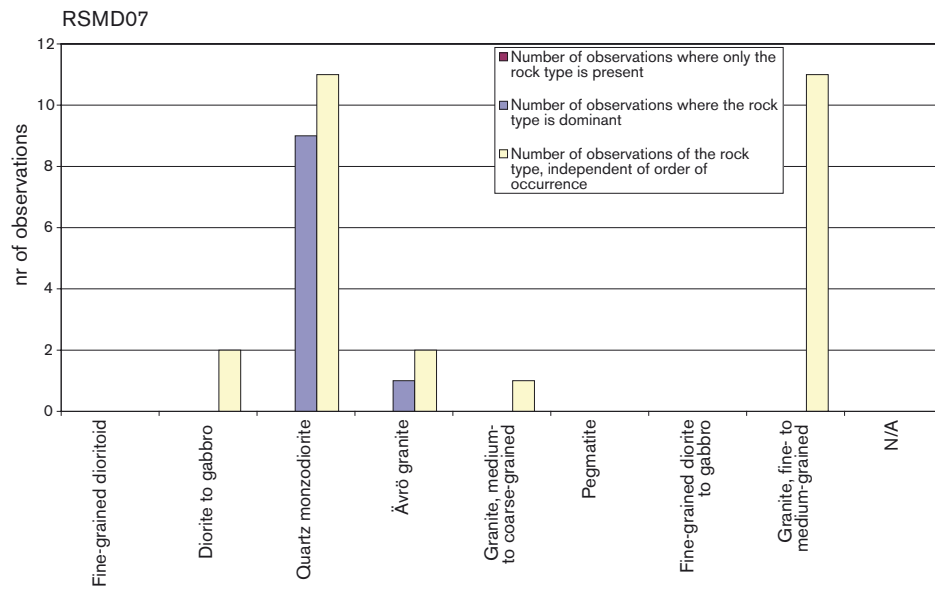


Figure A4-3. Qualitative assessment of dominant and subordinate rock types in rock domains based on surface outcrop data from the Laxemar subarea.

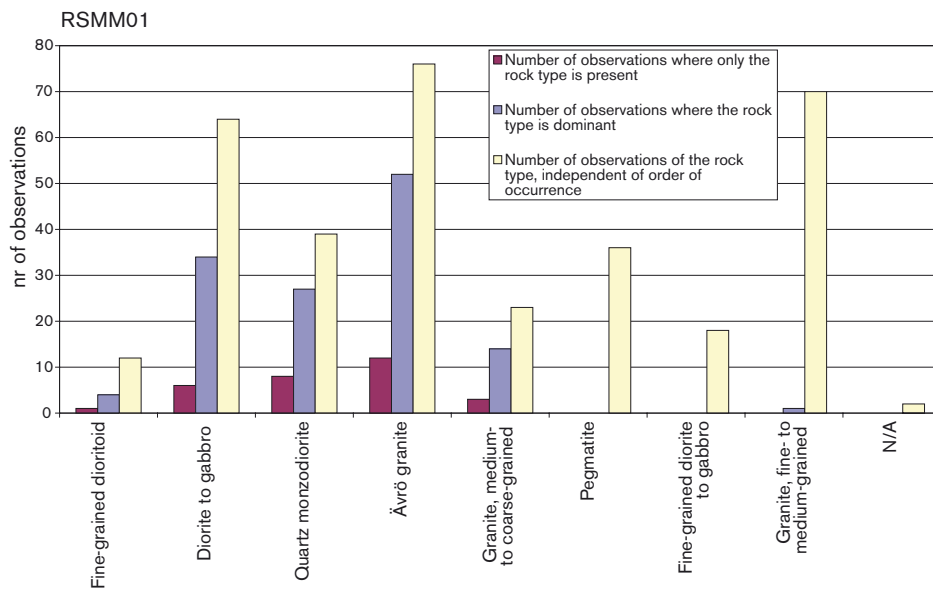
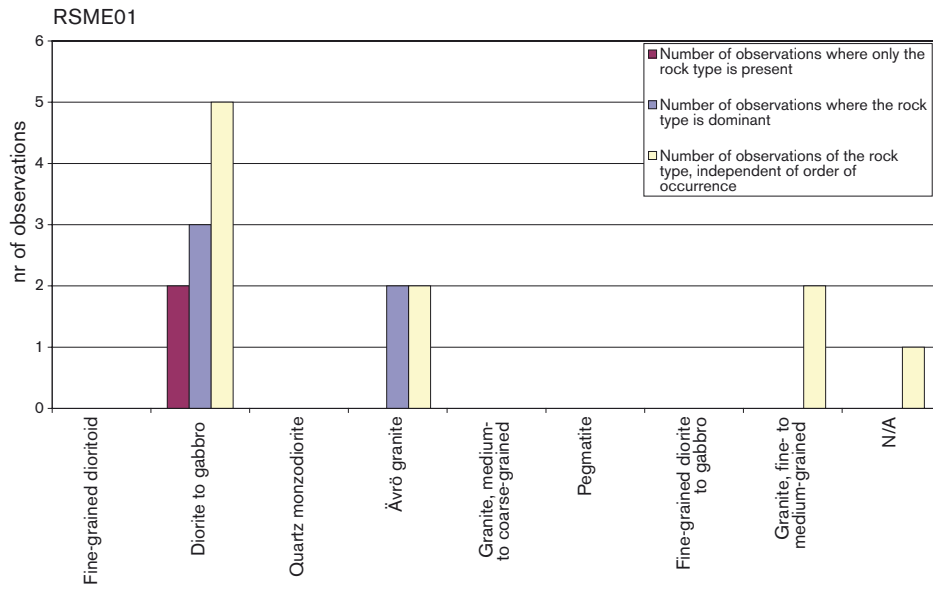


Figure A4-4. Qualitative assessment of dominant and subordinate rock types in rock domains based on surface outcrop data from the Laxemar subarea.

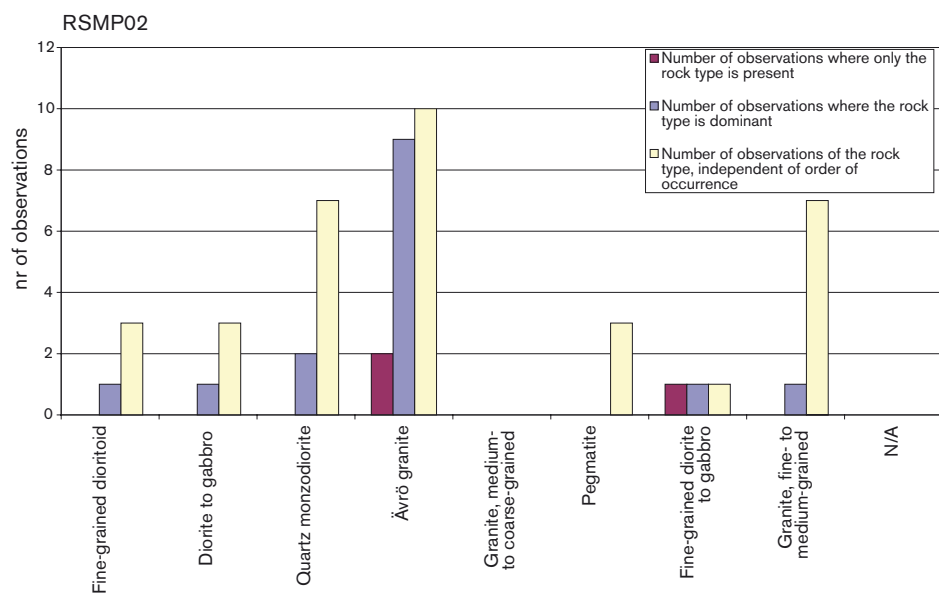
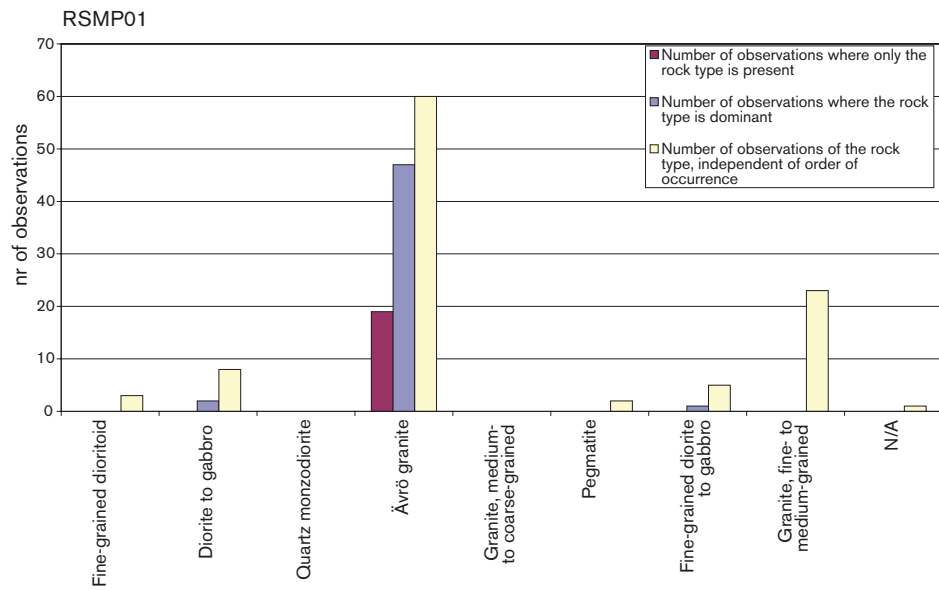


Figure A4-5. Qualitative assessment of dominant and subordinate rock types in rock domains based on surface outcrop data from the Laxemar subarea.

Property tables for deformation zones

ZSMEW002A				
Property	Estimate	Span	Basis for interpretation	Comments
Confidence in existence	High		Linked lineament, BH and geophysical ground survey	
Strike (regional scale)	090	± 20	Strong magnetic and topographic lineament	
Dip (regional scale)	65	± 10	Seismic relector and BH indicators	
Thickness, (including transition zones, regional scale)	100 m	20 to 200 m	Lineament, BH and geophysical ground survey	Complex zone, inferred anastomosing geometry.
Length (regional scale)	17.8 km	± 5 km	Linked lineaments	30 km, including extension outside the regional model area
Rock type	Ävrö granite dominates, with fine grained diorite gabbro		KAS03 and KLX06	
Ductile deformation	Yes		Mylonite KAS17. Field mapping	Brittle-ductile zone. Dominantly brittle.
Brittle deformation	Yes		Field indicators. Multiple crush zones KLX06 v. 1 only preliminary mapping available). Breccia and crush zones KAS03	Brittle-ductile zone. Dominantly brittle.
Alteration	Oxidation			
Water				
Fracture orientation	Not yet assessed			
Fracture frequency m ⁻¹	9		KAS03	Frac' frq'incl' crush (= 20 frac/m) (m ⁻¹)
Fracture filling	Ca 66%, Chl 67%, Ep 6%, He 46% Qtz 5%		KAS03	

BH	Geometrical intercept	Target intercept	Comment
KAS03	307–495	280–480	Brittle and ductile indicators.
KAS17	249–360		Only incomplete preliminary mapping available.
KLX06	300–430	300–400	Only preliminary mapping available.
HLX20	60–185		No results available.

ZSMEW007A				
Property	Estimate	Span	Basis for interpretation	Comments
Confidence in existence	High		Linked lineament, BH and geophysical ground survey	
Strike (regional scale)	278	± 20	Strong magnetic and topographic lineament	
Dip (regional scale)	43	± 10	Seismic relector and BH incators	Seismic reflector survey (P-04-215) reflector A, good agreement with strike and dip 43° N. Geophysical profiling; resistivity, magnetic; all suggest northern dip 40–55°.
Thickness, (including transition zones, regional scale)	50 m	20 to 60 m	Lineament, BH and geophysical ground survey	Complex zone. 50 m, based on inclusion of estimated likely transition zones. 10 m wide 'core' of more highly fractured rock based on general ref: geophysical profiling -refraction (P-04-134)
Length (regional scale)	3.3 km	± 200 m	Linked lineaments	
Ductile deformation	–			Brittle deformation zone
Brittle deformation	Yes		Rare field indicators, high facture frequency in BH's	Brittle deformation zone
Alteration	Oxidation		BH's	Red colouration
Water	Water bearing		BH's	No anaylsis available
Fracture orientation	Not yet assessed			
Fracture frequency m ⁻¹	10		KLX01, KLX02, KLX04	Frac' frq'incl' crush (= 20 frac/m) (m ⁻¹)
Fracture filling	Ca 41%, Chl 64%, Ep 23%, He 10% Qtz 1%		KLX01, KLX02, KLX04	

BH	Geometrical intercept	Target intercept	Comment
KLX01	972–1,044	1,000–1,020	Oxidation, high fracture frequency, narrow sections with crushed rock, several chlorite or calcite sealed fractures. Uncertainty = 3
KLX02	234–311	265–275	Orientated open fracture sets between BH length 260–280 m show good agreement.
KLX04	314–391	346–355	Brittle deformation with brecciation (sealed network). Low resistivity, variable sonic, very low susceptibility and small caliper anomaly. Radar reflectors at 350.7 m with the angle 70° to borehole axis and at 352.1 m with the angle 20° to borehole axis. Uncertainty = 3
HLX23	0–39		No results available- will require remodelling at a higer resolution with local lineament adjustment to include reults
HLX24			No results available- will require remodelling at a higer resolution with local lineament adjustment to include reults
HLX21	1–52		No results available- will require remodelling at a higer resolution with local lineament adjustment to include reults
HLX22			No results available- will require remodelling at a higer resolution with local lineament adjustment to include reults

ZSMEW009A				
Property	Estimate	Span	Basis for interpretation	Comments
Confidence in existence	High		Linked lineaments; Surface mapping; BHs; TASA (Äspö) tunnel intercept.	
Strike (regional scale)	085	± 15	Linked lineaments	
Dip (regional scale)	76	± 10	linked lineaments, TASA	
Thickness, (including transition zones, regional scale)	12 m	5 to 20 m	Linked lineaments; BHs; TASA (Äspö) tunnel intercept.	
Length (regional scale)	1.7 km	± 100 m	Linked lineaments	
Ductile deformation	Yes		KAS06 (66 m) mylonitic	Ductile-brittle zone
Brittle deformation	Yes		TASA (Äspö)	Ductile-brittle zone
Alteration	1.5 to 2 m thick central clay zone.		TASA (Äspö)	
Water	90 l/min 1.7 · 10 ⁻⁵ m ² /s		Inflow into TASA Inflow into TASA	Ref: PR 25-95-20 Ref: PR HRL96-19
Fracture orientation	Not analysed			
Fracture frequency m ⁻¹	14		KAS06	Frac' frq'incl' crush (= 20 frac/m) (m ⁻¹)
Fracture filling	Ca 65%, Chl 79%, Ep 6%, He 21% Qtz 1%		KAS06	

BH	Geometrical intercept	Target intercept	Comment
HAS14	0.2–49		Await results
HAS21	25–57		Await results
KAS06	59–76	60–75	Strong tectonization and several sections of crushed core. 1 m thick mylonitic section.
KAS07	562–604 (Base)		Not used in the current model to define geometry. (tectonization recorded -Ref: Geomod)
TASA		1,407–1,421	Ref: PR HRL96-19
Surface trench (Äspö)		x = 6367638 y = 1551412 z = 2.5	1.5 m thick mylonite

ZSMEW013A (EW1a)				
Property	Estimate	Span	Basis for interpretation	Comments
Confidence in existence	High		Linked lineaments, field mapping and BHs.	
Strike (regional scale)	85	105 to 065	Linked lineaments	105 in west curving round to 065
Dip (regional scale)	90	± 10	Linked lineaments and BHs.	Ref: Geomod EW1a
Thickness, (including transition zones, regional scale)	45 m	20 to 50 m	Linked lineaments and BHs.	
Length (regional scale)	4.4 km	2.5 to 4.4 km	Linked lineaments.	An alternative interpretation is to terminate the zone against ZSMNE005A
Ductile deformation	Yes		Field mapping and BH (mylonite)	Brittle-ductile zone
Brittle deformation	Yes		BH breccia and crush zones.	Brittle-ductile zone
Alteration	Epidotized			
Water				
Fracture orientation	Not yet assessed			
Fracture frequency m ⁻¹	5		KA1755A, KAS04	Frac' frq'incl' crush (= 20 frac/m) (m ⁻¹)
Fracture filling	Ca 57%, Chl 46%, Ep 23%, He 1%, Qtz 3%		KA1755A, KAS04	

BH	Geometrical intercept	Target intercept	Comment
KA1755A	188–234	180–230	A crush zone, with enhanced fracture frequency. A thin breccia/mylonite and a c. 5–7 m wide zone of tectonization have been recorded. The area as interpreted as EW-1a in /Stanfors et al. 1994/.
KAS04	100–185	87–158	Five thin mylonites at depths: 87, 140, 147, 153 and 158 m. Intense tectonization around the mylonite at 147 m. Ref: Geomod.
HLX03	0–19	–	Awaiting results
HAS01	4–100	–	No information

ZSMEW023A				
Property	Estimate	Span	Basis for interpretation	Comments
Confidence in existence	High		Linked lineaments; seismic refraction profiling; OKG tunnel intercept.	
Strike (regional scale)	275	± 15	Linked lineaments	
Dip (regional scale)	90	± 20	OKG	
Thickness, (including transition zones, regional scale)	20 m	5 to 50 m	Linked lineaments, seismic refraction profiling and field mapping	The upper 50 m limit is based on indications from OKG that suggest locally a more diffuse zone consisting of increased fracturing and only minor shears.
Length (regional scale)	3.8 km	± 200 m	Linked lineaments	
Ductile deformation	–		No indicators	Brittle zone
Brittle deformation	Yes		OKG	Brittle zone
Alteration	Chlorite and clay			Clay may be depth dependent and be associated with the weathering profile considering the relatively shallow intercept position.
Water	Low transmissivity		Local 'dripping' reported in OKG excavation mapping.	
Fracture orientation	Not analysed			
Fracture frequency	Not analysed			
Fracture filling	CHI, Ca, Clay		OKG	

BH	Geometrical intercept	Target intercept	Comment
OKG		Cold water intake ch. 065–110 m	OKG cold water intake ch 065–110 m increased fracturing with up to 1 m wide chlorite and clay filled shear zone.
HSH05	191–200 (Base)	–	Await results

ZSMEW038A				
Property	Estimate	Span	Basis for interpretation	Comments
Confidence in existence	High		Linked lineaments, tunnel mapping and BHs.	Considered a minor structure.
Strike (regional scale)	090	± 10	Linked lineaments and tunnel	Complex split geometry. Potentially involves a series of narrow mylonites in a number of BHs and the tunnel, with potential interference from other zones including ZSMNE006A. The current modelled geometry is an over simplification.
Dip (regional scale)	90	± 15	Linked lineaments, BHs and tunnel intercepts	
Thickness, (including transition zones, regional scale)	10 m	1 to 15 m	Linked lineaments, BHs and tunnel intercepts.	1 m thick in TASA; 10 m represents an envelope thickness.
Length (regional scale)	3.2 km	± 100 m	Linked lineaments.	
Ductile deformation	Yes		Tunnel mapping (mylonite) TASA ch. 1,180A minor mylonite, alternative intercepts exist.	Dominantly ductile zone. Possible brittle reactivation. Requires further review of Äspö data.
Brittle deformation	Yes		Inferred from tunnel mapping, transmissivity and seismic refraction profiling. Requires further study. Tunnel brittle evidence maybe associated with the development of other zones.	Dominantly ductile zone. Possible brittle reactivation. Requires further review of Äspö data.
Alteration				
Water	T = 1.3·10 ⁻⁶ m ² /s		TASA ch. 1,180	
Fracture orientation	Not yet assessed			
Fracture frequency m ⁻¹	13		KA1131B	Frac' frq'incl' crush (= 20 frac/m) (m ⁻¹)
Fracture filling	Ca 95%, Chl 70%, Ep 20%, He 0%, Qtz 0%		KA1131B	

BH	Geometrical intercept	Target intercept	Comment
HAV05	20–38	–	Awaiting results.
KAS09	220–239	249–253	Possible associated mylonite.
KBH02	538–547		
KA1131B	35–44	34–36	Mylonite
KA1061	100–109	74–75	Possible associated mylonite
TASA		1,180	(0.5–1 m thick)

ZSMEW900A				
Property	Estimate	Span	Basis for interpretation	Comments
Confidence in existence	High		Linked lineament, field mapping and geophysical ground survey	
Strike (regional scale)	100	± 20	Magnetic and topographic lineaments	Lineament interpretation needs further review.
Dip (regional scale)	70	± 20	Seismic reflector, field mapping and geophysical profiling.	Based generally on field measurements, seismic reflector L (P-04-215), geophysical profiling (P-04-134)
Thickness, (including transition zones, regional scale)	20 m	± 10	Lineament, geophysical ground survey	Based on inclusion of estimated likely transition zones. 10 m wide 'core' of more highly fractured rock based on general ref: geophysical profiling –refraction (P-04-134)
Length (regional scale)	1.7 km	1 to 2 km	Linked lineaments	Clear alternative lineament tie-ups are possible.
Ductile deformation	Yes		Single field indicator	Ductile-brittle deformation zone
Brittle deformation	Yes		Field indicators, inferred from seismic refraction survey	Ductile-brittle deformation zone
Alteration	–		Await results	
Water	–		Await results	
Fracture orientation			Await results	
Fracture frequency			Await results	
Fracture filling			Await results	

BH	Geometrical intercept	Target intercept	Comment
HLX25	169–182	166–185	Low resistivity, low sonic, variable density and low susceptibility.
HLX14	11–29	–	Await results

ZSMNE004A				
Property	Estimate	Span	Basis for interpretation	Comments
Confidence in existence	High		Linked lineament, Extensive field mapping and tunnel (Äspö) intercept. Seismic refraction.	
Strike (regional scale) 050		generally 030–070	Strong magnetic and topographic lineament; extensive field mapping	Curving geometry. However, the 090 trending eastwards extension has high uncertainty.
Dip (regional scale) 90	90	± 20	Extensive field mapping and tunnel (Äspö) intercept.	The vertical dip has been modified from Simp V 1.2 (70°S) to vertical ± 20° to allow for variations along entire zonelength. It may be preferable to model the zone with a steep dip to the S in the N and a vertical to N dip in the south with a smooth change over.
Thickness, (including transition zones, regional scale)	100 m	20 to 120 m	Linked lineament, tunnel and field mapping.	A ductile complex zone, inferred anastomosing geometry. The 100 m thickness is an envelope thickness containing the inferred splays.
Length (regional scale)	15.6 km	8 to > 15 km	Linked lineaments	Possible termination at ZSMNE024A or NE extension outside the regional model area. Limited data.
Ductile deformation	Yes		Extensive field mapping evidence.	Ductile-brittle zone.
Brittle deformation	–		TASA- highly fractured rock: see engineering comment below. Possible general association with KAV04 raised fracture frequency, though this is not clearly supported by fracture orientations.	Ductile-brittle zone.
Alteration				
Water	2.8·10 ⁻⁶ m ² /s		TASA ch. 300	
Fracture orientation	Not yet assessed			
Fracture frequency	Not yet assessed			
Fracture filling	Chl, Ca, Cy, Fe, Qz; clay		TASA ch.302–334	

BH	Geometrical intercept	Target intercept	Comment
HLX19	174–202	–	Awaiting results
KAV04	–	–	No geometrical intersection but the BH lies on the border of the modelled transition zone and may be responsible for the relatively high fracture frequency and degree of alteration throughout much of the BH though this is not clearly supported by fracture orientations.
TASA		302–334	

ZSMNE005A (Äspö shear zone)				
Property	Estimate	Span	Basis for interpretation	Comments
Confidence in existence	High		Linked lineaments – particularly magnetic. Field mapping results. BHs	
Strike (regional scale)	060	030 to 90	Linked lineaments	030 within the local model area, curving to 090 further north.
Dip (regional scale)	90	± 10	Field mapping	Modelled as vertical to allow for local variations. However, a dip of 90 to 80 SE is considered most probable.
Thickness, (including transition zones, regional scale)	250 m	50 to 300 m	Aerial magnetic survey, topography and field mapping	Complex zone, inferred anastomosing geometry.
Length (regional scale)	10.5 km	± 200 m	Linked lineaments	
Ductile deformation	Yes		Frequent evidence from field mapping	Ductile-brittle zone. Ductile clearly dominates but there has been clear brittle reactivation.
Brittle deformation	Yes		Weak evidence from field mapping. However, BHs show increased fracturing and brecciation.	Ductile clearly dominates but there has been clear brittle reactivation.
Alteration				
Water				/Rhen et al. 1997/: report the most conductive parts coincide with some narrow highly fractured sections or single open fractures which are probably not connected along the entire zone.
Fracture orientation	Not yet assessed			
Fracture frequency m ⁻¹	9		KA1755A, KA1754A, KA1751A, KAS04, KA3590G02, KAS02, KAS12	Frac' frq'incl' crush (= 20 frac/m) (m ⁻¹)
Fracture filling	Ca 45%, Chl 69%, Ep 14%, He 14%, Qtz 3%		KA1755A, KA1754A, KA1751A, KAS04, KA3590G02, KAS02, KAS12	

BH	Geometrical intercept	Target intercept	Comment
KA1755A	22–288	95–140	At core length 95–140 m generally > 10 fract./m, at nine sites > 20 fract./m. This wide zone coincides geometrically with EW-1b. Most of the zone is developed in fine-grained granite and partly in granodiorite. Only a thin zone of true mylonite, with a medium tectonized area of 2–4 m around it. RQD is less than 25 at several locations in the zone. At core length 203–213 m c. 10 fract./m except for a 1–2 m wide zone (ref: Geomod)
KA1754A	26–160 (Base)	90–115	A crush zone and surrounding tectonization at c. 90–115 m fits geometrically with EW-1b. The area has a very high fracture frequency and the rock is fine grained granite, granodiorite and “greenstone” (ref: Geomod)
KA1751A	45–150 (Base)	110–114	The rock is fine grained granite, granodiorite and greenstone. No major indications of deformation in the database. However, in /Stanfors et al. 1994/ a section between core length 140 and 150 m coincides with this area and is mapped as a fracture zone and as tectonized. At approximately 110 m there is a crush zone and a tectonized area developed in fine-grained granite and “greenstone” (ref: Geomod)

BH	Geometrical intercept	Target intercept	Comment
KAS04	2–464	131–437	Two mylonites. Also four areas with weak to intermediate tectonization. The rock is granodiorite and fine-grained granite (ref: Geomod)
KA3590G02	20–30 (Base)	19–30	Intermediate tectonization. The rock is granodiorite. (ref: Geomod)
KAS02	–	795–924	No longer geometrical intercept but keep indicator for review
KAS12	0 (Top)–269	19–286	
HLX09	99–151 (Base)	–	Awaiting BH results
HLX16	0–83	–	Awaiting BH results
KAS17	86–360	–	Only summary preliminary mapping available. Awaiting results

ZSMNE006A

Property	Estimate	Span	Basis for interpretation	Comments
Confidence in existence	High		Linked lineaments, BH and tunnel (Äspö) intercepts	
Strike (regional scale)	215	± 10	Linked lineaments	
Dip (regional scale)	65	± 20	Linked lineaments, BH and tunnel (Äspö) intercepts	
Thickness, (including transition zones, regional scale)	130 m	60 to 130 m	Linked lineaments, BH and tunnel (Äspö) intercepts	Model thickness of 130 m represents an envelope thickness containing narrower inferred splays. At Äspö NE1 is considered to consist of 3 main branches totaling 85 m as intercepted in the tunnel.
Length (regional scale)	2.1 km	2 to 4 km	Linked lineaments	An alternative interpretation allows the zone to continue further north eastwards.
Ductile deformation	Yes		Multiple 1cm thick Mylonite bands, tunnel mapping.	Dominantly brittle zone with minor ductile indicators
Brittle deformation	Yes		Breccia and fault gauge	Dominantly brittle zone with minor ductile indicators
Alteration	1 m wide central completely altered clay core			5–8 m wide partially clay altered.
Water				All 3 branches are water bearing
Fracture orientation	230/35, 341/45, 284/90, 045/30, 050/60, 094/60, 120/35, 310/38, 310/75			The first two sets are water bearing. The analysis did not include the 933 fractures in the 1 m core. See text for details.
Fracture frequency m ⁻¹	11		KA1131B, KAS07, KAS08, KAS11, KAS14, KBH02, KAS02	Frac' frq'incl' crush (= 20 frac/m) (m ⁻¹)
Fracture filling	Ca 60%, Chl 49%, Ep 27%, He 23%, Qtz 1%		KA1131B, KAS07, KAS08, KAS11, KAS14, KBH02, KAS02	

BH	Geometrical intercept	Target intercept	Comment
KA1061	94–209 (Base)	198–209	Ref: Geomod
KA1131B	47–203 (Base)	173–203	Ref: Geomod
KAS07	402–602 (Base)	497–602	Ref: Geomod
KAS08	440–590 (Base)	537–601	Ref: Geomod
KAS09	53–225	50–112	Ref: Geomod
KAS11	115–249	156–220	Ref: Geomod
KAS14	38–194	51–91	Ref: Geomod
KBH02	543–706 (Base)	667–706	Ref: Geomod
KAS02	740–924 (Base)	806–914	Ref: Geomod
KAS16	228–439	380–430	Ref: Geomod
TASA		1,240–1,325	Ref: Geomod

ZSMNE010A

Property	Estimate	Span	Basis for interpretation	Comments
Confidence in existence	High		Linked lineaments. Ref: v. 0. Verified by field control-epidote healed fractures	This zone has not been reviewed in Laxemar v. 1.2.
Strike (regional scale)	055	± 15	Linked lineaments	
Dip (regional scale)	90		Assumed. No information	
Thickness, (including transition zones, regional scale)	10 m	2 to 10 m	Ref: v. 0. Verified by field control-epidote healed fractures	
Length (regional scale)	3.4 km	± 200	Linked lineaments	
Ductile deformation	–		No data	Brittle zone.
Brittle deformation	Yes		Field control. Ref: v. 0.	Brittle zone.
Alteration			No data	
Water				
Fracture orientation				
Fracture frequency				
Fracture filling	Ep		Field control. Ref: v. 0.	

BH	Geometrical intercept	Target intercept	Comment
n.a	n.a	n.a	

ZSMNE011A				
Property	Estimate	Span	Basis for interpretation	Comments
Confidence in existence	High		Linked lineaments. Ref: v. 0. Verified by field control-ground magnetic and VLF measurements.	This zone has not been reviewed in Laxemar v. 1.2.
Strike (regional scale)	055	± 15	Linked lineaments	
Dip (regional scale)	90		Assumed. No information	
Thickness, (including transition zones, regional scale)	100 m	± 50	Linked lineaments	Ref: v. 0, 5–10 m 'cores' of highly fractured rock. 50–150 m wide transition envelope.
Length (regional scale)	8.5 km	8 to 12 km	Linked lineaments	Possible extension to SW.
Ductile deformation	Yes		Field evidence, Ref: v. 0.	Ductile-brittle zone.
Brittle deformation	Yes		Field control. Ref: v. 0. increased small scale fracturing, mesoscopic brittle and ductile-brittle deformation zones and epidote healed fractures	Ductile-brittle zone.
Alteration			No data	
Water			No data	
Fracture orientation			No data	
Fracture frequency			No data	
Fracture filling	Ep		Field control. Ref: v. 0.	

BH	Geometrical intercept	Target intercept	Comment
n.a	n.a	n.a	

ZSMNE012A (EW7-NE4)				
Property	Estimate	Span	Basis for interpretation	Comments
Confidence in existence	High		Linked lineaments, seismic reflector, BH and tunnel (Äspö) intercepts	
Strike (regional scale)	060	050 to 110	Linked lineaments	
Dip (regional scale)	45	± 10	Linked lineaments, BH and tunnel (Äspö) intercepts	
Thickness, (including transition zones, regional scale)	120 m	60 to 120 m	Linked lineaments, BH and tunnel (Äspö) intercepts	Model thickness of 120 m represents an envelope thickness containing narrower inferred splays. At Äspö this zone potentially incorporates both EW7 and NE4. Seismic refraction profiling indicate cores of fractured or altered rock with thicknesses of 15 to 20 m and velocities of 2,500–3,300 m/s

ZSMNE012A (EW7-NE4)				
Property	Estimate	Span	Basis for interpretation	Comments
Length (regional scale)	5.5 km	± 200 m	Linked lineaments	
Ductile deformation	Yes		Mylonite on northern boundary (TASA)	Ductile-brittle zone
Brittle deformation	Yes		Breccia and crushed mylonite.	Ductile-brittle zone
Alteration	Clay. Fracture fillings chlorite and epidote		TASA	
Water	Transmissivity 10 ⁻⁴ to 10 ⁻⁵ m ² /s		TASA	
Fracture orientation	Not yet assessed			
Fracture frequency m ⁻¹	9		KAV01, KAV04A, KBH02	Frac' frq'incl' crush (= 20 frac/m) (m ⁻¹)
Fracture filling	Ca 64%, Chl 48%, Ep 20%, He 14%, Qtz 3%		KAV01, KAV04A, KBH02	

BH	Geometrical intercept	Target intercept	Comment
HAV02	90–163 (Base)	90–150	Penetration rate indicates fractured or weak rock from c. 89–149 m depth.
HAV12	18–136	51–127	Penetration rate and BIPS indicate fractured or weak rock from c. 51–76 m with possible extension to 93 m. Low permeability. Between c. 100–127 m is water bearing. (only preliminary results available)
HAV13	0–121		Await results
HLX018	0–181 (Base)	16–181	Penetration rate indicates fractured or weak rock between 16–115 m, c. 147–151 m and c. 160–181 m. Water inflows at c. 53 m (1.5 l/min), c. 57 m (20 l/min), c. 67 m (21 l/min), c. 110 m (37–70 l/min) and c. 150 m (> 130 l/min). (only preliminary results available)
HMJ01	0–46 (Base)		No information
KAV01	401–630	400–580	Increased fracturing; alteration; low susceptibility and resistivity; low density. Mapped minor shear zones, breccias and mylonites.
KAV03	188–248	164–232	Sicada: 183–185 m brittle-ductile shear zone.
KAV04A	745–947	840–900	Increased number of crush zones. The deformation zone is characterized by an inhomogeneous brittle-cataclastic deformation. The focused resistivity (300) is markedly low along the section c. 860–900 m, but no other geophysical logging methods indicate significant anomalies.
KBH02	107–245	140–194	Sicada; 140.18 m–194.01 m code 42 = Brittle-ductile shear zone
TASA		779–858	

ZSMNE015A				
Property	Estimate	Span	Basis for interpretation	Comments
Confidence in existence	High		Linked lineament, field mapping, along with Clab 1, Clab 2 and OKG excavation mapping.	
Strike (regional scale)	050	± 20	Field and excavation mapping	070 in west curving to 035 eastwards
Dip (regional scale)	70	± 10	Clab 1, Clab 2 and OKG excavation mapping.	
Thickness, (including transition zones, regional scale)	10 m	3 to 15 m	Clab 1, Clab 2 and OKG excavation mapping.	Clab: 2–3 m thick breccia and 2–3 m thick schistose section.OKG: 5–7 m thick breccia.
Length (regional scale)	1.9 km	± 200	Linked lineaments	ZSMNE015A and B = 2.9 km
Ductile deformation	Yes		Field mapping; schistose banding in Clab	Ductile-brittle zone
Brittle deformation	Yes		Breccia in Clab 1 and 2	Ductile-brittle zone
Alteration	Cm wide clay bands		Clab 1 and Clab 2 excavation mapping.	May be depth/weathering dependent. Clab intercept is relatively shallow.
Water	Max' tunnel inflow recorded as 11 l/min		Clab 1 and Clab 2 excavation mapping.	
Fracture orientation				
Fracture frequency				
Fracture filling	Clay and chl		Clab 1 and Clab 2 excavation.	

BH	Geometrical intercept	Target intercept	Comment
Clab 1 access tunnel			Ref P-03-07 and P-03-86
Clab 2 access tunnel			Ref P-03-07 and P-03-86
OKG3 intake tunnel			Ref P-03-07 and P-03-86

ZSMNE015B				
Property	Estimate	Span	Basis for interpretation	Comments
Confidence in existence	High		Linked lineament, field mapping, along with OKG excavation mapping.	
Strike (regional scale)	080	± 10	Field and excavation mapping	
Dip (regional scale)	90	± 10	OKG excavation mapping.	
Thickness, (including transition zones, regional scale)	5 m	1 to 5 m	OKG excavation mapping.	OKG: irregular thickness 0.5–5 m thick breccia.
Length (regional scale)	1.0 km	± 100	Linked lineaments	ZSMNE015A and B = 2.9 km
Ductile deformation	–		No info'	Ductile-brittle zone (by association with ZSMNE015A)
Brittle deformation	Yes		'Crush zones' and Chlorite gouge reported on boundaries (OKG)	Ductile-brittle zone (by association with ZSMNE015A)
Alteration	Clay		OKG excavation mapping.	May be depth/weathering dependent. Clab intercept is relatively shallow.
Water	'Dry'		Nothing noted in OKG excavation mapping.	
Fracture orientation				
Fracture frequency				
Fracture filling	Clay and chl		OKG excavation.	

BH	Geometrical intercept	Target intercept	Comment
OKG cold water intake tunnel			Ref P-03-07 and P-03-86

ZSMNE016A				
Property	Estimate	Span	Basis for interpretation	Comments
Confidence in existence	High		Linked lineaments, seismic refraction, BH and tunnel (Äspö) intercepts	
Strike (regional scale)	030	± 20	Linked lineaments	
Dip (regional scale)	90	± 10	Linked lineaments, BH and tunnel (Äspö) intercepts	
Thickness, (including transition zones, regional scale)	15 m	± 10	Linked lineaments, BH and tunnel (Äspö) intercepts, seismic refraction profile	
Length (regional scale)	1.3 km	± 100 m	Linked lineaments	
Ductile deformation	–			Brittle deformation zone
Brittle deformation	Yes		TASA ch 350–370. Inferred from BH penetration rates and seismic refraction survey, 5–10 m wide low velocity zone 3,000 m/sec.	Brittle deformation zone
Alteration				
Water	Transmissivity 10 ⁻⁶ m ² /s		TASA ch. 350	
Fracture orientation				
Fracture frequency				
Fracture filling	Chlorite, calcite, epidote and clay.		Tunnel mapping	

BH	Geometrical intercept	Target intercept	Comment
HAV14	143–172	130–175	Penetration rate indicates fractured or weak rock (weakness zone) from c. 130–175 m. Water bearing between 164–169 m (85 l/min). (only preliminary results available)
HAV07	–	–	No intercept but in close proximity. Penetration rate indicates fractured or weak rock from c. 16–95 m.
TASA		350–370	

ZSMNE018A				
Property	Estimate	Span	Basis for interpretation	Comments
Confidence in existence	High		Linked lineament, Extensive field mapping evidence.	
Strike (regional scale)	080	± 10	Linked lineament, Extensive field mapping evidence.	
Dip (regional scale)	90	± 10	Field mapping	
Thickness, (including transition zones, regional scale)	50 m	± 25	Linked lineament and field mapping.	A ductile complex zone, inferred anastomosing geometry. The 50 m thickness is an envelope thickness containing the inferred splays.
Length (regional scale)	1.3 km	± 100	Linked lineaments	
Ductile deformation	Yes		Extensive field mapping evidence.	Ductile zone with weak evidence of brittle reactivation.
Brittle deformation	Yes		One clear brittle indicator. One other indicator associated with an inferred splay.	Ductile zone with weak evidence of brittle reactivation.
Alteration				
Water				No information
Fracture orientation	Not yet assessed			
Fracture frequency	Not yet assessed			
Fracture filling				

BH	Geometrical intercept	Target intercept	Comment
-	-	-	-

ZSMNE019A				
Property	Estimate	Span	Basis for interpretation	Comments
Confidence in existence	High		Linked lineament, ground geophysical profiling	
Strike (regional scale)	060	± 15	Linked lineament.	
Dip (regional scale)	90	± 20	None	Simple assumption
Thickness, (including transition zones, regional scale)	5 m	1 to 10 m	Linked lineament, ground geophysical profiling	
Length (regional scale)	3.7 km	± 200	Linked lineaments	
Ductile deformation	–			No information
Brittle deformation	–			No information
Alteration				No information
Water				No information
Fracture orientation				No information
Fracture frequency				No information
Fracture filling				No information

BH	Geometrical intercept	Target intercept	Comment
–	–	–	No intercepts

ZSMNE024A				
Property	Estimate	Span	Basis for interpretation	Comments
Confidence in existence	High		Linked lineaments, seismic reflector, seismic refractor, BHs and OKG cold water intake tunnel.	This zone should be viewed together with ZSMNE031A. Together they define a broad complex structural belt of deformation off the coast of Ävrö
Strike (regional scale)	225	215 to 235	Linked lineaments	
Dip (regional scale)	52	± 10	Linked lineaments, seismic reflector, and BHs. Reflector and KSH03A are the primary constraints	
Thickness, (including transition zones, regional scale)	80 m	± 20	Linked lineaments and BH	Model thickness of 80 m represents an envelope thickness containing narrower inferred splays. OKG suggests fractured cores 2 to 10 m thick. Seismic refraction profiling indicates cores of fractured or altered rock with thicknesses of up to 30 m and velocities of 3,400–4,200 m/s. This zone should be seen as contributing to a broader tectonic belt.
Length (regional scale)	11.6 km	10 to 15++km	Linked lineaments	Lineament data for ZSMNE024A and ZSMNE031A suggests this deformation belt extends beyond the boundaries of the regional model area.
Ductile deformation	–		BHs	Ductile-brittle zone. Major brittle element.

ZSMNE024A				
Property	Estimate	Span	Basis for interpretation	Comments
Brittle deformation	Yes		BHs and tunnel evidence	Ductile-brittle zone. Major brittle element.
Alteration	Chlorite		OKG	Noted as 'highly weathered' -OKG
Water				'moderately water bearing' -OKG
Fracture orientation	Not yet assessed			
Fracture frequency m ⁻¹	13		KSH01A, KSH03A, KAV01A, KAV04A	Frac' frq'incl' crush (= 20 frac/m) (m ⁻¹)
Fracture filling	Ca 51%, Chl 45%, Ep 18%, He 25%, Qtz 15%		KSH01A, KSH03A, KAV01A, KAV04A	

BH	Geometrical intercept	Target intercept	Comment
OKG			Moderately water bearing, highly weathered,
HAV11	95–178	124–180	Only preliminary results available. Penetration rate and BIPS figs' indicate fractured or weaker rock from c. 124–180 m; water bearing measured at 145 m c. 32 l/min and judged to originate from c. 129–142 m
KSH01A	542–669	540–631	DZ6, 540–609 m Partly increased fracturing. Partly heavy alteration. Indication: Low susceptibility, low resistivity. DZ7 609–614 m, Low-Grade, ductile shear-zone. DZ8, 614–631 m, Partly increased fracturing. Partly heavy alteration. Indication: Low susceptibility, low resistivity.
KSH03A	175–258	162–275	Inhomogeneous, low-grade, ductile deformation. High frequency of open and sealed fractures and crush zones. Brecciation between 220–235 m and mylonitization between 270–275 m. Marked low resistivity and, where available, lower sonic. Sonic data are missing between 203.5–255.2 m). Distinct, major caliper anomaly. Generally low magnetic susceptibility. A number of sections with increased fracturing may indicate minor deformation zones.
KAV01A	674–757 (Base)	660–757	Single hole interpretation includes no clear DZ in this location. However, examination of the log suggests that it is not unreasonable to suggest indicators are present.
KAV04A	937–1,004 (Base)	940–1,004	Single hole interpretation gives DZ1 840–900 m with the description: Increased number of crush zones. The deformation zone is characterized by an inhomogeneous brittle-cataclastic deformation. The focused resistivity (300) is markedly low along the section c. 860–900 m, but no other geophysical logging methods indicate significant anomalies. Note that ZSMNE012A is modelled with an interception from 840–900 m. Examination of the log suggests that it is not unreasonable to suggest deformation indicators continue below 900 m of KAV04A

ZSMNE031A				
Property	Estimate	Span	Basis for interpretation	Comments
Confidence in existence	High		Linked lineaments, seismic reflector, seismic refractor, BHs and OKG cold water intake tunnel.	This zone should be viewed together with ZSMNE024A. Together they define a broad complex structural belt of deformation off the coast of Ävrö
Strike (regional scale)	215	± 20	Linked lineaments	
Dip (regional scale)	52	± 20		Based on the assumption that this zone is intimately associated with ZSMNE024A. OKG intake tunnel suggests a shallower 40° dip
Thickness, (including transition zones, regional scale)	15 m	2 to 20 m	Linked lineaments and BH	Seismic refraction profiling indicates cores of fractured or altered rock with thicknesses of up to 15 m and velocities of 3,300–3,400 m/s. This zone should be seen as contributing to a broader tectonic belt.
Length (regional scale)	4.4 km	4.0 to 15++km	Linked lineaments	Lineament data for ZSMNE024A and ZSMNE031A suggests this deformation belt extends beyond the boundaries of the regional model area.
Ductile deformation	–			Brittle zone. Major brittle element.
Brittle deformation	Yes		BHs and tunnel evidence	Brittle zone. Major brittle element.
Alteration	Chl and clay		OKG	
Water	'Dry'		OKG	No inflow recorded in OKG
Fracture orientation	Not yet assessed			
Fracture frequency m ⁻¹	11		KSH01A, KSH03A,	Frac' frq'incl' crush (= 20 frac/m) (m ⁻¹)
Fracture filling	Ca 57%, Chl 52%, Ep 10%, He 29%, Qtz 15%		KSH01A, KSH03A,	

BH	Geometrical intercept	Target intercept	Comment
OKG			Brecciated zone with 2 m (apparent) thickness. Chlorite and clay on SE boundary with associated wedge failure in the roof.
KSH01A	682–704	687–693	Single hole interpretation: DZ10 686.5–692.5 m, Low-Grade, ductile shear-zone. DZ11 692.5–693 m, Increased fracturing. Indication: Low susceptibility, and density.
KSH03A	282–297	287–292	Note: Single hole interpretation: 162–275 m. However, indicators of deformation occur below this depth. eg 286.5–292 m Breccia.

ZSMNE040A				
Property	Estimate	Span	Basis for interpretation	Comments
Confidence in existence	High		Linked lineaments; magnetic, resistivity and seismic refraction profiling-	
Strike (regional scale)	030	± 10	Linked lineaments	
Dip (regional scale)	90	± 10	Magnetic and resistivity profiling.	Modelled as vertical to allow for local variations. However, resistivity profiling weakly indicates a steep (80°) dip to SE
Thickness, (including transition zones, regional scale)	20 m	5 to 20 m	Magnetic, resistivity and seismic refraction profiling	20 m represents an envelope width, inferred to contain discontinuous splays with widths of c. 5 m of fractured rock as inferred from seismic refraction profiling.
Length (regional scale)	1.4 km	± 100 m	Linked lineaments	
Ductile deformation	–			Brittle zone (preliminary assessment- but based on extremely weak evidence)
Brittle deformation	Yes		Inferred from seismic refraction low velocity. Possible associated field mapping indicators.	Brittle zone (preliminary assessment- but based on extremely weak evidence)
Alteration				
Water				
Fracture orientation				
Fracture frequency				
Fracture filling				

BH	Geometrical intercept	Target intercept	Comment
HLX01	0–30		Awaiting BH results
HLX04	21–82		Awaiting BH results

ZSMNE050A				
Property	Estimate	Span	Basis for interpretation	Comments
Confidence in existence	High		Linked lineaments. Field mapping (5 locations)	
Strike (regional scale)	045	035 to 065	Linked lineaments	
Dip (regional scale)	90	± 15	Field mapping	
Thickness, (including transition zones, regional scale)	50 m	20 to 70 m	Linked lineaments and field mapping	An envelope width containing transition zones and inferred splays.
Length (regional scale)	2.2 km	2.0 to 3.0 km	Linked lineaments	
Ductile deformation	Yes		Field mapping	Ductile zone
Brittle deformation	–		No data	Ductile zone
Alteration			No data	
Water			No data	
Fracture orientation			No data	
Fracture frequency			No data	
Fracture filling			No data	

BH	Geometrical intercept	Target intercept	Comment
n.a	n.a	n.a	

ZSMNE930A				
Property	Estimate	Span	Basis for interpretation	Comments
Confidence in existence	High		Linked lineament, Extensive field mapping evidence. Excavation evidence (OKG)	
Strike (regional scale)	065	± 10	Linked lineament, Extensive field mapping evidence.	
Dip (regional scale)	90	± 10	Field mapping and excavation evidence (OKG)	
Thickness, (including transition zones, regional scale)	5 m	1 to 30 m	Linked lineament, Extensive field mapping evidence. Excavation evidence (OKG)	A ductile complex zone, anastomosing geometry visible in the OKG excavations. The 30 m upper limit thickness is an envelope thickness containing the inferred splays with individual widths of 0.5 to 3 m.
Length (regional scale)	4.2 km	± 200 m	Linked lineaments	
Ductile deformation	Yes		Extensive field mapping evidence.	Ductile zone with weak evidence of brittle reactivation.
Brittle deformation	–		Weak indications probably associated with the weathering profile. The presence of well developed schistosity indicates deformation at depth.	Ductile zone with weak evidence of brittle reactivation.
Alteration	Clay			Note: the evidence of clay comes from the OKG excavations located at a shallow depth ie this may be related to a shallow weathering effect.

ZSMNE930A				
Property	Estimate	Span	Basis for interpretation	Comments
Water	Low transmissivity		No inflow indications marked on OKG excavation mapping	The clay is more likely to indicate a hydraulic barrier rather than a conductor.
Fracture orientation	Not yet assessed			Strongly developed schistosity (OKG excavation mapping)
Fracture frequency	Not yet assessed			
Fracture filling	Chlorite			

BH	Geometrical intercept	Target intercept	Comment
OKG	–	–	OKG 3 “turbine building shear zone”

ZSMNS001A–D				
Property	Estimate	Span	Basis for interpretation	Comments
Confidence in existence	High		Linked lineaments. Ref: v. 0. Verified by field control- ground magnetic and VLF measurements. The northern segment has also been verified by a refraction seismic survey /Rydström and Gereben 1989/	This zone has not been reviewed in Laxemar v. 1.2. Eastern side down thrown. Ref: /Kresten and Chyssler 1976/.
Strike (regional scale)	010	± 15	Linked lineaments	
Dip (regional scale)	90	± 15	Steep to vertical dip -VLF	
Thickness, (including transition zones, regional scale)	100 m	± 50 m	Linked lineaments	Ref: v. 0, 10 m ‘cores’ of highly fractured rock. 50–150 m wide transition envelope.
Length (regional scale)	A_3.4 km B_1.1 km C_2.2 km D_4.4 km	10 to > 11 km	Linked lineaments	Possible southward and northward extension beyond the regional model boundary
Ductile deformation	Yes		Field evidence, Ref: v. 0.	Ductile-brittle zone.
Brittle deformation	Yes		Field control. Ref: v. 0. Mesoscopic brittle-ductile shear zones along or close to the marked fracture zone	Ductile-brittle zone.
Alteration			No data	
Water			No data	
Fracture orientation			No data	
Fracture frequency			No data	
Fracture filling	Ep		Field control. Ref: v. 0.	

BH	Geometrical intercept	Target intercept	Comment
n.a	n.a	n.a	

ZSMNS009A				
Property	Estimate	Span	Basis for interpretation	Comments
Confidence in existence	High		Linked lineaments. Ref: v. 0. Verified by field control-ground magnetic and VLF measurements.	
Strike (regional scale)	010	± 10	Linked lineaments	
Dip (regional scale)	90	± 15	Steep to vertical dip -VLF	
Thickness, (including transition zones, regional scale)	80 m	± 40 m	Linked lineaments	Ref. v. 0. 5–50 m thickness has been inferred to represent the upper estimate of a highly fractured 'core' value. An 80 m width has been used in the model, including transition zones.
Length (regional scale)	9.8 km	10 to > 12 km	Linked lineaments	Possible southward extension beyond the regional model boundary
Ductile deformation	Yes		Field evidence, Ref: v. 0. increased small scale fracturing, mesoscopic brittle and brittle-ductile deformation zones and epidote-healed fractures	Ductile-brittle zone.
Brittle deformation	Yes		Field control. Ref: v. 0.	Ductile-brittle zone.
Alteration			No data	
Water			No data	
Fracture orientation			No data	
Fracture frequency			No data	
Fracture filling	Ep		Field control. Ref: v. 0.	

BH	Geometrical intercept	Target intercept	Comment
n.a	n.a	n.a	

ZSMNS017A and B (NNW4)				
Property	Estimate	Span	Basis for interpretation	Comments
Confidence in existence	High		Linked lineaments, tunnel mapping and BHs.	One of a number of parallel steep structures present in this area, ref: NNW4 Geomod.
Strike (regional scale)	335	± 10	Linked lineaments and tunnel	
Dip (regional scale)	83	± 10	Linked lineaments, BHs and tunnel intercepts	Ref: Geomod NNW4. The dip is a 'best fit' geometrical result, it should be treated as generally subvertical.
Thickness, (including transition zones, regional scale)	20 m	20 to 100 m	Tunnel mapping	The upper limit does not represent a single discrete structure but rather an envelope width containing an associated group of structures.
Length (regional scale)	17A 2.1 km 17B 1.1 km	± 100 m± 100 m	Linked lineaments.	
Ductile deformation	Yes		Tunnel mapping (mylonite) TASA ch. 2,015, 2,120, 2,920	Ductile-brittle zone. Important brittle component as indicated by high transmissivities.
Brittle deformation	Yes		Increased fracturing and crush zones KA2048B	Ductile-brittle zone. Important brittle component as indicated by high transmissivities.
Alteration	Weak to medium, Clay, Chl, Ca and Ep.			
Water	T = 2.1·10 ⁻⁴ m ² /s		TASA ch. 2,020	
Fracture orientation	Not yet assessed			
Fracture frequency m ⁻¹	11		KA2048B	Frac' frq'incl' crush (= 20 frac/m) (m ⁻¹)
Fracture filling	Ca 74%, Chl 38%, Ep 9%, He 28%, Qtz 0%		KA2048B	

BH	Geometrical intercept	Target intercept	Comment
KA2048B	6–67	28–46	8 fractures per m and crushed core c. 1 m total
TASA		2,010–2,020	Ref: Geomod and PR HRL-96-19
TASA		2,115–2,125	Ref: Geomod and PR HRL-96-19
TASA		2,910–2,930	Ref: Geomod and PR HRL-96-19

ZSMNS059A				
Property	Estimate	Span	Basis for interpretation	Comments
Confidence in existence	High		Linked lineament, field mapping and geophysical ground survey	
Strike (regional scale)	000	± 10	Strong magnetic and topographic lineament	
Dip (regional scale)	90	± 10	Seismic reflector, field mapping indicators and geophysical ground survey.	A seismic reflector interpreted as representing a splay of this zone has been identified as dipping 80° to the west field mapping results further south suggest 80–85° to the east. The zone will be modelled as being vertical with a ± 10° uncertainty.
Thickness, (including transition zones, regional scale)	50 m	20 to 60 m	Geophysical ground survey	Geophysical profiling indicates a complex zone; a width of 50 m has been used in the model as being representative of the zone over its entire length and covers inferred multiple splays and transition zones. Individual splays are inferred to have cores of more highly fractured rock that have widths varying between 5 m to 15 m, based on seismic refraction profiling results.
Length (regional scale)	5.3 km	± 200 m	Linked lineaments	Southern termination most uncertain.
Ductile deformation	Yes		Five field indicators	Brittle-ductile zone. No subsurface investigations yet to substantiate a brittle component.
Brittle deformation	Yes		Inferred from seismic refraction profiling results	Brittle-ductile zone. No subsurface investigations yet to substantiate a brittle component.
Alteration				No analysis available
Water				No analysis available
Fracture orientation				No analysis available
Fracture frequency				No analysis available
Fracture filling				No analysis available

BH	Geometrical intercept	Target intercept	Comment

ZSMNW025A				
Property	Estimate	Span	Basis for interpretation	Comments
Confidence in existence	High		Linked lineament, seismic refraction profiling	A minor structure
Strike (regional scale)	110	± 10	Linked lineament	
Dip (regional scale)	90	± 10	HSH01A	A dip of 88 gives a best fit with HSH01A. However, it seems unjustified to define such a specific dip based on such local evidence when surrounding investigations provide weak or no supporting indications.
Thickness, (including transition zones, regional scale)	10 m	1 to 15 m	Linked lineament and seismic refraction profiling	Variable width, considered discontinuous.
Length (regional scale)	1.9 km	± 100 m	Linked lineaments	Considered discontinuous
Ductile deformation	–		No info'	Brittle zone
Brittle deformation	Yes		increased fracturing c. 15/m	Brittle zone
Alteration				Await BH results
Water				Await BH results
Fracture orientation	Not yet assessed			
Fracture frequency m ⁻¹	7		HSH01A	Frac' frq'incl' crush (= 20 frac/m) (m ⁻¹)
Fracture filling	Ca 1%, Chl 83%, Ep 1%, He 0%, Qtz 14%		HSH01A	

BH	Geometrical intercept	Target intercept	Comment
HSH01A	170–197	160–171	Increased fracturing indicated by high penetration rate, low susceptibility and low resistivity. Alteration indicated by drill cuttings.
HSH04A	132–151		Await results
HSH06A	115–132		Await results

ZSMNW028A				
Property	Estimate	Span	Basis for interpretation	Comments
Confidence in existence	High		Linked lineaments; detailed topographic and magnetic study (ref: P-03-66) and BH.	
Strike (regional scale)	105	± 15	Linked lineaments	
Dip (regional scale)	90	± 10	Linked lineaments and BH	A dip of 83° gives a best fit with HAV09. However, oriented fractures in the hole suggest 250/88°. The zone is considered subvertical and it seems unjustified to define a more specific dip.
Thickness, (including transition zones, regional scale)	10 m	± 5 m	Linked lineaments and BH	
Length (regional scale)	1.1 km	± 100 m	Linked lineaments	
Ductile deformation	–		No information	Brittle zone
Brittle deformation	Yes		Increased fracturing in BH	Brittle zone
Alteration			Await results	
Water			Await results	
Fracture orientation	Not yet assessed			
Fracture frequency m ⁻¹	1		HAV09	Frac' frq'incl' crush (= 20 frac/m) (m ⁻¹)
Fracture filling	Ca 0%, Chl 0%, Ep 0%, He 0%, Qtz 0%		HAV09	-needs review and consensus with single hole interpretation.

BH	Geometrical intercept	Target intercept	Comment
HAV09	72–96	75–105	The zone is indicated by increased fracture frequency, high drill penetration rate, low resistivity, low magnetic susceptibility, low density, low p-wave velocity and distinct, marked caliper anomalies.

ZSMNW042A				
Property	Estimate	Span	Basis for interpretation	Comments
Confidence in existence	High		Linked lineaments, magnetic, resistivity and seismic refraction profiling	
Strike (regional scale)	105	± 10	Linked lineaments	
Dip (regional scale)	90	± 20	Linked lineaments. Dip-field mapping suggests dip to south, HLX15 orientated fractures suggest 75° to S or N. Surface geophysics suggest subvertical.	
Thickness, (including transition zones, regional scale)	80 m	30 to 80 m	Magnetic and topographic lineament widths.	Model width of 80 m represents an envelope width containing narrower inferred splays. Seismic refraction results indicate a narrower, 20 m wide fractured core.
Length (regional scale)	3.3 km	± 100 m	Linked lineaments	ZSMNW042A,B,C together = 8.3 km
Ductile deformation	Yes		Weak field indicators	Await BH results. current weak evidence suggests a ductile-brittle zone.
Brittle deformation	Yes		Weak field indicators	Await BH results. current weak evidence suggests a ductile-brittle zone.
Alteration				
Water				
Fracture orientation				
Fracture frequency				
Fracture filling				

BH	Geometrical intercept	Target intercept	Comment
HLX15	0–143		Await results
HLX26	40–151 (Base)		Await results
HLX27	136–165 (Base)		Await results
HLX28	72–154 (Base)		Await results
HLX29			Await results- no current geometrical intercept
KLX05			Await results- no current geometrical intercept

ZSMNW928A				
Property	Estimate	Span	Basis for interpretation	Comments
Confidence in existence	Medium		Seismic reflector and coincidence with BH deformation indicators	Based on seismic reflector N geometry /Juhlin et al. 2004b/. Relevant BH data has not been fully evaluated yet.
Strike (regional scale)	120	± 20	Seismic reflector 'N'/Juhlin et al. 2004b/	No surface expression. Based on seismic reflector N geometry /Juhlin et al. 2004b/
Dip (regional scale)	28	± 5	Seismic reflector 'N' /Juhlin et al. 2004b/	Based on seismic reflector N geometry /Juhlin et al. 2004b/
Thickness, (including transition zones, regional scale)	–	–	Seismic reflector 'N' /Juhlin et al. 2004b/	Modelled with zero thickness. Relevant BH data has not been fully evaluated yet.
Length (regional scale)	2.2 km	2 to 5 km	Seismic reflector survey	Length estimate limited by the extent of the survey coverage.
Rock type	Ävrö granite dominates, with fine grained diorite gabbro		KLX02 and KLX04	Preliminary- relevant BH data has not been fully evaluated yet.
Ductile deformation	Not yet assessed			Relevant BH data has not been evaluated yet.
Brittle deformation	Not yet assessed			
Alteration	Not yet assessed			
Water	Not yet assessed			
Fracture orientation	Not yet assessed			
Fracture frequency m ⁻¹	Not yet assessed			
Fracture filling	Not yet assessed			

BH	Geometrical intercept	Target intercept	Comment
KLX02	764	–	Not yet assessed
KLX04	898	–	Not yet assessed.

ZSMNW929A				
Property	Estimate	Span	Basis for interpretation	Comments
Confidence in existence	High		Linked lineament and BH intercepts.	
Strike (regional scale)	113	± 10	Magnetic and topographic lineaments	Lineament interpretation needs further review.
Dip (regional scale)	79	± 10	Lineament trace coupled with KLX02 and KLX04 single hole interpretations and orientated fractures in KLX04 between 870–970 BhI.	
Thickness, (including transition zones, regional scale)	50 m	20 to 50 m	Magnetic and topographic lineaments	Model width of 50 m represents an envelope width containing narrower inferred splays.
Length (regional scale)	1.9 km	± 100 m	Linked lineaments	
Ductile deformation	–		No indicators	Brittle deformation zone
Brittle deformation	Yes		BHs, increased fracture frequency and crush zones	Brittle deformation zone
Alteration	Oxidation			
Water	–			Not yet analysed
Fracture orientation	Not yet assessed			
Fracture frequency m ⁻¹	10		KLX02, KLX04	Frac' frq'incl' crush (= 20 frac/m) (m ⁻¹)
Fracture filling	Ca 51%, Chl 57%, Ep 13%, He 7%, Qtz 10%		KLX02, KLX04	.

BH	Geometrical intercept	Target intercept	Comment
KLX02	778–935	770–960	Generally increased frequency of open fractures and higher oxidation. The most intensive part of the zone is located between 845–880 m, which is indicated by distinct low p-wave velocity and partly somewhat lower resistivity. A number of sections with increased fracturing may indicate minor deformation zones.
KLX04	861–986	873–973	Repeated crush and sealed network. Alteration in upper part, but missing in the central part. High frequency of open fractures. Zone centre with strong inhomogeneous brittle deformation. The most intensely deformed part in this section is between c. 930 and 973 m. A radar reflector at 915.7 m has an angle of 31° to borehole axis and one reflector at 888.5 m has the angle 21° to borehole axis. Rock type is interpreted to be granite to quartz monzodiorite, generally porphyritic (Ävrö granite). Note: An intensely crushed part at 936–946 m may correlate with a seismic reflector (ZSMNE928A) with the orientation 120/30.

ZSMNW931A				
Property	Estimate	Span	Basis for interpretation	Comments
Confidence in existence	High		Linked lineaments. Ref: v. 0. Verified by field control-ground magnetic and VLF measurements.	Ground geophysics Ref: /Stanfors and Erlström 1995/
Strike (regional scale)	165	± 10	Linked lineaments	
Dip (regional scale)	90	± 15	Assumed	
Thickness, (including transition zones, regional scale)	50 m	50 to 100 m	Linked lineaments. Ref v. 0.	An envelope width containing transition zones and inferred splays.
Length (regional scale)	3.9 km	± 200 m	Linked lineaments	ZSMNW931A + B = 4.3 km
Ductile deformation	–		No data	Brittle zone.
Brittle deformation	Yes		Inferred from VLF	Brittle zone.
Alteration			No data	
Water			No data	
Fracture orientation			No data	
Fracture frequency			No data	
Fracture filling	Ep		No data	

BH	Geometrical intercept	Target intercept	Comment
n.a	n.a	n.a	

ZSMNW932A (formerly ZSMNW006A)				
Property	Estimate	Span	Basis for interpretation	Comments
Confidence in existence	High		Linked lineament and geophysical ground survey	Seismic refraction profiling did not identify any corresponding low velocity zone.
Strike (regional scale)	120	120 to 90	Linked lineaments	
Dip (regional scale)	90	± 20	geophysical ground survey identified no clear indicators.	
Thickness, (including transition zones, regional scale)	0 m	0 to 20 m	geophysical ground survey identified no clear indicators.	
Length (regional scale)	2.8 km	± 200 m	Linked lineaments	ZSMNW932A,B,C,D combined length 4.9 km
Ductile deformation	–		No evidence from field mapping	Awaiting BH results
Brittle deformation	–		No evidence from field mapping	Awaiting BH results
Alteration				Awaiting BH results
Water				Awaiting BH results
Fracture orientation				Awaiting BH results
Fracture frequency				Awaiting BH results
Fracture filling				Awaiting BH results

BH	Geometrical intercept	Target intercept	Comment
KLX03	505	–	Only summary preliminary mapping available. No strong indicators. Awaiting results
KLX05	624	–	Only summary preliminary mapping available. No strong indicators. Awaiting results

ZSMNW933A

Property	Estimate	Span	Basis for interpretation	Comments
Confidence in existence	High		Linked lineaments. Ref: v. 0. Verified by field control-ground magnetic and VLF measurements.	Ground geophysics Ref: /Stenberg and Sehlstedt 1989/
Strike (regional scale)	150	150 to 090 eastwards	Linked lineaments	
Dip (regional scale)	90	± 15	Assumed	
Thickness, (including transition zones, regional scale)	40 m	± 20	Linked lineaments. Ref v.0. ground geophysics VLF	Ref v. 0. ground geophysics VLF
Length (regional scale)	3.8 km	± 200	Linked lineaments	
Ductile deformation	–		No data	Brittle zone
Brittle deformation	Yes		Inferred from VLF	Brittle zone
Alteration			No data	
Water			No data	
Fracture orientation			No data	
Fracture frequency			No data	
Fracture filling	Ep		No data	

BH	Geometrical intercept	Target intercept	Comment
n.a	n.a	n.a	